

**FUNCTIONALIZATION OF POLYCAPROLACTONE THROUGH  
NOVEL BLOCK COPOLYMER DESIGN FOR CELL  
ENGINEERING AND GENE DELIVERY**

**LI ZIBIAO**

*(M. Eng., Shantou University)*

**A THESIS SUBMITTED  
FOR THE DEGREE OF DOCTOR OF PHILOSOPHY  
DEPARTMENT OF BIOENGINEERING  
NATIONAL UNIVERSITY OF SINGAPORE**

**2013**



## DECLARATION

I hereby declare that this thesis is my original work and it has been written by me in its entirety. I have duly acknowledged all the sources of information which have been used in the thesis. This thesis has also not been submitted for any degree in any university previously.



---

Li Zibiao

19-July-2013

### ACKNOWLEDGEMENTS

First and foremost I would like to express my sincere appreciation to Professor Li Jun, my supervisor, for his constant guidance, support and encouragement throughout my research. His insight to research and steady persistence in research work, which impressed me deeply, will be my greatest motivation in my future work. His critical comments have triggered and nourished my intellectual maturity; and also have promoted and enriched my research ability. I am really grateful to his directions.

I would like to thank Prof. Li Xiaoping and Prof. Chen Nanguang, who served as my oral qualification examiners and provided me comments on my research and thesis writing. I would also like to thank all my group members in Supramolecular Biomaterials Laboratory and IMRE, past and present, for their friendship and help throughout my research. Thanks go in particular to the sample seniors, Liu Kerh Li, Zhang Zhong-Xing, Loh Xian Jun, Wu Yunlong, Wang Chunxia, Liu Xiaohong and Ni Xiping who gave me great helps in research. It is my honor to be together with Ping Yuan, Yin Hui, Zhu Jing Ling, Liu Chengde, Li Jiajing, Zhao Feng, She Zhen, Wen Yuting, Song Xia and Colin SNG for doing research in the same group. Thank you.

I also want to thank Prof. Xu Kaitian and Prof. Chen Guo-Qiang for their supervision and training during my master study, who encouraged me to embark on a PhD study.

Finally, financial supports from National University of Singapore and A-STAR's Institute of Materials Research and Engineering are gratefully acknowledged.

Last but not mean the least, I'd like to thank my parents for their understanding and love in every aspect of my life. My greatest thank goes to my beloved wife, Yang Jing, who is willing to continuously support me with great love and sacrifice.

## TABLE OF CONTENTS

ACKNOWLEDGEMENTS .....	I
TABLE OF CONTENTS .....	II
SUMMARY .....	V
LIST OF SCHEMES .....	VII
LIST OF TABLES.....	VIII
LIST OF FIGURES.....	IX
LIST OF ABBREVIATIONS .....	XIV
LIST OF PUBLICATIONS .....	XVII
<b>CHAPTER 1        INTRODUCTION .....</b>	<b>18</b>
1.1 RESEARCH BACKGROUND .....	18
1.2 OBJECTIVE AND SCOPE OF STUDY .....	21
1.3 ORGANIZATION OF THE THESIS .....	22
1.4 REFERENCES .....	23
<b>CHAPTER 2        LITERATURE REVIEW .....</b>	<b>26</b>
2.1 BIODEGRADABLE POLYMERS AS BIOMATERIALS .....	26
2.1.1 <i>Biodegradable Polymers</i> .....	26
2.1.1.1 Natural polymers .....	27
2.1.1.2 Synthetic polymers .....	28
2.1.2 <i>Biodegradation</i> .....	31
2.1.2.1 Biodegradation mechanisms .....	32
2.1.2.2 Degradation products .....	35
2.1.2.3 Factors affecting biodegradation and degradation-monitoring techniques.....	38
2.2 BLOCK COPOLYMERS BASED ON BIODEGRADABLE ALIPHATIC POLYESTERS .....	39
2.2.1 <i>Block Copolymer Synthetic Strategies</i> .....	40
2.2.1.1 Step polymerization .....	40
2.2.1.2 Chain polymerization.....	43
2.2.2 <i>Block Copolymer Architectures</i> .....	45
2.2.2.1 Linear block copolymers.....	46
2.2.2.2 Brush block copolymers .....	49
2.2.2.3 Branch block copolymers .....	50
2.3 INCLUSION COMPLEX BETWEEN BIODEGRADABLE BLOCK COPOLYMERS AND CYCLODEXTRINS .....	51
2.4 BIOMEDICAL APPLICATIONS OF NOVEL BIODEGRADABLE BLOCK COPOLYMERS AND THEIR INCLUSION COMPLEXES .....	53

## Table of Contents

2.4.1 Biodegradable Block Copolymers for Tissue Engineering.....	53
2.4.2 Biodegradable Block Copolymers as Delivery Carriers .....	58
2.4.3 Biomedical Applications of Biodegradable Block Copolymers Based Inclusion Complexes .	60
2.5 REFERENCES .....	62
<b>CHAPTER 3 BIODEGRADABLE PCL-BASED HAIRY BLOCK COPOLYMERS: SYNTHESIS AND CHARACTERIZATION, THERMAL-SENSITIVE NANO-AGGREGATES AND SURFACE COATING FOR FACILE CELL RECOVERY.....</b>	<b>76</b>
3.1 INTRODUCTION .....	76
3.2 EXPERIMENTAL SECTION.....	78
3.2.1 Materials .....	78
3.2.2 Synthesis Methods .....	78
3.2.3 Methods and Characterization .....	79
3.2.4 Thermally Induced Cell Detachment .....	81
3.3 RESULTS AND DISCUSSION .....	82
3.3.1 Synthesis and Molecular Characterizations of the P(PPOMA)-PCL-P(PPOMA) Hairy Block Copolymers.....	82
3.3.2 Self-assembly of P(PPOMA)-PCL-P(PPOMA) Block Copolymer Solutions and Their Thermo-responsive Property Studies.....	85
3.3.3 Thermal and Crystallization Behavior .....	97
3.3.4 Temperature-dependent Cell Detachment and Viability Assay .....	99
3.4 CONCLUSIONS.....	104
3.5 REFERENCES .....	104
<b>CHAPTER 4 ENGINEERED BIODEGRADABLE PCL-BASED HYPERBRANCHED HYDROGEL WITH MECHANO-RESPONSIVE PROPERTY FOR POTENTIAL CELL DELIVERY APPLICATION.....</b>	<b>108</b>
4.1 INTRODUCTION .....	108
4.2 EXPERIMENTAL SECTION.....	110
4.2.1 Materials .....	110
4.2.2 Synthesis of Hyperbranched EGC Block Copolymers .....	110
4.2.3 Methods and Characterization .....	111
4.2.4 3D Cell Encapsulation and Sub-culture .....	113
4.3 RESULTS AND DISCUSSION .....	114
4.3.1 Synthesis and Characterization of Hyperbranched EGC Block Copolymers.....	114
4.3.2 Characterization of Hyperbranched EGC Hydrogels .....	120
4.3.3 Cell Encapsulation, Recovery and Sub-culture .....	129
4.4 CONCLUSION.....	133
4.5 REFERENCES .....	134
<b>CHAPTER 5 SUPRAMOLECULAR NANOCARRIERS CONSISTING OF BIODEGRADABLE PCL/CYCLODEXTRIN-BASED POLYROTAXANE FOR TARGETED GENE DELIVERY.....</b>	<b>137</b>
5.1 INTRODUCTION .....	137
5.2 EXPERIMENTAL SECTION.....	139
5.2.1 Materials .....	139
5.2.2 Synthesis of Polyrotaxane-Based Triblock Copolymers and FA-PEG-(D-PR-D) Conjugates .....	139
5.2.3 Methods and Characterization .....	141
5.2.4 Plasmid Amplification, Cell Lines and Gene Transfection Evaluation .....	142
5.3 RESULTS AND DISCUSSION .....	144
5.3.1 Synthesis and Characterization of Polyrotaxane-Based Triblock Copolymers (D-PR-D)...	144
5.3.2 Synthesis and Characterization of D-PR-D Triblock Copolymer Based Conjugates.....	149
5.3.3 pDNA Condensation and Particle Size Characterization.....	155
5.3.4 Cytotoxicity and In Vitro Transfection Efficiency Studies .....	159
5.4 CONCLUSION.....	164

## Table of Contents

---

5.5 REFERENCES .....	164
<b>CHAPTER 6 CONCLUSIONS AND FUTURE WORK.....</b>	<b>168</b>
6.1 CONCLUSIONS.....	168
6.2 POSSIBLE FUTURE RESEARCH .....	170
6.3 REFERENCES .....	171

### SUMMARY

Aliphatic polyesters comprise the earliest and most extensively investigation as biomaterials due to their biodegradability and biocompatibility. However, to be of practical interest, many other requirements have to be fulfilled. This is highly dependent on the specific applications at targeted living conditions. In this thesis, biodegradable block copolymers with various architectures containing aliphatic polycaprolactone (PCL) and different functional components were designed to manipulate the amphiphilicity, mechanical properties, degradation rate and functionalities of the desired products. The potential biomedical applications of the newly developed block copolymers were explored and demonstrated.

First, thermally sensitive block copolymers consisting of biodegradable PCL and hairy poly(propylene oxide) methacrylate (PPOMA) were synthesized by atom transfer radical polymerization (ATRP) to afford P(PPOMA)-PCL-P(PPOMA) structure, denoted as PCP. Due to the thermo-responsive property of the PPOMA segments, the PCP copolymer aqueous solutions self-assembled into controllable nano-aggregates as triggered by temperature. The thermo-responsive substrates were obtained by coating the PCP block copolymer solutions through drop-casting approach, and were examined for supporting cell adhesion and proliferation at 37 °C, and allowing effective cell detachment at 4 °C without using trypsin digestion. The thermally detached cells showed good proliferation ability in the cell sub-culture. The PCP block copolymer coated substrates allows for easy cell recovery under mild conditions and fast passage with good cell viability.

In addition to the PCP block copolymers coated surface as two dimensional (2D) cell culture and recovery substrates, a 3D cell encapsulation system in a thixotropic hydrogel for potential cell delivery application was developed. The mechano-responsive hydrogels were prepared from the hyperbranched polyurethane block copolymers comprising biodegradable PCL, hydrophilic poly(ethylene glycol) (PEG) and branch unit glycerol (EGC copolymers).



## Summary

---

The hydrogels possessed tunable viscoelasticity properties and provided tissue-like environment for cell encapsulation. The porous morphology of the hydrogels allowed the embedded cells to be stored in a 3D manner with good permeability for gas and nutrition. The encapsulated cells maintained good cell viability within the hydrogels and the recovered cells from the hydrogels also showed good proliferation ability after sub-culture. Together with the controlled biodegradability and injectability, the hydrogel system showed great potential as injectables for cell delivery, which is applicable to transfer cells into specific site for special disease treatment.

Finally, a novel targeted gene delivery carrier was synthesized from the combinational techniques of macromolecular self-assembly, ATRP and bioactive molecule conjugation. In the design strategy, a  $\alpha$ -cyclodextrin ( $\alpha$ -CD) based supramolecular architecture composed of a biodegradable PCL/ $\alpha$ -CD polyrotaxanes (PR) as central block and flanked by cationic poly(dimethylamino ethyl methacrylate) (PDMAEMA) segments were firstly prepared to give PDMAEMA-PR-PDMAEMA (D-PR-D) triblock copolymers. Then, these D-PR-D copolymers were further modified by folate-poly(ethylene glycol) (FA-PEG) to give the desired targeting gene delivery vector FA-PEG-(D-PR-D). The FA-PEG-(D-PR-D) polymers exhibited good ability to condense pDNA into nano-sized particles with positive surface charge at certain N/P ratios, and the incorporation of PEG imparted lower *in vitro* cellular toxicity as compared with the unconjugated D-PR-D copolymers. Gene transfection results showed the FA-PEG-(D-PR-D)/pDNA polyplexes exhibited higher transfection efficiency than that of PEG-(D-PR-D) in FR-positive KB cells but not FR-negative A549 cells. Folic acid competitive assay showed that the transfection efficiency of FA-PEG-(D-PR-D) in the presence of free folic acid was much lower than that of the supramolecules without free folic acid on FR-positive KB cells, indicating targeted gene delivery.

To sum up, block copolymers containing biodegradable aliphatic PCL and several functional components as building blocks were designed and synthesized in various architectures. The functionalities of these newly developed block copolymers as biomaterials were explored in different fields.

## **LIST OF SCHEMES**

Scheme 3.1. Synthesis route of P(PPOMA)-PCL-P(PPOMA) (PCP) hairy block copolymers by ATRP.....	82
Scheme 4.1. Synthesis route and schematic illustration of hyperbranched EGC block copolymer.....	115
Scheme 5.1. Synthetic procedure of Folate-PEG-NH <sub>2</sub> (A) and the final product FA-PEG-(D-PR-D) (B) with D-PR-D triblock copolymer as intermediate.....	145

## LIST OF TABLES

Table 2.1. Chemical structure of cyclic esters in corresponding to the most intensively studied aliphatic polyesters. ....	31
Table 2.2. Typical hydrolysable bonds in biodegradable polymers .....	35
Table 2.3. Final degradation products of some typical aliphatic polyesters. ....	37
Table 3.1. Molecular characteristics of PCP hairy block copolymers. <sup>a</sup> .....	83
Table 3.2. Solution properties of PCP hairy block copolymers.....	89
Table 3.3. Particle size characterization of PCP hairy block copolymer solutions. <sup>a</sup> .....	92
Table 3.4. Thermal properties of PCP hairy block copolymers.....	99
Table 4.1. Synthesis and molecular characteristics of hyperbranched EGC block copolymers. ....	116
Table 4.2. Thermal transitions of hyperbranched EGC block copolymers, hydrogels, and their precursors.....	120
Table 4.3. Rheological characteristics of hyperbranched EGC hydrogels at various concentrations and the hydrogel recovery time. ....	124
Table 5.1. Compositions and yields of PCL-diBr / $\alpha$ -CD based polypseudorotaxanes. <sup>a</sup> .....	146
Table 5.2. Molecular characteristics of PR-based triblock copolymers and conjugates.....	147

## LIST OF FIGURES

Figure 2.1. Some representative structures of nature polymers.....	28
Figure 2.2. Representative structures of synthetic biodegradable groups.....	29
Figure 2.3. Schematic illustration of surface erosion and bulk degradation mechanisms of biodegradable polymers.....	32
Figure 2.4. Schematic hydrolytic degradation of PCL, an aliphatic polyester. ....	36
Figure 2.5. Preparation of PHB- <i>alt</i> -PEG multiblock copolymers by esterification reaction of carboxylic acids with alcohols groups in building blocks. [This image was reproduced with permission from ref. <sup>75</sup> (J. Li, 2011) © 2011 American Chemical Society].....	41
Figure 2.6. Preparation of poly(PEG/PPG/PCL) multiblock copolymers by urethane reaction. [This image was reproduced with permission from ref. <sup>81</sup> (J. Li, 2011) © 2008 Elsevier].....	42
Figure 2.7. General mechanisms for the most studied CLRP (a) NMP [This image was reproduced with permission from ref. <sup>91</sup> (V. Sciannamea, 2008) © 2008 American Chemical Society]; (b) ATRP [This image was reproduced with permission from ref. <sup>92</sup> (J. S. Wang, 1995) © 1995 American Chemical Society]; and (c) RAFT [This image was reproduced with permission from ref. <sup>93</sup> (J. Chiefari, 1998) © 1998 American Chemical Society].....	43
Figure 2.8. Ring-opening polymerization of lactones or lactides by the (A) cationic, (B) anionic and (C) coordination-insertion mechanisms. [This image was reproduced with permission from ref. <sup>109</sup> (X. B. Xiong, 2012) © 2012 Elsevier].....	45
Figure 2.9. Types of block copolymers with various architectures. ....	46
Figure 2.10. Chemical structure of cyclodextrins and their physical dimensions. ....	51
Figure 2.11. Inclusion complexes structure formed between CDs and block copolymer with stereo-selectivity. [This image was reproduced with permission from ref. <sup>175</sup> (A. Harada, 2009) © 2009 American Chemical Society].....	52

## List of Figures

- Figure 2.12. (a) Structure of PNIPAAm-PHB-PNIPAAm triblock copolymers. (b) Illustration of the cell detachment process (b). [This image was reproduced with permission from ref.<sup>209</sup> (J. Li, 2009) © 2009 John Wiley and Sons]. ..... 55
- Figure 2.13. (a) Rheological characteristics of PEG-Silica based thixotropic hydrogel. (b) Live-dead assay after one week of culturing MCF-7 cells in 3D PEG-silica gels. [This image was reproduced with permission from ref.<sup>225</sup> (Y. S. Pek, 2008) © 2008 Nature Publishing Group]..... 57
- Figure 2.14. Structure of cationic polyrotaxanes with multiple OEI-grafted  $\beta$ -CD rings. [This image was reproduced with permission from ref.<sup>271</sup> (J. Li, 2006) © 2006 John Wiley and Sons]. ..... 60
- Figure 3.1.  $^1\text{H}$  NMR (A) and  $^{13}\text{C}$  NMR (B) spectra of PCP copolymer, PCP(530-2000-530) in  $\text{CDCl}_3$ ..... 84
- Figure 3.2.  $^1\text{H}$  NMR spectrum of PCP(3570-530-3570) (2 mg/mL) in  $\text{CDCl}_3$  (A) and  $\text{D}_2\text{O}$  (B) at 5 °C. .... 86
- Figure 3.3. Plots of  $I_{337}/I_{334}$  ratio of pyrene excitation spectra in water as a function of PCP copolymer concentration at different temperatures; A) PCP(3590-2000-3590); B) PCP(3570-530-3570). ..... 87
- Figure 3.4. Thermo-responsive behavior of PCP copolymer aqueous solutions. a) Poly(PPOMA) homopolymer at solution concentration of  $1.0 \times 10^3$  mg/L; b) PCP (3570-530-3570) at solution concentration of  $1.0 \times 10^3$  mg/L; c) PCP (3590-2000-3590) at solution concentration of 250 mg/L..... 90
- Figure 3.5. TEM micrographs (A) and particle size distributions (B) of PCP (3340-2000-3340) copolymer nano-aggregates at 5 °C and 35 °C. Solution concentration at 25 mg/L was used for the measurements..... 91
- Figure 3.6. Proposed mechanism for the reversible micelles to nano-aggregates transition between 5 °C and 35 °C..... 93
- Figure 3.7.  $^1\text{H}$  NMR spectrum of 2 mg/mL PCP (3570-530-3570) in  $\text{D}_2\text{O}$  solution at various temperatures, showing specific methyl and methylene protons signals in PPO units. .... 94
- Figure 3.8. (A) Thermodynamic diameter distribution of PCP (3570-530-3570) copolymer at 5 °C and 35 °C. a) Solution concentration is 500 mg/L, b) Solution concentration is 25 mg/L. (B) Graphics showing the reversible transition of PCP (3570-530-3570) at 500 mg/L triggered by temperature. .... 95
- Figure 3.9. (A) Static water contact angles of thermal-responsive surface coated by PCP block copolymers at various coating densities. (B) Photographs of water droplet on polymer coated surface at different temperatures. (a) Tissue culture polystyrene (TCPS), (b) PCP(3590-2000-3590) coated TCPS at density of  $6 \mu\text{g}/\text{cm}^2$ , (c) PCP(3570-530-3570) coated TCPS at density of  $6 \mu\text{g}/\text{cm}^2$ ..... 96
- Figure 3.10. Thermal and crystallinity studies of (A) TG/DTG curves of a) PPOMA prepolymer; b) PCP (2700-2000-2700); c) PCL2000-diBr. (B) DSC curves of PCP copolymers and its precursors. Data were collected from the second heating runs..... 98

## List of Figures

---

Figure 3.11. Phase contrast micrographs of L929 cells cultured on PCP(3590-2000-3590) coated substrates (A), temperature-induced detachment of the cells (B), and the sub-culture of the recovered cells (C). .....	100
Figure 3.12. Cell viability assay of L929 cells after 24 h culture on substrates coated with PCP copolymers at various coating densities. ....	101
Figure 3.13. Cell detachment number of L929 cells cultured on substrates coated with PCP copolymers at various coating densities. ....	102
Figure 3.14. Relative cell number after one day sub-culture for detached L929 cells from substrates coated with PCP copolymers at various coating densities. *Calculated by relating to trypsin treated cells. ....	103
Figure 4.1. $^1\text{H}$ NMR spectrum of EGC3 in $\text{CDCl}_3$ . ....	117
Figure 4.2. TG/DTG curves a) PCL530-diol, b) PEG2000, and c) EGC2. ....	118
Figure 4.3. DSC curves of hyperbranched EGC block copolymers, EGC2 hydrogel at 10% (w/v), and the precursors of EGC copolymers. a) data collected from reheating run; b) data collected from cooling process. ....	119
Figure 4.4. EGC hydrogel preparation and its various forms. a) Illustration of the hydrogel preparation by using sample EGC2 at 10% (w/v); b) Hydrogel injected out from the syringe needle. The red arrow indicates the byssoid hydrogel that was flowing out. The gel was loaded with dextran-FITC for better visibility; c) Hydrogel modeled in different shapes; d) SEM micrograph of the freeze-dried of EGC2-10% hydrogel. ....	120
Figure 4.5. SEM micrographs of the EGC hydrogels (Scale bar: 50 $\mu\text{m}$ ). ....	121
Figure 4.6. (A) Oscillatory stress sweep measurement of EGC2-10% hydrogel at 25 $^\circ\text{C}$ and constant angular frequency $\omega = 1$ rad/s. (B) Oscillatory time sweep measurement of EGC2-10% hydrogel at 25 $^\circ\text{C}$ and constant $\sigma = 5$ Pa after 30 seconds deformation using shear stress at the crossover point of $G'$ and $G''$ (1620 Pa). The recovery time $t_R$ is the time required for 100% recovery of elastic modulus to its original value before the deformation. ....	122
Figure 4.7. Oscillatory frequency sweep measurement of EGC2 hydrogel at 10% (w/v) at 25 $^\circ\text{C}$ . ....	123
Figure 4.8. Mass loss (%) of the EGC based hydrogels after incubation in PBS at pH 7.4 and 37 $^\circ\text{C}$ . ....	125
Figure 4.9. GPC profiles of samples (A) EGC1-10% hydrogel and (B) EGC2-10% hydrogel degradation products in chloroform extracts from the PBS buffer at various hydrolysis periods. ....	126
Figure 4.10. FTIR spectra of EGC1-10% hydrogel after different degradation periods. (a) original EGC1 copolymer, (b) Gel residue after 30 days of degradation, (c) Water soluble fractions after 30 days of degradation, and (d) Water soluble fractions after 90 days of degradation. ....	127
Figure 4.11. $^1\text{H}$ NMR spectra of EGC1-10% (w/v) hydrogel degradation products in (A) chloroform extracts and (B) in water extracts after 90 days. ....	128

## List of Figures

- Figure 4.12. L929 cell viability in the presence of hyperbranched EGC block copolymers at different concentrations. .... 129
- Figure 4.13. Viability of cells encapsulated in hydrogels. a) Micrograph of L929 cells entrapped in the upper surface of EGC2-10% (w/v) hydrogel; b) Confocal micrograph showing the spatial distribution of cells within the hydrogel; c-h) Showing the live-dead assay of the cells in EGC2-10% hydrogel and F127-20%, respectively. Healthy cells emit red fluorescence while injured/dead cells emit weak red/green fluorescence. All pictures were taken after three days encapsulation in hydrogels. .... 130
- Figure 4.14. Micrographs of recovered L929 cells cultured at different periods of incubation in tissue culture dishes. (a) trypsin-detached cells; (b) cells recovered from EGC2-10% hydrogel; (c) cells recovered from F127-20% hydrogel. .... 132
- Figure 4.15. Cell viability plot of the recovered L929 cells from hydrogels cultured for 5 days. EGC2-10% and F127-20% hydrogels were used in the study. Cells activity obtained from the freshly trypsin detached cells was used as control. .... 133
- Figure 5.1.  $^1\text{H}$  NMR spectra of pure  $\alpha$ -CD (A), PPR2 (B) in DMSO- $d_6$ , and D-PR-D-1 (C), FA-PEG-(D-PR-D-1) (D) in DMF- $d_7$ . .... 148
- Figure 5.2.  $^{13}\text{C}$  NMR spectra of D-PR-D-1 (A) and FA-PEG-(D-PR-D-1) (B) in DMF- $d_7$ . .... 149
- Figure 5.3. GPC traces of D-PR-D-2 triblock copolymer and the conjugated FA-PEG-(D-PR-D-2) polymer measured with light scattering and differential refractometer as detectors. DMF containing 0.1 M LiBr was used as eluent at 40 °C. .... 150
- Figure 5.4. CMC determination of D-PR-D-1 (A) by extrapolation of the difference in absorbance at 378 and 400 nm by using DPH as probe. CMC of FA-PEG-(D-PR-D-1) (B) is not determined in the measured concentration range. .... 151
- Figure 5.5. UV absorbance of folic acid PBS solutions (A) and the standard curve based folic acid content determination of FA-PEG-(D-PR-D) supramolecules (B). Light absorption of FA-PEG-(D-PR-D) solution was measured from 200 to 400 nm by UV-Vis spectrometer. .... 153
- Figure 5.6. Wide-angle X-ray diffraction patterns of  $\alpha$ -CD (A), PCL-diBr (B), dried PCL/ $\alpha$ -CD PPR2 (C), PCL/ $\alpha$ -CD PPR2 slurry in DMF (D), D-PR-D-1 (E) and FA-PEG-(D-PR-D-1) (F). The characteristic X-ray diffraction peaks of crystalline columnar  $\alpha$ -CD at  $2\theta = 19.8^\circ$  and  $22.6^\circ$  are labelled with \* and •, respectively. PEG peaks at around  $2\theta = 19.3^\circ$  and  $23.5^\circ$  are labelled with ○. .... 154
- Figure 5.7. Agarose gel electrophoresis retardation assays for D-PR-D-1/pDNA (A), FA-PEG-(D-PR-D-1)/pDNA (B), D-PR-D-2/pDNA (C), FA-PEG-(D-PR-D-2)/pDNA (D) and PEI/pDNA (E). Lane 1 (most left) is the pDNA control and Lanes 2 → 8 correspond to the polymer/pDNA polyplexes in different N/P ratios. .... 155
- Figure 5.8. Particle size (A) and zeta potential (B) of polyplexes formed by D-PR-D triblock copolymers and their conjugated supramolecules at different transfection N/P ratios. .... 156
- Figure 5.9. Particle size distribution and transmission electron micrographs of FA-PEG-(D-PR-D-2)/pDNA polyplexes at N/P of 4 (A) and 15 (B), respectively. .... 158
- Figure 5.10. Cytotoxicity of D-PR-D triblock copolymers and their conjugated supramolecules in comparison with PEI (25 kDa, branched) in KB cells (A) and A549 cells (B). .... 160

## List of Figures

---

Figure 5.11. *In vitro* gene transfection efficiency of D-PR-D/pDNA, PEG-(D-PR-D)/pDNA and FA-PEG-(D-PR-D)/pDNA polyplexes at various N/P ratios in serum supplemented folic acid-free RPMI-1640 medium at KB (A) and A549 (B) cell lines, in comparison with PEI (25 kDa, branched). Data represent mean  $\pm$  SD (n = 3, Student's *t*-test, \**P* < 0.05 as compared with the data of PEG-(D-PR-D)). ..... 161

Figure 5.12. Transfection efficiency of FA-PEG-(D-PR-D)/pDNA polyplexes in KB (A) and A549 (B) cell lines in the presence or absence of free folic acid at various N/P ratios. Data represent mean  $\pm$  SD (n = 3, Student's *t*-test, \**P* < 0.05 as compared with the data of FA-PEG-(D-PR-D)/free FA). ..... 163



## **LIST OF ABBREVIATIONS**

ATRP	Atom Transfer Radical Polymerization
CD	Cyclodextrin
CDI	1,1'-Carbonyldiimidazole
CGC	Critical Gelation Concentration
CMC	Critical Micelle Concentration
DCC	1,3- <i>N,N'</i> -Dicyclohexylcarbodiimide
DMAEMA	2-(Dimethylamino) Ethyl Methacrylate
DMEM	Dulbecco's Modified Eagle's Medium
DMF	Dimethylformamide
DMSO	Dimethyl Sulfoxide
DNA	Deoxyribonucleic Acid
DP	Degree of Polymerization
DSC	Differential Scanning Calorimetry
EA	Elemental Analyses
Et <sub>2</sub> O	Diethyl Ether
FA	Folic Acid
FR	Folate Receptor
FBS	Fetal Bovine Serum
FTIR	Fourier Transform Infrared Spectroscopy
GPC	Gel Permeation Chromatography

## List of Abbreviations

---

GPC/LS	Gel Permeation Chromatography/Light Scattering
HMDI	1,6-Hexamethylene Diisocyanate
HMTETA	1,1,4,7,10,10-hexamethyltriethylenetetramine
IC	Inclusion Complex
LCST	Lower Critical Solution Temperature
$M_n$	Number-averaged Molecular Weight
$M_w$	Weight-averaged Molecular Weight
MPEG	Methoxy Poly(ethylene glycol)
MTT	3-(4,5-Dimethylthiazol-2-yl)-2,5-diphenyl Tetrazolium Bromide
MTS	3-(4,5-dimethylthiazol-2-yl)-5-(3-carboxymethoxyphenyl)- 2-(4-sulfophenyl)-2H-tetrazolium
MWCO	Molecular Weight Cut Off
NMP	Nitroxide-mediated Polymerization
NMR	Nuclear Magnetic Resonance
PBS	Phosphate Buffered Saline
PCL	Poly( $\epsilon$ -caprolactone)
PDI	Polydispersity Index
PEG	Poly(ethylene glycol)
PEI	Poly(ethylene imine)
PEO	Poly(ethylene oxide)
PGA	Poly(glycolide)
PHA	Poly(hydroxyalkanoate)
PHB	Poly(hydroxybutyrate)
PLA	Poly(lactide)
PLGA	Poly(lactide- <i>co</i> -glycolide)
PPO	Poly(propylene oxide)
PPOMA	Poly(propylene oxide) Methacrylate
PPR	Polypseudorotaxane
PTMC	poly(trimethylene carbonate)
RAFT	Reversible Addition Fragmentation Chain Transfer

## List of Abbreviations

---

ROP	Ring-opening Polymerization
PR	Polyrotaxane
PTA	Phosphotungstic Acid
SEM	Scanning Electron Microscopy
TEM	Transmission Electron Microscopy
TEMPO	2,2,6,6-Tetramethyl-1-piperidinyloxy
TGA	Thermogravimetric Analysis
THF	Tetrahydrofuran
XRD	Wide Angle X-ray Diffraction
UV-Vis	Ultraviolet-Visible

## **LIST OF PUBLICATIONS**

1. **Z.B. Li**, J Li\*, “Control of Hyperbranched Structure of Polyurethane PCL/PEG Block Copolymers by Glycerol and Their Hydrogels for Potential Cell Delivery Application.” *The Journal of Physical Chemistry B*, **2013**, 117, 14763.
  
2. **Z.B. Li**, H. Yin, K.L. Liu, Z.X. Zhang, J Li\*, “Supramolecular Anchoring of DNA Polyplexes in Cyclodextrin-Based Polypseudorotaxane Hydrogel for Sustained Gene Delivery”. *Biomacromolecules*, **2012**, 13, 3162.
  
3. **Z.B. Li**, Z.X. Zhang, K.L. Liu, X.P. Ni, J Li\*, “Biodegradable Hyperbranched Amphiphilic Multiblock Polyurethane Copolymers Consisting of Poly(propylene glycol), Poly(ethylene glycol), and Polycaprolactone as in situ Thermogels”. *Biomacromolecules*, **2012**, 13, 3977.
  
4. **Z.B. Li**, Y. Yin, K.L. Liu, J Li\*, “Supramolecular Nanocarriers Consisting of Biodegradable Polyrotaxane for Specific Targeting in Gene Delivery”. To be submitted
  
5. **Z.B. Li**, J.L. Zhu, J Li\*, “Biodegradable Hairy Block Copolymers: Synthesis and Characterization, Thermal-Sensitive Nano-aggregates and Surface Coating for Facile Cell Recovery”. To be submitted

# CHAPTER 1 INTRODUCTION

This thesis contributes to some designed biodegradable block copolymers with promising applications in biomedical engineering. In this chapter, the research background is presented, followed by the objectives and scope of the study. Finally, a summary of the contents and the structure of this thesis are given in the end.

## 1.1 Research Background

Polymeric materials used in biomedical applications can date back 40 - 50 years, often in the situations of tissue replacement, tissue augmentation, tissue support and drug delivery carriers.<sup>1-3</sup> These materials are categorized into three main groups based on their behavior when intimately contact with living tissues: biostable, biodegradable and partially biodegradable polymers.<sup>4</sup> Since the last two decades of the twentieth century, we have witnessed a fast shift from biostable polymer to biodegradable polymers for biomedical and related applications.<sup>5,6</sup> The major reason for considering biodegradable over biostable polymers for biomedical applications lies in its adequate biocompatibility and biodegradability. This implies that in the future couple of years biodegradable polymer based devices with tolerable degradation rate will replace many of the permanent ones when implanted for short-term therapeutic applications.<sup>7,8</sup>

Biodegradable polymers are generally classified into natural biopolymers and synthetic polymers. As to the synthetic biodegradable polymers, aliphatic polyesters are the most extensively studied because of their immense diversity and synthetic versatility.<sup>9</sup> Almost the only high molecular weight compounds shown to be biodegradable are the aliphatic

polyesters.<sup>10</sup> The reasons are ascribed to the extremely hydrolysable ester linkages in the polymer backbone and the good fitness to the enzyme's active site by the flexible aliphatic polyester chains.<sup>11</sup> Aliphatic polyesters can be chemically synthesized by versatile synthetic techniques, including polycondensation of combinations of diols and dicarboxylic acids, self-polycondensation of hydroxyl acids and ring-opening polymerizations of lactones and lactides.<sup>12</sup> These effective techniques have diversified a new array of aliphatic polyesters, such as poly(glycolic acid) (PGA), poly(lactic acid) (PLA) and its copolymer poly(lactide-*co*-glycolide) (PLGA), poly(3-hydroxybutyrate) (PHB), polycaprolactone (PCL), poly(butylenes succinate) (PBS), poly(p-dioxanone) (PPDO) and poly(trimethylene carbonate) (PTMC) etc.<sup>13</sup> The successful performance of the first synthetic aliphatic polyesters that have been routinely employed with humans are PLA and PGA based co-/polymers for suture system in 1960s, in which the two constitutional elements would eventually lead to degradation products that are natural metabolites.<sup>4</sup> Aliphatic polyesters as biodegradable biomaterials are attracting increasing attention since then due to their good biocompatibility and controllable degradation profiles. Biodegradable polymers can degrade into harmless components after use, which promise to make unnecessary operations to remove the implanted structures. As the intended use of these biodegradable polymers is to be inserted in a living organism, the general demands of their degradation products have to be biocompatible, non-toxic and metabolized or eliminated by the living organism.<sup>14</sup>

Aliphatic polyesters traditionally are developed into rigid materials or fiber for applications in fracture fixation devices, interference screws or suture anchors.<sup>15, 16</sup> Advanced biomedical systems involved recently are for tissue engineering and delivery applications, capitalizing on their biodegradability and biocompatibility to create temporary scaffolds required for cell growth and particles in various sizes for controlled drug delivery.<sup>17-24</sup> Due to the complexity and diversity of the *in vivo* environment, finding a universal polymer that could be considered as an ideal polymeric biomaterial in living organisms remains a dream. Diverse specific properties such as a controlled biodegradability, desirable mechanical properties, suitable hydrophilic/hydrophobic balance and proper biological functionality are demanded to further expand the needs for more particular biomedical applications of this type of polyesters.<sup>9</sup> However, such polyesters are typically semi-crystalline, hydrophobic solid lacking in functionality. A strategy to overcome these shortcomings is fabrication of the aliphatic polyesters into block copolymers, which has been found as promising method to manipulate their amphiphilic behavior, mechanical and physical properties by adjusting the ratio of the constituting blocks or adding new blocks of the desired properties.<sup>25</sup> This technique has diversified a large number of novel and smart biomaterials. For example, amphiphilic block copolymers are prepared by combining a hydrophilic segment with the aliphatic polyester blocks.

The as-synthesized amphiphilic block copolymers can self-assemble into intriguing aggregates of varying shapes and sizes such as micelles, vesicles, liposomes and hydrogels.<sup>26-32</sup> Such that strategic tailoring of aliphatic polyesters in structure and functionality leads the desired products with superior properties and carries the potential to expand their application base to a wide variety of particular applications including target drug delivery, sustained gene delivery, injectables and three dimensional cell encapsulation in tissue engineering.<sup>29, 30, 32-39</sup>

The new functional segments selected to form block copolymers with aliphatic polyester are desired to match specific application. The biocompatibility is also a crucial consideration in designing the block copolymer structure. By modifying the backbone of the polymers, some of the characteristics can be changed to a significant extent in terms of degradation properties, mechanical properties and even biocompatibility.<sup>40</sup> In general, poly(ethylene glycol) (PEG), poly(propylene glycol) (PPG), poly(N-isopropylacrylamide) (PNIPAAm), amino acid, acrylic acid (AA) and hydroxyethyl methacrylate (HEMA) in certain molecular weight range are popular candidates in developing block copolymer based biomedical systems for drug delivery and tissue engineering applications.<sup>14, 30, 41-44</sup> On the other hand, polyethylenimine (PEI), poly-L-lysine (PLL), poly(N,N-diethylamino) ethyl methacrylate (DMAEMA), poly(N,N-diethylamino) ethyl methacrylate (DEAEM) and poly(N-3-dimethylamino) propyl methacrylamide (PDAPM) containing cationic portions in the molecular chains have been widely reported to form block copolymers at various molecular weight with aliphatic polyesters as effective gene delivery carriers.<sup>45-48</sup>

Several well developed methodologies leading to various architectures of well-defined block copolymers, such as linear, brush-type and branched architecture, have been reported.<sup>25, 49-51</sup> Block copolymers consisting of aliphatic polyesters have been synthesized extensively by direct coupling of well-defined homopolymers, living/controlled radical polymerization, cationic or anionic polymerization, ring opening polymerization and various combinations of the methods mentioned above.<sup>52</sup> On top of that, more complex functional supramolecular architectures through molecular recognition with other molecular entities are also promising technique to tailor block copolymers in structure-property and impart potential functionality.<sup>53-56</sup> For example, the dynamic equilibrium of block copolymers with cyclodextrins (CDs) can be used for morphologies transition and particle size control vehicle, which sheds new light of the biodegradable block copolymers in biomedical applications.<sup>31, 57-59</sup>

PCL is one of the most extensively studied aliphatic polyester in biomedical applications.<sup>60</sup> Its degradation products are less acidic as compared to other types of aliphatic polyesters, such as polylactide (PLA) and polyglycolide (PGA). PCL is used in Capronor which

has been commercialized as a commercially available 1-year implantable contraceptive device. The toxicology of PCL has been thoroughly studied and PCL has been generally regarded to be safe. Nevertheless, PCL is typically highly crystalline and hydrophobic, lacking of functionality. Therefore, strategic tailoring of the structure and functionality of PCL could expand its application considerably. Because of the presence of reactive groups, derivatives of PCL have been widely reported for block copolymer development in the most situations of drug delivery and tissue engineering applications.<sup>39, 61-64</sup> However, very little research has been done on the design of PCL-based block copolymers with specific and unique requirement for thermally induced cell detachment and suitable cell delivery carriers in tissue engineering. Furthermore, the exploitation of the host-guest interaction between CDs and the newly developed PCL block copolymers with the applications in site-specific gene delivery is still at its fancy state.

### 1.2 Objective and Scope of Study

The aim of this study was to design of PCL-based block copolymers with different functional components and well-defined macromolecular architectures to match the specific requirements of each individual biomedical application. The CDs involved supramolecular self-assembly and biological activity modifications of the developed block copolymers were explored. The specific objectives of this research are to:

- To construct brush-type block copolymers consisting of biodegradable PCL and thermal-responsive poly(propylene oxide) methacrylate (PPOMA) segments, and investigate the block copolymer coated surface as potential cell detachment substrates
- To control PCL/PEG based polyurethane block copolymers in hyperbranched structure and demonstrate their mechano-responsive hydrogels for potential three dimensional cell encapsulation and cell delivery
- To design new triblock copolymers comprising PCL/ $\alpha$ -CD as the biodegradable central block flanked by PDMAEMA segments, and further modify the supramolecular nanocarriers as a specific targeting gene vector by conjugation reaction

This research should have significant impact on understanding structure-property relationship of the newly developed PCL block copolymers in various architectures. Moreover,



this study could be helpful in clarifying block copolymer design considerations for specific biomedical applications, and the utilization of inclusion complexes as building blocks creates a new approach for designing site-specific delivery system.

This thesis mainly focuses on the design and synthesis of new block copolymers containing PCL and other functional groups. The possibility of using these materials as functional biomaterials was tested through *in vitro* experiments. The *in vivo* experiments are beyond the scope of this thesis.

### 1.3 Organization of the Thesis

Encompassing the objectives outlined previously, this thesis is organized into the following chapters:

Chapter 2: Literature review on the topic of biodegradable polymers as biomaterials, synthetic strategies of block copolymers and their architecture types, followed by a recent report on host-guest interaction between biodegradable block copolymers and cyclodextrins. Accounts on the biomedical applications of these biodegradable block copolymers will be mentioned in the end.

Chapter 3: Report on the synthesis of P(PPOMA)-PCL-P(PPOMA) brush-type triblock copolymers and the thermally responsive nano-aggregates in aqueous solutions. The triblock copolymers coated surfaces were assessed as potential cell detachment substrates as induced by temperature.

Chapter 4: Demonstration on the application of cell delivery through 3D cell encapsulation within mechano-responsive hydrogels developed from hyperbranched PCL/PEG based block copolymers. The rheological properties, biodegradation and the use of the hydrogels as a cell delivery carrier were characterized.

Chapter 5: Highlight on the synthesis of novel biodegradable polyrotaxane centered block copolymers and exploration of using  $\alpha$ -CD to introduce functional groups for the targeting group conjugation. Gene transfection experiments performed in different cell types were designed to examine the site-specific targeting effect.

Chapter 6: Conclusions on the work done and possible future directions.

### 1.4 References

1. D. J. Lyman and W. J. Seare, *Annu. Rev. Mater. Sci.*, 1974, **4**, 415-433.
2. D. F. Gibbons, *Annu. Rev. Biophys. Bioeng.*, 1975, **4**, 367-375.
3. T. Barrows, *Clin. Mater.*, 1986, **1**, 233-257.
4. S. Vainionpää, P. Rokkanen and P. Törmälä, *Prog. Polym. Sci.*, 1989, **14**, 679-716.
5. B. Karen and S. Shalaby, in *Absorbable and Biodegradable Polymers*, CRC Press, 2003.
6. E. Piskin, *J. Biomater. Sci. Polym. Ed.*, 1995, **6**, 775-795.
7. L. S. Nair and C. T. Laurencin, *Prog. Polym. Sci.*, 2007, **32**, 762-798.
8. D. F. Williams, *JMatS*, 1982, **17**, 1233-1246.
9. A.-C. Albertsson and I. Varma, in *Degradable Aliphatic Polyesters*, 2002, pp. 1-40.
10. R. Chandra and R. Rustgi, *Prog. Polym. Sci.*, 1998, **23**, 1273-1335.
11. Y. Tokiwa and T. Suzuki, *J. Appl. Polym. Sci.*, 1981, **26**, 441-448.
12. M. Okada, *Prog. Polym. Sci.*, 2002, **27**, 87-133.
13. I. Vroman and L. Tighzert, *Materials*, 2009, **2**, 307-344.
14. A. Marcos-Fernandez, G. A. Abraham, J. L. Valentin and J. San Roman, *Polymer*, 2006, **47**, 785-798.
15. D. Mark and P. Suzie, in *Polymeric Gene Delivery*, CRC Press, 2004.
16. R. S. Bezwada, D. D. Jamiolkowski, I.-Y. Lee, V. Agarwal, J. Persivale, S. Trenka-Benthin, M. Erneta, J. Suryadevara, A. Yang and S. Liu, *Biomaterials*, 1995, **16**, 1141-1148.
17. D. J. Mooney, D. F. Baldwin, N. P. Suh, L. P. Vacanti and R. Langer, *Biomaterials*, 1996, **17**, 1417-1422.
18. D. W. Hutmacher, T. Schantz, I. Zein, K. W. Ng, S. H. Teoh and K. C. Tan, *J. Biomed. Mater. Res.*, 2001, **55**, 203-216.
19. Q. Wu, Y. Wang and G. Q. Chen, *Artif. Cells, Blood Substitues, Immobilization Biotechnol.*, 2009, **37**, 1-12.
20. C. Shih-Jiuan and L. Robert, in *Polymeric Gene Delivery*, CRC Press, 2004.
21. M. Randall, in *Polymeric Gene Delivery*, CRC Press, 2004.
22. G. G. Pitt, M. M. Gratzl, G. L. Kimmel, J. Surles and A. Sohindler, *Biomaterials*, 1981, **2**, 215-220.
23. D. Fischer, Y. Li, B. Ahlemeyer, J. Krieglstein and T. Kissel, *Biomaterials*, 2003, **24**,

- 1121-1131.
24. S. Motala-Timol and D. Jhurry, *Eur. Polym. J.*, 2007, **43**, 3042-3049.
  25. N. Kumar, M. N. V. Ravikumar and A. J. Domb, *Adv. Drug Delivery Rev.*, 2001, **53**, 23-44.
  26. J. Li, X. P. Ni, X. Li, N. K. Tan, C. T. Lim, S. Ramakrishna and K. W. Leong, *Langmuir*, 2005, **21**, 8681-8685.
  27. Y. Y. Li, X. Z. Zhang, H. Cheng, J. L. Zhu, U. N. Li, S. X. Cheng and R. X. Zhuo, *Nanotechnology*, 2007, **18**, 1-8.
  28. C. Gong, S. Shi, P. Dong, B. Kan, M. Gou, X. Wang, X. Li, F. Luo, X. Zhao, Y. Wei and Z. Qian, *Int. J. Pharm.*, 2009, **365**, 89-99.
  29. B. Jeong, S. W. Kim and Y. H. Bae, *Adv. Drug Delivery Rev.*, 2002, **54**, 37-51.
  30. B. Jeong, Y. H. Bae, D. S. Lee and S. W. Kim, *Nature*, 1997, **388**, 860-862.
  31. J.-L. Zhu, K. L. Liu, Z. Zhang, X.-Z. Zhang and J. Li, *Chem. Commun.*, 2011, **47**, 12849-12851.
  32. A. Napoli, D. Sebok, A. Senti and W. Meier, in *Block Copolymers in Nanoscience*, ed. P. G. L. Prof Massimo Lazzari, Prof Sebastien Lecommandoux, 2008, pp. 39-71.
  33. D.-Q. Wu, T. Wang, B. Lu, X.-D. Xu, S.-X. Cheng, X.-J. Jiang, X.-Z. Zhang and R.-X. Zhuo, *Langmuir*, 2008, **24**, 10306-10312.
  34. D.-Q. Wu, Y.-X. Sun, X.-D. Xu, S.-X. Cheng, X.-Z. Zhang and R.-X. Zhuo, *Biomacromolecules*, 2008, **9**, 1155-1162.
  35. D.-Q. Wu, F. Qiu, T. Wang, X.-J. Jiang, X.-Z. Zhang and R.-X. Zhuo, *Bioconjugate Chem.*, 2009, **1**, 319-327.
  36. S. H. Park, B. G. Choi, M. K. Joo, D. K. Han, Y. S. Sohn and B. Jeong, *Macromolecules*, 2008, **41**, 6486-6492.
  37. S. J. Bae, M. K. Joo, Y. Jeong, S. W. Kim, W.-K. Lee, Y. S. Sohn and B. Jeong, *Macromolecules*, 2006, **39**, 4873-4879.
  38. A. Agarwal and S. K. Mallapragada, *Curr. Top. Med. Chem.*, 2008, **8**, 311-330.
  39. G. Gaucher, M.-H. Dufresne, V. P. Sant, N. Kang, D. Maysinger and J.-C. Leroux, *J. Controlled Release*, 2005, **109**, 169-188.
  40. M. Martina and D. W. Hutmacher, *Polym. Int.*, 2007, **56**, 145-157.
  41. X. J. Loh, K. B. C. Sng and J. Li, *Biomaterials*, 2008, **29**, 3185-3194.
  42. X. J. Loh, Z.-X. Zhang, Y.-L. Wu, T. S. Lee and J. Li, *Macromolecules*, 2009, **42**, 194-202.
  43. X. Tong, X. Zhang, L. Ye, A.-y. Zhang and Z.-g. Feng, *Soft Matter*, 2009, **5**, 1848-1855.

44. C. B. Liu, C. Y. Gong, Y. F. Pan, Y. D. Zhang, J. W. Wang, M. J. Huang, Y. S. Wang, K. Wang, M. L. Gou, M. J. Tu, Y. Q. Wei and Z. Y. Qian, *Colloids Surf. Physicochem. Eng. Aspects*, 2007, **302**, 430-438.
45. J. L. Zhu, H. Cheng, Y. Jin, S. X. Cheng, X. Z. Zhang and R. X. Zhuo, *J. Mater. Chem.*, 2008, **18**, 4433-4441.
46. S. Ribeiro, N. Hussain and A. T. Florence, *Int. J. Pharm.*, 2005, **298**, 354-360.
47. V. San Miguel, A. J. Limer, D. M. Haddleton, F. Catalina and C. Peinado, *Eur. Polym. J.*, 2008, **44**, 3853-3863.
48. M. D. Determan, J. P. Cox, S. Seifert, P. Thiyagarajan and S. K. Mallapragada, *Polymer*, 2005, **46**, 6933-6946.
49. J. K. Oh, *Soft Matter*, 2011, **7**, 5096-5108.
50. J. P. Jain and N. Kumar, *Biomacromolecules*, 2010, **11**, 1027-1035.
51. J. Z. Du, L. Y. Tang, W. J. Song, Y. Shi and J. Wang, *Biomacromolecules*, 2009, **10**, 2169-2174.
52. D. Taton and Y. Gnanou, in *Block Copolymers in Nanoscience*, ed. P. D. G. L. P. D. S. L. Prof. Dr. Massimo Lazzari, 2008, pp. 9-38.
53. A. Harada, J. Li and M. Kamachi, *Nature*, 1992, **356**, 325-327.
54. H. A. Klok and S. Lecommandoux, *Adv. Mater.*, 2001, **13**, 1217-1229.
55. H. X. X. Z. Yapei Wang, *Adv. Mater.*, 2009, **9999**, NA.
56. J. Li, C. Yang, H. Z. Li, X. Wang, S. H. Goh, J. L. Ding, D. Y. Wang and K. W. Leong, *Adv. Mater.*, 2006, **18**, 2969-2974.
57. H. S. Choi, T. Ooya, S. Sasaki, N. Yui, Y. Ohya, T. Nakai and T. Ouchi, *Macromolecules*, 2003, **36**, 9313-9318.
58. A. Harada and K. Kataoka, *Prog. Polym. Sci.*, 2006, **31**, 949-982.
59. J. Li and X. J. Loh, *Adv. Drug Delivery Rev.*, 2008, **60**, 1000-1017.
60. B. S. Kaith, H. Mittal, R. Jindal, M. Maiti and S. Kalia, in *Cellulose Fibers: Bio- and nano-polymer Composites*, eds. S. Kalia, B. S. Kaith and I. Kaur, Springer Berlin Heidelberg, 2011, pp. 425-451.
61. T. Kissel, Y. Li and F. Unger, *Adv. Drug Delivery Rev.*, 2002, **54**, 99-134.
62. C. Allen, D. Maysinger and A. Eisenberg, *Colloids Surf. B. Biointerfaces*, 1999, **16**, 3-27.
63. C. He, S. W. Kim and D. S. Lee, *J. Controlled Release*, 2008, **127**, 189-207.
64. H. Tian, Z. Tang, X. Zhuang, X. Chen and X. Jing, *Prog. Polym. Sci.*, 2012, **37**, 237-280.

## CHAPTER 2 LITERATURE REVIEW

### 2.1 Biodegradable Polymers as Biomaterials

As this thesis mainly focus on the design and synthesis of biodegradable block copolymers with specific properties as biomaterials, a brief review on biodegradable polymer main types and degradation behavior will be given first.

#### 2.1.1 Biodegradable Polymers

According to Albertsson and Karlsson's definition, biodegradation is defined as an event which takes place through the action of enzymes and/or chemical decomposition associated with living organisms (bacteria, fungi, yeasts and insect) or their secretion products.<sup>1</sup> However, it is also necessary to consider abiotic reactions involving chemical (oxidation and hydrolysis), physical (photo-degradation and thermal degradation), and environmental factors that may produce a synergistic effect to alter the polymer before, during or instead of biodegradation.<sup>2,3</sup> Therefore, strictly speaking, "biodegradation of a polymer" is defined as the deterioration of its physical and chemical properties and decrease of its molecular weight mass due to the conversion into CO<sub>2</sub>, H<sub>2</sub>O and CH<sub>4</sub> and other low molecular weight products under the influence of microorganisms in both aerobic and anaerobic conditions along with the abiotic chemical reactions.<sup>4-6</sup> Furthermore, all the residues and microbial mass eventually incorporated into the natural geochemical cycle should be nontoxic in the environmental assessments.<sup>3,7</sup> When applied biodegradable polymers as biomaterials, they enter into contact with a biological environment and the primary polymer hydrolyses and enzyme driven

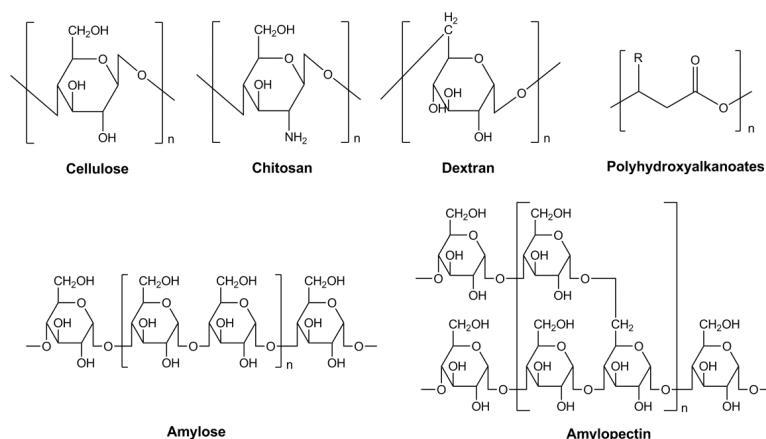
oxidations are responsible for the formation of fragments of lower molar mass in degradation processes.<sup>5, 8, 9</sup>

Currently biodegradable polymeric biomaterials can be broadly divided into two categories: natural and synthetic polymers.<sup>10</sup> Both of them have been extensively studied as biomaterials with several unique properties as well as deficiencies.

### *2.1.1.1 Natural polymers*

Natural polymers are formed in nature during the growth cycles of all organisms. They are generally produced within cells by complex metabolic process that involves in particular enzyme-catalyzed chain growth polymerization reactions of activated monomers.<sup>11</sup> As a class, natural polymers represent completely renewable resources due to their biodegradability and produced in nature.<sup>7</sup> They can be considered as the first biodegradable biomaterials. Application of natural polymers in medicine has long history than synthetic polymers. For example, collagen used as biomedical applications dates back thousands of years, but the utilization of biodegradable synthetic polymers started only in the late half of 1960s.<sup>12</sup> Even the biodegradation process of natural polymers is slow in contrast to the synthetic polymers, there is no concern at this point as they are produced in nature. Natural polymers possess remarkable advantages over synthetic ones when applied as biomaterials due to their inherent physiological activities, the ability to present selective cell adhesion driven by receptor-binding affinity, susceptibility to cell-triggered proteolytic degradation, similar mechanical properties to natural tissues and natural remodeling.<sup>13</sup> However, these inherent bioactivities of the natural polymers have their own deficiencies including risk of strong immunogenic response, unstable materials supply and the possibility of disease transmission.<sup>10</sup> Because of these, recent studies show a decreased demand of natural polymers. However, it still looks probable that some natural polymers will continue to play an important role as biomaterials and serve as specific biomedical devices, since they possess unique characteristics that synthetic polymers lack in some aspects.

The most widespread natural polymers are polysaccharides, such as cellulose, starch, dextrin, chitin, chitosan, hyaluronate, alginate and agarose.<sup>13-18</sup> Other important classes of natural polymers are polyesters such as polyhydroxyalkanoates (PHA), polypeptides such as collagen, gelatin, fibrin, albumin and silk fibroin.<sup>19-21</sup> Some of the representative structures of the nature polymers having high potential for biomedical applications are shown in Figure 2.1.



**Figure 2.1. Some representative structures of nature polymers.**

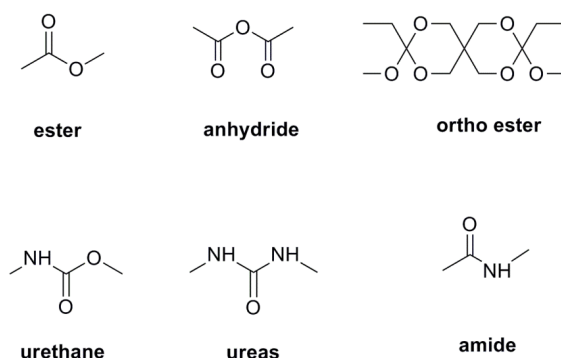
Natural polymers have been widely used in tissue engineering applications because these polymers are either components of or have similar macromolecular properties to the extracellular matrix (ECM). For example, collagens take 25% of the total protein mass of human body and they are the main proteins of the ECM.<sup>22</sup> Recently, polysaccharides have been applied in various delivery and targeting strategies either due to their ability to provide stabilization and form a skeleton on the appended sensory molecules. Alternatively, they can also behave as sensory devices to bring out the resultant targeted therapeutic effects.<sup>23</sup> Another category in natural polymers that has been extensively explored as biomaterials is PHAs properly because of their increasing production, adjustable physicochemical properties and excellent biocompatibility.<sup>19</sup> PHAs have similar properties to conventional plastics and completely biodegradable. They are intracellular biopolymers synthesized by many bacteria as intracellular carbon and energy storage granules. Microbial production of PHAs can produce the biodegradable polyesters with different side chain lengths of the repeating units and its various combination of block copolymer structure.<sup>24</sup> Bearing on these advantages, many properties of PHAs including mechanical properties, degradation rate and process ability are tunable to a suitable range, rendering the wide applications of PHAs family members as medical implant materials and drug delivery carriers.<sup>25, 26</sup>

### 2.1.1.2 Synthetic polymers

On the other hand, synthetic biodegradable polymers have become essential alternatives of natural polymers in various biomedical applications. There are several reasons for the tendency of using polymeric synthetic materials over natural ones in the future. First, as mentioned in 2.1.1.1 section, biologically derived biodegradable polymers may trigger strong

immunogenic response and disease transmission, possibly both situations that could be eliminated by using appropriate synthetic polymers. Another important reason lies in the fact that it is relatively difficult to modify the biologically derived biodegradable polymers by using chemical approaches and in most situations the bulk properties of the as-modified natural polymers may totally alter. However, with proper design, the synthetic polymers have more predictable properties and batch-to-batch uniformity, and they also have tailored property for specific applications, devoid of many of the disadvantages of natural polymers.<sup>27</sup>

Biodegradability of synthetic polymers can be commonly achieved by judicious addition of the chemical functional groups such as anhydride, ester, orthoester, urethane, urea and amide among others. For example polyester, polyurethane, polyurea, polyamide, polyanhydride, poly(amide-enamine), poly(ortho esters), poly(propylene fumarate), poly(akyl cyanoacrylates)s, synthetic poly(amino acids) and various combinations of the functional groups mentioned above have been widely studied as synthetic biodegradable polymers.<sup>9-11</sup> Some of the representative structures of the biodegradable functional groups are shown in Figure 2.2. Based on the type of the functional groups, synthetic biodegradable polymers are classified into three groups: (A) polyesters, (B) polymers containing both ester and other heteroatom-containing linkages in the main chains, and (C) polymers with heteroatom-containing linkages other than ester linkages in the main chains.<sup>28</sup>



**Figure 2.2. Representative structures of synthetic biodegradable groups.**

As to the synthetic biodegradable polymers, aliphatic polyesters comprise the earliest and most extensively investigation as biomaterials. For instance, poly(glycolic acid) (PGA) and poly(lactic acid) (PLA) and a range of their copolymers have historically researched as synthetic biomaterials in sutures, plates and fixtures for fracture fixation devices, scaffold for cell transplantation and other clinical applications.<sup>29</sup> Since the PGA and PLA based sutures were routinely employed for biodegradable materials in 1960s, a group family of aliphatic



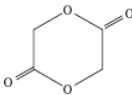
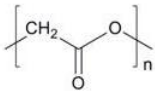
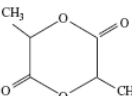
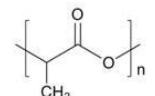
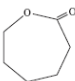
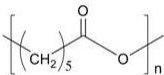
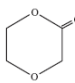
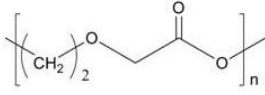
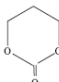
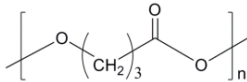
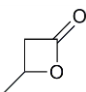
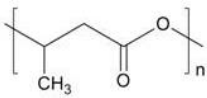
polyesters has been developed as biodegradable biomaterials.<sup>12, 30, 31</sup> The greatest advantage of aliphatic polyesters is their good biocompatibility and controllable degradation by simple hydrolysis in the aqueous environment such as body fluids. Almost the only high molecular weight compounds shown to be hydrolysable are aliphatic polyesters. This is due to the extremely hydrolysable backbone found in the polyesters. In addition, the polymer chains in the aliphatic polyesters can fit into the enzyme's active site, which makes them to be biodegradable by enzyme catalysts. This is one reason why flexible aliphatic polyesters are degradable and the rigid aromatic polyesters are not.<sup>32</sup> Furthermore, the degradation products are ultimately metabolized to carbon dioxide and water or are excreted through the kidney.<sup>11</sup> The most extensively studied biodegradable aliphatic polyesters are poly(glycolic acid) (PGA), poly(lactic acid) (PLA) and its copolymer poly(lactide-*co*-glycolide) (PLGA), polycaprolactone (PCL), poly(3-hydroxybutyrate) (PHB), poly(dioxanone) (PDO, PDX or PDXO) and poly(trimethylene carbonate) (PTMC).<sup>10-12, 28, 29, 33</sup>

Besides the immense diversity of aliphatic polyesters, another uniqueness of this type of biodegradable polymers is the synthetic versatility. Aliphatic polyesters can be developed from polycondensation of combinations of diols and dicarboxylic acids, self-polycondensation of hydroxyl acids and ring-opening polymerizations of lactones and lactides.<sup>30</sup> Synthesis of the aliphatic polyesters by polycondensation of diols with dicarboxylic acid traced back to Carothers' work in the 1930s.<sup>28</sup> However, high molecular weight polymers can only be achieved at very high conversions (> 98 - 99%) in condensation polymerization. Since the formation of the small byproducts, e.g. water, is involved during the polycondensation reactions, this is a task more difficult than the chain polymerization. Therefore, the development of biomaterials based on this approach has not been widely investigated.<sup>34</sup> A straightforward and more efficient route to synthesize aliphatic polyesters is ring-opening polymerization (ROP) of lactones and lactides.<sup>10</sup> The advantage of ROP compared with polycondensation is the effectiveness and flexibility in producing high molecular weight aliphatic homo- and copolyesters. A variety of monomers via ROP route have been reported in the successful synthesis of aliphatic polyesters.<sup>28</sup> The structures of cyclic lactones in corresponding to the most intensively studied aliphatic polyesters are tabulated in Table 2.1.

Aliphatic polyesters and its contained copolymers with tailored properties including features such as hydrophilicity, biodegradation rates and mechanical properties can be manipulated through the versatile synthesis approaches mentioned above. Specific properties are sometimes also achieved by introducing functional groups for further drug/targeting moiety

attachment. The biomedical applications of aliphatic polyesters and block copolymers will be reviewed in 2.4.

**Table 2.1. Chemical structure of cyclic esters in corresponding to the most intensively studied aliphatic polyesters.**

Cyclic esters	Polymer
 <p>Glycolide</p>	 <p>Poly(glycolide) PGA</p>
 <p>Lactide</p>	 <p>Poly(lactide) PLA</p>
 <p>Caprolactone</p>	 <p>Polycaprolactone PCL</p>
 <p>Dioxanone</p>	 <p>Poly(dioxanone) PDO</p>
 <p>Trimethyl carbonate</p>	 <p>Poly(trimethylene carbonate) PTMC</p>
 <p>Butyrolactone</p>	 <p>Poly(hydroxybutyrate) PHB</p>

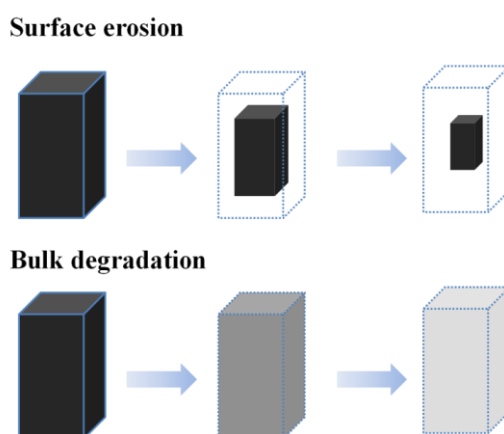
### 2.1.2 Biodegradation

In the context of biomedical applications, biodegradation may be defined as the gradual breakdown of a material mediated by a specific biological activity.<sup>35</sup> Degradation requirement in biomedicine is due to many reasons. The most important one means surgical intervention may not be required for removal at the end of its functional life, eliminating the need for a

second surgery.<sup>36</sup> In this way, biodegradation not only eliminates the risk of complications associated with the long-term presence of a foreign material but also allows for improved healing as viable tissue interacts and grows into the degrading construct.<sup>37</sup> In this section, the main mechanisms and the degradation products of biodegradable polymers used as biomedical devices will be reviewed. The factors that affected the degradation behavior and some degradation-monitoring techniques will be summarized at the end.

### 2.1.2.1 Biodegradation mechanisms

Bulk degradation (homogeneous) and surface erosion (heterogeneous) mechanisms are considered as the two general degradation mechanisms of the biodegradable polymers.<sup>38</sup> The two mechanisms and their difference are schematically illustrated in Figure 2.3.



**Figure 2.3. Schematic illustration of surface erosion and bulk degradation mechanisms of biodegradable polymers.**

During an application, degradation by surface erosion mechanism is featured by the weight loss from the materials surface only, resulting in predictable mass loss profiles. When the degradation process occurs under this mechanism, it is expected to deliver encapsulates at a constant rate and maintain the structural integrity and the mechanical properties. The materials get smaller but keep their original geometric shape. For example, poly(anhydrides) and poly(orthoesters) are the typical cases studied for surface-eroding polymeric materials.<sup>39, 40</sup> Bulk degradation, on the other hand, is characterized by hydrolysis of chemical bonds in the polymer chain at the center of the materials, which typically results in empty shell but

maintains the size for a consideration portion of time. This degradation behavior has been observed for PLA polymeric systems.<sup>41</sup>

Since many biodegradable polymers are intended to use in the biological environment, the subject of the degradation in such environments has become an important issue. As we know, the implantation environment is an isotonic saline solution containing a wide variety of extracellular active components and cells. The enzymes, which are proteins found both extra- and intracellularly within cells, play a crucial role in biodegradation.<sup>2, 10, 42</sup> In line with the biodegradation mechanisms, two principle types of reactions were regarded as the main means to lead the polymer degradation. They are categorized into (a) enzyme-mediated degradation and (b) hydrolysis degradation.<sup>35</sup>

### *(a) enzyme-mediated degradation*

Enzyme-mediated degradation of polymeric biomaterials may follow a surface erosion mechanism, in which the material is degraded gradually from the surface inwards. This is because the enzyme molecules are in big size and they cannot penetrate into the interior of the tightly packed structure of certain polymers.<sup>42</sup> According to the fundamental principles of catalysis, the enzyme provides a reaction path with a reduced energy of activation, specifically being able to bind and partially orient the reacting molecules with each other and with themselves in such a way as to maximize the occurrence of a productive reaction.<sup>35</sup> The binding and subsequent reaction takes place at a specific location, on the surface of an enzyme, called active site. Essentially most of the natural polymers are susceptible to undergo enzymatic degradation because the enzymatic polymerization reactions responsible for their synthesis in nature have closely related counterparts in nature for their enzymatic depolymerization: “what nature creates, nature can destroy”.<sup>43</sup> For the synthetic biodegradable polymers, in order to degrade by enzyme, the polymer chains must be flexible enough to fit into the active site of the enzyme. Flexible aliphatic polyesters can be degraded enzymatically, while more rigid aromatic polyesters are generally bioinert.<sup>32 10</sup>

Enzymatic oxidation and enzyme-catalyzed hydrolysis are the mostly considered reactions for enzyme-mediated degradation. It is well known that inflammatory cells, particularly leukocytes and macrophages, are able to produce highly reactive oxygen species such as superoxide ( $O_2^-$ ), hydrogen peroxide ( $H_2O_2$ ), nitric oxide (NO), and hypochlorous acid (HOCl) during the inflammatory response to foreign materials.<sup>44, 45</sup> The oxidation effect of these species may cause polymeric biomaterials chain scission and contribute to their degradation. Previous study showed that  $\cdot O_2^-$  could accelerate the degradation of aliphatic

polyesters by the cleavages of ester bonds via nucleophilic attack of  $\cdot\text{O}_2^-$ . These active anionic species subsequently could attack the main backbone chains via transesterification with a rapid reduction in molecular weight until thermodynamic equilibrium was reached. The resulting degradation products eventually lead to cyclic and/or linear oligomers.<sup>46</sup>

Another enzyme-driven reaction that has been widely investigated as a cause of degradation is hydrolysis. Hydrolysis reactions can take place with enzyme as catalysis which is known as hydrolases, including proteases, esterases, glycosidases and phosphatases among others. This class of enzymes functionalize as catalysis of several reactions in human body.<sup>47</sup> A commercial available surgical suture (Dexon) prepared from PGA is a good example to illustrate the enzyme activity toward the dramatic effect on degradation. Results showed those enzyme with esterase activity increased the rate of degradation.<sup>48</sup>

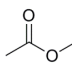
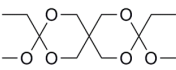
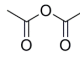
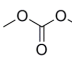
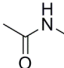
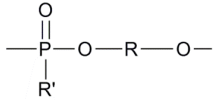
### *(b) Hydrolysis degradation*

The hydrolytic degradation and its based mechanism are currently the best understood and well-accepted in the biodegradation of biomedical polymeric materials. It is defined as the scission of chemical bonds in the polymer chains by the attack of water to form oligomers and finally monomers.<sup>35</sup> For hydrolytic decomposition, the polymer is unstable in water based environment. The prevailing mechanism under this approach occurs through the water penetration and erosion, attacking the chemical bonds in the amorphous phase and leading to a chain scission of long polymer chains into shorter water-soluble fragments. In respect to that, biodegradable polymers can be finally absorbed or extruded by the body leaving no trace.<sup>10</sup> Surprisingly, almost all the desirable biodegradable polymers are designed to break down by hydrolysis. The relatively shorter degradation period and ease of control in degradation period make them outstanding candidates for fabricating biomedical devices.

Regarding hydrolysis based biodegradation, water contacts with the water-labile bonds in the first step after implantation. This step may be achieved by either the direct access to the polymer surface or by penetration into the polymer matrix. Thereafter, the hydrolysis occurs on those water-labile bonds after the polymer absorbs water and swells. The second step accompanies by the progress of degradation of the implanted biomaterials.<sup>37</sup> Biodegradable polymers containing hydrolysable bonds are expected to experience a hydrolysis-mediated degradation. The functional groups susceptible to hydrolysis include esters, orthoesters, anhydrides, carbonates, amides, urethanes, ureas, etc.<sup>41</sup> Step polymerization and addition polymerization including ring-opening polymerization are the general routes that are used to

develop hydrolytically sensitive polymers for various biomedical applications.<sup>10</sup> Typical hydrolysis bonds in biodegradable polymers are presented in Table 2.2.

**Table 2.2. Typical hydrolysable bonds in biodegradable polymers**

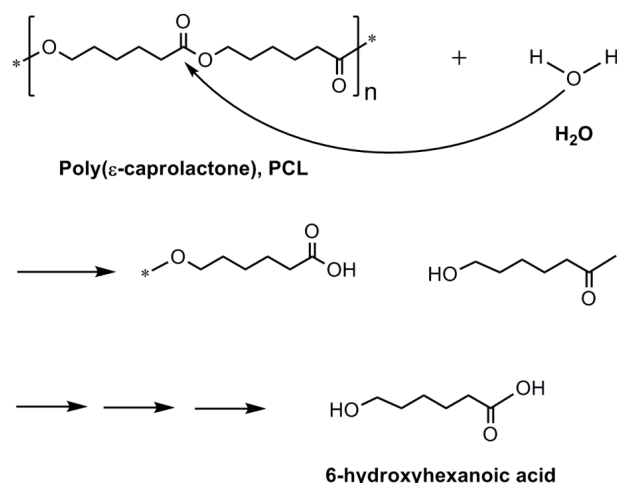
Polymer	bond
Polyester	
Polyorthoester	
Polyanhydride	
Polycarbonate	
Polyamino acid	
Polyphosphoesters	

### 2.1.2.2 Degradation products

Through the degradation mechanisms and approaches mentioned above, biodegradable natural polymers and synthetic polymers can degrade into various products corresponding to the components in each individual polymer. Naturally occurring polymers can actively experience enzymatic degradation, including proteins, poly(amino acid), poly(hydroxyalkanoates) (PHAs) and polysaccharides etc.<sup>43</sup> By lowering the activation energy they can induce an increase in reaction rates in an environment otherwise unfavorable for chemical reactions. The three dimensional structure of enzymes with folds and pocket creates certain regions on the surface with characteristic primary structures (i.e. specific amino acid sequences) which form an active site. At the active site the interaction between the enzyme and substrate takes place while others follow alternative chemical routes, leading to a chemical reaction, giving a particular product.<sup>10, 11</sup> For instance, collagen undergoes enzymatic degradation within the body to yield the corresponding amino acid.<sup>49</sup> Another example such as hyaluronic acid (HA) in polysaccharides groups, as natural occurring polymer, can also degrade

within the body by free radicals, such as nitric oxide found in the extracellular matrix, followed by endocytosis. It can alternatively undergo digestion by lysosomal enzymes to form mono and disaccharides, which will be further converted into ammonia, carbon dioxide and water via the Krebs cycles.<sup>50</sup>

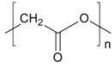
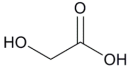
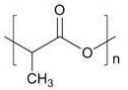
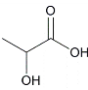
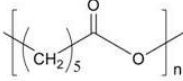
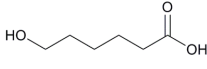
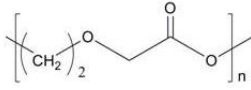
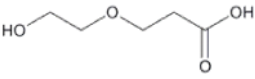
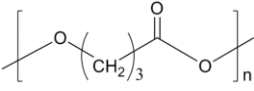

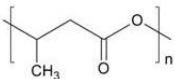
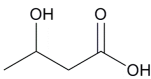
On the other hand, biodegradable synthetic polymers can degrade because of possessing the hydrolytically or enzymatically sensitive bonds. Their degradation results in a mixture of degradation products varying in chemical composition and molecular weight. For example, polyphosphoesters degrade under physiological conditions due to the hydrolytic and enzymatic cleavage of the phosphate bonds in the backbone. The ultimate breakdown products of the polymer are phosphate, alcohol and diols.<sup>51</sup> In our special interest of aliphatic polyesters, it is believed that chain scission occurs through simple hydrolysis, but kinetics of this hydrolysis are influenced by various factors (ions and enzymes etc).<sup>52</sup> The hydrolysis reaction is autocatalytic and the degradation products such as carboxylic acid participate in the transition state. Degradation occurs firstly within the amorphous parts because of the preferential water penetration but the crystalline regions also affect its degradation behavior.<sup>30, 53</sup> Among these aliphatic polyesters, PCL is known to be biocompatible and slowly hydrolytically and enzymatically degradable.<sup>54, 55</sup> The proposed degradation mechanism is hydrolysis of the polymer to oligomers and to 6-hydroxyhexanoic acid, an intermediate of  $\omega$ -oxidation. Biodegradation then proceeds through  $\beta$ -oxidation to acetyl-SCoA, which can undergo further degradation in citric acid cycle.<sup>56</sup> Polyester hydrolysis is schematically illustrated for PCL in Figure 2.4. Due to its good biodegradation and biocompatibility, sutures having PCL as a main component have been approved by FDA.



**Figure 2.4. Schematic hydrolytic degradation of PCL, an aliphatic polyester.**

Degradation products of the other intensively researched aliphatic polyesters are also reviewed in this section. PHA is a class of biopolyesters synthesized by microorganisms.<sup>57</sup> The degradation products of these biopolyesters are HA monomers, for example  $\beta$ -hydroxybutyric acid for poly(3-hydroxybutyrate) (PHB), which is one of the natural products that can be found in animal body.<sup>58, 59</sup>

**Table 2.3. Final degradation products of some typical aliphatic polyesters.**

Polymer	Degradation Products
 Poly(glycolide) PGA	 Glycolic acid
 Poly(lactide) PLA	 Lactic acid
 Polycaprolactone PCL	 6-hydroxyhexanoic acid
 Poly(dioxanone) PDO	 2-Hydroxyethoxypropanoic acid
 Poly(trimethylene carbonate) PTMC	 1,3-propanediol
 Poly(hydroxybutyrate) PHB	 Hydroxybutyric acid

Interestingly, PHAs polymerase is incapable of hydrolyzing the ester bonds in (S)-3HB units. This effect on (R)-3HB dimer is more obvious than higher oligomers, indicating the stereochemistry of PHB can influence the degradation product compositions.<sup>60</sup> Acetic acid and propanoic acid were formed as intermediate degradation products during the initial stages of PLA, PGA and its copolymer PLGA degradation, but they were no longer detected after prolonged aging.<sup>61-63</sup> Similarly, after hydrolytic degradation of PTMC and PDXO, the aliphatic



polyesters return to its ultimate building blocks, namely 1,3-propanediol and 2-hydroxyethoxypropanoic acid, respectively.<sup>64, 65</sup> The degradation products in corresponding to the most intensively investigated aliphatic polyesters are summarized in Table 2.3.

### 2.1.2.3 Factors affecting biodegradation and degradation-monitoring techniques

Various factors influence the degradation of polymers, which can be broadly classified into three main groups. They are: (i) the chemical and physical characteristics of polymer, (ii) the degradation conditions, and (iii) fabrication process.<sup>9</sup> Specifically, the rates of biodegradation of aliphatic polyesters are largely dependent on the types of chemical structure, molecular weight and distribution, morphology (e.g., crystallinity, size of spherulites, orientation), hydrophilicity, surface/volume ratio, as well as the environmental factors (e.g., enzyme, pH and temperature) in the degradation medium.<sup>30, 35</sup> A typical example on the comparison study between PCL and PGA based scaffolds can illustrate the effect of chemical structure on the biodegradation. PCL is much more hydrophobic than PGA due to the higher ratio of CH<sub>2</sub>/COO methylene/carboxylic groups, resulting a slower degradation rate.<sup>66</sup> Moreover, the crystallinity degree and the glass transition temperature ( $T_g$ ), termed as morphology, play an important role, because at 37 °C the polymer could behave as a glassy state, and the amorphous region in glassy state may be blocked by the semi-crystalline structure. Experimental *in vitro* and *in vivo* degradations showed that the crystalline polymers degrade slower than amorphous ones, e.g., PLLA and PDLA.<sup>60</sup> Other factors such as molecular weight, exposed surface area and shape geometry affect degradation rates as well.<sup>9, 30, 43</sup> Furthermore, depending on the type and intensity of ions in the degradation medium, various degradation phenomena can occur.<sup>35</sup> However, the thesis mainly focused on biomedical applications based on structure-property of the newly designed biomaterials, these environmental factors includes enzymes, pH and ions strength in the buffer solution are beyond the scope of the review in factors affecting biodegradation. Various techniques that have been developed to monitor the biodegradation progress are reviewed instead and presented in the following section.

Polymer degradation started from the gradual diffusion of water molecular into the polymer matrix at the early stages. This led to an increase of water uptake while the molecular weight, specimen weight loss and even mechanical strength were expected to be constant. At this stage, main changes took place on the outer surface of the polymer. However, these changes resulted in the eventual chemical changes because of hydrolysis. The hydrolytic cleavage of chemical bonds took place at the second stage, leading to a continuous decrease in

molecular weight, giving an increased weight loss and porosity of the polymer matrix. The mechanical properties also showed a marked decline.<sup>37</sup>

Based on the characteristic of degradation, the selection of characterization techniques should be made according to the degradation stage and the specific properties that are intended to investigate. During degradation, water uptake measurements can give some prediction of water absorption ability of the materials, and therefore indicate their tendency to be degraded by hydrolysis and make comparison at different hydrophobic/hydrophilic equilibrium. The changes in mass can be monitored by comparing the mass before and after degradation at specific time intervals, giving the extent of degradation by calculating the weight loss percentage. Molecular weight, on the other hand, is a crucial element needed to be well understood since it can affect many other properties such as mechanical properties, crystallinity behavior, weight loss and the morphology changes. The molecular weight change during the degradation can be easily determined by gel permeation chromatography (GPC). The molecular weight distribution, termed as polydispersity (PDI), can also be obtained by the GPC analysis to give the breadth of the molecular weight. The hydrolytic degradation results in surface chemistry change can be analyzed by several techniques including scanning electron microscopy (SEM), X-ray photo-electron spectroscopy (XPS) and Fourier transform infrared spectroscopy (FTIR). The formation of degradation products have been successfully characterized by high performance liquid chromatography (HPLC), mass spectroscopy (MS) and nuclear magnetic resonance (NMR).<sup>42, 58, 67-71</sup> Currently, the mechanical properties including testing tensile, bending, and compressive properties of biomaterials are commonly characterized by the standards described in the American Society for Testing and Materials (ASTM).<sup>37</sup>

### 2.2 Block Copolymers Based on Biodegradable Aliphatic Polyesters

In the synthetic biodegradable polymers, aliphatic polyesters comprise the earliest and most extensively investigated as biomaterials due to their biodegradability in a normal organism. They are members of a large group of polymers that can both be made from both natural origins for example PHAs and a variety of chemical reactions.<sup>29-31</sup> However, to be of practical interest, many other requirements, despite of the biodegradability, have to be fulfilled. This is highly dependent on the specific application at the targeted living conditions. For example, pure aliphatic polyesters cannot provide solutions because of lacking hydrophilicity

and their life-respecting applications as polymeric injectables (*e.g.* micelles and hydrogels) would thus be restricted. The most attractive strategy to modulate the range of accessible properties of aliphatic polyesters is to prepare biodegradable block copolymers. Biodegradable block copolymers are promising in manipulating their hydrophilicity, mechanical properties, degradation rate etc. by polymerizing different chemical structures and adjusting the ratio of constituting blocks. As such, the more advanced biomedical applications in the considered living system could be fulfilled and enlarged. In this section, block copolymer synthetic strategies and the block copolymer architectures containing aliphatic polyesters as building blocks will be reviewed.

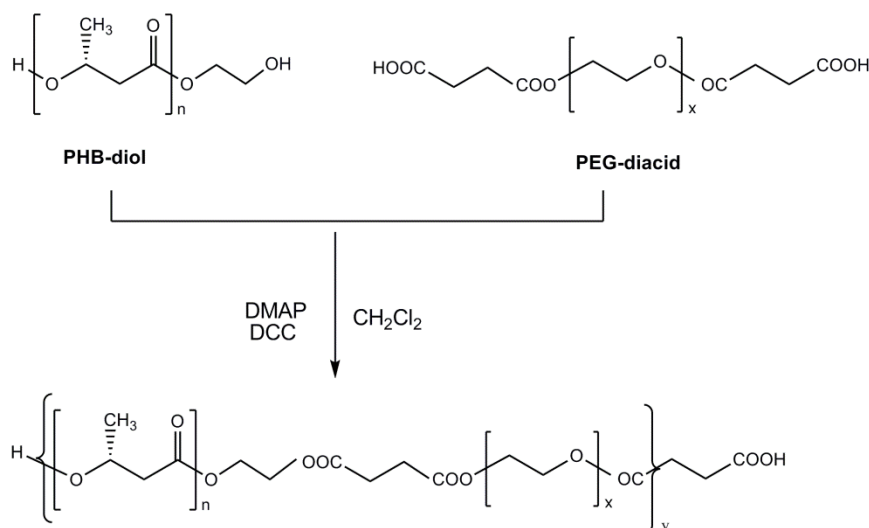
### 2.2.1 Block Copolymer Synthetic Strategies

Block copolymers are macromolecules that contain sequences, or blocks, of two or more different repeating units in one molecule.<sup>72</sup> For constructing block copolymers, there are four principal considerations: (a) linking polymer chain ends together through mutually-reactive functional groups; (b) polymerization by sequential addition of monomers; (c) polymerization of one monomer, after which the active end-group is converted and used to initiate the second monomer to give a different type of polymerization; (d) use of active site in prepolymer to initiate formation of another polymer by chain polymerization. These strategies can be achieved through step polymerization and chain polymerization. The following section will give the details of polymerization mechanisms and illustrate with specific examples.

#### 2.2.1.1 Step polymerization

Polymerizations in which the polymer chains grow step-wise by reactions that can occur between any two molecular species are known as step polymerization.<sup>73</sup> If the prepolymer chains are  $\alpha,\omega$ -functionalized, such reactions lead to block copolymer architecture which is akin to the step polymerization where the starting materials are end-functionalized monomers.<sup>74, 75</sup> The elimination of a small molecule (*e.g.* H<sub>2</sub>O, HCl) generated from the relevant chemical reactions symbolizes as condensation polymerization as opposed to the addition polymerization which the yielded polymers have identical molecular formula to those of reacting monomers in the repeat units.<sup>34, 76, 77</sup> The formation of polyesters from the reaction of carboxylic acid with alcohol groups is a classic example of polycondensation while the polyurethane preparation from RA<sub>2</sub> + RB<sub>2</sub> represents the typical polyaddition of diisocyanates

with diols. Due to the immense diversity and synthetic versatility of aliphatic polyesters, various reactive and functional groups can be introduced such as carboxyl, hydroxyl, amino, ketal, bromo, chloro and carbon-carbon bond.<sup>27, 78</sup> These functional groups facilitate to design and synthesize aliphatic polyesters based biodegradable block copolymers and diversify new materials with unique properties and advanced biomedical applications.

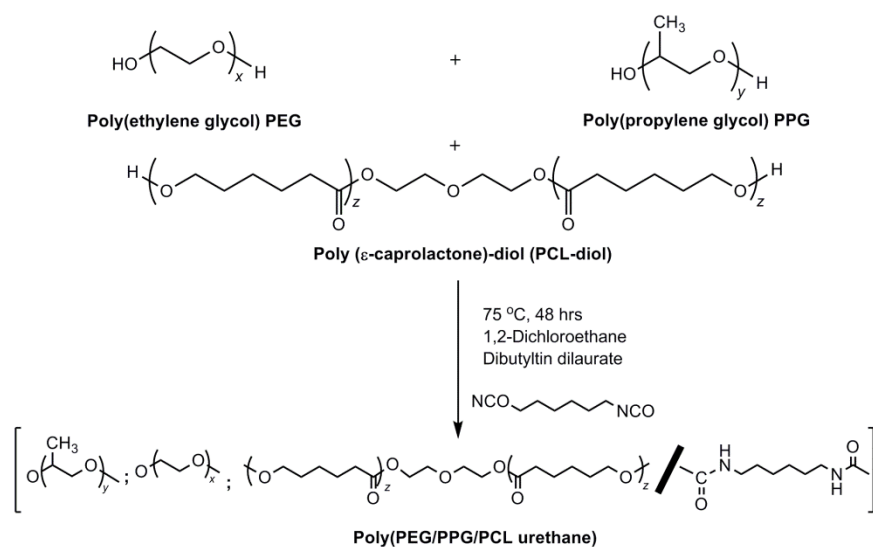


**Figure 2.5. Preparation of PHB-*alt*-PEG multiblock copolymers by esterification reaction of carboxylic acids with alcohol groups in building blocks. [This image was reproduced with permission from ref.<sup>75</sup> (J. Li, 2011) © 2011 American Chemical Society].**

Taking the preparation of poly(ethylene oxide)-poly[(R)-3-hydroxy butyrate]-poly(ethylene oxide) PEG-PHB-PEG triblock copolymer as an example to show the facile way in block copolymer fabrication. High molecular weight PHB was firstly modified into di-hydroxyl groups terminated prepolymer as building blocks at desired molecular weight range by transesterification. The subsequent polymerization of each individual segment through the condensation reaction of hydroxyl groups and monopropionic acid capped at MPEG end gave a well-defined PEG-PHB-PEG triblock copolymer structure. The incorporation of hydrophilic PEG into the backbone of the block copolymer brings new feature of the polymer property. For instance, PEG-PHB-PEG triblock copolymers can form micelle solution at very low critical micellization concentrations and its region-selective channel structure with  $\alpha$ -cyclodextrins could trigger polymer solution phase transformation which had broadened the system as a controlled drug release carrier in hydrogel formation.<sup>79, 80</sup> Similar technique was also adapted to the synthesis of PHB/PEG alternative block copolymer as presented in Figure

2.5. The obtained PHB-alt-PEG block copolymer showed interesting surface patterns and increased hydrophilicity.<sup>75</sup>

Another example can be used to elaborate the intelligence of step polymerization technique in the development of aliphatic polyester derived new biomaterials is poly(ester ether urethane) block copolymers. Polyaddition was involved in the reaction mechanism and showed as an effective approach in the block copolymer synthesis. For example, poly(PEG/PPG/PCL urethane)s multiblock copolymers were prepared from the direct coupling of each segment randomly via urethane linkage (Figure 2.6).



**Figure 2.6. Preparation of poly(PEG/PPG/PCL) multiblock copolymers by urethane reaction.** [This image was reproduced with permission from ref.<sup>81</sup> (J. Li, 2011) © 2008 Elsevier].

The resulted PEG/PPG/PCL block copolymers possessed functionality in water swelling capability triggered by temperature and its further exploration as hydrogel nanofiber was examined to support cell culture and showed controlled release of the encapsulated drugs.<sup>81, 82</sup> The incorporation of hydrophilic moiety led to a more rapid hydrolytic degradation, compared with the pure PCL nanofiber mats. Moreover, simple adjusting block copolymer compositions during the synthesis process could make the final products controllable in mechanical property and self-assembles in micelles and hydrogels.<sup>83</sup> Besides PCL, polyaddition approach was also adapted to prepare other aliphatic polyesters contained block copolymers such as PHB, PLA and PTMC for various explorations as potential biomaterials.<sup>68, 71, 84-89</sup>

2.2.1.2 Chain polymerization

On the other hand, polymerization in which a polymer chain grows only by reaction of monomer with a reactive end-group on growing chain are known as chain polymerization, and usually require an initial reaction between the monomer and an initiator to start growth of the chain.<sup>90</sup>

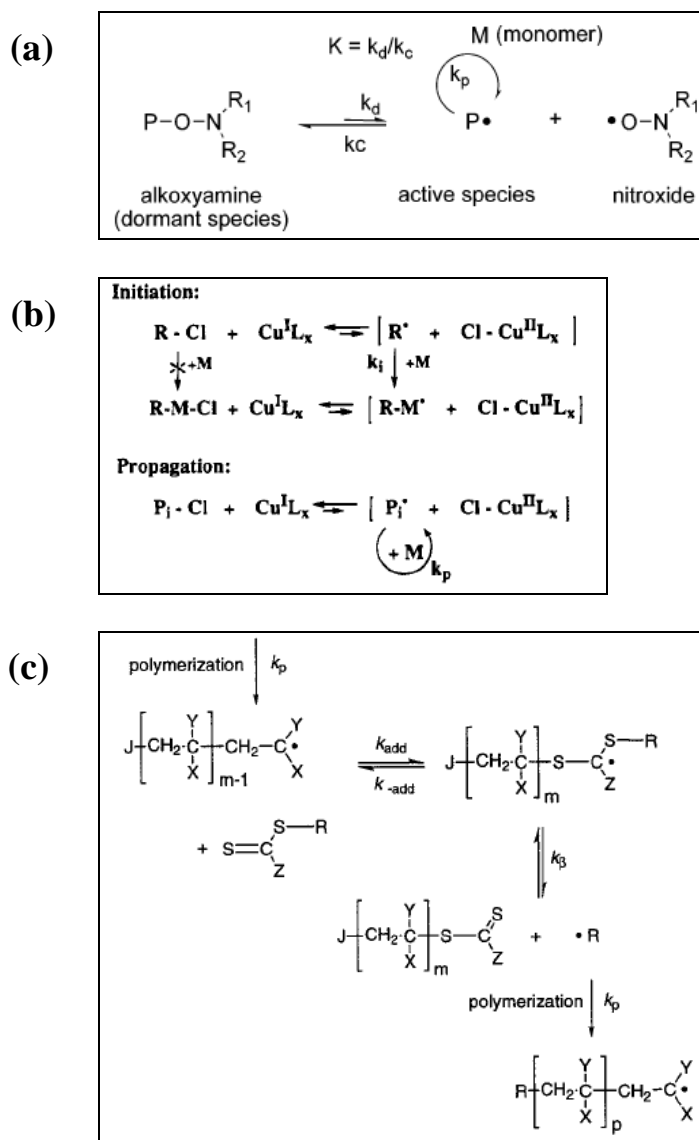
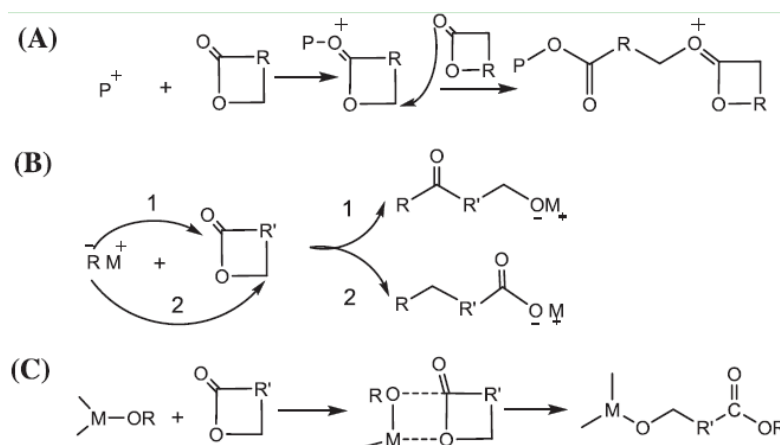


Figure 2.7. General mechanisms for the most studied CLRP (a) NMP [This image was reproduced with permission from ref.<sup>91</sup> (V. Sciannamea, 2008) © 2008 American Chemical Society]; (b) ATRP [This image was reproduced with permission from ref.<sup>92</sup> (J. S. Wang, 1995) © 1995 American Chemical Society]; and (c) RAFT [This image was reproduced with permission from ref.<sup>93</sup> (J. Chiefari, 1998) © 1998 American Chemical Society].

The initiating species may be a radical, anion or cation which leads to specified radical polymerization, anionic polymerization and cationic polymerization.<sup>94-95</sup> Despite of the difference in initiating species, they share three common steps, namely, chain initiation, propagation, and termination during the polymerization process. Among chain polymerization approaches, controlled/“living” radical polymerizations (CLRP) techniques offer many benefits including the ability to control molecular weight and polydispersity and to prepare block copolymers in complex architectures that are not yet already prepared by using other methodologies. In this section, the most recently studied CLRP techniques including nitroxide-mediated radical polymerization (NMP), atom transfer radical polymerization (ATRP) and reversible addition-fragmentation chain transfer (RAFT) will be discussed in their reaction mechanisms (Figure 2.7).<sup>91-93, 96, 97</sup>

For all the three CLRP mechanisms, they are established based on a rapid dynamic equilibration between a minute amount of growing free radicals and a large majority of the dormant species. The dormant chains may be alkyl halides (ATRP), degenerative transfer thioesters (RAFT) and alkoxyamines (NMP).<sup>96</sup> The combinations of CLRP with ROP, a high efficient approach in the synthesis of aliphatic polyesters, were widely employed in block copolymer design, and a variety of monomers under robust conditions have been polymerized into various architectures.<sup>28</sup>

ROP can be used to prepare aliphatic polyester based functional block copolymers, which cannot be easily prepared by other methods.<sup>98-106</sup> The main driving force for the ring-opening of cyclic esters in aliphatic polyesters preparation is the relief of bond-angle strain and/or steric repulsions between crowded into the center of the ring.<sup>107, 108</sup> ROP requires an initiator and in most cases proceeds by chain polymerization mechanisms. The precise mechanism of polymerization depends on the type of initiator, monomer and polymerization conditions. Three major reaction mechanisms are cationic, anionic, and coordination-insertion. However, high molecular weight polyesters have only been obtained by using anionic or coordination-insertion ring opening polymerization.<sup>108, 109</sup> The general mechanism of the three above mentioned ROP polymerization of lactones or lactides is presented in Figure 2.8. Block copolymers with various architectures have been prepared by either step polymerization, chain polymerization techniques, or its various combinations of different synthesis approaches, as reviewed in next section 2.2.2.

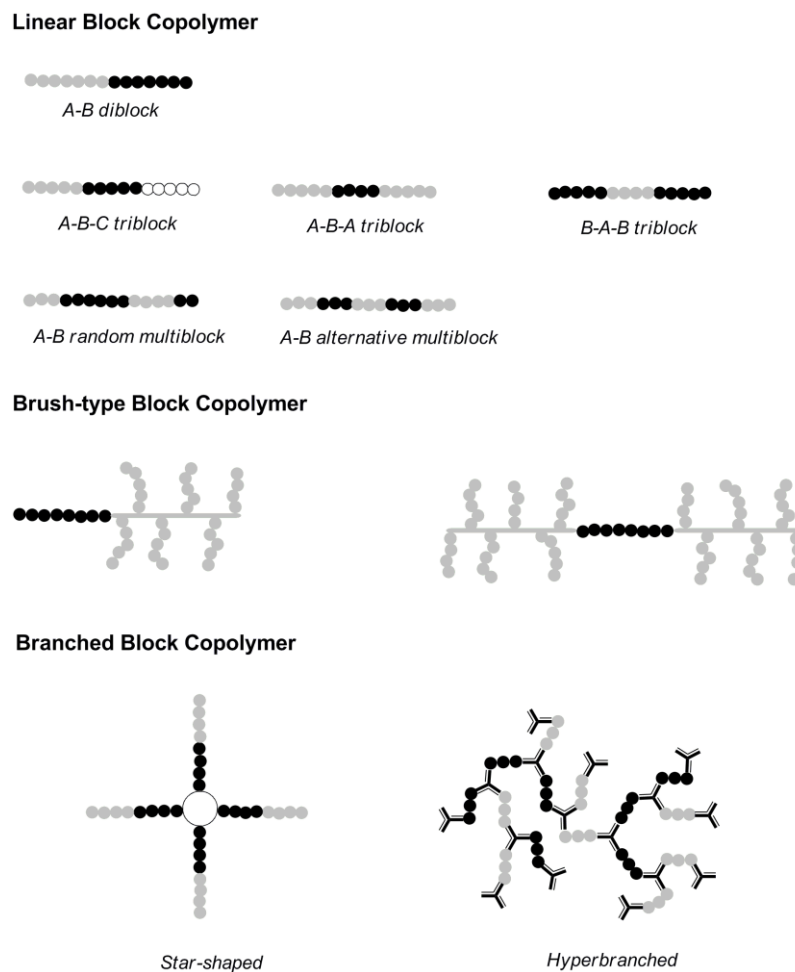


**Figure 2.8.** Ring-opening polymerization of lactones or lactides by the (A) cationic, (B) anionic and (C) coordination-insertion mechanisms. [This image was reproduced with permission from ref.<sup>109</sup> (X. B. Xiong, 2012) © 2012 Elsevier].

### 2.2.2 Block Copolymer Architectures

The rapid evolution of polymerization techniques has stimulated research into the development of new block copolymers with various architectures since the first report of PEG-poly(terephthalate) copolymer in late 70s.<sup>110</sup> This field has promptly developed and numerous applications have been identified. Block copolymers show controllable property which can meet specific criteria for advanced biomedical applications as compared with the unmodified pure polymers. This section gives the types of block copolymers architectures. According to the structures, block copolymers can be classified into linear (diblock, triblock, and multiblock), brush-type and branched block copolymers. The architectures of these types of block copolymers are demonstrated using monomer units A(●), B(●) and C (○) as shown in Figure 2.9. Biodegradable block copolymers containing aliphatic polyesters as building blocks and their unique properties when served as biomaterials will be reviewed in the next following sections.





**Figure 2.9.** Types of block copolymers with various architectures.

### 2.2.2.1 Linear block copolymers

(a) Diblock copolymer: the segment effect in the modification of mechanical property and hydrophilicity of block copolymers is obvious even in the simplest A-B diblock copolymers. Ring opening polymerization and direct coupling of two homopolymers are the two approaches used widely for constructing A-B diblock copolymers. For example, ring opening polymerization of  $\epsilon$ -caprolactone, L-lactide,  $\beta$ -butyrolactone using catalysts has been widely studied for building PCL, PLA and PHB contained biodegradable block polymers.<sup>105, 111, 112</sup> For the later, homopolymer chains must contain the necessary end groups to facilitate the coupling. The crystallization, morphology and drug release period of aliphatic polyesters vary from case to case. The mechanical performance as well as the degradation ratio can be adjusted

by forming A-B diblock copolymers, in which one behaves as hard segment while the other is soft segment. For example, PCL was employed as a drug carrier in long term drug delivery system because of its high crystallinity and low degradation rate. The degradation of the copolymers of PCL with other lactones, such as glycolide or lactide is ameliorated significantly, which can be used in tissue engineering as nerve guide materials.<sup>113, 114</sup> Mostly studied A-B diblock copolymers constituting of both aliphatic polyester are PLA-PCL,<sup>104, 115</sup> PDO-PCL,<sup>116</sup> PHB-PLA and PHB-PCL,<sup>117</sup> PLLA-PDLA,<sup>118</sup> PLA-PDO,<sup>100</sup> PCL-PHO (poly(3-hydroxyoctanoate)).<sup>119</sup> Alternatively, poly(ethylene glycol) (PEG) is nontoxic and cleared by the US Food and Drug Administration for internal use in the human body.<sup>120</sup> The second component PEG in the biodegradable block copolymers exhibits variously improved properties, such as biocompatibility, amphiphilicity, self-assembly, permeability, and controllable biodegradability. A-B polyester-polyether diblock copolymers such as PCL-PEG, PLA-PEG, PLGA-PEG, PTMC-PEG and PHB-PEG have been reported.<sup>120-124</sup> These polymers possess micellar property and have been studied for a long term circulating carriers for hydrophobic drugs after intravenous injection. Doxorubicin loading capacity in PLGA-PEG diblock copolymer formed micelles is greater than its counterparts PLA-PEG, relative to the physical entrapment of free doxorubicin in the inner PLGA core.<sup>125</sup> Different kinds of other applications have been thought for these materials, mainly as implantation and wound treatment.<sup>111, 112, 121, 123, 126</sup>

(b) Triblock copolymer: triblock copolymers comprising three different segments can be built into A-B-C triblock architecture. For example, PHB-PLA-PCL was synthesized via ring opening polymerization by using PHB-diol macroinitiator. The obtained triblock copolymers could combine the superiority of each precursor.<sup>127</sup> For example, tri-component aliphatic polyesters derived from PCL, PLA, PGA and its derivatives with different compositions were synthesized by ring opening polymerization. The fabricated triblock copolymers were shown to have variable degradation rates and most of them could disappear within a few months.<sup>128</sup> In the case of triblock copolymers with A and B segments, two segmental arrangements are possible, *i.e.* A-B-A or B-A-B, where A and B represents hard and soft or hydrophilic and hydrophobic segments, respectively. New resorbable and elastomeric A-B-A triblock copolymers, PLA-PDXO-PLA, have been successfully synthesized by introducing completely amorphous 1,5-dioxepan-2-one (DXO) flanked by hard PLA segment. This novel copolymers retained very good mechanical properties throughout *in vitro* degradation study over 59 days, indicating a potential biomedical application of artificial skin in tissue engineering.<sup>129</sup> Further report on the modification in crystallinity, biocompatibility,

degradation rate and mechanical property of aliphatic polyesters by forming triblock copolymers include PLA-PHB-PLA,<sup>130</sup> PLA-TMC-PLA,<sup>131</sup> PLGA-PCL-PLGA,<sup>113</sup> PLA-PCL-PLA.<sup>106</sup>

However, all these combinations did not alter the natural hydrophobicity of the resultant products, which limits the biomedical applications to some extent. Constructing of amphiphilic copolymers have been attracted great interest. In particular, PEG based triblock copolymers have been widely researched. A-B-A and B-A-B triblock copolymers consisting of aliphatic polyester (A) and PEG (B), for example, PCL-PEG-PCL,<sup>132</sup> PEG-PCL-PEG,<sup>133</sup> PEG-PHB-PEG,<sup>80, 134</sup> PLA-PEG-PLA,<sup>135</sup> PEG-PLA-PEG,<sup>136</sup> PHB-PEG-PHB,<sup>137</sup> PLGA-PEG-PLGA,<sup>138</sup> PEG-PLGA-PEG,<sup>139</sup> have been reported to form stable micelles in water environment. They have been extensively studied for drug delivery and enhanced gene delivery system.<sup>138, 139</sup>

Alternatively, physically cross-linked hydrogels generated by rapid swelling upon exposure to an aqueous environment were obtained from aliphatic polyester and PEG contained A-B-A and B-A-B triblock copolymers. Hydrogels are very attractive delivery systems for hydrophilic macromolecules such as proteins and DNA because they provide a protective environment and allow control of diffusion by adjusting cross-linking densities. Moreover, they show controlled degradation behavior and excellent biocompatibility.<sup>140</sup> A-B-A triblock copolymers, including PLA-PEG-PLA, PLGA-PEG-PLGA, PCL-PEG-PCL, poly(L-lactide-*co*- $\epsilon$ -caprolactone-*b*-ethyleneglycol-*b*-L-lactide-*co*- $\epsilon$ -caprolactone) (PLLC-PEG-PLLC), PTMC-PEG-PTMC have been researched for *in situ* forming hydrogels.<sup>124, 140</sup> Its analogy B-A-B type triblock copolymers such as PEG-PCL-PEG,<sup>141</sup> PEG-PLA-PEG,<sup>142, 143</sup> PEG-PLGA-PEG<sup>139</sup> can also form biodegradable injectable hydrogels with controlled drug release properties. Interestingly, a mixed suspension of the enantiomeric B-A-B triblock copolymers, polyoxyethylene-*b*-poly(L-lactide)-*b*-polyoxyethylene (PEG-PLLA-PEG) and polyoxyethylene-*b*-poly(D-lactide)-*b*-polyoxyethylene (PEG-PDLA-PEG), was found to induce reversible sol-to-gel transition, induced by the PEG helices.<sup>144</sup> In addition, both PEG-PHB-PEG and PHB-PEG-PHB triblock copolymers could form stable micelles in water whereas their complexation with cyclodextrins through host-guest interaction could induce hydrogel formation, which showed high potential in controlled drug delivery.<sup>80, 137, 145</sup>

(c) Multiblock copolymers: biodegradable multiblock copolymers can be built up by linking the functional groups located at the chain end of each component either in a random or an alternative manner, or by sequential polymerization of lactones/lactides by ROP technique.

One approach is to link each segment by a coupling reagent, including diisocyanates, dicarbonyl dichloride or diols. The reactions occurrences include urethane, esterification, chloroformylation reaction. These approaches are also feasible in the modification of biodegradation ratio, mechanical property and hydrophobic/hydrophobic balance of biodegradable polymers. For example, random PLA/PCL multiblock copolymers degraded faster than the respective homopolymers and performed more elastic feather at an elongation of 600%. It was reported to meet the requirement of vascular grafts in clinical use.<sup>146</sup> Similarly, highly elastic PHB/PCL, poly(3-hydroxybutyrate *-co-* 4-hydroxybutyrate) *-b-* poly(3-hydroxybutyrate *-co-* 3-hydroxyhexanoate) (P3/4HB/PHBHHx) and P3/4HB/poly(3-hydroxyhexanoate *-co-* 3-hydroxyoctanoate) random multiblock copolymers with urethane linkage also showed good hemocompatibility, cell compatibility and tunable biodegradability.<sup>147-149</sup> For PEG containing ones, PEG/PLA multiblock copolymer based three dimensional scaffolds showed prior cell proliferation and affinity than pure PLA.<sup>150</sup> More interesting, random PHB/PEG/poly(propylene glycol) (PPG), PLA/PEG/PPG multiblock copolymers formed thermo-responsive hydrogels which showed high potential in protein release and injectables.<sup>68, 71, 87</sup> PCL/PEG multiblock copolymers were synthesized by different approaches. The resultant polymers possessed high mechanical property and water swelling ratio.<sup>81, 151</sup> However, the alternative structure of multiblock copolymer showed some uniqueness. For example, PEG-*alt*-PHB multiblock copolymer coated mica present regular lamellar surface patterns under atomic force microscopy visualization.<sup>75</sup> PEG-*alt*-PHB multiblock copolymer based blends with poly[3-hydroxybutyrate-*co*-3-hydroxyvalerate] (PHBV) showed improved mechanical and biocompatibility.<sup>152</sup> Similar structure of PEG-*alt*-PHB multiblock copolymers prepared using urethane linkage possessed excellent hemocompatibility and adjustable biodegradability.<sup>153</sup>

### 2.2.2.2 Brush block copolymers

Current efforts towards the synthesis of brush-type block copolymers are focused on “controlled/living” radical polymerization of various (meth) acrylates or acrylamides using biodegradable segments as macroinitiator, or via ring opening polymerization to attach the biodegradable part into the brushes.<sup>154-159</sup> As compared with the linear block copolymers, the brush-type block copolymers may possess the advantage of allowing for more functional groups at the end of the brushes, which could be further modified either chemically or biologically to obtain desired properties. Previously, brush type block copolymers

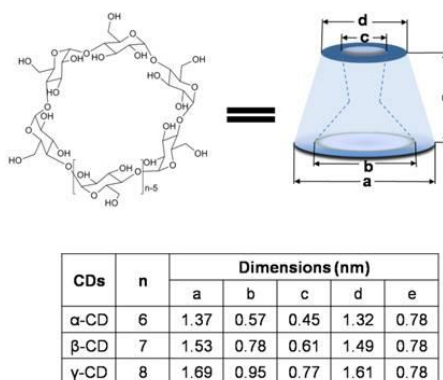
poly(poly(ethylene glycol)-methyl ether methacrylate-block-polystyrene) (P(PEGMA)-b-PS) and poly(glycidyl methacrylate)-block-poly(poly(ethylene glycol)methyl ether methacrylate) (P(GMA)-b-P(PEGMA)), which comprised of methacrylates macromonomers in the polymerization system were prepared by the consecutive ATRP and consecutive RAFT polymerizations, respectively.<sup>160</sup> The aggregation behavior study showed that both the brush block copolymers could form nano-size micelles. However, the interaction of the hydrophilic brushes with the aqueous environment could gradually lead to giant aggregates with diameters up to several micrometers and the non-biodegradable elements may be limited in biomedical applications. On the other hand, the study this type of block copolymers composed of biodegradable elements is in an urgent need. Recently, the synthesis of a novel biodegradable amphiphilic brush block copolymers consisting of PCL as one building segment and PEGylated polyphosphoester as the pendent brushes were reported through ring opening polymerization.<sup>161</sup> The obtained amphiphilic brush block copolymers formed micellar structures in water, and the CMCs were in the range of  $10^{-3}$  mg/mL. Such polymer micelles are expected to have wide utility in the field of drug delivery due to their controlled degradation behavior.<sup>161</sup> In another example, thermo-responsive hydrogels for cell encapsulation application were fabricated from brush structure block copolymers containing PCL, HEMA, NIPAAm and acrylic acid.<sup>162, 163</sup> Interestingly, the unique architecture of the brush structure copolymers also imparted superior properties. For instance, micelles self-assembled from HEMA-PCL-PEG brush copolymers performed larger drug loading capacity and prolonged release profile than those of PCL-PEG linear diblock copolymers.<sup>164</sup> Alternatively, pendent cationic group contained biodegradable brush like block copolymers have also been applied in effective gene delivery.<sup>165</sup>

### 2.2.2.3 Branch block copolymers

Commonly used linear biodegradable polymers are playing a prominent role in biomedical use. However, for some advanced applications, such as parenteral delivery and DNA protection in encapsulation, it is necessary to carefully adjust drug release and polymer degradation rates.<sup>70, 166</sup> The molecular architecture of biodegradable polymers, besides the abovementioned block copolymers approaches, can be exploited in branch structure to adjust polymer morphology and degradation. By incorporation of branching reagent containing multifunctional groups, branched structures can be obtained in suitable formulation from star-branched to hyperbranched structures. Star-shaped biodegradable block copolymers are constructed from a multifunctional core such as polyols functionalized as a initiator followed

by a ROP of the selected monomer.<sup>167</sup> For example, the three, four and six-armed star-shaped block copolymers containing PHB and PCL were synthesized by using trimethylol propane, pentaerythritol and dipentaerthritol as multifunctional cores, respectively. The obtained star-shaped block copolymers showed less blood clotting and more osteoblast cell growth than the corresponding PHB and PCL homopolymers.<sup>101</sup> Branch structure (PEG)<sub>3</sub>-PLA block copolymers were prepared from esterification reaction of citric acid and PEG with a subsequent ROP of lactide. (PEG)<sub>3</sub>-PLA has been explored for the formation of polymersomes with a controlled release of hydrophilic dye up to 18 days.<sup>168</sup> For hyperbranched block copolymers, one effective way to construct is through the introduction of branching unit route. The step-growth polycondensation takes place between the functional groups located at the end of selected blocks. Similar methods have been reported for hyperbranched polymer synthesis from A<sub>2</sub> + B<sub>3</sub> monomers with possible linkage of ester, amide, urea, urethane and ether.<sup>169</sup>

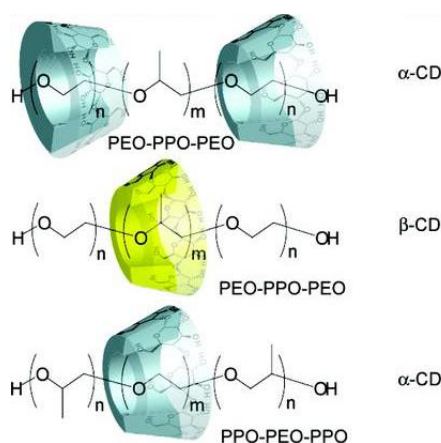
### 2.3 Inclusion Complex between Biodegradable Block Copolymers and Cyclodextrins



**Figure 2.10. Chemical structure of cyclodextrins and their physical dimensions.**

Cyclodextrins (CDs) are a class of cyclic oligosaccharide made up of D-(+)-glucose units linked up in α-1,4 fashion. CDs with 6, 7 and 8 sugar units are termed as α, β and γ CDs respectively. The torus-like molecules carry hydrophobic cavity with depth around 7.8 Å and internal diameter of 4.7-5.3, 6.0-6.5 and 7.3-8.3 Å for α, β and γ respectively (Figure 10). Their natural origin, biodegradability, biocompatibility and good water solubility are some of the advantages that account for their wide-spread use in pharmaceuticals and engineering.<sup>170, 171</sup>

Since the pioneering work of threading of CDs through PEG were reported by Harada, supramolecular structures based on CDs and block copolymers have drawn great attention.<sup>172-174</sup> Polymers covered with CD hosts may form polyrotaxanes or pseudopolyrotaxanes, in which depends on whether the CDs threaded polymeric chains are capped with bulky terminal groups or remain uncapped.<sup>175</sup> Examples of aliphatic polyesters can form inclusion complexes with CDs include PLA, PHB, PCL, poly(3-hydroxypropionate) and poly(4-hydroxybutyrate).<sup>175, 176</sup> In the case of biodegradable block copolymers, CDs may have site-selective favor on specific blocks to thread and have their properties significantly altered due to the shielding of cyclic CD rings.<sup>177</sup> For example, linear biodegradable triblock copolymers PPG-PCL-PPG were region-selectively complexed at the PCL blocks by  $\alpha$ -CD.<sup>178</sup> However, both blocks were complexed by  $\alpha$ -CD in biodegradable triblock copolymers PCL-PEG-PCL and PLA-PEG-PCL, because there is no preference for one block while PEG-PHB-PEG had full and partial coverage of  $\alpha$ -CD on the polyether and polyester blocks, respectively.<sup>79, 179-181</sup> The region-selectivity between CDs and block copolymers were also examined by PEO/PPO based block copolymers, as illustrated in Figure 2.11.



**Figure 2.11. Inclusion complexes structure formed between CDs and block copolymer with stereo-selectivity. [This image was reproduced with permission from ref.<sup>175</sup> (A. Harada, 2009) © 2009 American Chemical Society].**

The threading of  $\beta$ -CD onto the polymer backbone localized preferentially on the PPO block while  $\alpha$ -CD had site-selective behavior on PEG blocks to thread.<sup>145, 182-184</sup> In those cases of the CDs channeled biodegradable block copolymers, the modulation on the biodegradability can be achieved through inclusion complex formation with CDs.<sup>185</sup> Further, the inclusion complex structure and the coverage of CDs on the polymer chains can be used as novel tool to

achieve transformation such as sol to gel, assembling and de-assembling micelles which serves as possible trigger to release the drug encapsulated in the micelles, and tuning amphiphilicity of the building blocks, a potential size and shape controller of self-assemblies.<sup>80, 179, 184, 186, 187</sup> The hydroxyl groups in the exterior rings of CDs could provide functionality for potential conjugation of drugs and active biomolecules as targeting delivery carriers.<sup>188</sup>

### **2.4 Biomedical Applications of Novel Biodegradable Block Copolymers and Their Inclusion Complexes**

The main biomedical applications of biodegradable polymers can be classified into three groups: (A) temporary scaffold or support; (B) temporary barriers and (C) drug delivery devices.<sup>42, 189</sup> These applications are mainly focused on the characteristic of biodegradability while biodegradable block polymers based biomedical applications have extended to more advanced areas, such as delivery carriers in diversified formation, target specific delivery, as well as scaffold based tissue engineering and mimicking natural ECM. These advanced applications are not only involved in the biodegradability, but also the more important one, functionality of biodegradable block copolymers. This section will review the most promising biomedical applications of the aliphatic polyesters based biodegradable block copolymers in tissue engineering applications and delivery system.

#### **2.4.1 Biodegradable Block Copolymers for Tissue Engineering**

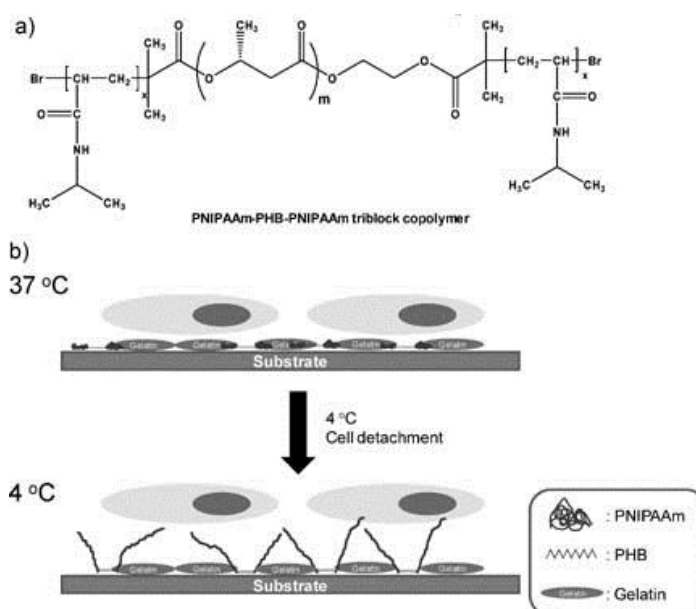
The typical application of biodegradable block copolymers served in biological system lies in tissue engineering, comprising of tissue replacement, tissue augmentation and tissue support. Recent treatment concepts based on scaffold-based tissue engineering show superior than standard tissue replacement and drug therapies as the engineered tissue aims not only to repair but also regenerate the target tissues.<sup>66, 190</sup> Biodegradable block copolymers, for example the most extensively studied di- and triblock copolymers based on aliphatic polyesters, are seen as promising alternatives to clinically established products.<sup>191</sup> These typical block copolymers are regarded as one instance biodegradable or certain partially biodegradable polymeric materials which can achieve tunable characteristics of the polymers to a significant extent such as degradation properties, mechanical properties, and even biocompatibility.<sup>192-194</sup> The complex requirements in mechanical strength and at the same time having a chemical structure which



allows for hydrolytic attack and breakdown in 3D scaffold design could be both fulfilled by using biodegradable block copolymers as the developing materials, which can be further targeted for specific tissue engineering application. For example, through careful selection of each segment and its control in length ratios in PCL/PGA diblock copolymer systems could lead the elongation up to 250% and recovery up to 98% after applied strain of 120%. The prepared scaffold supported rat smooth muscle cells growth and tissue formation *in vivo*, predicting a promising characteristic in mechanically dynamic environments application such as blood vessels, bladders and muscle tissue engineering.<sup>193</sup> Another challenges facing scaffold based tissue engineering is the ability to add bioactive molecules to enhance the biocompatibility.<sup>191</sup> Conventional biodegradable polymers lack this characteristic. However, it is worthy to point out that those bioactive molecules can be incorporated by introducing a functional side group in the backbone of block copolymers. This is an efficient strategy to overcome this limitation in cell therapy. For example, biodegradable amphiphilic ABA triblock copolymer consisting poly[(lactic acid)-*co*-(glycolic acid)-*alt*-( $\gamma$ -benzyl-glutamic acid)] and PEG (PLBG-PEG-PLBG) afforded pendant carboxyl groups after undergoing catalytic hydrogenation, which provided reactive groups for the attachment of biomolecules including oligosaccharides, drug molecules, and short peptides.<sup>195</sup> Scaffolds fabrication techniques containing biodegradable block copolymers with mimicking natural extracellular matrix have also being applied to meet the clinical needs for tissue engineering and are being developed at a rapid pace.<sup>196-198</sup>

In addition to the scaffold based tissue engineering, surface-modified substrates could assist to generate bioactive surface for cell culture, which can be exploited for the regeneration of various applications in tissue engineering. For example, the temperature responsive cell culture surface could be obtained by coating thermally responsive polymer onto a substrate from which the surface properties of the substrate can be changed by changing the temperature of the environment. This novel technique has been received significant attention due to the utilization of easy-controllable temperature as the solo trigger.<sup>87, 199, 200</sup> For example, Poly(N-isopropylacrylamide) (PNIPAAm) exhibits a lower critical solution temperature (LCST) transition temperature of 32 to 33 °C, with more hydrophilicity at low temperatures and precipitation out from solution at above the critical phase transition temperatures.<sup>201</sup> Hydrophobic surface modified by PNIPAAm at above its LCST can support cell adhesion and growth, and facilitate cells recovery through non-enzymatic method by cooling the temperature below LCST.<sup>202-205</sup> This experimental observation is explained by dehydration to hydration transition of PNIPAAm with temperature. Up to date, the synthesis of PNIPAAm based

triblock copolymers centered on a biodegradable aliphatic PCL or PHB segments using ATRP have been reported.<sup>206, 207</sup> Studies showed both triblock copolymers aqueous solutions possessed thermal sensitivity with temperature alternation across their corresponding LCST. More interestingly, PNIPAAm-PHB-PNIPAAm triblock copolymer micelle solutions coated surface afforded cell detachment with preserved cell-cell and cell-extracellular matrix interactions, unlike the typical approach of using proteases, such as trypsin, to detach cells (Figure 2.12).<sup>208, 209</sup> This mild technique of cell detachment has also been employed by many others reports for the generation of cell sheets.<sup>203-205</sup> However, most investigations related to temperature-induced cell adhesion and detachment is limited to those block copolymers consisting of PNIPAAm as culture surface.



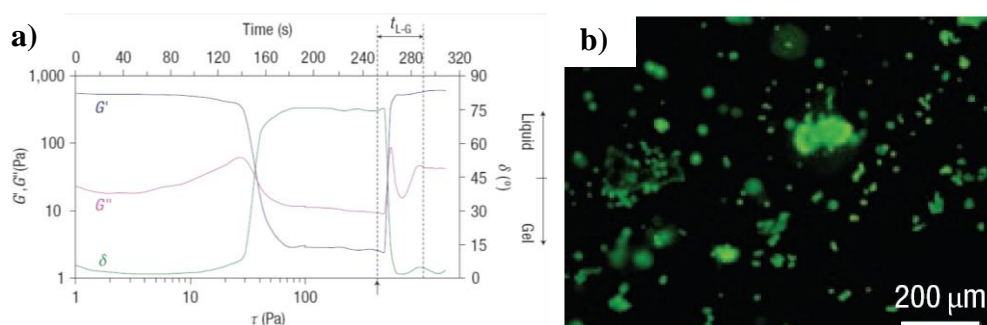
**Figure 2.12.** (a) Structure of PNIPAAm-PHB-PNIPAAm triblock copolymers. (b) Illustration of the cell detachment process (b). [This image was reproduced with permission from ref.<sup>209</sup> (J. Li, 2009) © 2009 John Wiley and Sons].

Poly(propylene oxide) (PPO) is another fascinating candidate when building thermo-sensitive block copolymers due to their good biocompatibility. The cloudy point of PPO contained polymer range from 14 °C to about 100 °C that is dependent on the polymer architectures and molecular weight.<sup>210, 211</sup> PPO contained triblock copolymers PEO-PPO-PEO, commercially know as Pluronic or Poloxamer, can undergo phase transition as triggered by temperature to form hydrogel formation. This polymer has been previously used in cell

engineering applications.<sup>212-214</sup> Temperature-induced L929 cells and normal human umbilical vein endothelial cells (HUVECs) detachment from F127 gels was investigated.<sup>214</sup> However, the problems come from the high hydrophilicity of F127 gels that tended to dissolve in the culture medium and suppressed its effect in cell recovery. Because cell growth on hydrophilic surfaces is not favorable and such a surface would inhibit the growth of cells.<sup>215</sup> The high flexibility of PEO segments in aqueous medium suppressed Pluronic coated substrates in plasma protein adsorption and platelet adhesion.<sup>216</sup> Therefore, immobilization of Pluronic on the surface of tissue culture flask were further carried out to improve the effectiveness for the cell culture and detachment as compared to the Pluronic gels.<sup>217</sup> Nevertheless, the cell density also tended to decrease sharply with increased surface concentration of immobilized Pluronic polymer. Moreover, the complicated chemical reactions involved in the immobilization process would limit its application to some extent. Therefore, the easy preparation and stable attachments of PPO based biodegradable thermo-responsive block copolymer onto the substrate is desired to benefit the strong hydrophobic interactions, as given by the hydrophobic segments such as aliphatic polyester segments. This process can avoid the complicated immobilization and spin-coating processes that have been commonly used in previously reports.<sup>213, 217</sup> The newly developed technique from thermo-responsive block copolymers treated surface could allow the isolation of cells under mild conditions, having potential to preserve cell-cell and cell-extracellular matrix (ECM) interactions. This is totally different from the traditional method of cell detachment using trypsin. The expected technology through PPO derived biodegradable block copolymer could provide a powerful tool for surface marker analysis and regenerative organs in tissue engineering.<sup>214, 217-219</sup>

In line with the cell engineering cultured on the two dimensional (2D) surface, 3D cell encapsulation has also gained increasing attention in recent years owing to its similarity to the *in vivo* environment.<sup>220</sup> Hydrogels that fabricated from a wide and diverse range of natural and synthetic polymers have been used to encapsulate cells.<sup>163, 212, 221-225</sup> In the past decades, *in situ* gelling stimuli-sensitive block copolymer based hydrogels have been reported extensively due to their proper gelation rate after injection.<sup>162, 163, 214, 222</sup> This kind of hydrogels is reversible polymer networks formed by physical interactions and exhibit a sol-gel phase transition in response to external stimuli. Nevertheless, many such physical hydrogels do not have enough stability and tenacity for holding cells. The research problems suffers from the weak gel strength and fast gel erosion, that show burst effects in biological environments, and cannot maintain a relatively stable environment for cell activity.<sup>71, 226</sup> For example, Pluronic F127 aqueous solutions have been most widely investigated as thermo-responsive hydrogels at above

certain concentrations. The polymer solutions can undergo sol-gel transition at physiological temperature.<sup>227</sup> However, the fast release of the entire encapsulates along with rapid hydrogel weight loss finished within 4 hour.<sup>71</sup> Its further exploration as cell encapsulation matrix within resulted in complete cell death by 5 days.<sup>213</sup> The high gel stiffness ( $G' > 1200$  Pa) of F127 hydrogel may account for this observation because the best performance for cell encapsulation in hydrogel has been previously demonstrated in the  $G'$  rang of 10 to 1000 Pa.<sup>221</sup> From this point of view, the thixotropic hydrogel shows easier mechanical control in viscoelastic property than the stimuli-responsive hydrogels and will become a new trend for the cell encapsulation materials development.



**Figure 2.13. (a) Rheological characteristics of PEG-Silica based thixotropic hydrogel. (b) Live-dead assay after one week of culturing MCF-7 cells in 3D PEG-silica gels. [This image was reproduced with permission from ref.<sup>225</sup> (Y. S. Pek, 2008) © 2008 Nature Publishing Group].**

In the rheological measurement of a thixotropic hydrogel, the elastic modulus  $G'$  diminishes as they are sheared. At the liquefied state, the elastic modulus becomes less than the viscous modulus ( $G' < G''$ ). However, the diminished  $G'$  of the hydrogel will eventually recover into its original state, in most cases within hours, when the tested hydrogel system is under no more or gentle agitation.<sup>225, 228, 229</sup> This unique properties render the mechano-stimuli as an much easier trigger and have made this kind of hydrogel more fascinating potential in 3D cell engineering application.<sup>225, 230</sup> Figure 2.13 shows a typical example of rheological characteristics of thixotropic hydrogel. Specifically, the typical  $G'$ ,  $G''$  and  $\delta$  of gels as a function of increasing shear stress  $\tau$  applied with time. At 150 s when  $G' = G''$ , liquefaction occurs and  $\tau = \tau_y =$  liquefaction stress. The time taken for  $G'$ ,  $G''$  and  $\delta$  to return to their original levels when shear stress was removed ( $t = 251$ s, indicated by the double arrow) is the liquid-gel transition time ( $t_{L-G}$ ). This PEG-Silica hydrogel has been reported as 3D cell encapsulation matrix and the spatially encapsulated cells could maintain good cell viability up to three weeks.<sup>225</sup> Besides the easy manipulation of cells encapsulation procedure in thixotropic

hydrogels by mechanical control, this kind of hydrogel could also afford other advantages such as other bioactive molecules including proteins, plasmid DNAs, drugs, even vaccines can be incorporated into the hydrogel without any contact with organic solvents by subjecting the hydrogel to a specific mechanical stress. Through novel block copolymer design, biodegradable components can be introduced into the hydrogel system. Together with the unique properties of hydrogel such as the similar soft-tissue-like property and porous structure, the combined biodegradable thixotropic hydrogel system could be expected to facilitate the exchange of oxygen, nutrients and other water-soluble metabolites. This could be beneficial in a variety of biomedical and pharmaceutical application in drug carriers, grow factor delivery, cell encapsulation, three-dimensional cell culture and tissue generation matrix.<sup>163, 225, 231-234</sup>

### 2.4.2 Biodegradable Block Copolymers as Delivery Carriers

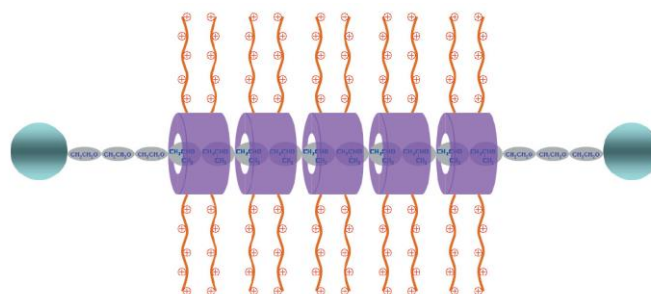
The great challenge in drug delivery is to maintain the optimum efficacy at a therapeutic concentration of the drug in the blood plasma. Below the certain concentrations, the drug efficacy decreases and the toxicity could be a big concern if the drug concentration is too high through repeat dosage.<sup>235</sup> Controlled drug delivery technology offers numerous advantages compared to conventional dosage forms including improved efficacy, reduced toxicity, and improved patient compliance and convenience.<sup>236</sup> Biodegradable block copolymers, especially for the amphiphilic ones, can provide the sustained release of the encapsulated molecules. The amphiphilic block copolymers can self-assemble into different morphologies.<sup>80, 237-239</sup> The most common and well-studied self-assembly behavior of the aliphatic polyester and PEG based block copolymers are micelles and hydrogels. Micelles, as a colloidal carrier system, have been receiving much attention in the field of drug targeting because of their high loading capacity for drugs as well as their unique disposition characteristics in the body. The process of micellization in aqueous milieu is driven by the core segregation, induced by hydrophobic interaction and hydrogen bonding of constituent block copolymers. The segregated aliphatic polyester core embedded in the hydrophilic palisade PEG is shown to function as a reservoir for genes, enzymes, and a variety of drugs with diverse characteristics.<sup>240, 241</sup> For example, the PLA-PEG-PLA (ABA) type and PEG-PLA-PEG (BAB) type micelles, the diffusion-controlled release of paclitaxel drug is the slowest for the BAB polymers. Compared with PLA particles, all the micellar particles tested of both BAB and ABA types showed a controllable release profile.<sup>136</sup>

On the other hand, hydrogels are an alternative formula which can provide controlled release effect of encapsulates. They are a special class of polymers that possess unique swelling behavior and 3D structure.<sup>242</sup> Due to its similarity to the *in vivo* environment, hydrogels with respect to pharmaceutical delivery have been an attractive topic of extensive research in the past decades.<sup>243-245</sup> The copolymerization of hydrophilic segment such as PEG with aliphatic polyesters has yielded some interesting *in situ* hydrogels.<sup>246</sup> Thermo-responsive properties were given by incorporating suitable chain length of polyester and its appropriate ratio with PEG and other functional blocks.<sup>86, 246</sup> In contrast to the permanent chemically cross-linked hydrogel networks, *in situ*-forming hydrogels are injectable fluids before administration but immediately turn into standing hydrogels within the desired tissue, organ, or body cavity.<sup>247</sup> This unique characteristic of the *in situ*-forming hydrogels exempts the surgical procedure for placement, and various therapeutic formulations can be incorporated by simple mixing.<sup>248</sup> For example, Jeong and his colleagues have investigated a group of aliphatic polyesters and PEG based thermogels as injectables for delivery applications.<sup>142</sup> From then, new biodegradable block copolymers based thermogelling system containing aliphatic polyesters as building blocks which can eventually lead to a hydrogel formation includes PLA, PCL, PTMC, PHB and their various combinations in different architectures have been widely investigated for delivery applications.<sup>87, 139, 249-256 71</sup>

In addition to encapsulation of drugs, the biodegradable block copolymers derived delivery system could also be extended to delivery of protein, gene and other active biomolecules when selecting proper functional segments as building blocks.<sup>109, 140 165, 257</sup> For delivery technology, block copolymers in various formations other than micelles and hydrogels have been explored, including micro- and nanoparticles, polymersomes and vesicles.<sup>247, 258-261</sup> All of these aggregates were reported in controlled or sustained fashion with prerequisite protection of the encapsulates from degradation or loss of its bioactivity. Particularly, block copolymer are able to provide targeting and specific delivery with further modification or conjugation of a desirable and bioactive molecules onto backbone or branches of the copolymers through various coupling reactions (e.g., antibody, ligand).<sup>140, 262-264</sup>

### 2.4.3 Biomedical Applications of Biodegradable Block Copolymers Based Inclusion Complexes

Inclusion complexes between polymers chains and CD hosts may form polyrotaxanes or pseudopolyrotaxanes with the difference of whether the CDs threaded polymeric chains are capped with bulky terminal groups or not.<sup>175</sup> The hydroxyl groups in CD rings provide various possibilities for chemical modifications and their supramolecular assemblies have been widely investigated as new biomaterials.<sup>265-270</sup> For example, as shown in Figure 2.14, oligoethylenimine-grafted  $\beta$ -CDs threaded on a PEO/PPO block copolymer chains were synthesized to give cationic supramolecules for efficient gene delivery.<sup>271</sup> The cationic supramolecular gene delivery vectors showed good DNA binding ability, low cytotoxicity, and high gene transfection efficacy that is comparable to one of the most effective gene delivery polymers studied to date (PEI).<sup>170</sup> However, the obtained cationic supramolecular product is non-biodegradable and accumulation of cationic polymers in lysosomal compartment might lead to a medical condition classified as macromolecular syndrome or lysosomal storage disease.<sup>272</sup> To make this kind of stable polymer biocleavable while maintain the good transfection efficiency, a new polyrotaxane through disulfide cleavage located at the end of the polyrotaxane were prepared.<sup>273</sup> The subsequent supramolecular dissociation of the noncovalent linkages between  $\alpha$ -CDs and PEG was verified to further enhanced gene delivery.



**Figure 2.14. Structure of cationic polyrotaxanes with multiple OEI-grafted  $\beta$ -CD rings.** [This image was reproduced with permission from ref.<sup>271</sup> (J. Li, 2006) © 2006 John Wiley and Sons].

However, lack of affinity could make the systems unable to differentiate receptor-mediated endocytosis of human cancer cell lines from the non-specific uptake of normal tissues when applied them as gene vectors. Receptor-mediated targeting gene delivery based on this kind of polyrotaxanes and the assemblies have been further designed very

recently.<sup>274</sup> In this new system, folate (FA) molecules were functioned as blockers on cationic polyrotaxanes ends, in the placement of disulfide cleavage bond of the cleavable polyrotaxanes.<sup>273</sup> Here, the FA molecules served as ligand for FA-receptor abundant tumor cells and enhanced antitumor effect in the nude mice was observed. Nevertheless, the design sacrificed the degradation properties and will also face a safety issue caused from the polymer accumulation after repeated administrations. Gene delivery carriers consisting biodegradable polyrotaxanes and specific targeting effect are far more promising. The combination of biodegradation and bioactive functions look likely as the future direction of cationic polyrotaxanes. The reaction groups in CDs could functionalize as the potential conjugation or grafting of drugs and active biomolecules as targeting delivery system. However, studies in this direction have been achieved limited success.<sup>275</sup>

Biodegradable aliphatic polyesters such as PLA, PHB, PCL, poly(3-hydroxypropionate) (P3HP) and poly(4-hydroxybutyrate) (P4HB) have been reported to form inclusion complexes with CDs through self-assembly.<sup>175, 176</sup> For the biodegradable block copolymers built from biodegradable aliphatic polyesters and other functional blocks, CDs showed site-selective favor on specific blocks to thread. Besides the development trend of using this kind of materials as gene delivery carriers, this technology has also diversified a variety of self-assembled systems which showed high potential for other biological applications. This includes sustained gene delivery, drug delivery and cell encapsulations etc.<sup>177, 270, 276</sup> For instance, supramolecular hydrogels self-assembled from biodegradable PCL/PEG based block copolymers such as PCL-PEG, PCL-PEG-PCL, and PEG-PCL-PEG were reported for controlled drug delivery and cell encapsulation studies.<sup>179, 223, 277</sup> Ternary block copolymers containing PEG, PCL and PDMAEMA was fabricated into supramolecular hydrogel with  $\alpha$ -CD which has extended the biodegradable block copolymer based inclusion complexes to sustained gene delivery.<sup>278</sup> Alternatively, PHB in both atactic and isotactic conformation were reported to form block copolymers with PEG in various architectures and their inclusion complexes with CDs triggered solution transformation from micelles to hydrogels, which supported a well-controlled release profile of the encapsulated molecules without burst release.<sup>145, 223, 228, 279, 280</sup> This kind of supramolecular hydrogels rely on the threading of sufficient CD molecules onto PEG chains to form polypseudorotaxanes that subsequently aggregate into crystalline domains that in turn act as physical cross-links of the hydrogel.<sup>281</sup> The comprehensive summaries of using supramolecular hydrogels as delivery systems and tissue engineering were reviewed in Li's report.<sup>170, 276, 279, 282</sup>



### 2.5 References

1. A.-C. Albertsson and S. Karlsson, in *Chemistry and technology of biodegradable polymer*, ed. G. J. L. Griffin, Blackie, Glasgow (United Kingdom), 1994, ch. 2, pp. 7-17.
2. W. Amass, A. Amass and B. Tighe, *Polym. Int.*, 1998, **47**, 89-144.
3. X.-L. Wang, K.-K. Yang and Y.-Z. Wang, *J. Macromol. Sci., Polym. Rev.*, 2003, **43**, 385-409.
4. B. S. Kaith, H. Mittal, R. Jindal, M. Maiti and S. Kalia, in *Cellulose Fibers: Bio- and nano-polymer Composites*, eds. S. Kalia, B. S. Kaith and I. Kaur, Springer Berlin Heidelberg, 2011, pp. 425-451.
5. A. Calmon-Decriaud, V. Bellon-Maurel and F. Silvestre, in *Blockcopolymers - Polyelectrolytes - Biodegradation*, eds. V. Bellon-Maurel, A. Calmon-Decriaud, V. Chandrasekhar, N. Hadjichristidis, J. Mays, S. Pispas, M. Pitsikalis and F. Silvestre, Springer Berlin / Heidelberg, 1998, vol. 135, pp. 207-226.
6. G. Luckachan and C. Pillai, *J. Polym. Environ.*, 2011, **19**, 637-676.
7. P. L. Nayak, *J. Macromol. Sci., Polym. Rev.*, 1999, **39**, 481-505.
8. Y. Cha and C. G. Pitt, *Biomaterials*, 1990, **11**, 108-112.
9. L. Fambri, C. Migliaresi, K. Kesenci and E. Piskin, in *Biodegradable Polymers*, ed. R. Barbucci, Springer US, 2002, pp. 119-187.
10. L. S. Nair and C. T. Laurencin, *Prog. Polym. Sci.*, 2007, **32**, 762-798.
11. R. Chandra and R. Rustgi, *Prog. Polym. Sci.*, 1998, **23**, 1273-1335.
12. S. Vainionpää, P. Rokkanen and P. Törmälä, *Prog. Polym. Sci.*, 1989, **14**, 679-716.
13. Y. Ikada, in *Integrated Biomaterials Science*, ed. R. Barbucci, Springer US, 2002, pp. 1-23.
14. R. A. J. Warren, *Annu. Rev. Microbiol.*, 1996, **50**, 183-212.
15. J. Simon, H. P. Müller, R. Koch and V. Müller, *Polym. Degrad. Stab.*, 1998, **59**, 107-115.
16. H. F. Zobel, *Starch - Stärke*, 1988, **40**, 44-50.
17. D. Klemm, B. Heublein, H.-P. Fink and A. Bohn, *Angew. Chem. Int. Ed.*, 2005, **44**, 3358-3393.
18. C. K. S. Pillai, W. Paul and C. P. Sharma, *Prog. Polym. Sci.*, 2009, **34**, 641-678.

19. G. Q. Chen, *Chem. Soc. Rev.*, 2009, **38**, 2434-2446.
20. Q. Wu, Y. Wang and G. Q. Chen, *Artif. Cells, Blood Substitues, Immobilization Biotechnol.*, 2009, **37**, 1-12.
21. G. I. Williams and R. P. Wool, *Appl. Compos. Mater.*, 2000, **7**, 421-432.
22. L. David, C. Fulin and H. Dietmar, in *Handbook of Carbohydrate Engineering*, CRC Press, 2005, vol. null, pp. 837-893.
23. V. Sihorkar and S. P. Vyas, *Int. J. Pharm. Pharm. Sci.*, 2001, **4**, 138-158.
24. G.-Q. Chen and R.-C. Luo, *Polyhydroxyalkanoate Blends and Composites*, John Wiley & Sons, Inc., 2009.
25. G.-Q. Chen and Q. Wu, *Biomaterials*, 2005, **26**, 6565-6578.
26. C. W. Pouton and S. Akhtar, *Adv. Drug Delivery Rev.*, 1996, **18**, 133-162.
27. H. Tian, Z. Tang, X. Zhuang, X. Chen and X. Jing, *Prog. Polym. Sci.*, 2012, **37**, 237-280.
28. M. Okada, *Prog. Polym. Sci.*, 2002, **27**, 87-133.
29. A. G. Pathiraja and A. Raju, *Eur. Cells. Mater.*, 2003, **5**, 1-16.
30. A.-C. Albertsson and I. Varma, in *Degradable Aliphatic Polyesters*, 2002, pp. 1-40.
31. M. Lindblad, Y. Liu, A.-C. Albertsson, E. Ranucci and S. Karlsson, in *Degradable Aliphatic Polyesters*, 2002, pp. 139-161.
32. Y. Tokiwa and T. Suzuki, *J. Appl. Polym. Sci.*, 1981, **26**, 441-448.
33. I. Vroman and L. Tighzert, *Materials*, 2009, **2**, 307-344.
34. U. Edlund and A. C. Albertsson, *Adv. Drug Delivery Rev.*, 2003, **55**, 585-609.
35. D. F. Williams and S. P. Zhong, *Int. Biodeterior. Biodegrad.*, 1994, **34**, 95-130.
36. D. K. Gilding and A. M. Reed, *Polymer*, 1979, **20**, 1459-1464.
37. A. Helena and R. Rui, in *Biodegradable Systems in Tissue Engineering and Regenerative Medicine*, CRC Press, 2004, vol. null.
38. A. Göpferich, *Biomaterials*, 1996, **17**, 103-114.
39. A. Göpferich, *Biomaterials*, 1997, **18**, 397-403.
40. A. K. Burkoth, J. Burdick and K. S. Anseth, *J. Biomed. Mater. Res.*, 2000, **51**, 352-359.
41. S. Li, *J. Biomed. Mater. Res.*, 1999, **48**, 342-353.

42. T. Hayashi, *Prog. Polym. Sci.*, 1994, **19**, 663-702.
43. R. Lenz, in *Biopolymers I*, eds. R. Langer and N. Peppas, Springer Berlin / Heidelberg, 1993, vol. 107, pp. 1-40.
44. J. W. Coleman, *Int. Immunopharmacol.*, 2001, **1**, 1397-1406.
45. R. S. Labow, Y. Tang, C. B. McCloskey and J. P. Santerre, *J. Biomater. Sci. Polym. Ed.*, 2002, **13**, 651-665.
46. K.-H. Lee and C. C. Chu, *J. Biomed. Mater. Res.*, 2000, **49**, 25-35.
47. C. A. Finch, *Polym. Int.*, 1995, **37**, 83-84.
48. J. M. Schakenraad, M. J. Hardonk, J. Feijen, I. Molenaar and P. Nieuwenhuis, *J. Biomed. Mater. Res.*, 1990, **24**, 529-545.
49. L. Meinel, S. Hofmann, V. Karageorgiou, C. Kirker-Head, J. McCool, G. Gronowicz, L. Zichner, R. Langer, G. Vunjak-Novakovic and D. L. Kaplan, *Biomaterials*, 2005, **26**, 147-155.
50. M. I. Tammi, A. J. Day and E. A. Turley, *J. Biol. Chem.*, 2002, **277**, 4581-4584.
51. Q. Li, J. Wang, S. Shahani, D. D. N. Sun, B. Sharma, J. H. Elisseeff and K. W. Leong, *Biomaterials*, 2006, **27**, 1027-1034.
52. T. G. Park, S. Cohen and R. Langer, *Macromolecules*, 1992, **25**, 116-122.
53. T. Mathisen and A.-C. Albertsson, *J. Appl. Polym. Sci.*, 1990, **39**, 591-601.
54. R. S. Bezwada, D. D. Jamiolkowski, I.-Y. Lee, V. Agarwal, J. Persivale, S. Trenka-Benthin, M. Erneta, J. Suryadevara, A. Yang and S. Liu, *Biomaterials*, 1995, **16**, 1141-1148.
55. G. G. Pitt, M. M. Gratzl, G. L. Kimmel, J. Surlles and A. Sohindler, *Biomaterials*, 1981, **2**, 215-220.
56. M. Hakkarainen and A.-C. Albertsson, in *Chromatography for Sustainable Polymeric Materials*, eds. A.-C. Albertsson and M. Hakkarainen, Springer Berlin / Heidelberg, 2008, vol. 211, pp. 85-116.
57. Y. Saito and Y. Doi, *Int. J. Biol. Macromol.*, 1994, **16**, 99-104.
58. Y. Doi, Y. Kanesawa, M. Kunioka and T. Saito, *Macromolecules*, 1990, **23**, 26-31.
59. X. Y. Chen, X. D. Yang, J. Y. Pan, L. Wang and K. T. Xu, *J. Biomed. Mater. Res. B Appl. Biomater.*, 2010, **92B**, 447-455.
60. M. Hakkarainen, *Adv. Polym. Sci.*, 2002, **157**, 113-138.
61. J.-H. Zhu, Z.-R. Shen, L.-T. Wu and S.-L. Yang, *J. Appl. Polym. Sci.*, 1991, **43**, 2099-2106.

62. C. M. Agrawal, K. A. Athanasiou and J. D. Heckman, in *Porous Materials for Tissue Engineering*, 1997, vol. 250, pp. 115-128.
63. A. A. Ignatius and L. E. Claes, *Biomaterials*, 1996, **17**, 831-839.
64. A.-C. Albertsson and M. Eklund, *J. Appl. Polym. Sci.*, 1995, **57**, 87-103.
65. A. Löfgren and A.-C. Albertsson, *J. Appl. Polym. Sci.*, 1994, **52**, 1327-1338.
66. D. W. Hutmacher, *Biomaterials*, 2000, **21**, 2529-2543.
67. A. M. Reed and D. K. Gilding, *Polymer*, 1981, **22**, 499-504.
68. X. J. Loh, Y. X. Tan, Z. Y. Li, L. S. Teo, S. H. Goh and J. Li, *Biomaterials*, 2008, **29**, 2164-2172.
69. D. F. Williams, *JMatS*, 1982, **17**, 1233-1246.
70. A. Breitenbach, Y. X. Li and T. Kissel, *J. Controlled Release*, 2000, **64**, 167-178.
71. X. J. Loh, S. H. Goh and J. Li, *Biomaterials*, 2007, **28**, 4113-4123.
72. F. S. Bates and G. H. Fredrickson, *Annu. Rev. Phys. Chem.*, 1990, **41**, 525-557.
73. J. K. Stille, *J. Chem. Educ.*, 1981, **58**, 862.
74. J. Li, X. Li, X. P. Ni and K. W. Leong, *Macromolecules*, 2003, **36**, 2661-2667.
75. X. Li, K. L. Liu, J. Li, E. P. S. Tan, L. M. Chan, C. T. Lim and S. H. Goh, *Biomacromolecules*, 2006, **7**, 3112-3119.
76. Y. Ikeda, S. Kohjiya, S. Takesako and S. Yamashita, *Biomaterials*, 1990, **11**, 553-560.
77. J. Kloss, M. Munaro, G. P. D. Souza, J. V. Gulmine, S. H. Wang, S. Zawadzki and L. Akcelrud, *J. Polym. Sci., Part A: Polym. Chem.*, 2002, **40**, 4117-4130.
78. A. H. Arkin and B. Hazer, *Biomacromolecules*, 2002, **3**, 1327-1335.
79. J. Li, X. Li, X. P. Ni, X. Wang, H. Z. Li and K. W. Leong, *Biomaterials*, 2006, **27**, 4132-4140.
80. J. Li, X. P. Ni, X. Li, N. K. Tan, C. T. Lim, S. Ramakrishna and K. W. Leong, *Langmuir*, 2005, **21**, 8681-8685.
81. X. J. Loh, K. B. C. Sng and J. Li, *Biomaterials*, 2008, **29**, 3185-3194.
82. X. J. Loh, P. Peh, S. Liao, C. Sng and J. Li, *J. Controlled Release*, 2010, **143**, 175-182.
83. X. J. Loh, B. J. H. Yee and F. S. Chia, *J. Biomed. Mater. Res., Part A*, 2012, **100A**, 2686-2694.
84. X. J. Loh, W. Guerin and S. M. Guillaume, *J. Mater. Chem.*, 2012, **22**, 21249-21256.

85. X. J. Loh, S. H. Goh and J. Li, *J. Phys. Chem. B*, 2009, **113**, 11822-11830.
86. X. J. Loh and J. Li, *Expert Opin. Ther. Pat.*, 2007, **17**, 965-977.
87. X. J. Loh, S. H. Goh and J. Li, *Biomacromolecules*, 2007, **8**, 585-593.
88. X. J. Loh, K. K. Tan, X. Li and J. Li, *Biomaterials*, 2006, **27**, 1841-1850.
89. X. Li, X. J. Loh, K. Wang, C. B. He and J. Li, *Biomacromolecules*, 2005, **6**, 2740-2747.
90. D. Colombani, *Prog. Polym. Sci.*, 1997, **22**, 1649-1720.
91. V. Sciannamea, R. Jerome and C. Detrembleur, *Chem. Rev.*, 2008, **108**, 1104-1126.
92. J.-S. Wang and K. Matyjaszewski, *J. Am. Chem. Soc.*, 1995, **117**, 5614-5615.
93. J. Chiefari, Y. K. Chong, F. Ercole, J. Krstina, J. Jeffery, T. P. T. Le, R. T. A. Mayadunne, G. F. Meijs, C. L. Moad, G. Moad, E. Rizzardo and S. H. Thang, *Macromolecules*, 1998, **31**, 5559-5562.
94. J. M. Catala, F. Bubel and S. O. Hammouch, *Macromolecules*, 1995, **28**, 8441-8443.
95. S. Penczek, M. Cypryk, A. Duda, P. Kubisa and S. Słomkowski, *Prog. Polym. Sci.*, 2007, **32**, 247-282.
96. W. A. Braunecker and K. Matyjaszewski, *Prog. Polym. Sci.*, 2007, **32**, 93-146.
97. C. J. Hawker, A. W. Bosman and E. Harth, *Chem. Rev.*, 2001, **101**, 3661-3688.
98. K. Letchford and H. Burt, *Eur. J. Pharm. Biopharm.*, 2007, **65**, 259-269.
99. C. B. Liu, C. Y. Gong, Y. F. Pan, Y. D. Zhang, J. W. Wang, M. J. Huang, Y. S. Wang, K. Wang, M. L. Gou, M. J. Tu, Y. Q. Wei and Z. Y. Qian, *Colloids Surf. Physicochem. Eng. Aspects*, 2007, **302**, 430-438.
100. B. Li, S. C. Chen, Z. C. Qiu, Q. K. K. Yang, S. P. Tang, W. J. Yu and Y. Z. Wang, *Polym. Bull.*, 2008, **61**, 139-146.
101. L. P. Wu, L. Wang, X. J. Wang and K. T. Xu, *Acta Biomater.*, 2010, **6**, 1079-1089.
102. Y. Lemmouchi, M. C. Perry, A. J. Amass, K. Chakraborty and E. Schacht, *J. Polym. Sci., Part A: Polym. Chem.*, 2007, **45**, 3975-3985.
103. J. L. Hedrick, M. Trollsas, C. J. Hawker, B. Atthoff, H. Claesson, A. Heise, R. D. Miller, D. Mecerreyes, R. Jerome and P. Dubois, *Macromolecules*, 1998, **31**, 8691-8705.
104. J. K. Kim, D.-J. Park, M.-S. Lee and K. J. Ihn, *Polymer*, 2001, **42**, 7429-7441.
105. K. L. Liu, S. H. Goh and J. Li, *Polymer*, 2008, **49**, 732-741.
106. G. Maglio, A. Migliozzi and R. Palumbo, *Polymer*, 2003, **44**, 369-375.

107. N. Nomura, R. Ishii, M. Akakura and K. Aoi, *J. Am. Chem. Soc.*, 2002, **124**, 5938-5939.
108. A.-C. Albertsson and I. K. Varma, *Biomacromolecules*, 2003, **4**, 1466-1486.
109. X.-B. Xiong, Z. Binkhathlan, O. Molavi and A. Lavasanifar, *Acta Biomater.*, 2012, **8**, 2017-2033.
110. D. K. Gilding and A. M. Reed, *Polymer*, 1979, **20**, 1454-1458.
111. C. He, J. Sun, C. Deng, T. Zhao, M. Deng, X. Chen and X. Jing, *Biomacromolecules*, 2004, **5**, 2042-2047.
112. L. Jongpaiboonkit, Z. H. Zhou, X. P. Ni, Y. Z. Wang and J. Li, *J. Biomater. Sci. Polym. Ed.*, 2006, **17**, 747-763.
113. Q. Cai, J. Z. Bei and S. G. Wang, *Polym. Adv. Technol.*, 2000, **11**, 159-166.
114. D. W. Grijpma, G. J. Zondervan and A. J. Pennings, *Polym. Bull.*, 1991, **25**, 327-333.
115. L. Piao, J. Sun, Z. Zhong, Q. Liang, X. Chen, J.-H. Kim and X. Jing, *J. Appl. Polym. Sci.*, 2006, **102**, 2654-2660.
116. J. Albuérne, L. Marquez, A. J. Muller, J. M. Raquez, P. Degee, P. Dubois, V. Castelletto and I. W. Hamley, *Macromolecules*, 2003, **36**, 1633-1644.
117. M. S. Reeve, S. P. McCarthy and R. A. Gross, *Macromolecules*, 1993, **26**, 888-894.
118. L. Li, Z. Zhong, W. H. de Jeu, P. J. Dijkstra and J. Feijen, *Macromolecules*, 2004, **37**, 8641-8646.
119. L. Timbart, E. Renard, V. Langlois and P. Guerin, *Macromol. Biosci.*, 2004, **4**, 1014-1020.
120. K. J. Zhu, X. Z. Lin and S. L. Yang, *J. Appl. Polym. Sci.*, 1990, **39**, 1-9.
121. S. Zhou, X. Deng and H. Yang, *Biomaterials*, 2003, **24**, 3563-3570.
122. F. Ravenelle and R. H. Marchessault, *Biomacromolecules*, 2002, **3**, 1057-1064.
123. R. Gref, A. Domb, P. Quellec, T. Blunk, R. H. Müller, J. M. Verbavatz and R. Langer, *Adv. Drug Delivery Rev.*, 1995, **16**, 215-233.
124. E. Bat, D. W. Grijpma and J. Feijen, *J. Controlled Release*, 2008, **132**, e37-e39.
125. H. S. Yoo and T. G. Park, *J. Controlled Release*, 2001, **70**, 63-70.
126. S. Stolnik, L. Illum and S. S. Davis, *Adv. Drug Delivery Rev.*, 1995, **16**, 195-214.
127. L. P. Wu, S. T. Chen, Z. B. Li, K. T. Xu and G. Q. Chen, *Polym. Int.*, 2008, **57**, 939-949.

128. Q. Cai, J. Z. Bei and S. G. Wang, *J. Biomater. Sci., Polym. Ed.*, 2000, **11**, 273-288.
129. M. Ryner and A.-C. Albertsson, *Biomacromolecules*, 2002, **3**, 601-608.
130. S. Hiki, M. Miyamoto and Y. Kimura, *Polymer*, 2000, **41**, 7369-7379.
131. J. H. Kim and J. H. Lee, *Polym. J.*, 2002, **34**, 203-208.
132. C. B. Liu, C. Y. Gong, M. J. Huang, J. W. Wang, Y. F. Pan, Y. D. Zhang, G. Z. Li, M. L. Gou, K. Wang, M. J. Tu, Y. Q. Wei and Z. Y. Qian, *J. Biomed. Mater. Res. B Appl. Biomater.*, 2008, **84B**, 165-175.
133. N.-V. Cuong, M.-F. Hsieh, Y.-T. Chen and I. Liao, *J. Appl. Polym. Sci.*, 2010, **117**, 3694-3703.
134. X. Li, K. Y. Mya, X. P. Ni, C. B. He, K. W. Leong and J. Li, *J. Phys. Chem. B*, 2006, **110**, 5920-5926.
135. L. Liu, C. Li, X. Li, Z. Yuan, Y. An and B. He, *J. Appl. Polym. Sci.*, 2001, **80**, 1976-1982.
136. G. He, L. L. Ma, J. Pan and S. Venkatraman, *Int. J. Pharm.*, 2007, **334**, 48-55.
137. K. L. Liu, J.-I. Zhu and J. Li, *Soft Matter*, 2010, **6**, 2300-2311.
138. J. H. Jeong, S. W. Kim and T. G. Park, *Pharm. Res.*, 2004, **21**, 50-54.
139. B. Jeong, Y. H. Bae and S. W. Kim, *J. Controlled Release*, 2000, **63**, 155-163.
140. T. Kissel, Y. X. Li and F. Unger, *Adv. Drug Delivery Rev.*, 2002, **54**, 99-134.
141. C. Gong, S. Shi, P. Dong, B. Kan, M. Gou, X. Wang, X. Li, F. Luo, X. Zhao, Y. Wei and Z. Qian, *Int. J. Pharm.*, 2009, **365**, 89-99.
142. B. Jeong, Y. H. Bae, D. S. Lee and S. W. Kim, *Nature*, 1997, **388**, 860-862.
143. F. Li, S. Li, A. El Ghzaoui, H. Nouailhas and R. Zhuo, *Langmuir*, 2007, **23**, 2778-2783.
144. T. Mukose, T. Fujiwara, J. Nakano, I. Taniguchi, M. Miyamoto, Y. Kimura, I. Teraoka and C. W. Lee, *Macromol. Biosci.*, 2004, **4**, 361-367.
145. J. Li, X. Li, Z. Zhou, X. Ni and K. W. Leong, *Macromolecules*, 2001, **34**, 7236-7237.
146. D. Cohn and A. F. Salomon, *Biomaterials*, 2005, **26**, 2297-2305.
147. Z. F. Chen, S. T. Cheng and K. T. Xu, *Biomaterials*, 2009, **30**, 2219-2230.
148. Z. F. Chen, S. T. Cheng, Z. B. Li, K. T. Xu and G. Q. Chen, *J. Biomater. Sci.-Polym. Ed.*, 2009, **20**, 1451-1471.
149. Q. Liu, S. Cheng, Z. Li, K. Xu and G.-Q. Chen, *J. Biomed. Mater. Res., Part A*, 2009, **90A**, 1162-1176.

150. Y. Wan, W. Chen, J. Yang, J. Bei and S. Wang, *Biomaterials*, 2003, **24**, 2195-2203.
151. J. H. You, S. W. Choi, J. H. Kim and Y. T. Kwak, *Macromol. Res.*, 2008, **16**, 609-613.
152. X. Li, K. L. Liu, M. Wang, S. Y. Wong, W. C. Tjiu, C. B. He, S. H. Goh and J. Li, *Acta Biomater.*, 2009, **5**, 2002-2012.
153. J. Y. Pan, G. Y. Li, Z. F. Chen, X. Y. Chen, W. F. Zhu and K. T. Xu, *Biomaterials*, 2009, **30**, 2975-2984.
154. M. W. Neiser, S. Muth, U. Kolb, J. R. Harris, J. Okuda and M. Schmidt, *Angew. Chem. Int. Ed.*, 2004, **43**, 3192-3195.
155. J.-B. Kim, W. Huang, C. Wang, M. Bruening and G. L. Baker, in *Polymer Brushes*, ed. W. J. B. K. C. C. J. R. Rigoberto C. Advincula, 2005, pp. 105-117.
156. J. Pyun, T. Kowalewski and K. Matyjaszewski, in *Polymer Brushes*, ed. W. J. B. K. C. C. J. R. Rigoberto C. Advincula, 2005, pp. 51-68.
157. S. G. Boyes, A. M. Granville, M. Baum, B. Akgun, B. K. Mirous and W. J. Brittain, in *Polymer Brushes*, ed. W. J. B. K. C. C. J. R. Rigoberto C. Advincula, 2005, pp. 151-165.
158. F. Tasaka, Y. Ohya and T. Ouchi, *Macromolecules*, 2001, **34**, 5494-5500.
159. L. He, Y. Zhang, L. Ren, Y. Chen, H. Wei and D. Wang, *Macromol. Chem. Phys.*, 2006, **207**, 684-693.
160. Cheng, Zhu, E. T. Kang and K. G. Neoh, *Langmuir*, 2005, **21**, 7180-7185.
161. J.-Z. Du, D.-P. Chen, Y.-C. Wang, C.-S. Xiao, Y.-J. Lu, J. Wang and G.-Z. Zhang, *Biomacromolecules*, 2006, **7**, 1898-1903.
162. D.-Q. Wu, F. Qiu, T. Wang, X.-J. Jiang, X.-Z. Zhang and R.-X. Zhuo, *ACS Appl. Mater. Interfaces*, 2009, **1**, 319-327.
163. D.-Q. Wu, Y.-X. Sun, X.-D. Xu, S.-X. Cheng, X.-Z. Zhang and R.-X. Zhuo, *Biomacromolecules*, 2008, **9**, 1155-1162.
164. J. Z. Du, L. Y. Tang, W. J. Song, Y. Shi and J. Wang, *Biomacromolecules*, 2009, **10**, 2169-2174.
165. J. L. Zhu, H. Cheng, Y. Jin, S. X. Cheng, X. Z. Zhang and R. X. Zhuo, *J. Mater. Chem.*, 2008, **18**, 4433-4441.
166. C. G. Oster, M. Wittmar, U. Bakowsky and T. Kissel, *J. Controlled Release*, 2006, **111**, 371-381.
167. K. Stridsberg, M. Ryner and A.-C. Albertsson, in *Degradable Aliphatic Polyesters*, 2002, pp. 41-65.
168. J. P. Jain and N. Kumar, *Biomacromolecules*, 2010, **11**, 1027-1035.



169. C. R. Yates and W. Hayes, *Eur. Polym. J.*, 2004, **40**, 1257-1281.
170. J. Li and X. J. Loh, *Adv. Drug Delivery Rev.*, 2008, **60**, 1000-1017.
171. J. W. Steed and J. L. Atwood, in *Supramolecular Chemistry (Second Edition)*, 2009, pp. 307-384.
172. A. Harada, J. Li and M. Kamachi, *Nature*, 1992, **356**, 325-327.
173. A. Harada, J. Li and M. Kamachi, *Nature*, 1993, **364**, 516-518.
174. A. Harada, J. Li and M. Kamachi, *Nature*, 1994, **370**, 126-128.
175. A. Harada, A. Hashidzume, H. Yamaguchi and Y. Takashima, *Chem. Rev.*, 2009, **109**, 5974-6023.
176. K.-m. Shin, T. Dong, Y. He, Y. Taguchi, A. Oishi, H. Nishida and Y. Inoue, *Macromol. Biosci.*, 2004, **4**, 1075-1083.
177. G. Wenz, B. H. Han and A. Muller, *Chem. Rev.*, 2006, **106**, 782-817.
178. J. Lu, I. D. Shin, S. Nojima and A. E. Tonelli, *Polymer*, 2000, **41**, 5871-5883.
179. S.-P. Zhao, L.-M. Zhang and D. Ma, *J. Phys. Chem. B*, 2006, **110**, 12225-12229.
180. X. Li, J. Li and K. W. Leong, *Macromolecules*, 2003, **36**, 1209-1214.
181. H. S. Choi, T. Ooya, S. Sasaki, N. Yui, Y. Ohya, T. Nakai and T. Ouchi, *Macromolecules*, 2003, **36**, 9313-9318.
182. J. Li, X. P. Ni, Z. H. Zhou and K. W. Leong, *J. Am. Chem. Soc.*, 2003, **125**, 1788-1795.
183. J. Li, X. P. Ni and K. Leong, *Angew. Chem. Int. Ed.*, 2003, **42**, 69-72.
184. C. A. Dreiss, E. Nwabunwanne, R. Liu and N. J. Brooks, *Soft Matter*, 2009, **5**, 1888-1896.
185. X. Shuai, F. E. Porbeni, M. Wei, T. Bullions and A. E. Tonelli, *Macromolecules*, 2002, **35**, 2401-2405.
186. J. Li, A. Harada and M. Kamachi, *Polym. J.*, 1994, **26**, 1019-1026.
187. H. X. X. Z. Yapei Wang, *Adv. Mater.*, 2009, **9999**, NA.
188. N. Schaschke, I. Assfalg-Machleidt, W. Machleidt, T. Laßleben, C. P. Sommerhoff and L. Moroder, *Biorg. Med. Chem. Lett.*, 2000, **10**, 677-680.
189. J. M. Dang and K. W. Leong, *Adv. Drug Delivery Rev.*, 2006, **58**, 487-499.
190. D. W. Hutmacher, J. T. Schantz, C. X. F. Lam, K. C. Tan and T. C. Lim, *J Tissue Eng Regen Med*, 2007, **1**, 245-260.

191. M. Martina and D. W. Hutmacher, *Polym. Int.*, 2007, **56**, 145-157.
192. S. M. Li, I. Molina, M. B. Martinez and M. Vert, *J. Mater. Sci. Mater. Med.*, 2002, **13**, 81-86.
193. S.-H. Lee, B.-S. Kim, S. H. Kim, S. W. Choi, S. I. Jeong, I. K. Kwon, S. W. Kang, J. Nikolovski, D. J. Mooney, Y.-K. Han and Y. H. Kim, *J. Biomed. Mater. Res., Part A*, 2003, **66A**, 29-37.
194. D. Cohn, T. Stern, M. F. González and J. Epstein, *J. Biomed. Mater. Res.*, 2002, **59**, 273-281.
195. H. Guan, Z. Xie, P. Zhang, C. Deng, X. Chen and X. Jing, *Biomacromolecules*, 2005, **6**, 1954-1960.
196. D. J. Mooney, D. F. Baldwin, N. P. Suh, L. P. Vacanti and R. Langer, *Biomaterials*, 1996, **17**, 1417-1422.
197. J. L. Drury and D. J. Mooney, *Biomaterials*, 2003, **24**, 4337-4351.
198. B. Dhandayuthapani, Y. Yoshida, T. Maekawa and D. S. Kumar, *Int. J. Polym.Sci.*, 2011, **2011**, 1-19.
199. Z. M. O. Rzaev, S. Dincer and E. Piskin, *Prog. Polym. Sci.*, 2007, **32**, 534-595.
200. P. Bhargava, Y. F. Tu, J. X. Zheng, H. M. Xiong, R. P. Quirk and S. Z. D. Cheng, *J. Am. Chem. Soc.*, 2007, **129**, 1113-1121.
201. Y. Xia, X. Yin, N. A. D. Burke and H. D. H. Stöver, *Macromolecules*, 2005, **38**, 5937-5943.
202. K. Uchida, K. Sakai, E. Ito, O. Hyeong Kwon, A. Kikuchi, M. Yamato and T. Okano, *Biomaterials*, 2000, **21**, 923-929.
203. H. Hatakeyama, A. Kikuchi, M. Yamato and T. Okano, *Biomaterials*, 2005, **26**, 5167-5176.
204. T. Shimizu, M. Yamato, A. Kikuchi and T. Okano, *Biomaterials*, 2003, **24**, 2309-2316.
205. K. Nishida, M. Yamato, Y. Hayashida, K. Watanabe, N. Maeda, H. Watanabe, K. Yamamoto, S. Nagai, A. Kikuchi, Y. Tano and T. Okano, *Transplantation*, 2004, **77**, 379-385.
206. X. J. Loh, Z.-X. Zhang, Y.-L. Wu, T. S. Lee and J. Li, *Macromolecules*, 2009, **42**, 194-202.
207. X. J. Loh, Y. L. Wu, W. T. J. Seow, M. N. I. Norimzan, Z. X. Zhang, F. Xu, E. T. Kang, K. G. Neoh and J. Li, *Polymer*, 2008, **49**, 5084-5094.
208. X. J. Loh, W. C. D. Cheong, J. Li and Y. Ito, *Soft Matter*, 2009, **5**, 2937-2946.

209. X. J. Loh, J. S. Gong, M. Sakuragi, T. Kitajima, M. Z. Liu, J. Li and Y. Ito, *Macromol. Biosci.*, 2009, **9**, 1069-1079.
210. V. G. De Bruijn, L. J. P. Van den Broeke, F. A. M. Leermakers and J. T. F. Keurentjes, *Langmuir*, 2002, **18**, 10467-10474.
211. K. Mortensen, W. Brown and E. Joergensen, *Macromolecules*, 1994, **27**, 5654-5666.
212. F. Cellési, N. Tirelli and J. A. Hubbell, *Macromol. Chem. Phys.*, 2002, **203**, 1466-1472.
213. S. F. Khattak, S. R. Bhatia and S. C. Roberts, *Tissue Eng.*, 2005, **11**, 974-983.
214. A. Higuchi, T. Yamamoto, K. Sugiyama, S. Hayashi, T. M. Tak and T. Nakagawa, *Biomacromolecules*, 2005, **6**, 691-696.
215. A. Higuchi, S. Tamiya, T. Tsubomura, A. Katoh, C.-S. Cho, T. Akaike and M. Hara, *J. Biomater. Sci. Polym. Ed.*, 2000, **11**, 149-168.
216. A. Higuchi, K. Sugiyama, B. O. Yoon, M. Sakurai, M. Hara, M. Sumita, S.-i. Sugawara and T. Shirai, *Biomaterials*, 2003, **24**, 3235-3245.
217. A. Higuchi, N. Aoki, T. Yamamoto, T. Miyazaki, H. Fukushima, T. M. Tak, S. Jyujyoji, S. Egashira, Y. Matsuoka and S. H. Natori, *J. Biomed. Mater. Res., Part A*, 2006, **79A**, 380-392.
218. T. Amanuma, H. Iwata, H. Kanehiro, H. Kuge, Y. Nakajima, K. Ohashi, T. Okano, M. Tsutsumi, M. Yamato, J. Yang and T. Yokoyama, *Nat. Med.*, 2007, **13**, 880-885.
219. M. A. Laflamme and C. E. Murry, *Nat. Biotechnol.*, 2005, **23**, 845-856.
220. E. Cukierman, R. Pankov, D. R. Stevens and K. M. Yamada, *Science*, 2001, **294**, 1708-1712.
221. K. Bott, Z. Upton, K. Schrobback, M. Ehrbar, J. A. Hubbell, M. P. Lutolf and S. C. Rizzi, *Biomaterials*, 2010, **31**, 8454-8464.
222. T. Konno and K. Ishihara, *Biomaterials*, 2007, **28**, 1770-1777.
223. D. Q. Wu, T. Wang, B. Lu, X. D. Xu, S. X. Cheng, X. J. Jiang, X. Z. Zhang and R. X. Zhuo, *Langmuir*, 2008, **24**, 10306-10312.
224. C. R. Nuttelman, M. A. Rice, A. E. Rydholm, C. N. Salinas, D. N. Shah and K. S. Anseth, *Prog. Polym. Sci.*, 2008, **33**, 167-179.
225. Y. S. Pek, A. C. A. Wan, A. Shekaran, L. Zhuo and J. Y. Ying, *Nat Nanotechnol*, 2008, **3**, 671-675.
226. Y. Li, J. Rodrigues and H. Tomas, *Chem. Soc. Rev.*, 2012, **41**, 2193-2221.
227. L. E. Bromberg and E. S. Ron, *Adv. Drug Delivery Rev.*, 1998, **31**, 197-221.

228. J. Li, X. Li, X. Ni, X. Wang, H. Li and K. W. Leong, *Biomaterials*, 2006, **27**, 4132-4140.
229. R. Barbucci, D. Pasqui, R. Favaloro and G. Panariello, *Carbohydr. Res.*, 2008, **343**, 3058-3065.
230. Y. S. Pek, A. C. A. Wan and J. Y. Ying, *Biomaterials*, 2010, **31**, 385-391.
231. Y. H. Bae and S. W. Kim, *Adv. Drug Delivery Rev.*, 1993, **11**, 109-135.
232. A. K. A. Silva, C. Richard, M. Bessodes, D. Scherman and O.-W. Merten, *Biomacromolecules*, 2009, **10**, 9-18.
233. D.-Q. Wu, T. Wang, B. Lu, X.-D. Xu, S.-X. Cheng, X.-J. Jiang, X.-Z. Zhang and R.-X. Zhuo, *Langmuir*, 2008, **24**, 10306-10312.
234. R. A. Stile, W. R. Burghardt and K. E. Healy, *Macromolecules*, 1999, **32**, 7370-7379.
235. J. Roseman T and H. Yalkowsky S, in *Controlled Release Polymeric Formulations*, AMERICAN CHEMICAL SOCIETY, 1976, vol. 33, ch. 4, pp. 33-52.
236. K. E. Uhrich, S. M. Cannizzaro, R. S. Langer and K. M. Shakesheff, *Chem. Rev.*, 1999, **99**, 3181-3198.
237. Y. Lin;, Y. Qiao;, Y. Yan; and J. Huang;, *Soft Matter*, 2009, **5**, 7.
238. J.-F. Gohy, in *Block Copolymers in Nanoscience*, ed. P. D. G. L. P. D. S. L. Prof. Dr. Massimo Lazzari, 2008, pp. 91-116.
239. T. J. Deming, *Soft Matter*, 2005, **1**, 28-35.
240. Y. Bae, H. Cabral and K. Kataoka, in *Block Copolymers in Nanoscience*, ed. P. D. G. L. P. D. S. L. Prof. Dr. Massimo Lazzari, 2008, pp. 73-89.
241. K. Kataoka, A. Harada and Y. Nagasaki, *Adv. Drug Delivery Rev.*, 2001, **47**, 113-131.
242. A. S. Hoffman, *Adv. Drug Delivery Rev.*, 2002, **54**, 3-12.
243. T. Kissel, Y. Li and F. Unger, *Adv. Drug Delivery Rev.*, 2002, **54**, 99-134.
244. Y. Zhang, W. Zhu, B. Wang and J. Ding, *J. Controlled Release*, 2005, **105**, 260-268.
245. S. V. Graeter, J. Huang, N. Perschmann, M. López-García, H. Kessler, J. Ding and J. P. Spatz, *Nano Lett.*, 2007, **7**, 1413-1418.
246. L. Klouda and A. G. Mikos, *Eur. J. Pharm. Biopharm.*, 2008, **68**, 34-45.
247. C. He, S. W. Kim and D. S. Lee, *J. Controlled Release*, 2008, **127**, 189-207.
248. E. Ruel-Gariépy and J.-C. Leroux, *Eur. J. Pharm. Biopharm.*, 2004, **58**, 409-426.

249. S. H. Park, B. G. Choi, M. K. Joo, D. K. Han, Y. S. Sohn and B. Jeong, *Macromolecules*, 2008, **41**, 6486-6492.
250. S. C. Lee, Y. Chang, J.-S. Yoon, C. Kim, I. C. Kwon, Y.-H. Kim and S. Y. Jeong, *Macromolecules*, 1999, **32**, 1847-1852.
251. B. Jeong, Y. H. Bae and S. W. Kim, *Macromolecules*, 1999, **32**, 7064-7069.
252. S. J. Bae, J. M. Suh, Y. S. Sohn, Y. H. Bae, S. W. Kim and B. Jeong, *Macromolecules*, 2005, **38**, 5260-5265.
253. S. J. Bae, M. K. Joo, Y. Jeong, S. W. Kim, W.-K. Lee, Y. S. Sohn and B. Jeong, *Macromolecules*, 2006, **39**, 4873-4879.
254. B. Jeong, C. F. Windisch, M. J. Park, Y. S. Sohn, A. Gutowska and K. Char, *J. Phys. Chem. B*, 2003, **107**, 10032-10039.
255. M. J. Hwang, J. M. Suh, Y. H. Bae, S. W. Kim and B. Jeong, *Biomacromolecules*, 2005, **6**, 885-890.
256. B. Jeong, S. W. Kim and Y. H. Bae, *Adv. Drug Delivery Rev.*, 2002, **54**, 37-51.
257. H. Tian, C. Deng, H. Lin, J. Sun, M. Deng, X. Chen and X. Jing, *Biomaterials*, 2005, **26**, 4209-4217.
258. N. Kumar, M. N. V. Ravikumar and A. J. Domb, *Adv. Drug Delivery Rev.*, 2001, **53**, 23-44.
259. G. Gaucher, M.-H. Dufresne, V. P. Sant, N. Kang, D. Maysinger and J.-C. Leroux, *J. Controlled Release*, 2005, **109**, 169-188.
260. C. Y. Gong, S. Shi, X. H. Wang, Y. J. Wang, S. Z. Fu, P. W. Dong, L. J. Chen, X. Zhao, Y. Q. Wei and Z. Y. Qian, *J. Phys. Chem. B*, 2009, **113**, 10183-10188.
261. M. K. Nguyen and D. S. Lee, *Macromol. Biosci.*, 2010, **10**, 17.
262. E. S. Gil and S. M. Hudson, *Prog. Polym. Sci.*, 2004, **29**, 1173-1222.
263. J. K. Oh, *Soft Matter*, 2011, **7**, 5096-5108.
264. E. K. Park, S. B. Lee and Y. M. Lee, *Biomaterials*, 2005, **26**, 1053-1061.
265. C. Yang, H. Li, S. H. Goh and J. Li, *Biomaterials*, 2007, **28**, 3245-3254.
266. C. Yang, X. P. Ni and J. Li, *Polymer*, 2009, **50**, 4496-4504.
267. C. Yang, X. Wang, H. Li, S. H. Goh and J. Li, *Biomacromolecules*, 2007, **8**, 3365-3374.
268. C. Yang, J. Yang, X. Ni and J. Li, *Macromolecules*, 2009, **42**, 3856-3859.
269. C. A. Yang, H. Z. Li, X. Wang and J. Li, *J. Biomed. Mater. Res., Part A*, 2009, **89A**, 13-23.

270. A. Harada and K. Kataoka, *Prog. Polym. Sci.*, 2006, **31**, 949-982.
271. J. Li, C. Yang, H. Z. Li, X. Wang, S. H. Goh, J. L. Ding, D. Y. Wang and K. W. Leong, *Adv. Mater.*, 2006, **18**, 2969-2974.
272. P. Dubruel and E. Schacht, *Macromol. Biosci.*, 2006, **6**, 789-810.
273. T. Ooya, H. S. Choi, A. Yamashita, N. Yui, Y. Sugaya, A. Kano, A. Maruyama, H. Akita, R. Ito, K. Kogure and H. Harashima, *J. Am. Chem. Soc.*, 2006, **128**, 3852-3853.
274. Y. Zhou, H. Wang, C. Wang, Y. Li, W. Lu, S. Chen, J. Luo, Y. Jiang and J. Chen, *Mol. Pharm.*, 2012, **9**, 1067-1076.
275. N. Yui and T. Ooya, *Chem. Eur. J.*, 2006, **12**, 6730-6737.
276. L. Jun, *NPG Asia Mater*, 2010, **2**, 112-118.
277. X. Li and J. Li, *J. Biomed. Mater. Res., Part A*, 2008, **86A**, 1055-1061.
278. Z. Li, H. Yin, Z. Zhang, K. L. Liu and J. Li, *Biomacromolecules*, 2012, **13**, 3162-3172.
279. K. L. Liu, Z. Zhang and J. Li, *Soft Matter*, 2011, **7**, 11290-11297.
280. K. L. Liu, J. L. Zhu and J. Li, *Soft Matter*, 2010, **6**, 2300-2311.
281. K. L. Liu, S. H. Goh and J. Li, *Macromolecules*, 2008, **41**, 6027-6034.
282. J. Li, F. Zhao and J. Li, *Appl. Microbiol. Biotechnol.*, 2011, **90**, 427-443.

## **CHAPTER 3 BIODEGRADABLE PCL-BASED HAIRY BLOCK COPOLYMERS: SYNTHESIS AND CHARACTERIZATION, THERMAL-SENSITIVE NANO-AGGREGATES AND SURFACE COATING FOR FACILE CELL RECOVERY**

### **3.1 Introduction**

Block copolymers can self-assemble into intriguing aggregates of varying shapes and sizes in such as micelles, vesicles, polymersomes, fibers, liposomes and hydrogels.<sup>1-5</sup> Recently, intense efforts have been directed to the development of materials that respond to external stimulus, such as pH, temperature, redox potential, light, magnetic field, electrostatic absorption, and ultrasound.<sup>6-8</sup> These stimuli-sensitive properties can be achieved by introducing stimulus responsive functional groups into the copolymer backbone to form graft,<sup>9</sup> branched,<sup>10</sup> or block copolymers.<sup>11</sup> Different aggregation processes corresponding to appropriate stimulus could be used as triggers for novel biotechnological applications including programmed delivery of encapsulated drugs and tissue regeneration.<sup>12-15</sup>

Thermally responsive polymers with tunable properties stimulated by external temperature have been received significant attention due to the utilization of temperature as the only trigger.<sup>16-18</sup> Poly(N-isopropylacrylamide) (PNIPAAm), for instance, exhibits a lower critical solution temperature (LCST) transition temperature of 32 to 33 °C, being hydrophilic at low temperatures and precipitating at above the critical phase transition temperatures.<sup>19</sup> The copolymerization with other components such as butylmethacrylate (BMA), acrylic acid (AAc), poly(DL-lactic acid) (PDLLA), poly(lactic-*co*-glycolic acid) (PLGA) or poly( $\epsilon$ -caprolactone) (PCL) has been widely studied for the temperature-induced delivery of calcitonin, insulin, and

other drug delivery applications.<sup>20-24</sup> Recently, several researchers have reported the hydrophobic surface modified by PNIPAAm at above its LCST can support cell adhesion and growth, and facilitate cells recovery through non-enzymatic method by cooling the temperature below LCST.<sup>25-28</sup> This observation is explained by dehydration to hydration transition of PNIPAAm with temperature. Previously, we reported the synthesis of PNIPAAm based triblock copolymers centred on a biodegradable aliphatic PCL or poly((R)-hydroxybutyrate) (PHB) segments using atom transfer radical polymerization (ATRP), respectively.<sup>29, 30</sup> Studies showed that the copolymers aqueous solutions possessed thermal sensitivity with temperature alternation across their corresponding LCST. More interestingly, PNIPAAm-PHB-PNIPAAm triblock copolymer micelle solution coated surface afforded cell detachment with preserved cell-cell and cell-extracellular matrix interactions, unlike the typical approach of using proteases, such as trypsin, to detach cells.<sup>31, 32</sup> Similarly, the mild technique of cell detachment has been employed by other researchers for the generation of cell sheets.<sup>26-28</sup> However, most of the investigations related to temperature-induced cell adhesion and detachment are limited to those using PNIPAAm as culture surface.

Poly(propylene oxide) (PPO) is another fascinating candidate when building thermo-sensitive block copolymers as biomaterials. PPO contained polymers show transition temperatures range from 14 °C to 100 °C, depending on the polymer architecture and molecular weight.<sup>33, 34</sup> The wide temperature transition range makes PPO more promising in designing versatile thermo-responsive copolymers for temperature-dependent cell detachment. The copolymers of poly(ethylene oxide)-poly(propylene oxide)-poly(ethylene oxide) (PEO-PPO-PEO), commercially known as Pluronic or Poloxamer, possesses excellent transformation from micelle to gel at specific temperatures and concentrations via micellar bridge mechanism.<sup>18, 34</sup> Temperature-induced L929 cells and normal human umbilical vein endothelial cells (HUVECs) detachment from F127 gels were investigated.<sup>35</sup> However, the high hydrophilicity of F127 gels tends to dissolve in the culture medium and suppresses the effect in cell recovery. It has been previously reported that the cell growth on hydrophilic surfaces is not favorable and such a surface would inhibit the growth of the cells.<sup>36</sup> The high flexibility of PEO segments in aqueous medium suppressed Pluronic coated substrates in plasma protein adsorption and platelet adhesion.<sup>37</sup> Immobilization of Pluronic on the surface of tissue culture flask showed more effective for the cell culture compared to the Pluronic gels.<sup>38</sup> Nevertheless, the cell density also decreased sharply with increasing surface concentration of immobilized Pluronic. The complicated chemical reactions involved in the immobilization process also limit its applications.



Herein, novel P(PPOMA)-PCL-P(PPOMA) hairy block copolymers with thermally responsive properties were designed for cell recovery applications. The central biodegradable PCL segment in the targeted block copolymer structure served to enhance the copolymer absorption to tissue cell culture surface by self-assembly of hydrophobic interaction. Instead of chemical reaction and spin coating, an easy drop-casting approach to prepare homogeneous coatings for temperature-induced cell detachment was illustrated. P(PPOMA)-PCL-P(PPOMA) copolymers formed micelles with a hydrophilic PPO corona and hydrophobic PCL core at low temperature. More interestingly, the micelle formation self-assembled into hydrophobic nano-associations after the PPO phase transition at temperature above LCST. The copolymer coated substrates supported a high cell growth in good viability as compared with the cells cultured on Tissue Culture Polystyrene (TCPS). After a period of culture, the cells could be detached effectively by cooling at 4 °C for 30 min without trypsin treatment.

### 3.2 Experimental Section

#### 3.2.1 Materials

Dihydroxyl-terminated poly( $\epsilon$ -caprolactone) (PCL-diol,  $M_n = 2000$  and 530), 2-bromoisobutryl bromide (98%), Poly(propylene oxide) methacrylate (PPOMA,  $M_n = 375$ ), 1,1,4,7,10,10-hexamethyltriethylenetetramine (HMTETA, 99%), copper(I) bromide (CuBr, 99%), Ethyl 2-bromoisobutyrate (EBiB, 98%), triethylamine (>99%) and 2-propanol (>99.5%) were obtained from Aldrich Chemical Co. of Milwaukee, WI. Purified nitrogen was used in all reactions.

#### 3.2.2 Synthesis Methods

##### Synthesis of P(PPOMA)-PCL-P(PPOMA) Hairy Block Copolymer by ATRP

PCL-diBr macroinitiator was prepared according to the previously reported method with revisions.<sup>30,39</sup> Typically, 5.0 mmol PCL-diol ( $M_n = 2000$ ) was dissolved in 50 mL of anhydrous tetrahydrofuran (THF) containing 10 mmol of triethylamine in a 250 mL round bottom flask. Reaction was carried out at 4 °C. 2-Bromoisobutryl bromide (10.5 mmol), a slight excess of the stoichiometric amount of -OH groups, was added into the flask dropwisely through an

equalizing funnel. After addition, the reaction was sealed and kept at room temperature for another 24 h. After reaction, the resultant solution was centrifuged to remove triethylamine·HCl salt before it was poured into excess hexane for precipitation. After another cycle of THF dissolution, hexane re-precipitation and double washing with water, the purified PCL-diBr was obtained. Finally, the PCL-diBr was dried under reduced pressure (yield, 70%).

Hairy block copolymers poly(propylene oxide) methacrylate-poly( $\epsilon$ -caprolactone)-poly(propylene oxide) methacrylate (P(PPOMA)-PCL-P(PPOMA)) were synthesized using a feed ratio [PPOMA (53.3 mmol,  $M_n$  = 375 g/mol)]/[Br-PCL-Br (1.1 mmol,  $M_n$  = 2100 g/mol)]/[CuBr (1.1 mmol)]/[HMTETA (2.2 mmol)] of 48:1:1:2. Reaction was performed in a 50 mL flask equipped with a magnetic stir bar. PPOMA, PCL-diBr, and HMTETA were introduced into the flask containing 25 mL of 2-propanol. After the reactants were dissolved completely, the reactant mixture was degassed by bubbling nitrogen for 30 min. CuBr was added into the flask under nitrogen atmosphere. The reaction was further purged with nitrogen for 10 min. The flask was then sealed and kept under nitrogen atmosphere and polymerization was allowed to proceed under continuous stirring at 45 °C for 0.5 – 5.5 h. The reaction was stopped by diluting with THF and exposing the system to air for 1 h. The copper catalyst complex was removed by passing through a short neutral aluminium oxide column. THF was removed under reduced pressure to give a concentrated solution. Products were collected by precipitation in excess hexane. By changing the macroinitiator into PCL-diBr ( $M_n$  = 530), another series of hairy block copolymers were synthesized. Poly(PPOMA) without PCL segment was prepared as a control..

### 3.2.3 Methods and Characterization

**Molecular Characterization.**  $^1\text{H}$  and  $^{13}\text{C}$  NMR spectra were recorded on a Bruker AV-400 NMR spectrometer at room temperature. Chemical shift at 7.3 ppm and 4.7 ppm were referred to the solvent peaks  $\text{CHCl}_3$  and  $\text{H}_2\text{O}$ , respectively. Gel permeation chromatography (GPC) is not an accurate method for molecule weight determination of brush-structure macromolecules.<sup>40</sup> Instead, molecular weight was evaluated by integrating the proton chemical shifts -OCH- and -OCH<sub>2</sub>- in PPO units from 3.25 - 3.71 ppm and the area of -CH<sub>2</sub>- in PCL unit at 4.1 ppm. Polydispersity of PCP hairy copolymer was estimated by GPC analysis (Shimadzu SCL-10A). THF was used as eluent at a flow rate of 0.30 mL/min at 40 °C.

**Thermal Analysis.** Thermogravimetric analyses (TGA) were conducted using the TA Instruments SDT 2960. Samples were heated at 20 °C/min to 800 °C under nitrogen flow rate

of 70 mL/min. Differential scanning calorimetry (DSC) were performed on TA Instruments 2920 differential scanning calorimeter with an auto-refrigerated cooling system and calibrated using indium. Each sample was tested by the following protocol: heating from room temperature to 170 °C at 20 °C/min, holding at 170 °C for 2 min, cooling from 170 to -30 °C at 5 °C/min, and reheating from -30 to 170 °C at 5 °C/min. Data were collected from the second heating runs.

#### **Critical Aggregation Concentration Determination by Fluorescence Spectroscopy.**

Steady-state fluorescence spectra were recorded on a Shimadzu RF-5301PC spectrofluorophotometer. Excitation spectra were monitored at 390 nm. Slit widths for both excitation and emission sides were maintained at 3.0 nm. Sample solutions were prepared by adding a predetermined amount of block copolymer solution into an aqueous pyrene solution of known concentration, and the solutions were allowed to stand for 1 day for equilibration. The concentration of pyrene was kept at  $6.0 \times 10^{-7}$  M.

**Lower Critical Solution Temperature Determination.** Lower critical solution temperature (LCST) was measured by UV-Vis spectrophotometer. The LCST was determined by the temperature which exhibited a 50% reduction in optical transmittance of the aqueous copolymer solutions. During the measurements, temperature was increased by 2 °C interval and equilibrated for 5 min before each transmittance value was record. The concentrations used in the measurements were at  $1 \times 10^3$  mg/L and  $2.5 \times 10^2$  mg/L for the two PCL(  $M_n = 530$  and  $M_n = 2000$ ) initiated copolymers, respectively. Poly(PPOMA) homopolymer with the similar molecular weight ( $M_n = 8000$ ) to the PCP copolymers was used as control.

**Particle Size Measurements.** Particle size and size distribution were determined by dynamic light scattering (DLS) using a Brookhaven 90Plus particle size analyzer with angle detection of 90°. Polymer solution (25 mg/L) was passed through a 0.45 mm pore-sized syringe filter before the measurement. Each analysis lasted for 10 runs at predetermined temperatures (5 °C or 35 °C). For the reversible transition test, polymer solutions were equilibrated at the two abovementioned temperatures overnight between each measurement run. Six parallel analyses were carried out and the average value was reported. Homopolymer poly(PPOMA) aqueous solution was used as control.

**Transmission Electron Microscopy.** Samples were imaged on a JEOL JEM-2010F FasTEM field emission transmission electron microscope (TEM) operated at 100 kV. Samples were prepared by directly depositing one drop (10  $\mu$ L) of the copolymer solution (25 mg/L) containing 0.01 wt% phosphotungstic acid (PTA) onto 200 mesh copper grids, which were

coated in advance with supportive Formvar films and carbon (Agar Scientific). The samples were kept for 24 h at 5 °C or 35 °C before TEM imaging.

### 3.2.4 Thermally Induced Cell Detachment

**Coating of Copolymers on Cell Culture Substrates.** 1 mL of PCP (3590-2000-3590) and PCP (3570-530-3570) copolymer aqueous solution at given concentrations were added into culture plate wells, respectively. After addition, the plates were left to dry overnight and sterilized by exposure to UV light for 1 h before cell seeding. The coated density of copolymer in the cell culture plates are in the range of 0.6 - 60  $\mu\text{g}\cdot\text{cm}^{-2}$ .

**Contact Angle Measurements.** Static water contact angles of PCP block copolymer coated TCPS substrates were measured by the sessile method at room temperature under an air atmosphere using an NRL-100-0-(230) contact angle goniometer (Rame-Hart, New Jersey). The droplet volume used for measurement was 3  $\mu\text{L}$ . *Telescope with a magnification power of  $\times 23$*  was equipped with a protractor of 0.1° graduation. Each contact angle reported was averaged from 5 readings from different parts of the substrate surface.

**Cells and Media.** L929 mouse fibroblasts were obtained from ATCC and cultivated in Dulbecco's Modified Eagle Medium (DMEM) containing 10% fetal bovine serum (FBS) and 1% penicillin/streptomycin. Cells were grown as a monolayer and passaged upon confluence using trypsin (0.5%, w/v in PBS). L929 cells were harvested from culture by incubating in trypsin solution for 5 min. The cells were centrifuged and the supernatant was discarded. Three mL of serum-supplemented DMEM was added to neutralize any residual trypsin. The cells were re-suspended in serum-supplemented DMEM at a concentration of  $2 \times 10^4$  cells/mL. The cells were cultivated at 37 °C and 5%  $\text{CO}_2$ .

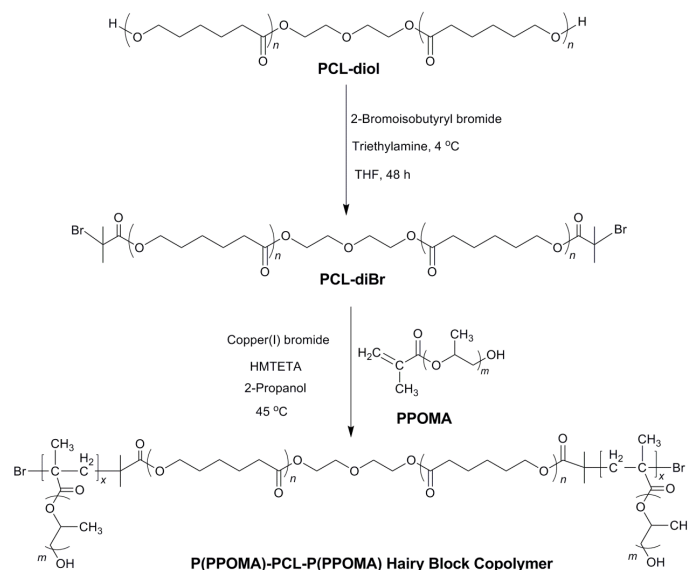
**Cell Cultivation.** In order to evaluate the biocompatibility of the hairy block copolymers when using as coating surface at various densities, *in vitro* cytotoxicity test was carried out using the 3-(4,5-dimethylthiazol-2-yl)-2,5-diphenyltetrazolium bromide (MTT) assay in L929 cell lines. The cells at density of  $3 \times 10^4$  cells/well were seeded in 24-well microtiter plates (Nunc, Wiesbaden, Germany) that were pre-coated with PCP copolymer at densities of 0.06, 0.6, 6, and 60  $\mu\text{g}/\text{cm}^2$ , and cultured in complete DMEM supplemented with 10% FBS at 37 °C, 5%  $\text{CO}_2$ . After 24 h, 10  $\mu\text{L}$  of sterile-filtered MTT stock solution in PBS (5 mg/mL) was added to each well, reaching a final MTT concentration of 0.5 mg/mL. After 5 h, unreacted dye was removed by aspiration. The formazan crystals were dissolved in dimethyl sulfoxide (DMSO) (100  $\mu\text{L}$ /well), and the absorbance was measured using a microplate reader

(Spectra Plus, TECAN) at a wavelength of 570 nm. The relative cell viability (%) related to control cells cultured on uncoated tissue culture polystyrene (TCPS) was calculated with  $[A]_{test}/[A]_{control} \times 100\%$ , where  $[A]_{test}$  is the absorbance of the wells with different coating densities and  $[A]_{control}$  is the absorbance of the control wells.<sup>29</sup> All experiments were conducted with six repetitions and averaged.

**Cell Detachment and Sub-culture of the Detached Cells.** The cells were seeded at a cell density of  $3 \times 10^4$  cells/well in 24-well microtiter plates which were pre-coated with PCP copolymers. After 24 h, the cells were detached by cooling at 4 °C for 30 min and the culture medium was pipetted for 30 times. The detached cell number was counted using a hemocytometer. Six readings were taken and the average results were reported. For PCP copolymer coated surfaces, the coating densities at 0.06, 0.6, 6, and 60  $\mu\text{g}/\text{cm}^2$  were used. The cells harvested from the uncoated cell culture surface of TCPS and the trypsinized cells under the standard cell culture conditions were used as controls, respectively. After cell detachment, the cell suspension was further sub-cultured at 37 °C for 24 h and the relative cell number was calculated by relating to the trypsin treated cells in MTT assay.

### 3.3 Results and Discussion

#### 3.3.1 Synthesis and Molecular Characterizations of the P(PPOMA)-PCL-P(PPOMA) Hairy Block Copolymers



**Scheme 3.1. Synthesis route of P(PPOMA)-PCL-P(PPOMA) (PCP) hairy block copolymers by ATRP.**

The synthesis route of thermo-responsive P(PPOMA)-PCL-P(PPOMA) hairy block copolymers was shown in Scheme 3.1. PCL-diBr macroinitiator was prepared from PCL-diol by the reaction of hydroxyl end groups in PCL-diol with 2-bromoisobutyryl bromide. PCL with two different molecule weights ( $M_n = 530$  and  $2000$ ) were used in this step.  $^1\text{H}$  NMR spectrum of PCL-diBr is similar to that reported previously.<sup>30, 39</sup> The extent of the substitution of PCL-diol were obtained by calculating the ratio of the signal at 4.1 ppm due to methylene protons in PCL, and the signal at 1.92 ppm from the methyl protons in the 2-bromoisobutyryl fragment. Substitution of hydroxyl group was estimated to be 98% for PCL-diBr ( $M_n = 530$ ) and 95% for PCL-diBr ( $M_n = 2000$ ).

**Table 3.1. Molecular characteristics of PCP hairy block copolymers.**<sup>a</sup>

Samples	Reaction Time (h)	Copolymer Composition (wt%)		$M_n$ (g/mol) <sup>d</sup>	PDI <sup>e</sup>
		PCL <sup>b</sup>	P(PPOMA) <sup>c</sup>		
PPOMA375	/ <sup>f</sup>	/ <sup>f</sup>	/ <sup>f</sup>	380	1.30
PCP(3590-2000-3590)	5.5	21.8 (16.1)	78.2 (83.9)	9180	1.21
PCP(3340-2000-3340)	2.0	23.0 (18.9)	77.0 (81.1)	8680	1.41
PCP(2700-2000-2700)	1.5	27.0 (24.9)	73.0 (75.1)	7410	1.48
PCP(530-2000-530)	0.5	65.4 (75.1)	34.6 (24.9)	3060	1.56
PCP(3570-530-3570)	2.0	6.9 (10.8)	93.1 (89.2)	7680	1.45
PCP(1450-530-1450)	0.5	15.9 (17.4)	84.1 (82.6)	3440	1.53
P(PPOMA8000)	3.0	/ <sup>f</sup>	/ <sup>f</sup>	8000	1.15

<sup>a)</sup> P(PPOMA)-PCL-P(PPOMA) are denoted PCP, P for PPOMA, where C represents for PCL. The numbers in the parentheses show the indicative block length of each block in g/mol.

<sup>b)</sup> PCL content in the block copolymers was determined by  $^1\text{H}$  NMR. The value in the parentheses was determined by TGA.

<sup>c)</sup> P(PPOMA) content in the block copolymers determined by  $^1\text{H}$  NMR. The value in the parentheses was determined by TGA.

<sup>d)</sup> Calculated from  $^1\text{H}$  NMR.

<sup>e)</sup> Polydispersity was determined by GPC.

<sup>f)</sup> Not determined.

P(PPOMA)-PCL-P(PPOMA) hairy copolymers were synthesized in 2-propanol at 45 °C via ATRP. Two series of hairy block copolymers with different PCL segment lengths and different PPOMA lengths were synthesized by changing the reactant feedings and reaction time. PCL block flanked by the pendent PPO segments led the final polymer chain to a

brush-type structure. According to previous study, GPC was not an accurate method in the molecular weight determination of macromolecules of this type of architecture.<sup>40</sup>

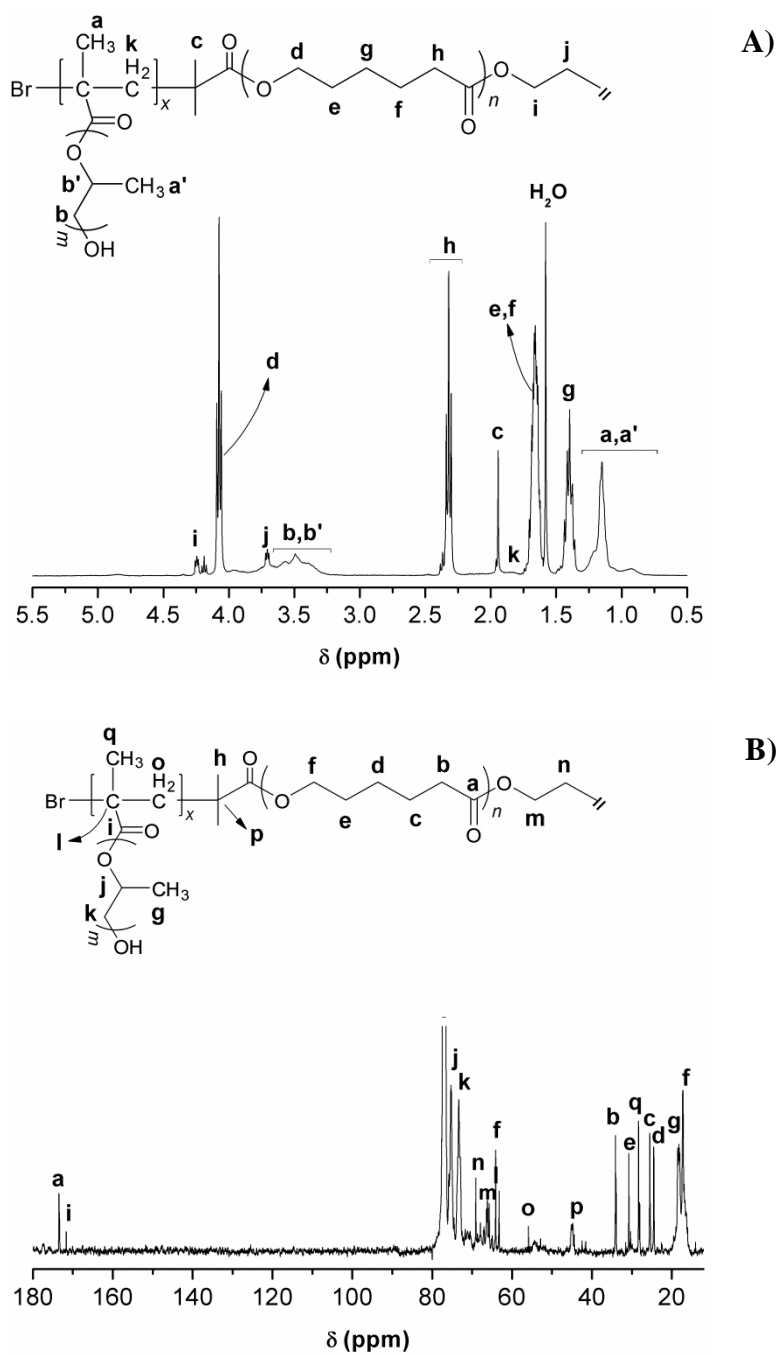


Figure 3.1.  $^1\text{H}$  NMR (A) and  $^{13}\text{C}$  NMR (B) spectra of PCP copolymer, PCP(530-2000-530) in  $\text{CDCl}_3$ .

Instead, the molecular weight was calculated from the integrations of the peaks at 3.25 - 3.71 ppm for  $-OCH-$  and  $-OCH_2-$  of PPO units and at 4.1 ppm for  $-CH_2-$  of PCL, where molecular weight of PCL is known. GPC was used to evaluate the polydispersity. The molecular characteristics were summarized in Table 3.1. In general, molecular weight is reaction-time-dependent. The longer reaction time affords higher molecular weight within the designed time frame and PCL-diBr with shorter length possessed higher reactivity. As can be seen in Table 3.1, the molecular weight of PCL530-diBr initiated PCP block copolymers are higher than those started from PCL2000-diBr at the same polymerization time. In addition, all hairy block copolymers have low polydispersity, indicating that all the molecule chains propagated uniformly within the reaction system.

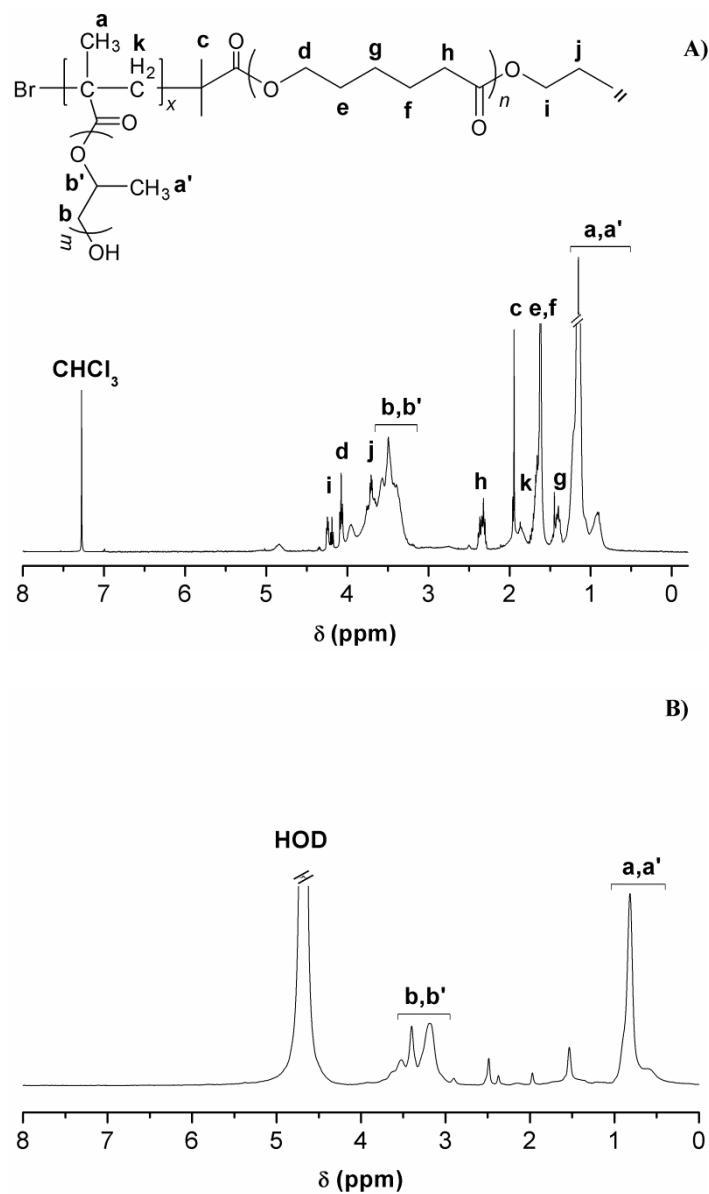
The chemical structure of P(PPOMA)-PCL-P(PPOMA) hairy copolymer was characterized by  $^1H$  NMR and  $^{13}C$  NMR spectroscopy (Figure 3.1A and B). Figure 3.1A shows the typical  $^1H$  NMR spectra of the sample PCP (530-2000-530) in  $CDCl_3$ , in which all proton signals belong to PCL and PPOMA segments are confirmed. Signals corresponding to methylene protons alpha to the ester group of PCL segments are observed at 4.1 ppm, the signal at 3.2 - 3.6 ppm are assigned to methenyl and methylene protons in PPO and the peak associated with methyl protons in PPOMA is found at 1.1 ppm. From  $^1H$  NMR, the molecular weights and composition of the hairy block copolymers were calculated and the results were also summarized in Table 3.1. For  $^{13}C$  NMR in Figure 3.1B, the signal at 17.7 ppm are assigned to the methyl carbon of PPO and the signals at 27.4 ppm are associated with methyl carbon of PPOMA, the signals corresponding to the methylene carbon alpha to the ester group of PCL segment are observed at 64.5 ppm. More importantly, the methyl carbon peak associated with 2-bromoisobutyryl fragment, originally at 31.1 ppm, was shifted to 16.7 ppm; this indicates that the bromide end of macroinitiator has reacted with PPOMA prepolymer. All these results demonstrate the successful synthesis of the hairy block copolymers.

### 3.3.2 Self-assembly of P(PPOMA)-PCL-P(PPOMA) Block Copolymer Solutions and Their Thermo-responsive Property Studies

Core-Shell Micelle Formation: NMR spectroscopy was also used to investigate the solvent effect on the micelle structure.<sup>41,42</sup>  $CDCl_3$  is a good non-selective solvent for PCL and PPOMA while  $D_2O$  is a good selective solvent for PPO at low temperature (5 °C) but poor for

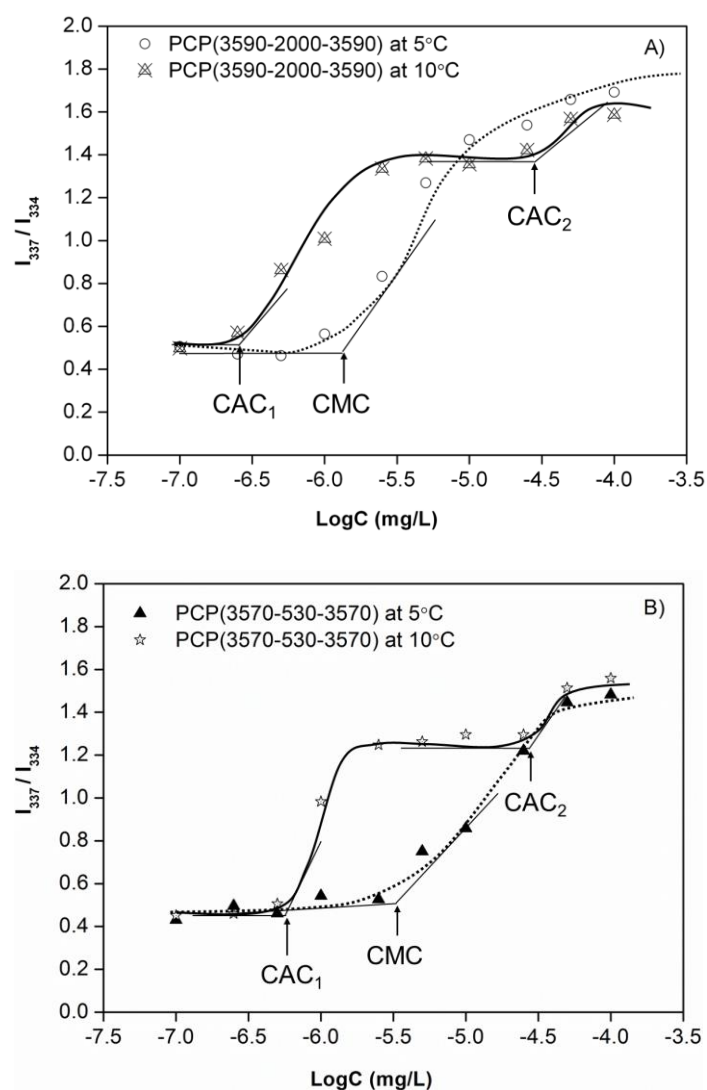


PCL. In  $\text{CDCl}_3$ , the peaks due to PCL and PPOMA segments are sharp and well-defined. (Figure 3.2A)



**Figure 3.2.**  $^1\text{H}$  NMR spectrum of PCP(3570-530-3570) (2 mg/mL) in  $\text{CDCl}_3$  (A) and  $\text{D}_2\text{O}$  (B) at 5 °C.

In  $\text{D}_2\text{O}$  at 5 °C, PPOMA is shown as sharp peak, but the PCL peaks are collapsed (Figure 3.2B). This shows that the molecular motion of PCL is slow in water, indicating a hydrophobic core structure made up of PCL with the hydrophilic PPOMA as the corona structure at 5 °C, confirming the core-corona structure of the micelle.<sup>43,44</sup>



**Figure 3.3.** Plots of  $I_{337}/I_{334}$  ratio of pyrene excitation spectra in water as a function of PCP copolymer concentration at different temperatures; A) PCP(3590-2000-3590); B) PCP(3570-530-3570).

Critical Aggregation Concentration Determination: Fluorescence probe technique is a powerful tool to study aggregation behavior of amphiphilic block copolymers.<sup>2, 45, 46</sup> When the copolymer concentration in an aqueous solution of pyrene is increased, both emission and excitation spectra undergo significant changes upon micellization of the copolymer system. The fluorescence excitation spectra show a change in the vibrational fine structure and a shift in the low energy band from about 334 to 337 nm. These changes are caused by the transfer of pyrene molecules from the polar water environment to the hydrophobic micellar cores and thus can reflect location information of pyrene molecules in the solution. According to Astafievat et al,

the (0,0) absorption band change of pyrene is more sensitive to the true onset of aggregation than the lifetime measurement or fluorescence emission changes.<sup>45</sup> Therefore, the critical aggregation concentration (CAC) values of PCP hairy copolymers in aqueous solutions were determined using the fluorescence excitation spectra of the pyrene probe.

Figure 3.3 shows the intensity ratio of  $I_{337}/I_{334}$  of pyrene excitation spectra as a function of the logarithm of copolymer concentrations for the samples PCP (3590-2000-3590) and PCP (3570-530-3570), respectively. Experiments under two different temperatures (5 °C and 10 °C) were carried out to investigate temperature effect on the aggregation behavior. As can be seen from Figure 3.3, the  $I_{337}/I_{334}$  versus log C plots present a sigmoid curve at 5 °C. A negligible change in the intensity ratio of  $I_{337}/I_{334}$  is observed in the low concentration range of each PCP hairy block copolymer. With an increase in the copolymer concentration, the intensity ratio exhibits a substantial increase above certain concentration, reflecting the incorporation of pyrene into the PCL hydrophobic region of the micelles. The sudden increase at the threshold concentration in the excitation spectra are defined as the CAC. It is the critical concentration of the polymer solution which can associate into aggregates in a dynamic process. When the aggregate formation is micelle, it is also named as critical micelle concentration (CMC).<sup>47</sup> Therefore, the CAC of the PCP hairy block copolymers, also known as CMC at low temperature for our studied copolymers, were determined from the cross-over point in the low concentration range (Figure 3.3). Results are listed in Table 3.2. The extremely low CMC range from 0.60 - 2.45 mg/L for P(PPOMA)-PCL-P(PPOMA) indicates a very strong self-assembly tendency of the hairy block copolymers toward formation of micelles in aqueous solution. Table 3.2 shows that both hydrophobic PCL segment lengths and hydrophilic PPOMA lengths have significant effect on CMC values of the hairy copolymers. Longer PCL chains give lower CMC while the incorporation of more PPOMA units increases it. This is because the higher molecule weight PCL is more hydrophobic than lower ones, which provides a greater driving force for the self-assembly of the copolymers into micelles in aqueous solution at 5 °C. The PCP hairy copolymers with higher PPOMA contents are more hydrophilic at 5 °C, which increases their CMC values.<sup>29, 48</sup> The CMC values of the PCP hairy copolymers are much lower than those of the PNIPPAM-PCL-PNIPPAM<sup>30</sup> and PEO-PCL-PEO<sup>11</sup> copolymers, indicating the weaker hydrophilic PPOMA segments compared to PNIPPAM and PEG. The polymethacrylate linkage in the copolymer backbone may also enhance the self-assembly tendency.<sup>47</sup>

**Table 3.2. Solution properties of PCP hairy block copolymers.**

Polymers	CMC <sup>a</sup> at 5 °C (mg/L)	CAC <sub>1</sub> <sup>b</sup> at 10 °C (mg/L)	CAC <sub>2</sub> <sup>b</sup> at 10 °C (mg/L)	LCST <sup>c</sup> (°C)
PCP(3590-2000-3590)	0.95	0.20	23.10	10.9
PCP(3340-2000-3340)	0.89	0.30	12.30	10.8
PCP(2700-2000-2700)	0.63	0.35	13.26	10.5
PCP(530-2000-530)	0.60	0.25	7.24	/ <sup>d</sup>
PCP(3570-530-3570)	2.45	0.48	27.52	12.8
PCP(1450-530-1450)	1.20	0.28	40.71	6.2
P(PPOMA8000)	/ <sup>d</sup>	/ <sup>d</sup>	/ <sup>d</sup>	12.4

<sup>a)</sup> Critical micelle concentration (CMC) in water was determined by the pyrene probe technique at 5 °C.

<sup>b)</sup> Critical aggregation concentration (CAC) in water was determined by the pyrene probe technique at 10 °C.

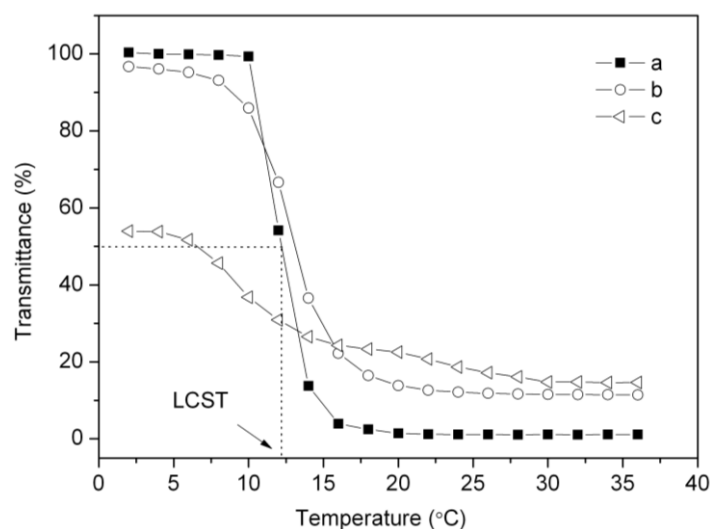
<sup>c)</sup> Lower Critical Solution Temperature (LCST) was determined by recording the temperature that led to a 50% decrease in the optical transmittance of the PCP copolymer aqueous solution at 500 nm; Following polymer concentrations were used for the measurements: Poly(PPOMA) homopolymer and PCL530 derived PCP block copolymers ( $1.0 \times 10^3$  mg/L). PCL2000 derived PCP block copolymers (250 mg/L).

<sup>d)</sup> Not determined.

At the temperature is increased to 10 °C, the plots present a double sigmoid curve in which the first inflection indicates the initial critical aggregation concentration (CAC<sub>1</sub>). CAC<sub>1</sub> values are much lower than the CMC of the corresponding PCP hairy copolymer (Table 3.2). This is because the CAC depends upon the hydrophobic/hydrophilic balance.<sup>47</sup> Increased temperature makes the PPOMA more hydrophobic which leads to a lower CAC.<sup>49</sup> The second inflection is due to the fact that there are two distinct events occurring. The primary event is the initial polymer chain association at lower concentrations and the secondary event is the aggregates of the formed particles at higher concentrations (CAC<sub>2</sub>).<sup>30</sup> The particles size change in PCP copolymer aqueous solution and their corresponding morphology studies at different temperatures will be discussed later.

Thermo-responsive Behavior of PCP Copolymer Solutions: PCP hairy block copolymers can form micelles with hydrophobic PCL core and hydrophilic PPO corona at 5 °C. When the temperature is increased, the hydrophobicity of PPO segments increases and PPO chains in the micelle corona collapse. The increased hydrophobicity of the micelles leads to the change from micelle formation into larger hydrophobic nanoparticles via particle aggregations. The thermo-sensitivity of PCP hairy block copolymers solutions were demonstrated by the optical transmittance change of the tested solutions as a function of temperature. Linear PPO contained polymers exhibit a temperature-sensitive phase transition in the temperature range of 14 to

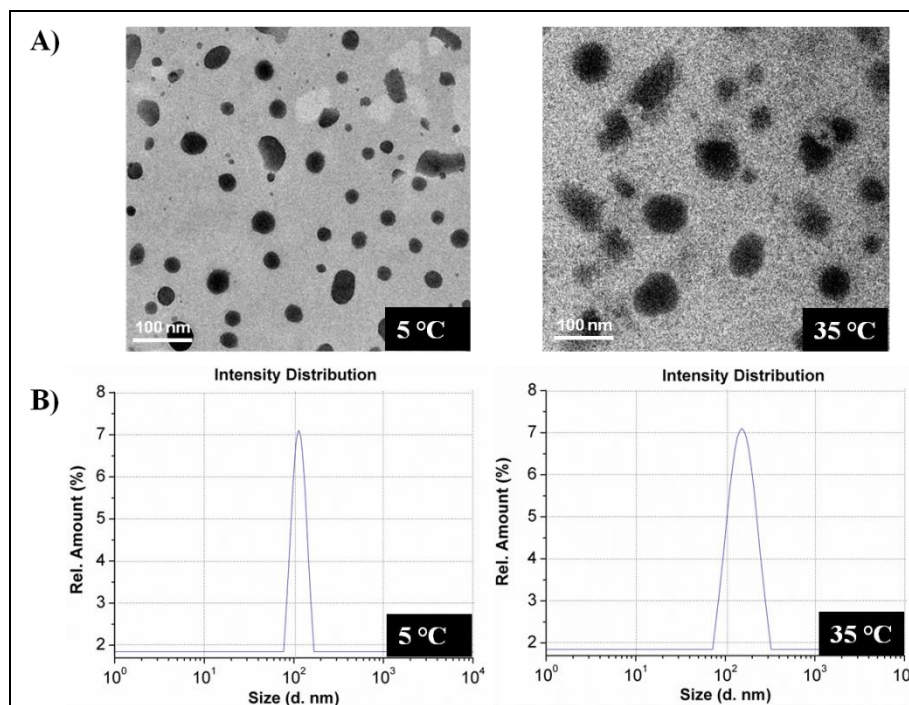
about 100 °C.<sup>33, 34</sup> This temperature is known as the cloud point temperature and has been used to determine the lower critical solution temperature (LCST). The LCST values of PCP hairy block copolymers are presented in Table 3.2.



**Figure 3.4.** Thermo-responsive behavior of PCP copolymer aqueous solutions. a) Poly(PPOMA) homopolymer at solution concentration of  $1.0 \times 10^3$  mg/L; b) PCP (3570-530-3570) at solution concentration of  $1.0 \times 10^3$  mg/L; c) PCP (3590-2000-3590) at solution concentration of 250 mg/L.

At temperature below LCST, PPO is a hydrophilic moiety. The micellar solutions as formed from PCP block copolymers at this temperature have higher optical transmittance. Above this temperature, PPO becomes hydrophobic and collapses to form larger nano-aggregates. This leads to a significant decrease in the transmittance of the tested polymer solutions. In this article, the LCST is defined as the temperature exhibiting a 50% decrease in optical transmittance of an aqueous copolymer solution at 500 nm (Figure 3.4). All the PCP block copolymer solutions show a similar LCST at around 10 °C which is much lower than previously reported data of PEO-PPO-PEO copolymer.<sup>33</sup> This may be resulted from the different polymer/solvent interactions arising from the changes in the hydrophilic/hydrophobic balance between two copolymer structures. The highly hair-like structure with short PPO pendent segments ( $M_n = 375$ ) in PCP block copolymer, unlike linear PPO segment in PEO-PPO-PEO copolymers, provides weaker hydrophilicity due to the hydrophobic polymethacrylate linkage in the copolymer backbone.<sup>47</sup> It can be seen from the results that there is no significant change in the LCST values with the incorporation of PCL, compared to the P(PPOMA) homopolymer (Figure 3.4). This is similar to previously reported studies on

PNIPAAm-PCL-PNIPAAm and PCL-PNIPAAm-PCL copolymer aqueous micellar solutions.<sup>30</sup>  
<sup>50</sup> PCL-PNIPAAm-PCL copolymer solutions showed no decrease in the LCST values upon incorporation of PCL in the copolymer. The authors suggested that the copolymers formed phase-separated core-shell micelle structures in aqueous solution.<sup>50</sup>



**Figure 3.5.** TEM micrographs (A) and particle size distributions (B) of PCP (3340-2000-3340) copolymer nano-aggregates at 5 °C and 35 °C. Solution concentration at 25 mg/L was used for the measurements.

Particle Size Measurements: Morphology and size distribution of the particles before and after PPO phase transition were investigated by TEM observation and dynamic light scattering (DLS), respectively (Figure 3.5 and Table 3.3). P(PPOMA) homopolymers aqueous solution at concentration of 25 mg/L cannot self-assemble into micelles at 5 °C, implying that the driving force from polymethacrylate linkage is not strong enough to induce the self-assembly. However, a particle size measurement was detected at about 170 nm and a significant increase in count rate (0 → 29.7 kcps) after the aqueous solution was equilibrated at 35 °C overnight. This is due to the change in the hydrophilic/hydrophobic balance of the P(PPOMA) solution.<sup>51</sup> The count rate from DLS corresponds to the light scattering intensities and its values are used as the indication of the mean particle size number in kcps (kilo counts per second).<sup>52</sup> All PCP hairy copolymers, because of the higher driving force lead from the incorporation of hydrophobic PCL segment, can form micelles morphology with relatively

larger count rates. The mean diameter of PCP hairy copolymer micelles at 5 °C measured by DLS is in the range of 90 - 200 nm, which is precisely controlled by the composition and molecular weight of the copolymers (Table 3.3). The polydispersity of the micelles, estimated by the cumulant method, is fairly low (0.03 - 0.17), which suggests a narrow size distribution.<sup>53</sup>  
<sup>54</sup> At 35 °C, the nano-aggregates are increased to 150 - 490 nm through the thermo-induced hydrophobic PPO associations and interactions.<sup>55</sup> This leads to a more polydisperse distribution of the particles (0.14 - 0.34).

**Table 3.3. Particle size characterization of PCP hairy block copolymer solutions.<sup>a</sup>**

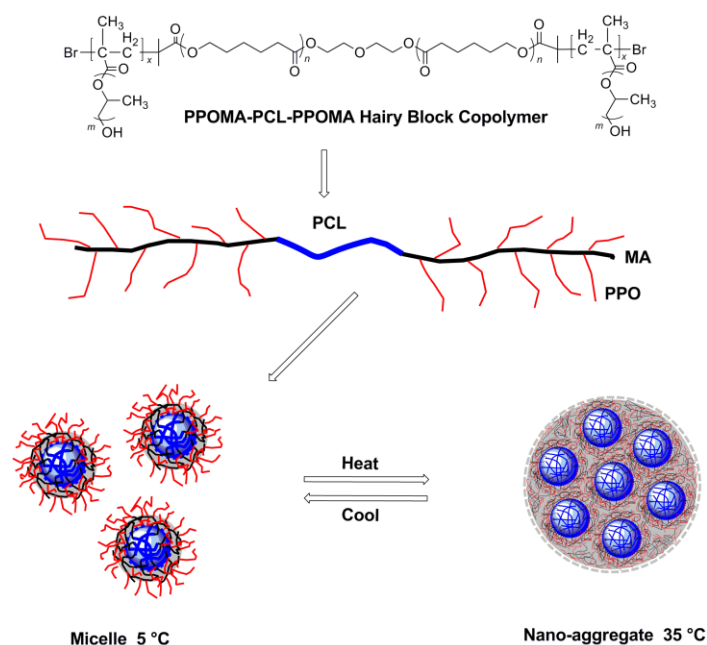
Polymers	5 °C		35 °C	
	Particle Size (nm) <sup>b</sup>	Count Rate (kcps)	Particle Size (nm) <sup>b</sup>	Count Rate (kcps)
PCP(3590-2000-3590)	113 ± 2 (0.06)	38.9	153 ± 3 (0.23)	61.1
PCP(3340-2000-3340)	117 ± 3 (0.10)	29.8	173 ± 6 (0.21)	70.1
PCP(2700-2000-2700)	175 ± 2 (0.09)	33.2	200 ± 4 (0.14)	119.9
PCP(530-2000-530)	200 ± 22 (0.03)	2.9	479 ± 20 (0.26)	146.1
PCP(3570-530-3570)	93 ± 7 (0.17)	4.5	147 ± 19 (0.15)	53.9
PCP(1450-530-1450)	101 ± 3 (0.15)	10.7	304 ± 41 (0.32)	30.1
P(PPOMA8000)	/ <sup>c</sup>	/ <sup>c</sup>	170 ± 2 (0.34)	29.7

<sup>a)</sup> PCP hairy block copolymers concentration in aqueous solution is 25 mg/L.

<sup>b)</sup> Numbers in the parentheses shows the polydispersity of the particle size.

<sup>c)</sup> Samples are not suitable for particle size test due to the very low count rate.

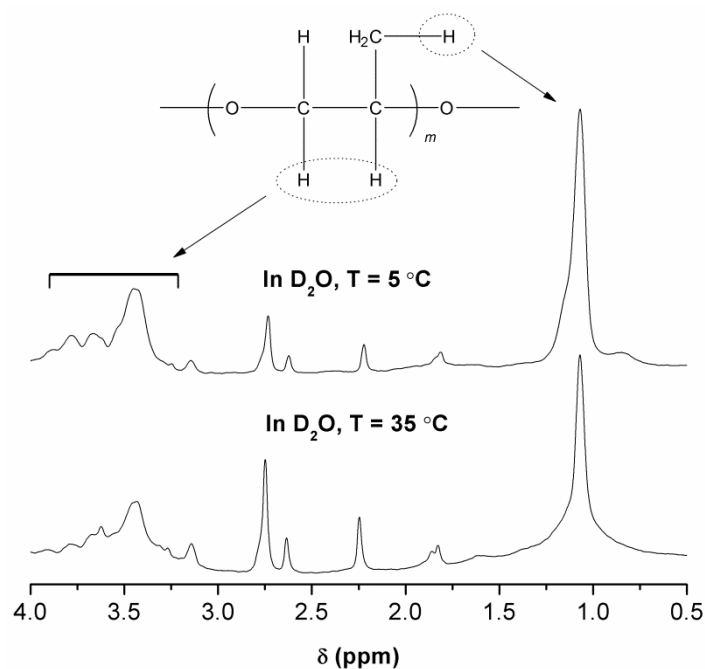
The transition mechanism was proposed in Figure 3.6. At 5 °C, the PPO segments are hydrophilic with good chain mobility in aqueous solution. The driving force from the hydrophobic interaction between PCL segments induces the PCP copolymer chains to self-assemble into micelles with hydrophobic PCL core and hydrophilic PPO as the corona.



**Figure 3.6. Proposed mechanism for the reversible micelles to nano-aggregates transition between 5 °C and 35 °C.**

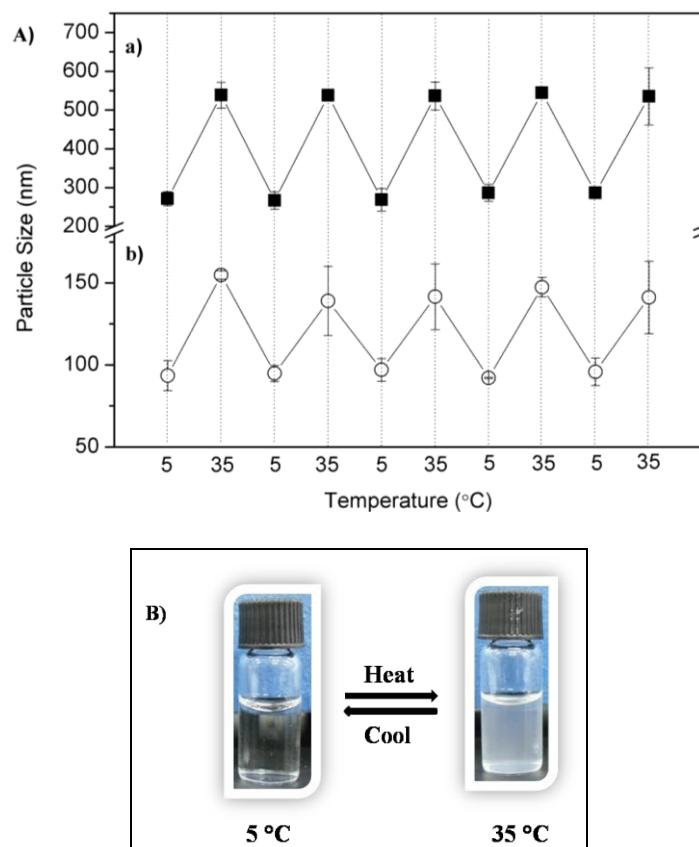
In the NMR spectra at this temperature, the PCL peaks are not observed, supporting the hydrophobic PCL core formation (Figure 3.2B and Figure 3.7). In addition, the signals corresponding to methyl and methylene proton vibrations are split in doublets, indicating good PPO/D<sub>2</sub>O interaction. At 35 °C, the PPO segments become dehydrated and collapse, and the hydrophobic interaction of PPO chains make the micelles to form larger compact aggregates. The relative intensity of the signals corresponds to methyl and methylene group in PPO segments reduces and the well-split peaks for those protons collapse when the temperature is increased from 5 °C to 35 °C (Figure 3.7), indicating the reduced PPO segment motion in D<sub>2</sub>O. This is attributed to the fact that PPO transforms from hydrophilic to hydrophobic phase when the temperature is increased above the LCST, causing a lower hydrodynamic PPO/D<sub>2</sub>O interaction.<sup>56, 57</sup> Detailed <sup>1</sup>H NMR spectroscopy studies on the PEO-PPO-PEO triblock copolymers, PPO contained poly(ether ester urethane)s and 2-(diethylamino)ethyl methacrylate-poly(propylene oxide) (DEA-PPO) copolymers in D<sub>2</sub>O at various temperatures were reported previously.<sup>56-58</sup> Our results are similar to the reported data.





**Figure 3.7.**  $^1\text{H}$  NMR spectrum of 2 mg/mL PCP (3570-530-3570) in  $\text{D}_2\text{O}$  solution at various temperatures, showing specific methyl and methylene protons signals in PPO units.

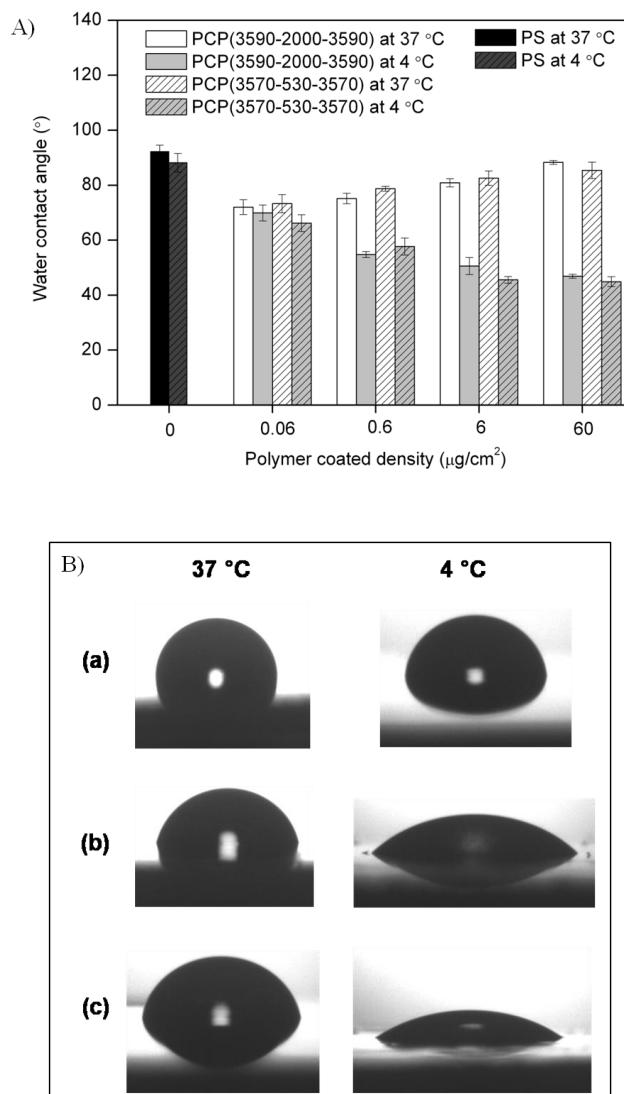
In the present study, the diameters of the nano-aggregates decrease as the PPOMA units become longer at both 5 °C and 35 °C, i.e., PCL block copolymers with shorter PPOMA units form relatively larger aggregates, while PCP copolymers with longer PPOMA units form smaller aggregates. This is an anomalous self-assembly behavior similar to the PNIPAAm-PHB-PNIPAAm and the poly(2-(methacryloyloxy)ethyl phosphorylcholine)-poly(2-hydroxypropyl methacrylate) (PMPC-PHPMA) block copolymers.<sup>29,59</sup> This phenomenon occurs because the PPOMA units become more hydrophobic at 35 °C and this effect is intensified as the degree of polymerization is increased. Therefore, shorter PPOMA units lead to the formation of loose aggregates, whereas longer ones formed more compact aggregates.<sup>59</sup> From TEM micrographs, spherical morphologies are observed for the self-assembled particles, but the estimated diameters are different from the DLS results. This has to be related to the fact that DLS measures the hydrodynamic diameter of particles in an aqueous environment whereas the TEM micrographs show the dehydrated solid state of the nano-aggregates. It could be assumed that the dehydration and subsequent collapse of the PPOMA chain ends when the sample is dried at 35 °C overnight made the smaller diameter from TEM observation. This observation was also reported in other papers.<sup>20, 50</sup>



**Figure 3.8. (A) Thermodynamic diameter distribution of PCP (3570-530-3570) copolymer at 5 °C and 35 °C. a) Solution concentration is 500 mg/L, b) Solution concentration is 25 mg/L. (B) Graphics showing the reversible transition of PCP (3570-530-3570) at 500 mg/L triggered by temperature.**

Reversible Transition Demonstration: Figure 3.8 shows the reversible micelles to nano-aggregates transition of PCP (3570-530-3570) hairy block copolymer solution triggered by temperature. PCP block copolymers at two different concentrations of 500 mg/L and 25 mg/L were studied at temperatures of 5 °C and 35 °C for this demonstration. The micelles are easily re-dispersed and rearranged into larger hydrodynamic diameter associations by increasing the temperature to 35 °C. Cooling the temperature to 5 °C and allowing the solution to equilibrate overnight regenerate the micelle morphology, indicating that the morphological changes are reversible (Figure 3.8A). Five cycles of the transition were conducted in our tests. The particle diameters are in good agreement in each cycle for micelles and nano-aggregates, respectively. This reversal is due to the reversible hydrophobic to hydrophilic transition of PPO segments in the micelle corona as induced by temperature. Similar reversible behavior of PPO containing block copolymer was also reported previously.<sup>57</sup> The morphological changes are also accompanied with the change of optical transmittance of the PCP copolymer solution, as

shown in Figure 3.8B. Increase of temperature results in instantaneous particle aggregation, as judged by the decrease in optical transmittance. The cloudy solutions turned bluish color of the reversible micelles again at 5 °C. Thus, the corresponding micelles at 5 °C and larger nano-aggregate at 35 °C can be transitioned between each morphological state repeatedly, in a fully reversible manner.

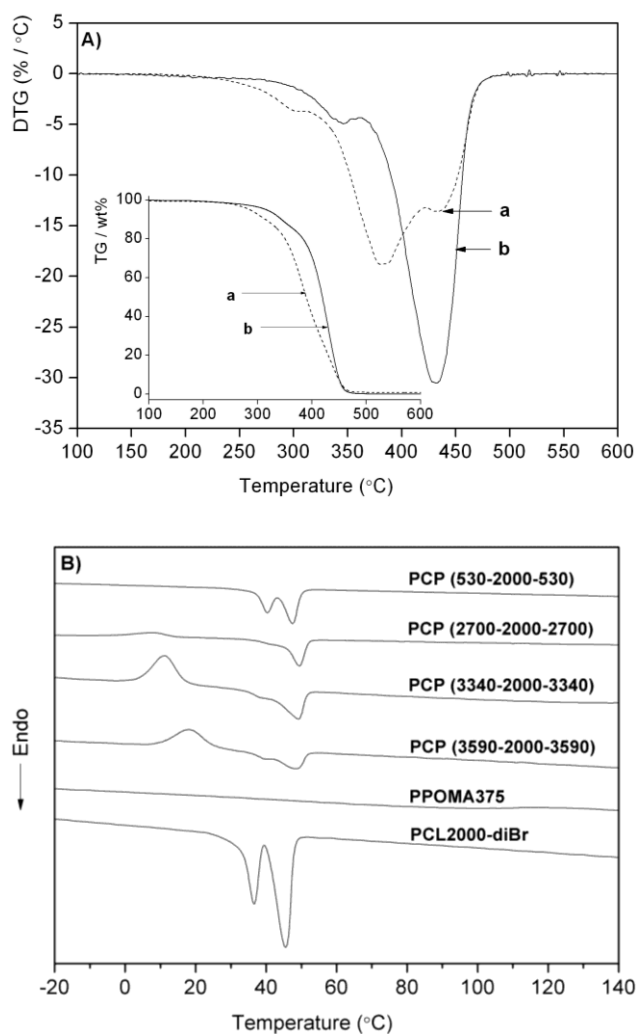


**Figure 3.9.** (A) Static water contact angles of thermal-responsive surface coated by PCP block copolymers at various coating densities. (B) Photographs of water droplet on polymer coated surface at different temperatures. (a) Tissue culture polystyrene (TCPS), (b) PCP(3590-2000-3590) coated TCPS at density of 6  $\mu\text{g}/\text{cm}^2$ , (c) PCP(3570-530-3570) coated TCPS at density of 6  $\mu\text{g}/\text{cm}^2$ .

Surface hydrophilicity of the PCP Block copolymers coated substrate was evaluated by contact angle measurements. All the PCP block copolymers coated substrates were tested in the coating density range of 0.06 to 60  $\mu\text{g}/\text{cm}^2$  at 37 °C and 4 °C, respectively. The results were shown in Figure 3.9. For bare TCPS substrate without PCP copolymer coatings, the contact angle of a water droplet was measured to be  $92.2^\circ \pm 2.4^\circ$  at 37 °C. The obvious thermal response in their hydrophilicities was not observed when cooled to 4 °C (Figure 3.9A and B image (a)). For the PCP(3590-2000-3590) and PCP(3570-530-3570) copolymers coated substrates, changes in the hydrophilicities were observed upon cooling at polymer coating density above 0.06  $\mu\text{g}/\text{cm}^2$ . For example, the PCP(3590-2000-3590) block copolymer, when coated at 6  $\mu\text{g}/\text{cm}^2$ , showed a change in the contact angle from  $80.9^\circ \pm 1.5^\circ$  at 37 °C to  $50.6^\circ \pm 3.1^\circ$  at 4 °C. The PCP(3570-530-3570) block copolymer, on the other hand, showed a change in the contact angle from  $82.6^\circ \pm 2.6^\circ$  at 37 °C to  $45.5^\circ \pm 1.2^\circ$  at 4 °C at the same coating density (Figure 3.9A and B image (b) and (c)). The reduced thermal response of PCP(3590-2000-3590) surface, compared with PCP(3570-530-3570) surface, may be affected by the block copolymer compositions. However, with increasing coating density, higher wettability was achieved on both PCP copolymers coated substrates upon exposure to lower temperature. Based on these results, it is evident that the coating of PCP copolymers imparted thermal response property of normal TCPS surface as functional substrates, which is a promising characteristic for temperature induced cell detachment application.

### 3.3.3 Thermal and Crystallization Behavior

Thermal stability and crystallization property of PCP hairy copolymers were evaluated using TGA and DSC (Figure 3.10). Numerical values corresponding to the thermal transition and the crystallinity are tabulated in Table 3.4. As depicted in the TG/DTG curves of PCP (2700-2000-2700) and the precursors, the PCP block copolymers undergo stepwise thermal degradation process, and exhibit two DTG peaks arising from the decomposition of P(PPOMA) and PCL. The compositions of the copolymers can be calculated from the two step degradation profile (Table 3.1). The results are in excellent agreement with the values calculated from  $^1\text{H}$  NMR. The low temperature in TGA thermograms is corresponded to the decomposition of P(PPOMA) moieties and it is retarded with the incorporation of PCL segment from 193 °C to 289 - 321 °C (Table 3.4). This implies that the introduction of PCL would make the P(PPOMA) in the copolymer more thermally stable than the PPOMA precursor.



**Figure 3.10. Thermal and crystallinity studies of (A) TG/DTG curves of a) PPOMA prepolymer; b) PCP (2700-2000-2700); c) PCL2000-diBr. (B) DSC curves of PCP copolymers and its precursors. Data were collected from the second heating runs.**

From DSC, no crystallization and melting behavior were detected of PCL530-diBr macroinitiator derived PCP copolymers because the short PCL molecule chains cannot retain the crystallinity.<sup>60</sup> In Figure 3.10B, the melting endotherms and crystallinity derived from PCL2000-diBr in the reheating run are shown. It is interesting to note from Table 3.4 that PCL melting points are slightly increased with the copolymerization of PPOMA and the cold exothermic crystallization peaks appear when the PPOMA units content increases up to 72 wt % in the sample PCP(2700-2000-2700). Further, the cold crystallization temperatures,  $T_c$ , shifts to a higher position with the increasing PPOMA unit number (8.2  $\rightarrow$  11.8 °C). This indicates that the flexibility of PCL chains in the PCP copolymer are restricted by the presence

of PPOMA segments.<sup>61</sup> However, the final crystallinity degrees of PCL,  $X_c$ , in each copolymer are similar to the PCL precursor (Table 3.4). These results reveal that the rate of the non-isothermal crystallization of PCL segments in copolymers is restricted compare to free PCL segments but eventually lead to the crystallinity of PCL in the similar extent, albeit the different copolymer compositions.

**Table 3.4. Thermal properties of PCP hairy block copolymers.**

Samples	$T_m$ (°C) <sup>a</sup>	$T_c$ (°C) <sup>b</sup>	$\Delta H_{PCL}$ (J/g) <sup>c</sup>	$X_c$ (%) <sup>d</sup>	$T_d$ (°C) <sup>e</sup>
PPGMA375	/ <sup>f</sup>	/ <sup>f</sup>	/ <sup>f</sup>	/ <sup>f</sup>	193.0
PCL2000-diBr	45.6	/ <sup>f</sup>	61.8	45.4	343.4
PCP(3590-2000-3590)	47.8	18.1	12.4	41.8	321.7
PCP(3340-2000-3340)	49.1	11.5	13.3	42.4	306.1
PCP(2700-2000-2700)	49.4	8.2	15.9	43.3	314.6
PCP(530-2000-530)	47.5	/ <sup>f</sup>	40.5	45.9	318.5
PCP(3570-530-3570)	/ <sup>f</sup>	/ <sup>f</sup>	/ <sup>f</sup>	/ <sup>f</sup>	301.8
PCP(1450-530-1450)	/ <sup>f</sup>	/ <sup>f</sup>	/ <sup>f</sup>	/ <sup>f</sup>	289.3

<sup>a)</sup> Melting point was determined by the second heating run in DSC measurement. For PCL2000-diBr having multipeak endotherm because of melting recrystallization, the  $T_m$  value for the second peak is given.

<sup>b)</sup> Peak temperature of the cold crystallized exotherm thermograms.

<sup>c)</sup> Enthalpy change during melting determined by DSC second heating run.

<sup>d)</sup> Crystallinity was calculated from the melting enthalpies. Reference values of 136 J/g for completely crystallized PCL was used.<sup>60</sup>

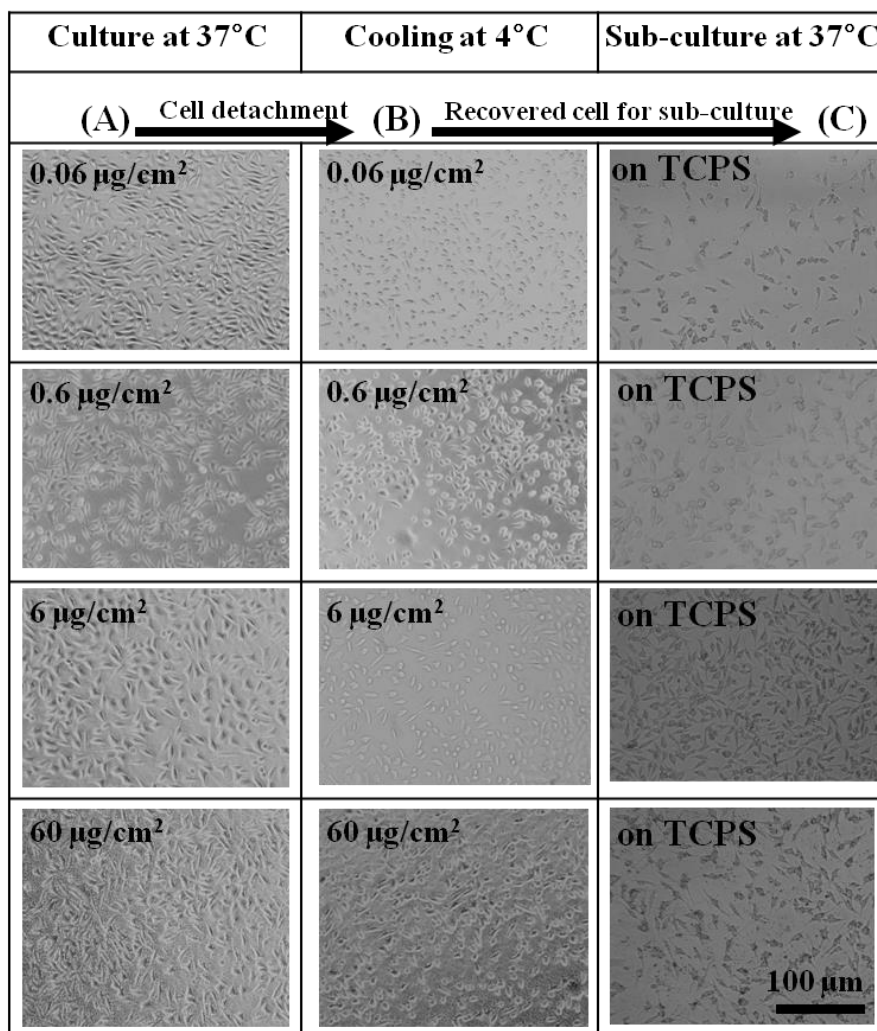
<sup>e)</sup> Decomposition temperature was recorded at 10% weight loss at the TGA curves.

<sup>f)</sup> Not determined.

### 3.3.4 Temperature-dependent Cell Detachment and Viability Assay

Cell Cultivation on PCP Block Copolymer Coated Substrates: Among all the PCP block copolymers, the specimens PCP(3590-2000-3590) and PCP(3570-530-3570) with the longest P(PPOMA) segments while containing different PCL blocks were selected for the cell detachment study, since the longer P(PPOMA) segments could be expected to give rise to greater thermal response. The cell growth and morphology of the L929 cells cultured on PCP copolymer coated surface at densities of 0.06, 0.6, 6, and 60  $\mu\text{g}/\text{cm}^2$  were examined by phase contrast microscopy as indices of cell behavior and function.<sup>35</sup> As shown in Figure 3.11A, most

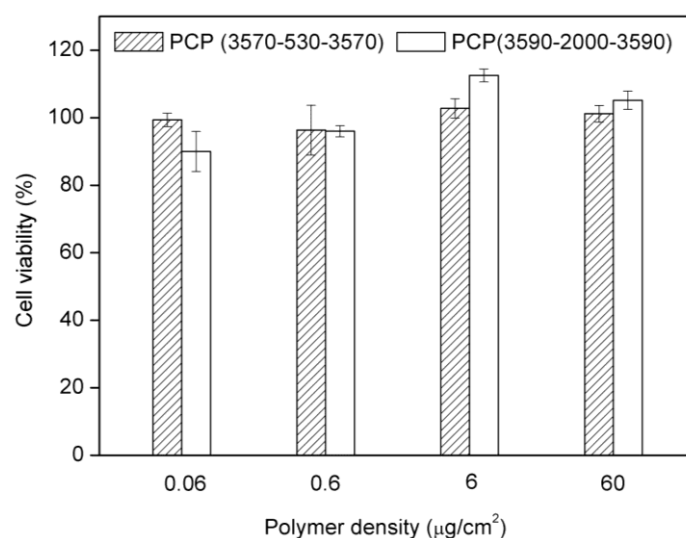
of the cells with good adhesion morphology are observed on all PCP copolymer coated substrates, which is similar to the previously reported L929 cells morphology observation cultured on TCPS.<sup>36</sup> These results demonstrate that the cells cultured on PCP copolymer coated substrates maintained good cell function. Assuming that the density of the copolymer is 1 to 1.1 g/cm<sup>3</sup>, the calculated thickness of the layer used for cell culture studies is about 0.6 - 600 nm. PCP copolymers coated substrates in this thickness range support a good cell adhesion and spreading without aggregated condition.



**Figure 3.11. Phase contrast micrographs of L929 cells cultured on PCP(3590-2000-3590) coated substrates (A), temperature-induced detachment of the cells (B), and the sub-culture of the recovered cells (C).**

Quantification of cell viability in response to the coating densities after 24 h were investigated by MTT assay, using cells cultured on the uncoated substrates TCPS as control.

The results are presented in Figure 3.12. All the PCP copolymers coated surfaces show high viability on L929 cells over a coating density range from 0.06 to 60  $\mu\text{g}/\text{cm}^2$ . As compared with the cells cultured on Pluronic gel and Pluronic-immobilized surface, the later ones with more hydrophilic surface, as imparted from PEG blocks in Pluronic, are unfavourable for cell growth.<sup>35, 38</sup> However, in the present study, a high cell attachment and spreading enhanced surfaces were developed by coating the PCP block copolymers, properly due to the improved hydrophobicity at 37 °C.<sup>62</sup> From the MTT assay results, the PCP copolymers synthesized in this work suggest good biocompatibility as surface coating materials for cell culture.

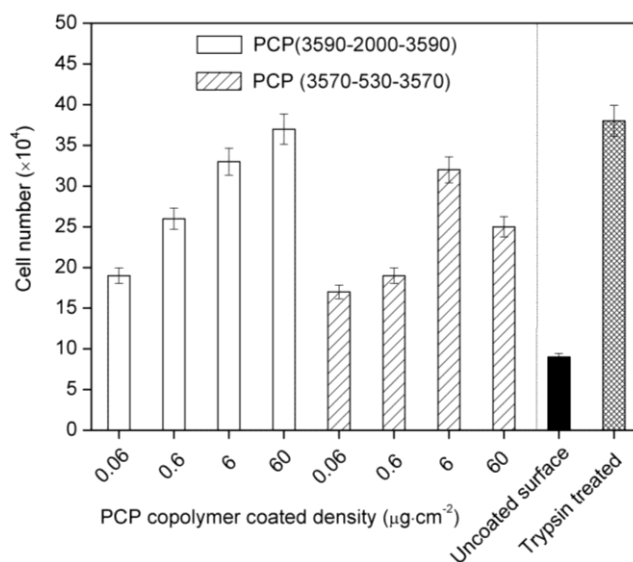


**Figure 3.12. Cell viability assay of L929 cells after 24 h culture on substrates coated with PCP copolymers at various coating densities.**

Temperature-induced Cell Detachment and Sub-culture of the Detached Cells: L929 cells were cultivated on two series of PCP copolymers coated substrates with respect to different coating densities for 24 h. Thereafter, temperature-induced cell detachment was examined by incubating at 4 °C for a period of 30 min. Figure 3.11 column A → B shows a typical morphological change of the L929 cells cultured on PCP(3590-2000-3590) copolymer coated substrates at densities 0.06, 0.6, 6, and 60  $\mu\text{g}/\text{cm}^2$ . Upon cooling, the L929 cells tended to coagulate independently with less discernible cell spreading at this stage. From the surface contact angle study of the PCP copolymers coated surfaces, P(PPOMA) segments became hydrophilic after being cooled to 4 °C. This would thus lead to a higher hydrophilicity through P(PPOMA) chains transition from dehydrated at 37 °C to hydrated at 4 °C, which is a similar



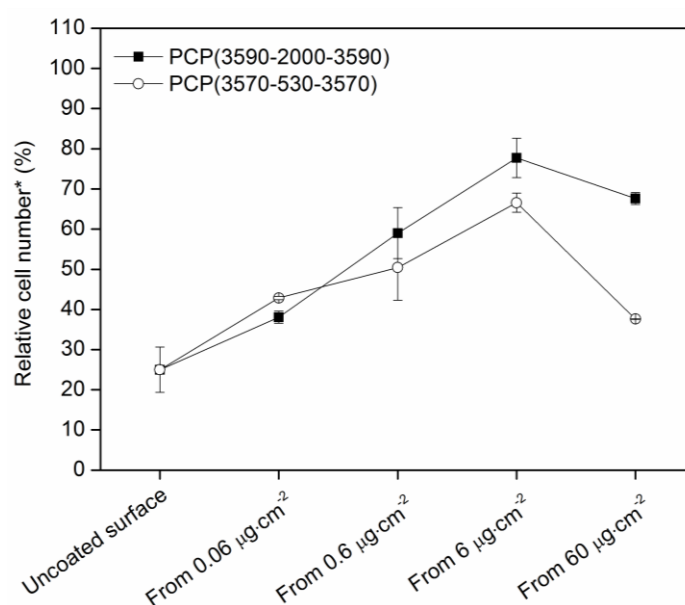
tendency to PNIPAAm.<sup>31, 32</sup> Due to the change of hydrophobic-hydrophilic properties, cell adhesion to the PCP copolymer coated surface became weak. The cells morphology correlates with the cellular activities and functions; a strong cell adhesion and spreading often favour proliferation while a round cell shape is required for cell-specific functions.<sup>63, 64</sup> Similar to previous studies, the thermally detached cells were harvested by gentle pipetting of the culture medium.<sup>35, 38</sup> The cell detachment efficiency was further evaluated and compared with those that were obtained by typical trypsin digestion methods. As shown in Figure 3.13, coating densities play a crucial role in the determination of the detached cell number, and at the tested range of coating densities for both PCP(3590-2000-3590) and PCP(3570-530-3570) copolymers, each optimal detachment efficiency is comparable to those from traditional trypsinization approach. On the other hand, most of the L929 cells on the uncoated substrates surface remained attached when the cells were treated in the same protocol. These results clearly show the temperature-dependent detachment effect of L929 cells from the PCP copolymer coated substrates. As compared with thermo-sensitive surface consisting of PNIPAAm to generate cell sheets, the PCP copolymer coated substrates are favourable for the cell cultivation in passage because the cells can be detached as mainly single or small colonies in our study. This is properly due to the weak cell-cell interaction by decreasing temperature, as accounted previously.<sup>38</sup>



**Figure 3.13.** Cell detachment number of L929 cells cultured on substrates coated with PCP copolymers at various coating densities.

Finally, the recovered cells from the thermal responsive PCP copolymer coated surface were further re-cultured on a normal TCPS. After 24 h incubation, the morphologies of the cells

attached and spread on to the plate surface are shown in Figure 3.11C. In this experiment, 100  $\mu\text{L}$  of the cell suspension harvested from the temperature-sensitive surfaces were used for the cell seeding. However, the cells show different morphologies and viabilities in response to the each coating density. A spread cell is defined as any cell that is not spherical but has more than two corners.<sup>36</sup> For the cells recovered from uncoated and low PCP copolymer amount coated surface, cells are in low number and most of them are in round shape and spread slowly (Figure 3.11C, right upper image). With increasing of the coating density, the recovered cells show good spreading ratio and viability which is similar to the previously reported cell culture of trypsinized cells.<sup>38</sup> The relative cell number of the sub-cultured cells after 24 h was also calculated by relating to the trypsin treated cells in MTT assay.



**Figure 3.14. Relative cell number after one day sub-culture for detached L929 cells from substrates coated with PCP copolymers at various coating densities. \*Calculated by relating to trypsin treated cells.**

As presented in Figure 3.14, the relative cell number correlates with the PCP copolymer coated densities on the substrates. It is proportional to the coating density at the initial stage, since a greater amount of polymer can provide greater thermal response and this could be expected to recover the cells easier with good cell function.<sup>31</sup> However, the relative cell numbers decreased when polymer densities are increased up to 60  $\mu\text{g}/\text{cm}^2$ . This may be resulted from the introduction of the detached polymers as impurities in cell suspension (Figure 3.11, right bottom image). Based on the results obtained so far, the PCP copolymers can be

used as thermal responsive surface coatings for easy cell detachment and replating, bypassing the need for the use of trypsin in the cell harvesting process. This could have important implications for cell engineering applications.

### 3.4 Conclusions

In summary, thermally sensitive PCP hairy block copolymers having two P(PPOMA) blocks linked to a central PCL block were firstly synthesized by ATRP. The molecular characterizations of the copolymers were performed by NMR, GPC, TGA and DSC. PCP block copolymers solutions formed micelles with a hydrophobic PCL core and a hydrophilic PPO shell at 5 °C, as inferred from the <sup>1</sup>H NMR spectra recorded in two environments (CDCl<sub>3</sub> and D<sub>2</sub>O). The micelle formation transformed into larger nano-aggregates morphology with the change of PPO segments from hydrophilic to hydrophobic at elevated temperature. The PCP block copolymer coated substrates as prepared from the easy drop-casting method were examined to have good biocompatibility for cell growth and adhesion characteristics at 37 °C. Temperature-induced cell detachment from the PCP copolymers coated surfaces without using trypsin enzymatic methods enabled the isolation of cells under mild conditions. The optimal coating densities for PCP copolymers with different compositions were determined. The sub-culture of the recovered cells on normal TCPS showed proliferation ability. This technique allows for saving of valuable time in harvesting and passage during cell culture process, which could have important implications in clinical applications.

### 3.5 References

1. X. J. Loh and J. Li, *Expert Opin. Ther. Pat.*, 2007, **17**, 965-977.
2. J. Li, X. P. Ni, X. Li, N. K. Tan, C. T. Lim, S. Ramakrishna and K. W. Leong, *Langmuir*, 2005, **21**, 8681-8685.
3. H.-W. Jun, S. E. Paramonov and J. D. Hartgerink, *Soft Matter*, 2006, **2**, 177-181.
4. T. J. Deming, *Soft Matter*, 2005, **1**, 28-35.
5. Y. Lin, Y. Qiao, Y. Yan and J. Huang, *Soft Matter*, 2009, **5**, 3047-3053.
6. B. Jeong, Y. H. Bae, D. S. Lee and S. W. Kim, *Nature*, 1997, **388**, 860-862.

7. Y. Osada, H. Okuzaki and H. Hori, *Nature*, 1992, **355**, 242-244.
8. A. Suzuki and T. Tanaka, *Nature*, 1990, **346**, 345-347.
9. G. Y. Zhou, *Smart Materials & Structures*, 2003, **12**, 139-146.
10. Z. Shi, Y. Zhou and D. Yan, *Macromol. Rapid Commun.*, 2008, **29**, 412-418.
11. C. Y. Gong, S. Shi, X. H. Wang, Y. J. Wang, S. Z. Fu, P. W. Dong, L. J. Chen, X. Zhao, Y. Q. Wei and Z. Y. Qian, *J. Phys. Chem. B*, 2009, **113**, 10183-10188.
12. E. S. Lee, H. J. Shin, K. Na and Y. H. Bae, *J. Controlled Release*, 2003, **90**, 363-374.
13. P. S. Xu, E. A. Van Kirk, W. J. Murdoch, Y. H. Zhan, D. D. Isaak, M. Radosz and Y. Q. Shen, *Biomacromolecules*, 2006, **7**, 829-835.
14. M. A. Laflamme and C. E. Murry, *Nat. Biotechnol.*, 2005, **23**, 845-856.
15. T. Amanuma, H. Iwata, H. Kanehiro, H. Kuge, Y. Nakajima, K. Ohashi, T. Okano, M. Tsutsumi, M. Yamato, J. Yang and T. Yokoyama, *Nat. Med.*, 2007, **13**, 880-885.
16. Z. M. O. Rzaev, S. Dincer and E. Piskin, *Prog. Polym. Sci.*, 2007, **32**, 534-595.
17. P. Bhargava, Y. F. Tu, J. X. Zheng, H. M. Xiong, R. P. Quirk and S. Z. D. Cheng, *J. Am. Chem. Soc.*, 2007, **129**, 1113-1121.
18. X. J. Loh, S. H. Goh and J. Li, *Biomacromolecules*, 2007, **8**, 585-593.
19. Y. Xia, X. Yin, N. A. D. Burke and H. D. H. Stöver, *Macromolecules*, 2005, **38**, 5937-5943.
20. Y. Y. Li, X. Z. Zhang, H. Cheng, J. L. Zhu, U. N. Li, S. X. Cheng and R. X. Zhuo, *Nanotechnology*, 2007, **18**, 8.
21. D. Schmaljohann, *Adv. Drug Delivery Rev.*, 2006, **58**, 1655-1670.
22. S. Q. Liu, Y. W. Tong and Y.-Y. Yang, *Biomaterials*, 2005, **26**, 5064-5074.
23. C. Ramkissoon-Ganorkar, F. Liu, M. Baudys and S. W. Kim, *J. Biomater. Sci. Polym. Ed.*, 1999, **10**, 1149-1161.
24. F. Kohori, K. Sakai, T. Aoyagi, M. Yokoyama, M. Yamato, Y. Sakurai and T. Okano, *Colloids Surf. B. Biointerfaces*, 1999, **16**, 195-205.
25. K. Uchida, K. Sakai, E. Ito, O. Hyeong Kwon, A. Kikuchi, M. Yamato and T. Okano, *Biomaterials*, 2000, **21**, 923-929.
26. H. Hatakeyama, A. Kikuchi, M. Yamato and T. Okano, *Biomaterials*, 2005, **26**, 5167-5176.
27. T. Shimizu, M. Yamato, A. Kikuchi and T. Okano, *Biomaterials*, 2003, **24**, 2309-2316.

28. K. Nishida, M. Yamato, Y. Hayashida, K. Watanabe, N. Maeda, H. Watanabe, K. Yamamoto, S. Nagai, A. Kikuchi, Y. Tano and T. Okano, *Transplantation*, 2004, **77**, 379-385.
29. X. J. Loh, Z.-X. Zhang, Y.-L. Wu, T. S. Lee and J. Li, *Macromolecules*, 2009, **42**, 194-202.
30. X. J. Loh, Y. L. Wu, W. T. J. Seow, M. N. I. Norimzan, Z. X. Zhang, F. Xu, E. T. Kang, K. G. Neoh and J. Li, *Polymer*, 2008, **49**, 5084-5094.
31. X. J. Loh, W. C. D. Cheong, J. Li and Y. Ito, *Soft Matter*, 2009, **5**, 2937-2946.
32. X. J. Loh, J. S. Gong, M. Sakuragi, T. Kitajima, M. Z. Liu, J. Li and Y. Ito, *Macromol. Biosci.*, 2009, **9**, 1069-1079.
33. V. G. De Bruijn, L. J. P. Van den Broeke, F. A. M. Leermakers and J. T. F. Keurentjes, *Langmuir*, 2002, **18**, 10467-10474.
34. K. Mortensen, W. Brown and E. Joergensen, *Macromolecules*, 1994, **27**, 5654-5666.
35. A. Higuchi, T. Yamamoto, K. Sugiyama, S. Hayashi, T. M. Tak and T. Nakagawa, *Biomacromolecules*, 2005, **6**, 691-696.
36. A. Higuchi, S. Tamiya, T. Tsubomura, A. Katoh, C.-S. Cho, T. Akaike and M. Hara, *J. Biomater. Sci. Polym. Ed.*, 2000, **11**, 149-168.
37. A. Higuchi, K. Sugiyama, B. O. Yoon, M. Sakurai, M. Hara, M. Sumita, S.-i. Sugawara and T. Shirai, *Biomaterials*, 2003, **24**, 3235-3245.
38. A. Higuchi, N. Aoki, T. Yamamoto, T. Miyazaki, H. Fukushima, T. M. Tak, S. Jyujyoji, S. Egashira, Y. Matsuoka and S. H. Natori, *J. Biomed. Mater. Res., Part A*, 2006, **79A**, 380-392.
39. F. J. Xu, J. Li, S. J. Yuan, Z. X. Zhang, E. T. Kang and K. G. Neoh, *Biomacromolecules*, 2008, **9**, 331-339.
40. K. Zhang and G. N. Tew, *ACS Macro Letters*, 2012, **1**, 574-579.
41. B. Jeong, Y. H. Bae and S. W. Kim, *Macromolecules*, 1999, **32**, 7064-7069.
42. B. H. Lee, Y. M. Lee, Y. S. Sohn and S.-C. Song, *Macromolecules*, 2002, **35**, 3876-3879.
43. B. Jeong, Y. Han Bae and S. Wan Kim, *Colloids Surf. B. Biointerfaces*, 1999, **16**, 185-193.
44. B. Jeong, C. F. Windisch, M. J. Park, Y. S. Sohn, A. Gutowska and K. Char, *J. Phys. Chem. B*, 2003, **107**, 10032-10039.
45. I. Astafieva, X. F. Zhong and A. Eisenberg, *Macromolecules*, 1993, **26**, 7339-7352.

46. M. Wilhelm, C. L. Zhao, Y. Wang, R. Xu, M. A. Winnik, J. L. Mura, G. Riess and M. D. Croucher, *Macromolecules*, 1991, **24**, 1033-1040.
47. H. Hussain, K. Y. Mya and C. B. He, *Langmuir*, 2008, **24**, 13279-13286.
48. X. J. Loh, K. B. C. Sng and J. Li, *Biomaterials*, 2008, **29**, 3185-3194.
49. P. Alexandridis, J. F. Holzwarth and T. A. Hatton, *Macromolecules*, 1994, **27**, 2414-2425.
50. C. Chang, H. Wei, C.-Y. Quan, Y.-Y. Li, J. Liu, Z.-C. Wang, S.-X. Cheng, X.-Z. Zhang and R.-X. Zhuo, *J. Polym. Sci., Part A: Polym. Chem.*, 2008, **46**, 3048-3057.
51. X. Y. Xiong, K. C. Tam and L. H. Gan, *J. Appl. Polym. Sci.*, 2006, **100**, 4163-4172.
52. J. Oishi, K. Kawamura, J.-H. Kang, K. Kodama, T. Sonoda, M. Murata, T. Niidome and Y. Katayama, *J. Controlled Release*, 2006, **110**, 431-436.
53. A. Harada and K. Kataoka, *Macromolecules*, 1998, **31**, 288-294.
54. A. Harada and K. Kataoka, *Macromolecules*, 1995, **28**, 5294-5299.
55. C. He, S. W. Kim and D. S. Lee, *J. Controlled Release*, 2008, **127**, 189-207.
56. X. J. Loh, S. H. Goh and J. Li, *J. Phys. Chem. B*, 2009, **113**, 11822-11830.
57. S. Liu, N. C. Billingham and S. P. Armes, *Angew. Chem. Int. Ed.*, 2001, **40**, 2328-2331.
58. J.-H. Ma, C. Guo, Y.-L. Tang and H.-Z. Liu, *Langmuir*, 2007, **23**, 9596-9605.
59. J. Madsen, S. P. Armes, K. Bertal, S. MacNeil and A. L. Lewis, *Biomacromolecules*, 2009, **10**, 1875-1887.
60. J. Kloss, M. Munaro, G. P. D. Souza, J. V. Gulmine, S. H. Wang, S. Zawadzki and L. Akcelrud, *J. Polym. Sci., Part A: Polym. Chem.*, 2002, **40**, 4117-4130.
61. G. R. Saad, Y. J. Lee and H. Seliger, *J. Appl. Polym. Sci.*, 2002, **83**, 703-718.
62. N. Faucheux, R. Schweiss, K. Lützow, C. Werner and T. Groth, *Biomaterials*, 2004, **25**, 2721-2730.
63. T. Konno and K. Ishihara, *Biomaterials*, 2007, **28**, 1770-1777.
64. D. Mooney, L. Hansen, J. Vacanti, R. Langer, S. Farmer and D. Ingber, *J. Cell. Physiol.*, 1992, **151**, 497-505.

## **CHAPTER 4 ENGINEERED BIODEGRADABLE PCL-BASED HYPERBRANCHED HYDROGEL WITH MECHANO-RESPONSIVE PROPERTY FOR POTENTIAL CELL DELIVERY APPLICATION**

### **4.1 Introduction**

The three dimensional (3D) cell encapsulation using hydrogel has gained increasing attention in recent years owing to the similarity of the hydrogels and the *in vivo* environment.<sup>1</sup> A wide and diverse range of natural and synthetic polymers have been used to fabricate hydrogels for cell encapsulation.<sup>2-8</sup> Among them, *in situ* gelling stimuli-responsive block copolymer hydrogels, which are reversible polymer networks formed by physical interactions and exhibit a sol-gel phase transition in response to external stimuli, have been studied extensively for injectable cell delivery systems.<sup>2, 4, 9, 10</sup> However, many such physical hydrogels do not have enough stability and tenacity for holding cells. The low gel stability results fast gel erosion and burst effects in biological environments.<sup>11, 12</sup> For instance, commercially available Pluronic triblock copolymers of poly(ethylene glycol)-poly(propylene glycol)-poly(ethylene glycol) (PEG-PPG-PEG) have been widely investigated as thermo-responsive hydrogels, and their polymer solutions can undergo sol-gel transition at physiological temperatures.<sup>13</sup> Rapid weight loss and fast release of the encapsulated protein from Pluronic copolymer hydrogels were observed.<sup>12</sup> It was also reported that cells encapsulated within pure Pluronic hydrogels completely died in five days.<sup>14</sup> It was also reported that the optimal G' for a PEG-based

hydrogel is between 10 and 1000 Pa for 3D cell encapsulation, and at high stiffness (elastic modulus,  $G' > 1200$  Pa) the hydrogel matrix acts as a barrier for cells cultured in 3D.<sup>3</sup>

The viscoelastic property of a thixotropic hydrogel can be easily controlled. In the rheological measurement, the elastic modulus  $G'$  diminishes as the shear rate increases. In the fluid state, the elastic modulus is smaller than viscous modulus  $G''$ . However, the diminished  $G'$  of the hydrogel will eventually restore towards its original value, in most cases within hours, when there is no more agitation.<sup>8, 15, 16</sup> This unique property is very important and renders thixotropic hydrogels suitable for injectable delivery systems. The mechano-stimulus can be easily triggered so this kind of hydrogel is promising for potential 3D cell encapsulation application.<sup>8, 17</sup> The recovered rheological property of a mechano-responsive hydrogel can provide a soft-tissue-like environment and the porous structure of hydrogel networks with interconnectivity can provide space for cells and allow free exchange of oxygen, nutrients and other water-soluble metabolites.<sup>11</sup> With additional biodegradability through incorporating biodegradable components in the hydrogel design, Thixotropic hydrogels have shown great potential in a variety of biomedical and pharmaceutical applications, such as drug and growth factor delivery, cell encapsulation, three-dimensional cell encapsulation, sustained gene delivery and tissue regeneration.<sup>2, 8, 18-22</sup>

In the present study, we demonstrate a new design of three-component amphiphilic biodegradable hyperbranched block copolymers, and the copolymers can form mechano-responsive hydrogels after water swelling. The starting materials poly( $\epsilon$ -caprolactone) (PCL), poly(ethylene glycol) (PEG) and Glycerol (Gly) are selected with following considerations. First, PCL-diol with molecular weight of 530 is chosen. PCL is a biodegradable polyester and has been extensively investigated as biomedical materials. The degradation products of PCL are naturally occurring metabolite in the human body. Sutures having PCL as a main component have been approved by the Food and Drug Administration (FDA) for use in surgeries, attesting to its safe application in humans.<sup>23-25</sup> The PCL-diol with low molecular weight in the block copolymers may have low crystallinity and this could improve the water uptake capability of the prepared hydrogel.<sup>26</sup> Second, the incorporation of PEG in the hydrogel networks is an well-accepted strategy since PEG chains are hydrophilic and exhibit excellent biocompatibility and good blood compatibility.<sup>27</sup> PEG in the hydrogels can enhance water swelling ability, hydrogel permeability and solute release.<sup>28-32</sup> Finally, the tri-functional Gly with three hydroxyl groups is used as a branching unit. It has been reported to have low toxicity and has been approved by FDA in frozen cell storage.<sup>33</sup>



The abovementioned three components, PEG, Gly, and PCL were linked via urethane linkages to give hyperbranched block copolymers (EGC copolymers). The use of the branching agent Gly is expected to further enhance the mechanical strength of the otherwise weak physical PCL/PEG hydrogels. We found that the resultant hyperbranched copolymer hydrogels demonstrated superior elastic property and higher water swelling capability, which can provide the encapsulated cells with a comfortable environment. The cells embedded within the hydrogels maintained their activity and the recovered cells from thereof also showed good viability in the sub-culture. Bearing the biodegradability of the EGC copolymers in nature, the as-prepared hydrogels may afford a potential cell storage vehicle used for injectable cell delivery application.

## 4.2 Experimental Section

### 4.2.1 Materials

Hydroxyl-terminated poly( $\epsilon$ -caprolactone) (PCL-diol,  $M_n = 530$ ) and hydroxyl-terminated poly(ethylene glycol) (PEG,  $M_n = 2000$ ) were purchased from Aldrich. They were vacuum-dried at 75 °C overnight before use. Glycerol (Gly, 99%), dibutyltin dilaurate (95%), 1,6-hexamethylene diisocyanate (HDI) (98%), diethyl ether, 1,2-dichloroethane (99.8%) and 2-propanol were also purchased from Aldrich. 1,2-dichloroethane was distilled over  $\text{CaH}_2$  before use.

### 4.2.2 Synthesis of Hyperbranched EGC Block Copolymers

Hyperbranched block copolymers synthesized from PEG, Glycerol and PCL are denoted as EGC, where E represents for PEG, G for glycerol, and C for PCL. During the syntheses, PCL-diol was fixed at  $1.89 \times 10^{-3}$  mole, PEG at  $(1.25 - 2.25) \times 10^{-3}$  mole and Gly at  $(2.71 - 5.43) \times 10^{-4}$  mole. HDI was used as a coupling reagent and the amount added was equivalent to the hydroxyl groups in the reaction. Typically, 1.0 g of PCL-diol ( $M_n = 530$ ,  $1.89 \times 10^{-3}$  mol), 4.5 g of PEG ( $M_n = 2000$ ,  $2.25 \times 10^{-3}$  mol), and 0.05 g of glycerol (Gly,  $5.43 \times 10^{-3}$  mol) were dried in a 250 mL three-necked flask at 75 °C under high vacuum overnight. Then, 60 mL of anhydrous 1,2-dichloroethane was added to the flask, and any trace of water in the system was removed through azeotropic distillation with about 45 mL of 1,2-dichloroethane being left in

the flask. When the flask was cooled down to 75 °C, 0.83 g of HDI ( $0.80 \times 10^{-3}$  mol) and two drops of dibutyltin dilaurate ( $\sim 8 \times 10^{-3}$  g) were added sequentially. The reaction mixture was stirred at 75 °C under a nitrogen atmosphere for 72 hours. At the end of the reaction, 1 mL of 2-propanol was added and the system was allowed to age for another two hours to prevent the allophanate reaction. The resultant polymers were precipitated from diethyl ether and further purified by redissolving in 1,2-dichloroethane followed by precipitation in methanol/diethyl ether (1/100, v/v) to remove remaining dibutyltin dilaurate. A series of products were prepared through this method.<sup>34</sup> The polymer compositions and molecular weight data are listed in Table 4.1.

### 4.2.3 Methods and Characterization

**Molecular Characterization.** <sup>1</sup>H NMR spectra were recorded on a Bruker AV-400 NMR spectrometer at room temperature. Chemical shift at 7.3 ppm was referred to the solvent peaks, CHCl<sub>3</sub>. Gel permeation chromatography (GPC) analysis was carried out with a Shimadzu SCL-10A and LC-8A system equipped with a Shimadzu RID-10A refractive index detector. THF was used as the eluent at a flow rate of 0.30 mL/min at 40 °C. Monodispersed PEG standards were used to obtain a calibration curve. Branch length between two branch units was theoretically calculated based on the feed ratio and molecular weight.

**Thermal Analysis.** Thermogravimetric analyses (TGA) were conducted using the TA Instruments SDT 2960. Samples were heated at 20 °C·min<sup>-1</sup> to 800 °C under nitrogen flow rate of 70 mL·min<sup>-1</sup>. Differential scanning calorimetry (DSC) was performed on TA Instruments 2920 differential scanning calorimeter with a refrigerated cooling system and calibrated using indium. Each dry sample was tested by the following protocol: heating from room temperature to 175 °C at 5 °C·min<sup>-1</sup>, holding at 175 °C for 2 min, cooling from 175 to -30 °C at 5 °C·min<sup>-1</sup>, isothermal for 5 min, and reheating from -30 to 175 °C at 5 °C min<sup>-1</sup>. For hydrogel test, the measuring temperature range was set at 0 to 70 °C, by considering the frozen and evaporative effect of water. Data were collected from the cooling and the second heating runs.

**Hydrogel Preparation and Injectability Test.** Hydrogels based on the hyperbranched EGC block copolymers were prepared from direct water swelling process at predetermined polymer concentrations. Each sample was allowed to age overnight at room temperature for equilibrium. The hydrogel was determined by the formation of a firm gel that remained intact when the sample vial was inverted by 180°. <sup>35</sup> Critical gelation concentration (CGC) was the lowest concentration of the polymer that can form hydrogel formation. A 1-mL Luer Injekt

syringe with loaded hydrogel (10%, w/v) and a Sterican needle of 1.10 mm diameter attached to the syringe tip was used to demonstrate the injectability of the formed hydrogels.<sup>36</sup>

**Scanning Electron Microscopy (SEM) Examination.** The freeze-dried structure of the hydrogels was characterized by SEM images, recorded on a JSM-5600 microscope (JEOL, Japan) at acceleration voltage of 5 kV. Hydrogel samples were freeze dried at -50 °C overnight, and were sputter-coated with a thin layer of gold for 10 s to make the samples conductive before testing.

**Rheological Characterization.** Rheological tests were conducted on a Thermo Haake RS600 rheometer with Peltier plate-temperature control. Parallel plate geometry (35 mm diameter) at a gap of 1 to 2 mm was used for the measurement of hydrogels at various concentrations. In each experiment, hydrogel sample that had been aged for at least 2 days was carefully loaded onto the measuring geometry, and allowed to age for another 30 min at 25 °C to get rid of any shear history introduced during the transfer. Oscillatory stress sweeps were performed by applying increasing shear stress logarithmically from 0.50 Pa at a fix angular frequency of 1 rad/s. Oscillatory frequency sweeps were done from 100 to 0.10 rad/s at a constant shear stress of either 5.0 Pa. Upon reaching the crossover point in stress sweep, the applied shear stresses were fixed and maintained for 30 s for hydrogel deformation. Then the shear stresses were reduced to 5 Pa to monitor structural recovery. A 100% recovery of elastic modulus from the destroyed hydrogel formation was defined as the recovery time,  $t_R$ . Data collected from commercial Pluronic 127 (20%, w/v) at 37 °C was used as control.

**Hydrolytic Degradation of EGC Hydrogels.** EGC hydrogels at different concentrations were prepared by water swelling process within a porous cellulose cassette (pore size: ~100  $\mu$ m) in a sample vial. After equilibration overnight to give a firm hydrogel formation, hydrogels were packed into dimensions of 20 mm  $\times$  11 mm  $\times$  7 mm specimens. Each hydrogel sample was placed into 20 mL of phosphate buffer solution in a test tube, which was incubated and shaken at 50 rpm in a water bath at 37 °C. The buffer solution had a pH of 7.4, and contained 8.0 g of NaCl, 0.2 g of KCl, 1.44 g of Na<sub>2</sub>HPO<sub>4</sub>, and 0.24 g of K<sub>2</sub>H<sub>2</sub>PO<sub>4</sub> in 1 L of solution. Samples were taken out at predetermined time intervals and experiments were done in triplicate. The residual gel was lyophilized and weighed to give the mass loss profile by using the following equation  $\text{Mass loss (\%)} = [1 - (W_t/W_0)] \times 100\%$ , where  $W_0$  and  $W_t$  are the initial weight and the weight of the copolymer in the gel residual at time  $t$ , respectively.  $W_t$  was obtained by weighting the dehydrated residual hydrogel after lyophilization. The dissolved and/or degraded copolymers in the buffer solutions were also analyzed according to the previous method we developed.<sup>12</sup> The changes of the molecular characteristics of the hydrogels

were monitored by using GPC and NMR methods described above. FT-IR spectra recorded on Bio-Rad 165 FT-IR spectrophotometer were further used to investigate the degradation products in molecular environment. Pressed pellets prepared by grinding the samples with KBr at 1:100 ratio were used in the measurement.

### 4.2.4 3D Cell Encapsulation and Sub-culture

**Cytotoxicity Study.** The *in vitro* cytotoxicity test of the hyperbranched block copolymers was carried out using the MTT assay in L929 cell lines. Cells were seeded in a 96-well microtiter plate (Nunc, Wiesbaden, Germany) at a density of  $6 \times 10^4$  cells/well, and cultured in complete DMEM supplemented with 10% FBS at 37 °C, 5% CO<sub>2</sub>. After 24 h, culture medium was replaced with serum-supplemented culture medium containing copolymers of known concentrations, and the cells were incubated for a further 48 h. Then, 10 μL of sterile-filtered MTT stock solution in PBS (5 mg/mL) was added to each well, reaching a final MTT concentration of 0.5 mg/mL. After 5 h, unreacted dye was removed by aspiration. The formazan crystals were dissolved in DMSO (100 μL/well), and the absorbance was measured using a microplate reader (Spectra Plus, TECAN) at a wavelength of 570 nm. The relative cell viability (%) related to control cells cultured in media without polymers was calculated with  $[A]_{test}/[A]_{control} \times 100\%$ , where  $[A]_{test}$  is the absorbance of the wells with polymers and  $[A]_{control}$  is the absorbance of the control wells.<sup>37</sup> All experiments were conducted with six repetitions and averaged.

**Cell Encapsulation and Live-dead Assays.** Swollen hydrogels within 8-well chamber slides (Lab-Tek, USA) at a concentration of 10% (w/v) were freeze dried to prepare the hydrogel scaffolds. Before the cell seeding experiments, the scaffolds within the glass chamber were exposed under UV-light for 1 h for sterilization. L929 cells ( $5 \times 10^5$  in 200 μL suspension) were added into each well containing the hydrogel scaffold, and the cells were mixed well with the hydrogel. After incubation for 1 h in an incubator (37 °C, 5% CO<sub>2</sub>), the cells entrapped in the hydrogel (10%, w/v) were obtained. The cells were further incubated for 72 h with addition of fresh DMEM on the top of the hydrogel every 24 h. The 3D distribution of the cells within the hydrogels was visualized by confocal laser scanning microscopy FV1000 (CLSM, Olympus Japan).

For Live-dead assays of the encapsulated cells, the cells were stained with a live/dead cell vitality assay kit (C<sub>12</sub>-Resazurin/SYTOX Green) followed by CLSM measurements.<sup>38</sup> Samples were visualized at excitation wavelength of 543 nm and emission wavelength of 619

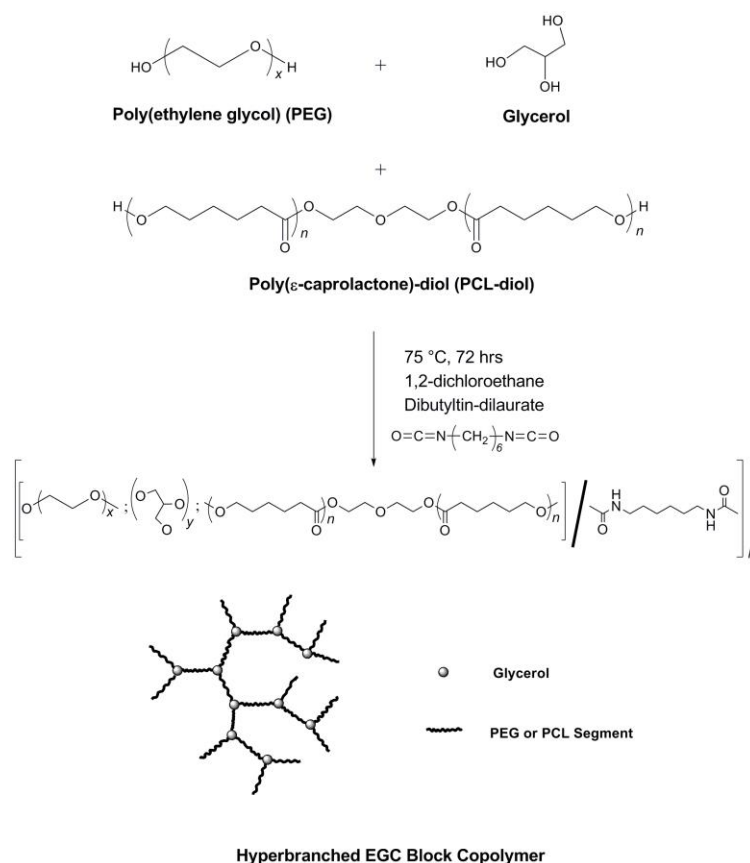
nm for the red color image. Excitation wavelength of 488 nm and emission wavelength of 519 nm were selected for the green fluorescence image collection. All the samples were measured under the same conditions.

**Cell Recovery and Sub-culture.** The cell-encapsulated hydrogel in the glass chamber was taken out and agitated in fresh DMEM. After that, the mixture was transferred into 2-mL centrifuge tube and centrifuged at 1000 rpm for 5 min (twice) to collect the cell suspension. The cell suspension was dispersed equally into 6 wells in a 24-well plate, followed by further culture for 5 days before MTT assay.

### 4.3 Results and Discussion

#### 4.3.1 Synthesis and Characterization of Hyperbranched EGC Block Copolymers

Previously, we reported the synthesis and water swelling behavior of amphiphilic multiblock poly(ester ether urethanes) consisting of PEG, PCL and poly(propylene glycol) (PPG) blocks.<sup>23</sup> Each prepolymer terminated with hydroxyl group was linked with HDI as a chain extender to form linear block copolymers. The obtained copolymers can be casted into films with good mechanical property. In this study, hyperbranched block copolymers comprising these components were designed and synthesized. Glycerol was used as a tri-functional branching agent and HDI as a coupling reagent. The reaction of  $-OH$  of PCL, PEG and Glycerol with  $-NCO$  of HDI in the presence of dibutyltin dilaurate led to hyperbranched architecture of the final copolymers. Recently, we applied a similar protocol to produce hyperbranched amphiphilic polyurethane multiblock copolymers consisting of PEG, PPG, and PCL as thermogels.<sup>39</sup> The synthesis route and schematic illustration of the hyperbranched block copolymers in this paper is presented in Scheme 4.1.



**Scheme 4.1. Synthesis route and schematic illustration of hyperbranched EGC block copolymer.**

In the synthesis, a lower concentration of PEG, PCL and glycerol prepolymers (~12 wt%) in 1,2-dichloroethane was used in comparison with previous study (~25 wt%), since the viscosity of the polymer solution increased significantly with the polymerization, which may lead to a crosslinked product at high concentration.<sup>23</sup> Addition of 2-propanol at the end of the reaction was used to consume any unreacted –NCO groups. As such, the allophanate reaction, occurring between the –NCO and the urethane group can be eliminated.<sup>40</sup> Hydrophobic PCL incorporated in the polymer frame was to enhance the gel properties as well as to make the polymer biodegradable.

A series of hyperbranched EGC block copolymers with different branch length were synthesized, and their molecular weights and molecular weight distributions were determined by GPC (Table 4.1). The observation of unimodal peaks in GPC chromatographs of the purified products the successful polymerization.<sup>41, 42</sup> In addition, all polymers synthesized had low polydispersity (1.34 – 1.41) and high molecular weight ( $2.02 \times 10^4$  –  $3.74 \times 10^4$ ). The sample EGC3 recorded lower molecular weight on GPC than EGC1 and EGC2 due to the shorter

branch length which made the sample dissolved poorly in THF. The filtration process before injecting the solution into GPC column would have excluded the high molecular weight component of the sample EGC3. The average branch length between two adjacent glycerol units for each polymer was theoretically calculated based on the feed ratio and molecular weight. The results are also tabulated in Table 4.1.

**Table 4.1. Synthesis and molecular characteristics of hyperbranched EGC block copolymers.**

Copolymer <sup>a</sup>	Feeding ( $\times 10^3$ mol)			PEG Content (wt %)		Branch length <sup>c</sup>	$M_n$ <sup>d</sup>	PDI <sup>d</sup>	CGC ( $\times 10^2$ g/mL) <sup>e</sup>
	PCL	Gly	PEG	Measured <sup>b</sup>					
				Feeding	Measured <sup>b</sup>				
EGC1	1.89	0.26	2.25	81	83	7079	37400	1.41	8
EGC2	1.89	0.51	2.25	80	79	3625	46500	1.37	6
EGC3	1.89	0.51	1.13	70	71	2157	20200	1.34	/ <sup>f</sup>

<sup>a)</sup> Hyperbranched block copolymers are denoted EGC, where E represents for PEG, G for glycerol, and C for PCL.

<sup>b)</sup> Calculated from TGA thermograms.

<sup>c)</sup> Theoretical branch length calculated based on the feed ratio and molecular weight.

<sup>d)</sup> Determined from GPC.

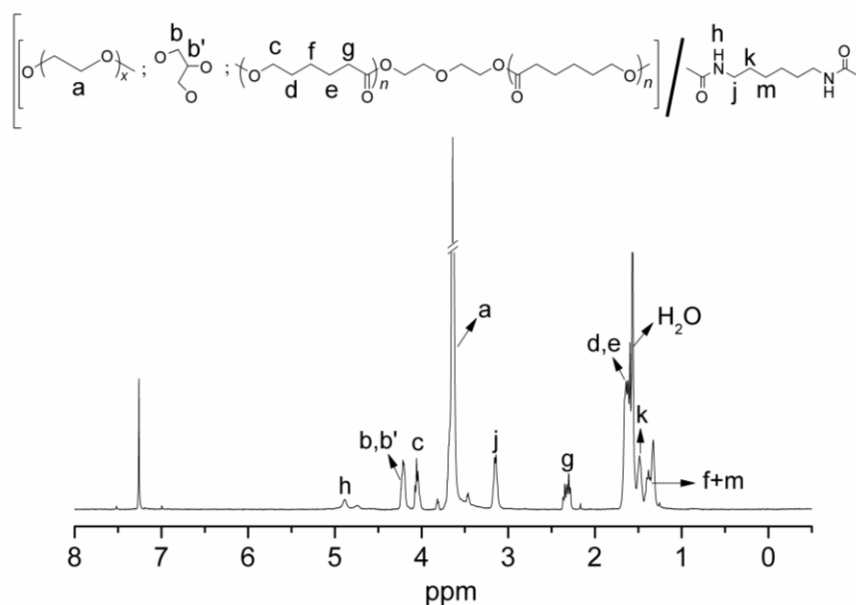
<sup>e)</sup> Critical gelation concentration determined by inverting vial method.

<sup>f)</sup> EGC3 cannot form gel.

Glycerol serves as a tri-functional branching agent. Its amount in the feeding plays a crucial role in determining the branch length of the final products. For samples EGC1 and EGC2 with fixed feeding amount of PCL-diol ( $1.89 \times 10^{-3}$  mol) and PEG ( $2.25 \times 10^{-3}$  mol), the branch length decreased from 7079 to 3625 by increasing the glycerol amount from  $2.6 \times 10^{-4}$  to  $5.1 \times 10^{-4}$  mol in the reaction system. However, it should be noted that the resultant hyperbranched block copolymers can hardly be fabricated into hydrogels when the branch length is too short or too long. When the theoretical branch length was longer than 7079, the resulting polymer dissolved completely in water. While the theoretical branch length was shorter than or equal to 2157 (EGC3), the polymers were rigid, brittle and poor in water-swelling. Hence, we only measured and analyzed the two samples with branch lengths of 7079 and 3625 in next sections.

The chemical structure of the hyperbranched EGC block copolymers was verified by <sup>1</sup>H NMR spectroscopy. Figure 4.1 shows the <sup>1</sup>H NMR spectrum of EGC3 in CDCl<sub>3</sub>, in which all proton signals belong to PEG, glycerol and PCL portions are confirmed. The signals at 3.6 ppm corresponds to the methylene protons in PEG segments, those at 4.1 ppm to the methylene

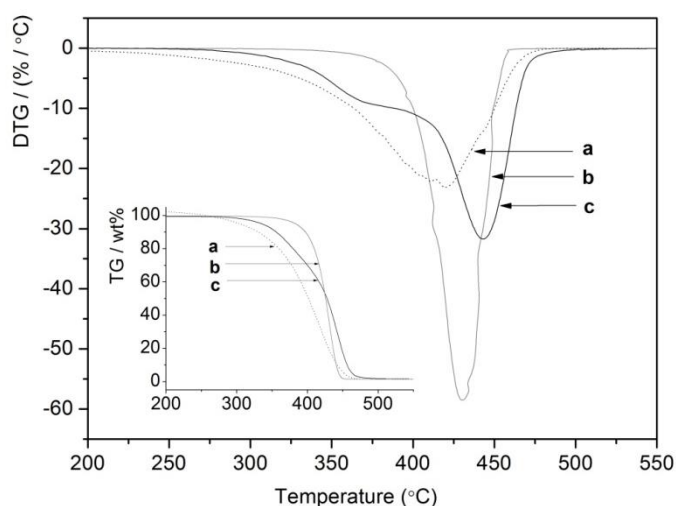
protons alpha to the ester group of PCL segments,<sup>23</sup> and those at 4.2 ppm to the methenyl and methylene protons in glycerol. The new peaks found at 4.9 ppm are attributed to the urethane linkage generated from the reaction between hydroxyl groups and isocyanate groups in HDI ( $-\text{OH} + -\text{NCO} \rightarrow -\text{NHCOO}-$ ). The above observation, together with the concomitant increase in the molecular weight of the copolymers indicate that the polymerization reaction was successful.



**Figure 4.1.** <sup>1</sup>H NMR spectrum of EGC3 in CDCl<sub>3</sub>.

The thermal Properties: Thermal stability and crystallization property were evaluated using TGA and DSC (Figures 4.2 & 4.3). Numerical values corresponding to the thermal transition and the crystallinity are tabulated in Table 4.2. As depicted in the TG/DTG curves of EGC2 and its precursors (Figure 4.2), the block copolymers undergo stepwise thermal degradation, and exhibit two DTG peaks arising from the decomposition of PCL and PEG, respectively. The compositions of the hyperbranched block copolymers can be calculated from the two step degradation profile. Results estimated from TGA are in excellent agreement with the values in the feeding (Table 4.1). The weight loss at low temperatures in TGA thermograms corresponds to the decomposition of PCL moieties and it is retarded by the incorporation of PEG segment by 10 to 30 °C (Table 4.2). This implies that the introduction of PEG would make the PCL in the copolymers more thermal stable than the PCL precursor.

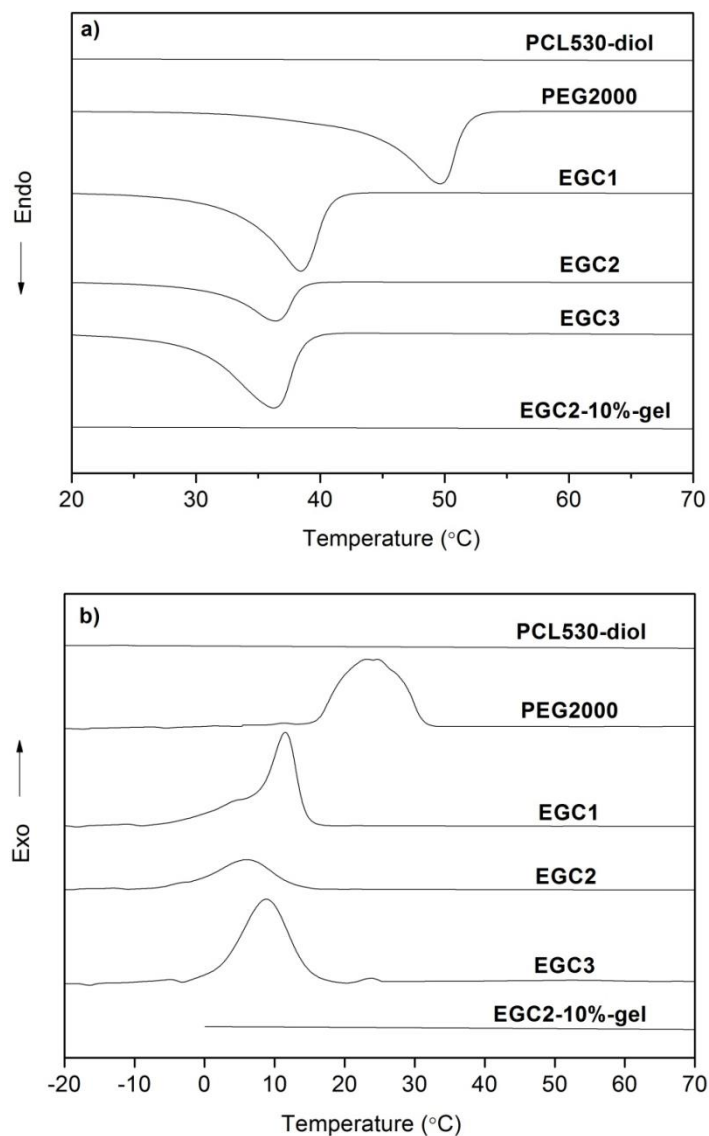




**Figure 4.2.** TG/DTG curves a) PCL530-diol, b) PEG2000, and c) EGC2.

From DSC, no crystallization and melting were detected for PCL block because the short PCL chains cannot retain its crystallinity.<sup>26</sup> The melting endotherms and crystallinity of PEG and EGC block copolymers in solidified and hydrogel states are shown in Figure 4.3. The melting points,  $T_m$ , are detected to be around 37°C for samples EGC1, EGC2, and EGC3, which is much lower than 49.6 °C, the  $T_m$  of pure PEG (Table 4.2). Moreover, The  $T_m$  of EGC copolymers shifts to a lower temperature with decrease in the branch length (Figure 4.3a). This may be due to the fact that the hyperbranched structure makes the molecular chains pack more loosely than pure PEG.<sup>43</sup> The crystallinity,  $X_c$ , calculated from melting endotherm also reveals that the presence of the hyperbranched structure limits the mobility of PEG chains to crystallize to a large extent and this effect is proportional to the branch length of the hyperbranched block copolymers as well as the polymer molecular weight and compositions (Table 4.2).<sup>44</sup>

For the exothermic crystallization peaks (Figure 4.3b), the crystallization temperature,  $T_c$ , recorded during the cooling process indicates that the nonisothermal crystallinity of PEG from melting state in the hyperbranched polymers is retarded to lower temperatures as compared with pure PEG (24.7 → 11.5 °C) (Table 4.2). The further decrease in the branch length of samples EGC2 and EGC3 leads the  $T_c$  below 10 °C. All these results prove that the hyperbranched structure not only affects the crystallinity but also the crystallization rate of PEG in the polymer.<sup>44</sup> More importantly, the hyperbranched EGC block copolymers in hydrogel state do not show any crystallinity behavior, which can provide a mild aqueous environment for cell encapsulation. Otherwise, the sharp crystal structure may cause damage to the cell membrane and make the materials not applicable for cell encapsulation application.<sup>45</sup>



**Figure 4.3.** DSC curves of hyperbranched EGC block copolymers, EGC2 hydrogel at 10% (w/v), and the precursors of EGC copolymers. a) data collected from reheating run; b) data collected from cooling process.

Therefore, the thermal study of the hyperbranched EGC block copolymers in different states indicates: (1) the powder morphology of dried samples possesses various extents of crystallinity; (2) Its subsequent water-swelling in the hydrogel formation under physiological environment could eliminate PEG crystals and potentially provide a vehicle for cell encapsulation.

**Table 4.2. Thermal transitions of hyperbranched EGC block copolymers, hydrogels, and their precursors.**

Samples	$\Delta H_m$ (J/g) <sup>a</sup>	$T_m$ (°C) <sup>b</sup>	$X_c$ (%) <sup>c</sup>	$\Delta H_c$ (J/g) <sup>d</sup>	$T_c$ (°C) <sup>e</sup>	$T_d$ (°C) <sup>f</sup>
PCL530	/	/	/	/	/	328.6
PEG2000	118.1	49.6	57.6	123.3	24.7	397.3
EGC1	64.7	38.7	35.2	65.1	11.5	338.8
EGC2	58.8	35.4	34.9	57.9	5.8	356.3
EGC3	50.1	34.7	34.1	54.1	8.8	316.4
EGC gel <sup>g</sup>	/	/	/	/	/	/

a) Enthalpy change during melting determined in the DSC second heating run.

b) Melting point determined in the DSC second heating run.

c) Crystallinity degree calculated from melting enthalpies. Reference values of 205.0 J/g for completely crystallized PEG was used.<sup>26</sup>

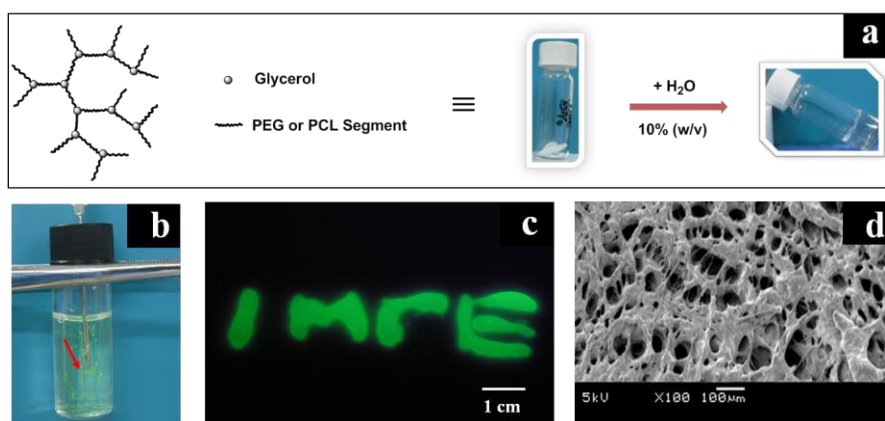
d) Exothermic enthalpies obtained from cooling scan.

e) Crystallization temperature obtained from cooling scan.

f) Decomposition temperature recorded at 10% weight loss on TGA thermograms.

g) All hydrogels prepared from EGC1 and EGC2 samples were recorded no crystallinity of PEG.

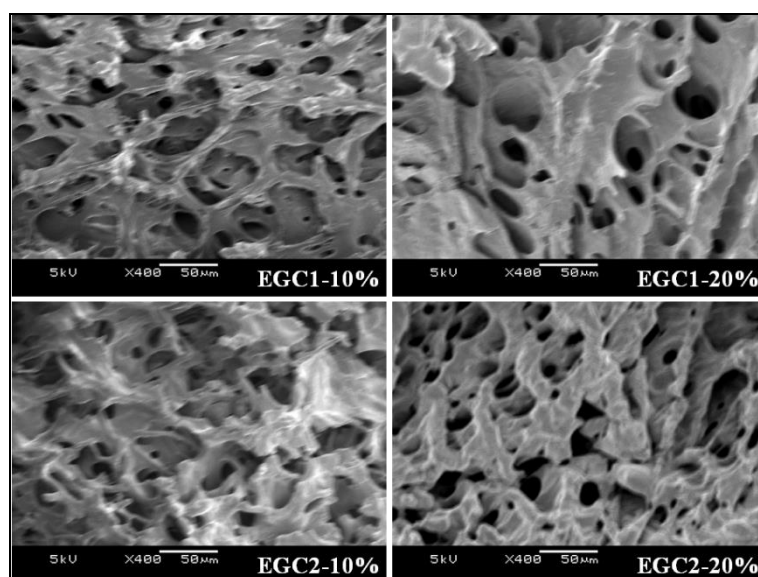
#### 4.3.2 Characterization of Hyperbranched EGC Hydrogels



**Figure 4.4.** EGC hydrogel preparation and its various forms. a) Illustration of the hydrogel preparation by using sample EGC2 at 10% (w/v); b) Hydrogel injected out from the syringe needle. The red arrow indicates the byssoid hydrogel that was flowing out. The gel was loaded with dextran-FITC for better visibility; c) Hydrogel modeled in different shapes; d) SEM micrograph of the freeze-dried of EGC2-10% hydrogel.

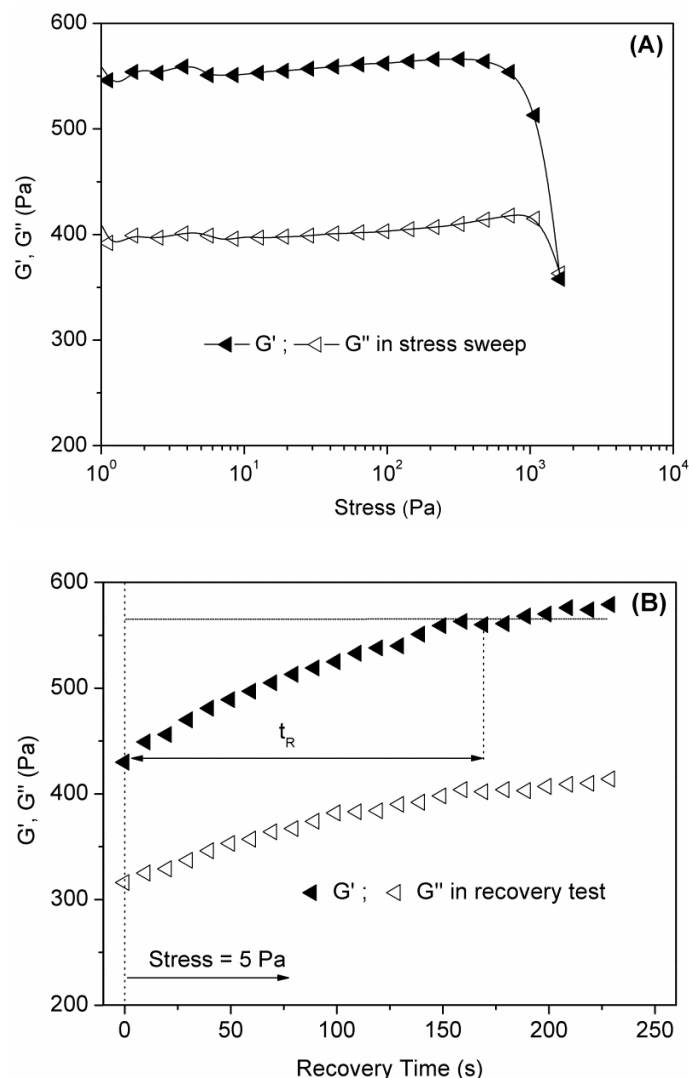
Hydrogel Formulations and Rheological Characterizations: Hydrogels were prepared by mixing the hyperbranched EGC block copolymers with deionized water at given concentrations

(Figure 4.4a). The CGCs of the samples EGC1 and EGC2 were found to be between 6% and 8% (w/v). These values are much lower than those reported for the linear PEG-PCL-PEG and PCL-PEG-PCL block copolymers based hydrogels (15~20 wt%).<sup>46 47</sup> Figure 4.4a shows the photographs of the stable hydrogel formation of sample EGC2 at 10% (w/v). The hydrogel at this concentration can be injected through a 1.10 mm diameter syringe needle under normal pressure, which renders the hydrogel suitable for injection (Figure 4.4b). As such, it could be modeled into different shapes easily. Figure 4.4c shows the various shapes of EGC2-10% hydrogel loaded with Dextran-FITC. Nevertheless, EGC3 behaved rigid, brittle and poor in water swelling due to its low PEG content and short branch length, which cannot form a hydrogel formation.



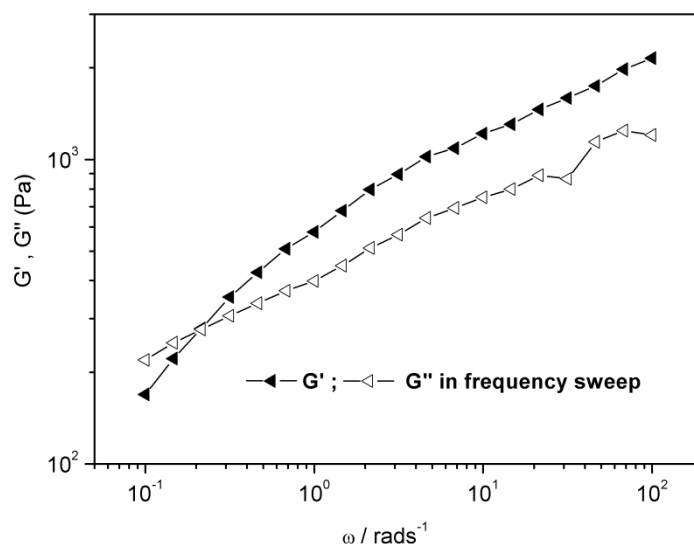
**Figure 4.5. SEM micrographs of the EGC hydrogels (Scale bar: 50  $\mu\text{m}$ ).**

The freeze-dried EGC hydrogel were characterized by SEM. The SEM graph of the cross section of EGC2 hydrogel after lyophilisation is shown in Figure 4.5. It shows that the hydrogel has a porous structure. The average pore diameters of the hydrogels made of EGC1 at 10 and 20% (w/v) are 25 and 15  $\mu\text{m}$ , respectively, whereas those are 15 and 10  $\mu\text{m}$ , respectively, for EGC2 hydrogels at the same concentrations (Figure 4.5). The high water content and porous structure in the hydrogel could provide good permeability for nutrition and gases, which is an important characteristic for encapsulating cells.<sup>4</sup>



**Figure 4.6. (A) Oscillatory stress sweep measurement of EGC2-10% hydrogel at 25 °C and constant angular frequency  $\omega = 1$  rad/s. (B) Oscillatory time sweep measurement of EGC2-10% hydrogel at 25 °C and constant  $\sigma = 5$  Pa after 30 seconds deformation using shear stress at the crossover point of  $G'$  and  $G''$  (1620 Pa). The recovery time  $t_R$  is the time required for 100% recovery of elastic modulus to its original value before the deformation.**

Rheological characterization of EGC hydrogels was performed. As shown in Figure 4.6, an oscillatory stress sweep measurement on EGC2-10% (w/v) shows that the hydrogel, within its linear viscoelastic range of up to almost 500 Pa in terms of shear stress, has an elastic modulus ( $G'$ ) dominating over its viscous modulus ( $G''$ ) with a magnitude of 560 Pa, which indicates the gel formation. The hydrogel formation evidence also came from the frequency sweep measurements, which generally shows its  $G'$  greater than  $G''$  (Figure 4.7).



**Figure 4.7. Oscillatory frequency sweep measurement of EGC2 hydrogel at 10% (w/v) at 25 °C.**

From Table 4.3, the  $G'$  of EGC2-10% hydrogel is nearly 12 times lower than F127-20% hydrogel, implying the low stiffness of EGC2-10% hydrogel under experimental conditions. In addition, a shear stress of 1620 Pa is required to destroy the network structure of EGC2-10% hydrogel that is manifested by a  $G'/G''$  crossover into liquid-like phase.<sup>8</sup> On the other hand, F127-20% hydrogel yields at a shear stress of only 111 Pa. It is thought that hydrogels formed from the hyperbranched EGC block copolymers can stand larger strain, because the hyperbranched architecture can uniformly disperse the deformation.<sup>48</sup>

The complete elastic modulus  $G'$  data obtained from the oscillatory stress sweep measurements, together with the polymer concentrations of the EGC1 and EGC2 hydrogels, are presented in Table 4.3. As demonstrated,  $G'$  and yield stress increase with an increase in the polymer concentration for both hydrogel series. Surprisingly, the shear stress that leads to EGC2-25% hydrogel failure can reach 12000 Pa comparing with 111 Pa for F127-20% hydrogel. This indicates that the hyperbranched polymer hydrogels possess superior viscoelasticity properties to the commercial F127 hydrogel.

The mechanically reversible gel-liquid-gel transition was demonstrated in Figure 4.6. In gel state,  $G'$  is larger than  $G''$ , and the gel starts to liquefy when  $G' = G''$ . As the gel becomes liquefied,  $G'$  becomes less than  $G''$ .<sup>8</sup> In the recovery test, the hydrogel was firstly destroyed by maintaining the shear stress at the  $G'/G''$  crossover point for 30 s followed by monitoring the  $G'$  and  $G''$  recovery versus time using a fixed shear stress of 5 Pa. The increasing of  $G'$  and

$G''$  with time in the gel recovery process was recorded, and the data are shown in Figure 4.6. Here, the recovery time is defined the time required for a 100% recovery of the  $G'$  to its original value from the destroyed gel.

**Table 4.3. Rheological characteristics of hyperbranched EGC hydrogels at various concentrations and the hydrogel recovery time.**

Samples	$G'$ (Pa)	$G''$ (Pa)	$\tau$ (Pa) <sup>a</sup>	$\gamma$ (%) <sup>b</sup>	$t_R$ (sec) <sup>c</sup>
EGC1-10%	308	257	884	355	54
EGC1-12%	502	392	1620	449	110
EGC1-15%	1140	789	2970	678	130
EGC1-25%	4780	3290	1240	360	147
EGC2-10%	560	401	1620	608	177
EGC2-12%	590	414	2430	579	194
EGC2-15%	1500	967	5450	690	210
EGC2-25%	4980	3260	12000	640	410
F127-20%	6640	1170	111	6.8	<sup>d</sup>

<sup>a)</sup> Shear stress recorded at the crossover point of  $G'$  and  $G''$ .

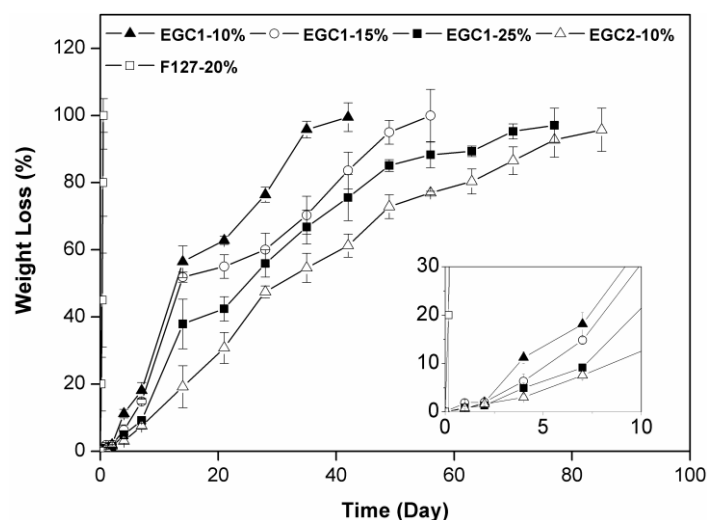
<sup>b)</sup> Deformation at yield point.

<sup>c)</sup> Hydrogel recovery time in second defined by a 100% recovery of  $G'$  from a destroyed gel at yield point.

<sup>d)</sup> Recovered immediately.

As it can be seen from Table 4.3, at the onset of the liquefied hydrogel, the deformation ratio of the tested hydrogels reach to 355–690%, which subsequently affects the recovery time. Depending on the hydrogel composition and concentration, the recovery time varies from 54 to 410 s. So, the hydrogels are thixotropic. The driving force for the hydrogel recovery may be the H-bonding interaction between the oxygen-rich chains and the urethane linkage formed during the polymerization.<sup>40</sup> Hydrogels with shorter branch length and higher concentration have lower water swelling ratio comparing with the fully swollen hydrogels, which would thus lead to a longer recovery time due to the less efficient H-bonding interaction effect.

Hydrolytic Degradation of EGC Hydrogels: EGC hydrogels at predetermined concentration can be obtained after incubation the copolymers in PBS buffer for 1 day, after which the hydrolytic degradation process was investigated by monitoring the weight loss of the hydrogels. As shown in Figure 4.8, all the gels were experiencing a steady mass loss with the increasing incubation period. This observation may be due to the surface erosion occurred on the packed gels when immersed in large quantity of PBS buffer solution. Moreover, the hydrogel erosion could be controlled by the gel composition. With increase of gel concentration, the time required for completely erosion increased. Therefore, by adjusting the hydrogel concentration and EGC block copolymer composition, the erosion time of EGC based gels can be tuned from 40 days up to 90 days. F127 hydrogels on the other hand experienced a complete weight loss within one day under the designed experimental conditions, indicating its poor stability as injectable hydrogels.

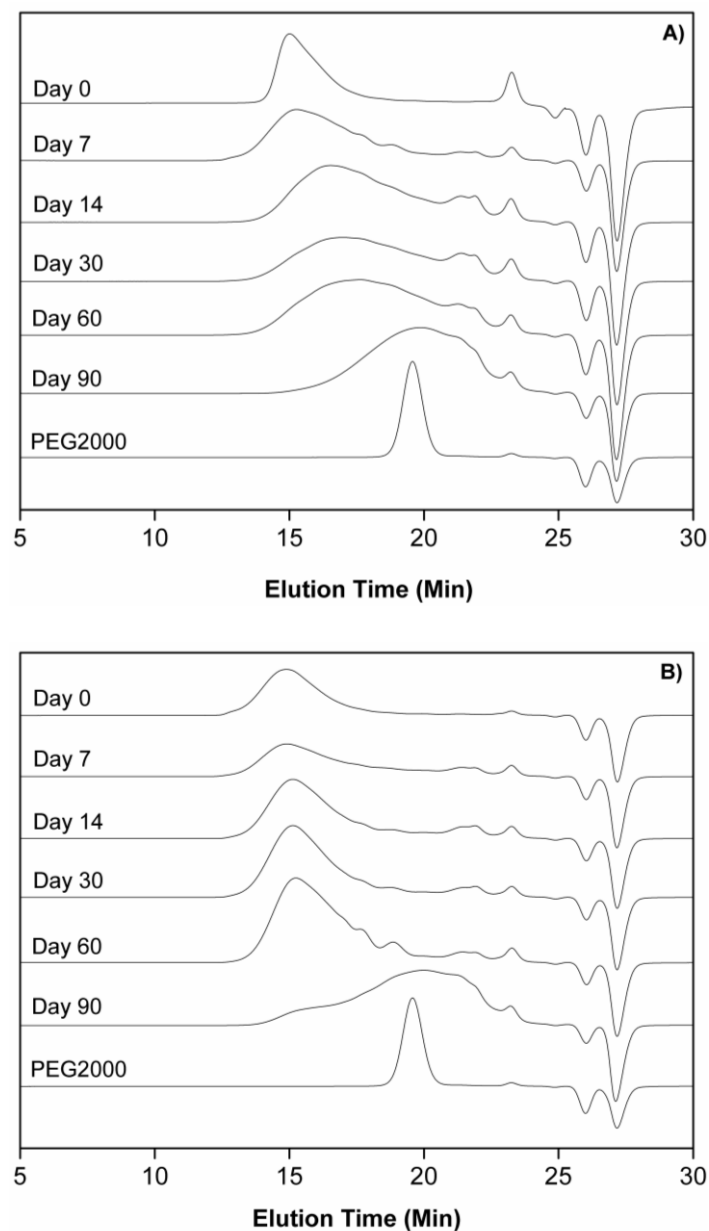


**Figure 4.8.** Mass loss (%) of the EGC based hydrogels after incubation in PBS at pH 7.4 and 37 °C.

The molecular weight change at various degradation periods was monitored by GPC. As shown in Figure 4.9, the measurements of the degraded residuals extracted from the PBS buffer showed a change of the copolymers during hydrolytic degradation from narrow unimodal to broad molecular weight distributions. The broaden GPC shapes may be generated from some new-born lower molecular weight components which came from the chain scission of the ester bonds in PCL units.<sup>49</sup> The molecular weight kept going down with the degradation proceeding



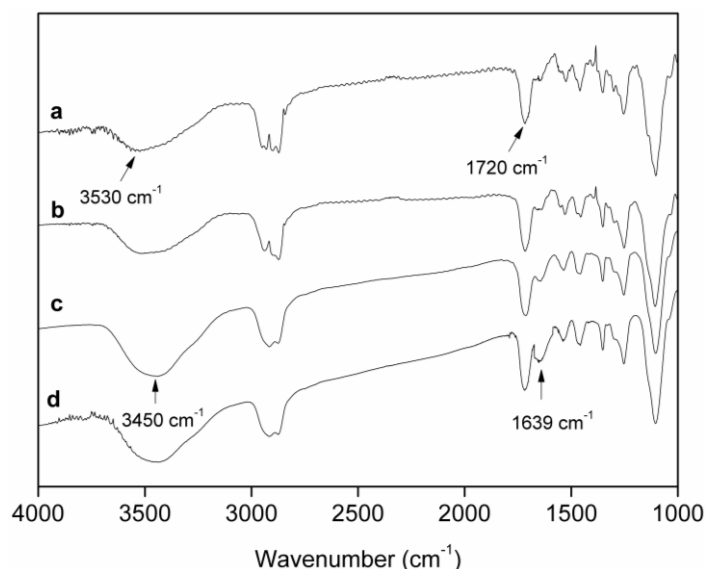
to 3 months. Almost all the residual samples degraded into lower molecular weight components, as compared with one of the starting materials, PEG2000.



**Figure 4.9.** GPC profiles of samples (A) EGC1-10% hydrogel and (B) EGC2-10% hydrogel degradation products in chloroform extracts from the PBS buffer at various hydrolysis periods.

Interestingly, EGC1 copolymer started to degrade after 15 days incubation whereas EGC2 copolymer with higher molecular weight and shorter branch length did not show obvious

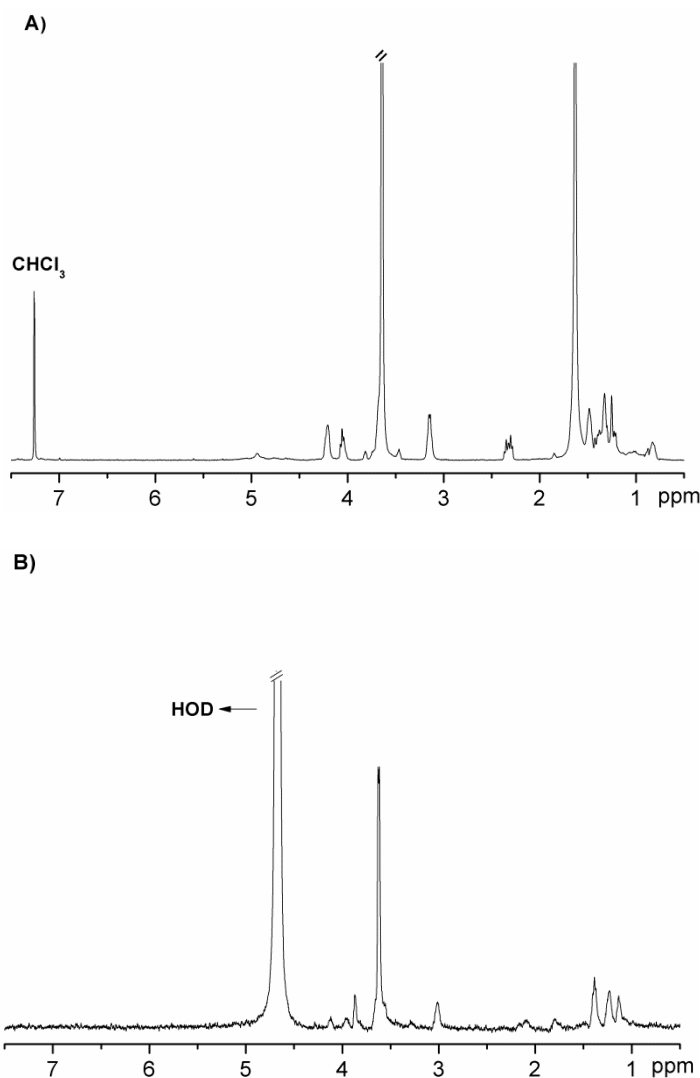
decrease in molecular weight up to 30 days (Figure 4.9). As stated above, the molecular weight and branch length played a crucial role in weight loss and molecular degradation. Previously, we reported that amphiphilic poly(PPG/PEG/PCL urethane) that is more hydrophilic than pure PCL increased the degradation rate of the PCL segments in the copolymers and the arrangement of polymer segments into hyperbranched structure could further increase the degradation rate of poly(PPG/PEG/PCL urethane).<sup>39, 50</sup> The present study shows that the copolymers comprising PCL at molecular weight of 530 has slower degradation rate as compared with the copolymer synthesized from PCL-triol ( $M_n = 300$ ) as biodegradable segments, although both copolymers are in hyperbranched architecture.



**Figure 4.10.** FTIR spectra of EGC1-10% hydrogel after different degradation periods. (a) original EGC1 copolymer, (b) Gel residue after 30 days of degradation, (c) Water soluble fractions after 30 days of degradation, and (d) Water soluble fractions after 90 days of degradation.

The changes in molecular structures of the copolymer hydrogels after various periods of degradation were also monitored by FTIR spectroscopy. A typical example for EGC1-10% hydrogel is shown in Figure 4.10. In the original un-degraded sample, the  $\text{-C=O}$  in ester peak corresponding to the repeating CL units in PCL can be observed at  $1720\text{ cm}^{-1}$ , along with a small peak at  $1530\text{ cm}^{-1}$  which corresponds to the stretching vibrations of NH bonds.<sup>51</sup> The gel residue obtained after 30 days of hydrolysis showed a shift of the peak to  $1639\text{ cm}^{-1}$ , as generated from  $\text{-C=O}$  carboxylic stretching. This confirms that the ester bonds were hydrolyzed to the carboxylic acid groups.<sup>12</sup> Furthermore, the ratio of the peak height at  $1720$

$\text{cm}^{-1}$  to that at  $1639 \text{ cm}^{-1}$  showed a concomitant decrease with increasing degradation time, as recorded on the water-soluble fraction of the hydrolysis products (Figure 4.10 curves c  $\rightarrow$  d). This result implies a further scission of ester bond in PCL segments with increasing incubation time, leading to more carboxylic acid groups in the degradation products, giving a stronger signal in FTIR spectra.



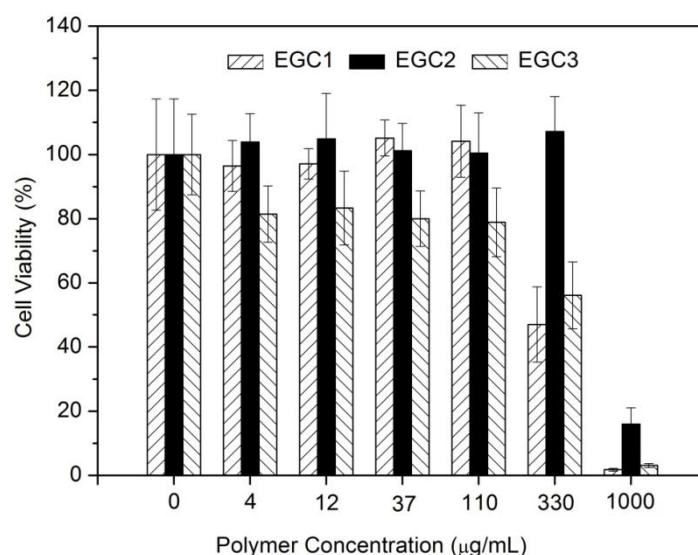
**Figure 4.11.**  $^1\text{H}$  NMR spectra of EGC1-10% (w/v) hydrogel degradation products in (A) chloroform extracts and (B) in water extracts after 90 days.

In Figure 4.10 a  $\rightarrow$  d, in the  $-\text{OH}$  stretching region, the peak at  $3530 \text{ cm}^{-1}$  showed a shift to  $3450 \text{ cm}^{-1}$ , during which two peaks were observed. The  $3530 \text{ cm}^{-1}$  peak corresponds to the  $-\text{OH}$  stretch of the hydroxyl moiety while the peak observed at round  $3450 \text{ cm}^{-1}$  corresponds to the  $-\text{OH}$  stretch of the carboxylic acid moiety.<sup>12</sup> It can be observed that the peak corresponding

to the –OH stretch of the carboxylic acid moiety is absent in the FTIR spectrum of the original un-degraded polymer sample. The degradation products of EGC1-10% hydrogel in chloroform extract and PBS buffer were measured by  $^1\text{H}$  NMR, respectively. At 3.7, 2.4 and 4.1 ppm, methylene proton signals were observed as  $\text{HOCH}_2$ -,  $-\text{OCOCH}_2$ -, and  $-\text{C}(=\text{O})\text{OCH}_2$ - in  $\text{CDCl}_3$  whereas 3.6 and 4.2 ppm were found as  $-\text{OCH}_2\text{CH}_2\text{O}$ - and  $-\text{CHCH}_2\text{O}$ - in both  $\text{CDCl}_3$  and  $\text{D}_2\text{O}$  as solvents (Figure 4.11). Therefore, the identified degraded products are 6-hydroxycaproic acid and its oligomers, PEG and glycerol contained fragments.<sup>52</sup>

### 4.3.3 Cell Encapsulation, Recovery and Sub-culture

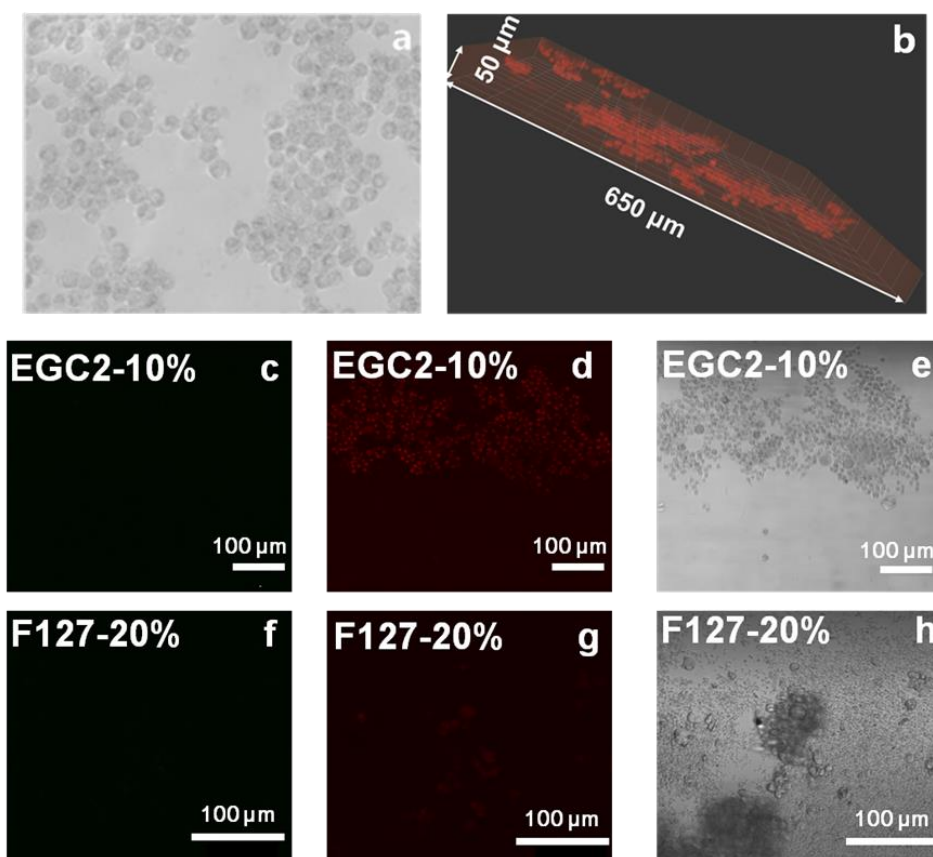
Cytotoxicity Assay: MTT assay was performed to investigate the cytotoxicity of the EGC polymers. The effect of the polymer concentration on the proliferation of L929 cells was studied. As shown in Figure 4.12, there is no significant difference in cell viability when the concentration of the polymer is between 40  $\mu\text{g}/\text{mL}$  and 110  $\mu\text{g}/\text{mL}$ . The cell viability was still higher than 50%, even when the polymer concentration of EGC1 and EGC3 was 330  $\mu\text{g}/\text{mL}$ . The results demonstrated that the hyperbranched block copolymers prepared in this paper show low cell cytotoxicity.



**Figure 4.12.** L929 cell viability in the presence of hyperbranched EGC block copolymers at different concentrations.

Cell Encapsulation and Live-dead Assays: Hydrogel prepared from the hyperbranched EGC block copolymers with longer branch length are vulnerable in gel erosion and dissolution,

so EGC1 polymer based hydrogel are not suitable for cell encapsulation at low concentration. Thus, cell encapsulation was carried out in EGC2 hydrogel, which had very low weight loss percentage in the hydrolytic degradation experiment (Figure 4.8). A uniform cell encapsulated hydrogel can be obtained by simply adding the cell suspension into the polymer scaffold and incubate it for 1 h at 37 °C. The 3D distribution of the cells within the hydrogel can be expected, as the cell suspension can penetrate through the porous structure of the polymer scaffold and the hydrogel formed around the entrapped cells.



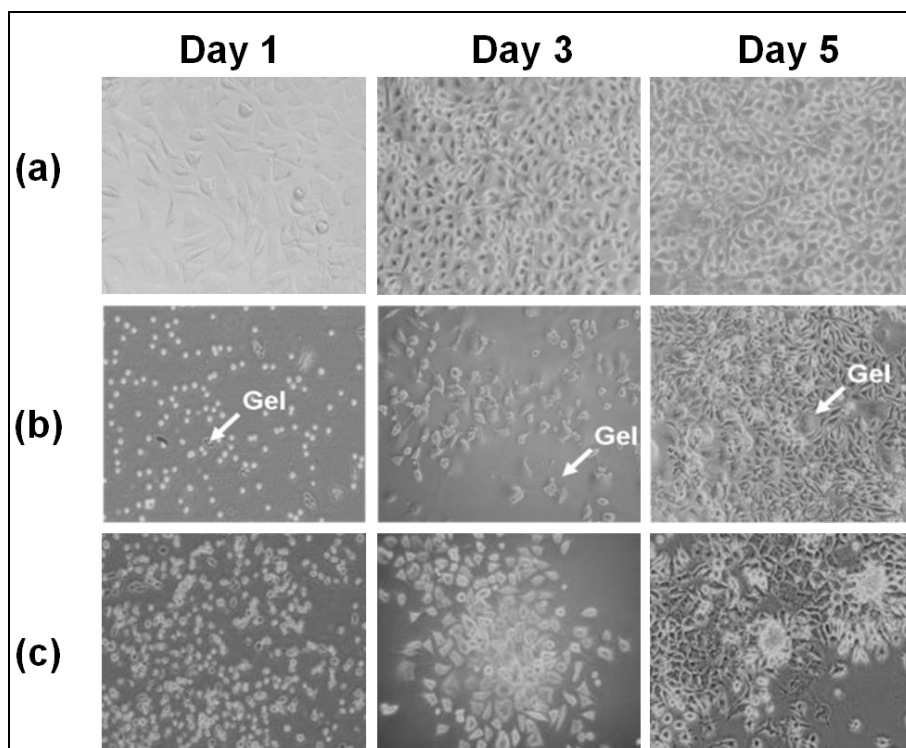
**Figure 4.13. Viability of cells encapsulated in hydrogels. a) Micrograph of L929 cells entrapped in the upper surface of EGC2-10% (w/v) hydrogel; b) Confocal micrograph showing the spatial distribution of cells within the hydrogel; c–h) Showing the live-dead assay of the cells in EGC2-10% hydrogel and F127-20%, respectively. Healthy cells emit red fluorescence while injured/dead cells emit weak red/green fluorescence. All pictures were taken after three days encapsulation in hydrogels.**

Figure 4.13a shows the phase contrast microscope image of L929 cells in the upper surface of the EGC2-10% hydrogel. The cell morphology was circular with no discernible cell spreading in the EGC2 hydrogel during the three days culture period. The cell morphology correlates with the cellular activities and functions; a strong cell adhesion and spreading often

favor proliferation while a round cell shape is required for cell-specific functions.<sup>10, 53, 54</sup> The average cell number ( $4.7 \times 10^5$ ) as counted by hemocytometer after hydrogel encapsulation did not show increase in comparison to the seeded cell number in the hydrogel scaffold ( $4.7 \times 10^5$ ). This may be explained by the high hydrophilicity of EGC2 hydrogels because cell growth in highly hydrophilic environment is known to be strongly suppressed.<sup>55</sup> The fibroblasts used in this study are anchorage-dependent cells (ADCs) and the proliferation of these cells requires spreading to a substrate.<sup>56</sup> This finding is accordance with the cells encapsulated in poly(vinyl alcohol) (PVA) complex network hydrogel and F127 thermogels, which the cells can hardly proliferate but maintain the activity within the hydrogel.<sup>4, 10</sup>

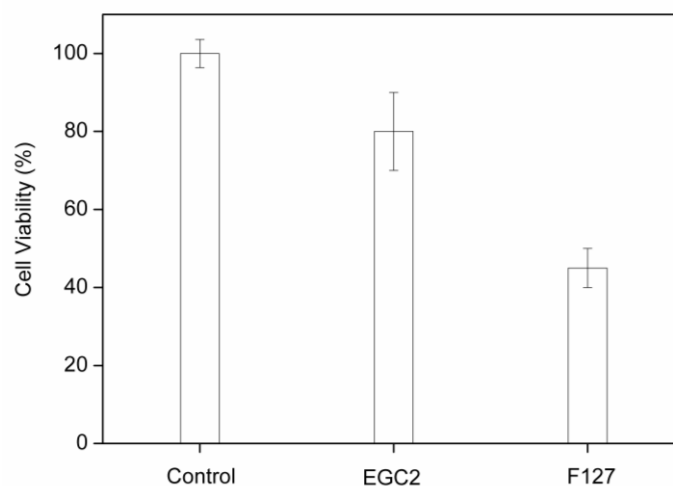
The spatial distribution of the encapsulated cells within the hydrogel was evaluated by confocal laser scanning microscopy (CLSM). Before imaging, the cells at determined culture period were stained for live-dead assay, namely, dead cells emit mostly green fluorescence whereas the healthy, metabolically active cells emit mostly red fluorescence in the applied kit.<sup>38</sup> Slices taken at each depth of the hydrogel by CLSM were rebuilt into a 3D image, which reflected the true situation of the cells within the gel. As can be seen in Figure 4.13b, the image of the slices taken at the cuboid region with 50  $\mu\text{m}$  height and 650  $\mu\text{m}$  width shows that the cells encapsulated within EGC2 hydrogel maintain high activity after three days culture and are spatially distributed uniformly. The porous structure within the hydrogel can not only provide high nutrition and gas permeability needed for the cells entrapped but also allow the cells distribution in a 3D manner.

Figure 4.13 (c  $\rightarrow$  h) shows the live-dead results of cells entrapped in EGC2 in contrast to F127 hydrogels. Obviously, cells in EGC2 hydrogels maintain higher activity than those encapsulated in F127 hydrogels, although no obvious dead cells were detected in both samples (no green fluorescence). The cells in F127 emitted very weak red fluorescence due to the fact that the injured cells have lower metabolic activity and, consequently, reduced red fluorescence emission.<sup>38</sup> Further prolongation of cell incubation time in F127 gels will result in cell death.<sup>14</sup> As suggested by Bott K et al., PEG-based hydrogel with higher gel stiffness ( $G' > 1200$  Pa) acts as a barrier for cells cultured in 3D and the best performance may be achieved with  $G'$  ranging from 10 to 1000 Pa.<sup>3</sup> Our rheological results show that by varying polymer composition, the gel stiffness can be tuned to a suitable range for 3D cell encapsulation. These results suggest that the hyperbranched EGC block copolymer based hydrogels show superiority in cells encapsulation application to F127 hydrogels.



**Figure 4.14. Micrographs of recovered L929 cells cultured at different periods of incubation in tissue culture dishes. (a) trypsin-detached cells; (b) cells recovered from EGC2-10% hydrogel; (c) cells recovered from F127-20% hydrogel.**

Cell Recovery and Sub-culture: The cells-encapsulated hydrogel was dissolved by addition of DMEM followed by gentle trituration. The cells recovered from the hydrogel were seeded on the tissue culture dishes. Figure 4.14 shows the morphological images of the recovered L929 cells cultured for different cell culture periods in comparison with those of cells recovered from trypsin detachment. The cells recovered from hydrogels adhered and proliferated slower than the trypsin-detached cells at day one. The residual PEG from the hydrogel fragment in the cell culture medium can form PEG-hydration with water, which may influence the cell adhesion onto the surface of culture dishes.<sup>57</sup> However, as shown in Figure 4.14b, the EGC2-10% hydrogels had no adverse effects on the health of cells, and their morphology at day 5 became normal.<sup>4</sup> MTT assay of the cell viability at day 5 is presented in Figure 4.15. The results confirmed the good viability of the cells recovered from the EGC2-10% hydrogel. However, for the F127-20% gel, the cell growth was suppressed as compared to those recovered from the EGC2-10% hydrogel.<sup>55, 58</sup>



**Figure 4.15. Cell viability plot of the recovered L929 cells from hydrogels cultured for 5 days. EGC2-10% and F127-20% hydrogels were used in the study. Cells activity obtained from the freshly trypsin detached cells was used as control.**

#### 4.4 Conclusion

A series of hyperbranched EGC block copolymer were designed and characterized, and the glycerol was used to control the hyperbranched structure of the copolymers. Thixotropic hydrogels were formed from these copolymers, which had tunable rheological properties particularly suitable for live cell encapsulation. The fabricated EGC hydrogels underwent hydrolytic degradation in a controllable manner. Cells were encapsulated into the hydrogels, which were found to homogeneously distribute within the hydrogels. The encapsulated cells maintained good cell viability and the recovered cells from the hydrogels showed good proliferation ability. Based on our results, it can be concluded that the hydrogels could provide a mild and suitable 3D environment for cells just like a cell suspension. Together with its injectable property in nature, the hydrogels could be promising injectable systems for cell delivery application.



## 4.5 References

1. E. Cukierman, R. Pankov, D. R. Stevens and K. M. Yamada, *Science*, 2001, **294**, 1708-1712.
2. D.-Q. Wu, Y.-X. Sun, X.-D. Xu, S.-X. Cheng, X.-Z. Zhang and R.-X. Zhuo, *Biomacromolecules*, 2008, **9**, 1155-1162.
3. K. Bott, Z. Upton, K. Schrobback, M. Ehrbar, J. A. Hubbell, M. P. Lutolf and S. C. Rizzi, *Biomaterials*, 2010, **31**, 8454-8464.
4. T. Konno and K. Ishihara, *Biomaterials*, 2007, **28**, 1770-1777.
5. D. Q. Wu, T. Wang, B. Lu, X. D. Xu, S. X. Cheng, X. J. Jiang, X. Z. Zhang and R. X. Zhuo, *Langmuir*, 2008, **24**, 10306-10312.
6. F. Cellési, N. Tirelli and J. A. Hubbell, *Macromol. Chem. Phys.*, 2002, **203**, 1466-1472.
7. C. R. Nuttelman, M. A. Rice, A. E. Rydholm, C. N. Salinas, D. N. Shah and K. S. Anseth, *Prog. Polym. Sci.*, 2008, **33**, 167-179.
8. Y. S. Pek, A. C. A. Wan, A. Shekaran, L. Zhuo and J. Y. Ying, *Nat Nanotechnol*, 2008, **3**, 671-675.
9. D.-Q. Wu, F. Qiu, T. Wang, X.-J. Jiang, X.-Z. Zhang and R.-X. Zhuo, *ACS Appl. Mater. Interfaces*, 2009, **1**, 319-327.
10. A. Higuchi, T. Yamamoto, K. Sugiyama, S. Hayashi, T. M. Tak and T. Nakagawa, *Biomacromolecules*, 2005, **6**, 691-696.
11. Y. Li, J. Rodrigues and H. Tomas, *Chem. Soc. Rev.*, 2012, **41**, 2193-2221.
12. X. J. Loh, S. H. Goh and J. Li, *Biomaterials*, 2007, **28**, 4113-4123.
13. L. E. Bromberg and E. S. Ron, *Adv. Drug Delivery Rev.*, 1998, **31**, 197-221.
14. S. F. Khattak, S. R. Bhatia and S. C. Roberts, *Tissue Eng.*, 2005, **11**, 974-983.
15. J. Li, X. Li, X. Ni, X. Wang, H. Li and K. W. Leong, *Biomaterials*, 2006, **27**, 4132-4140.
16. R. Barbucci, D. Pasqui, R. Favaloro and G. Panariello, *Carbohydr. Res.*, 2008, **343**, 3058-3065.
17. Y. S. Pek, A. C. A. Wan and J. Y. Ying, *Biomaterials*, 2010, **31**, 385-391.
18. Y. H. Bae and S. W. Kim, *Adv. Drug Delivery Rev.*, 1993, **11**, 109-135.
19. A. K. A. Silva, C. Richard, M. Bessodes, D. Scherman and O.-W. Merten, *Biomacromolecules*, 2009, **10**, 9-18.

20. D.-Q. Wu, T. Wang, B. Lu, X.-D. Xu, S.-X. Cheng, X.-J. Jiang, X.-Z. Zhang and R.-X. Zhuo, *Langmuir*, 2008, **24**, 10306-10312.
21. R. A. Stile, W. R. Burghardt and K. E. Healy, *Macromolecules*, 1999, **32**, 7370-7379.
22. Z. Li, H. Yin, Z. Zhang, K. L. Liu and J. Li, *Biomacromolecules*, 2012, **13**, 3162-3172.
23. X. J. Loh, K. B. C. Sng and J. Li, *Biomaterials*, 2008, **29**, 3185-3194.
24. R. S. Bezwada, D. D. Jamiolkowski, I.-Y. Lee, V. Agarwal, J. Persivale, S. Trenka-Benthin, M. Erneta, J. Suryadevara, A. Yang and S. Liu, *Biomaterials*, 1995, **16**, 1141-1148.
25. G. G. Pitt, M. M. Gratzl, G. L. Kimmel, J. Surles and A. Sohindler, *Biomaterials*, 1981, **2**, 215-220.
26. J. Kloss, M. Munaro, G. P. D. Souza, J. V. Gulmine, S. H. Wang, S. Zawadzki and L. Akcelrud, *J. Polym. Sci., Part A: Polym. Chem.*, 2002, **40**, 4117-4130.
27. J. Y. Pan, G. Y. Li, Z. F. Chen, X. Y. Chen, W. F. Zhu and K. T. Xu, *Biomaterials*, 2009, **30**, 2975-2984.
28. C. T. Chen, R. F. Eaton, Y. J. Chang and A. V. Tobolsky, *J. Appl. Polym. Sci.*, 1972, **16**, 2105-2114.
29. J. Yu, S. Sundaram, D. Weng, J. M. Courtney, C. R. Moran and N. B. Graham, *Biomaterials*, 1991, **12**, 119-120.
30. N. Yui, K. Kataoka, A. Yamada, Y. Sakurai, K. Sanui and N. Ogata, *Makromol. Chem. Rapid Commun.*, 1986, **7**, 747-750.
31. Y. Ikeda, S. Kohjiya, S. Takesako and S. Yamashita, *Biomaterials*, 1990, **11**, 553-560.
32. N. Yui, K. Kataoka, A. Yamada and Y. Sakurai, *J. Controlled Release*, 1987, **6**, 329-342.
33. C. R. Valeri, G. Ragno, L. E. Pivacek, G. P. Cassidy, R. Srey, M. Hansson-Wicher and M. E. Leavy, *Vox Sang.*, 2000, **79**, 168-174.
34. X. J. Loh, S. H. Goh and J. Li, *Biomacromolecules*, 2007, **8**, 585-593.
35. E. Behravesh, A. K. Shung, S. Jo and A. G. Mikos, *Biomacromolecules*, 2001, **3**, 153-158.
36. W. Rungseevijitprapa and R. Bodmeier, *Eur. J. Pharm. Sci.*, 2009, **36**, 524-531.
37. X. J. Loh, Z.-X. Zhang, Y.-L. Wu, T. S. Lee and J. Li, *Macromolecules*, 2009, **42**, 194-202.
38. M. J. White, M. J. DiCaprio and D. A. Greenberg, *J. Neurosci. Methods*, 1996, **70**, 195-200.

39. Z. Li, Z. Zhang, K. L. Liu, X. Ni and J. Li, *Biomacromolecules*, 2012, **13**, 3977-3989.
40. G. Hild, *Prog. Polym. Sci.*, 1998, **23**, 1019-1149.
41. X. J. Loh, K. K. Tan, X. Li and J. Li, *Biomaterials*, 2006, **27**, 1841-1850.
42. Z. B. Li, X. D. Yang, L. P. Wu, Z. F. Chen, Y. T. Lin, K. T. Xu and G. Q. Chen, *J. Biomater. Sci. Polym. Ed.*, 2009, **20**, 1179-1202.
43. G. R. Saad, Y. J. Lee and H. Seliger, *Macromol. Biosci.*, 2001, **1**, 91-99.
44. G. R. Saad, Y. J. Lee and H. Seliger, *J. Appl. Polym. Sci.*, 2002, **83**, 703-718.
45. Anon, *Calcif. Tissue Int.*, 2006, **78**, S52-S52.
46. C. Gong, S. Shi, P. Dong, B. Kan, M. Gou, X. Wang, X. Li, F. Luo, X. Zhao, Y. Wei and Z. Qian, *Int. J. Pharm.*, 2009, **365**, 89-99.
47. S. J. Bae, M. K. Joo, Y. Jeong, S. W. Kim, W. K. Lee, Y. S. Sohn and B. Jeong, *Macromolecules*, 2006, **39**, 4873-4879.
48. A. S. Hoffman, *Adv. Drug Delivery Rev.*, 2002, **54**, 3-12.
49. J. R. Schoonover, D. G. Thompson, J. C. Osborn, E. B. Orler, D. A. Wroblewski, A. L. Marsh, H. Wang and R. A. Palmer, *Polym. Degrad. Stab.*, 2001, **74**, 87-96.
50. X. J. Loh, P. Peh, S. Liao, C. Sng and J. Li, *J. Controlled Release*, 2010, **143**, 175-182.
51. Q. Liu, S. Cheng, Z. Li, K. Xu and G.-Q. Chen, *J. Biomed. Mater. Res., Part A*, 2009, **90A**, 1162-1176.
52. Y. Geng and D. E. Discher, *J. Am. Chem. Soc.*, 2005, **127**, 12780-12781.
53. C. S. Chen, M. Mrksich, S. Huang, G. M. Whitesides and D. E. Ingber, *Biotechnol. Progr.*, 1998, **14**, 356-363.
54. D. Mooney, L. Hansen, J. Vacanti, R. Langer, S. Farmer and D. Ingber, *J. Cell. Physiol.*, 1992, **151**, 497-505.
55. A. Higuchi, S. Tamiya, T. Tsubomura, A. Katoh, C.-S. Cho, T. Akaike and M. Hara, *J. Biomater. Sci. Polym. Ed.*, 2000, **11**, 149-168.
56. Y. Fu, K. Xu, X. Zheng, A. J. Giacomini, A. W. Mix and W. J. Kao, *Biomaterials*, 2012, **33**, 48-58.
57. J. D. Andrade, S. Nagaoka, S. Cooper, T. Okano and S. W. Kim, *ASAIO J.*, 1987, **33**, 75.
58. X. J. Loh, S. H. Goh and J. Li, *J. Phys. Chem. B*, 2009, **113**, 11822-11830.

**CHAPTER 5 SUPRAMOLECULAR NANOCARRIERS  
CONSISTING OF BIODEGRADABLE  
PCL/CYCLODEXTRIN-BASED POLYROTAXANE FOR  
TARGETED GENE DELIVERY**

### **5.1 Introduction**

Due to the inherent obstacles associated with the viral-based gene vectors, such as immunogenicity and mutagenicity, synthetic polymers are being developed as alternatives to viral vectors.<sup>1</sup> These synthetic polymers-based carriers as non-viral vectors are able to provide formulation design flexibility and a specific route of vector administration.<sup>2</sup> Poly(dimethylamino)ethyl methacrylate (PDMAEMA) is a methacrylated-based synthetic polymer containing tertiary amine groups which can condense DNA effectively and provide pH buffering capacity to the polymer.<sup>3</sup> They can be prepared by versatile radical polymerization methods and produced easily in large amount. However, the major drawback in terms of the biological properties is the fact that PDMAEMA and its vinyl derivatives are non-degradable, toxic at high molecular weight and lack of specificity.<sup>4</sup> Previous studies show that the accumulation of PDMAEMA derived polymers in lysosomal compartment may lead to a medical condition classified as macromolecular syndrome or lysosomal storage disease.<sup>5</sup>

Recent efforts are hence directed towards the design of PDMAEMA containing biodegradable block copolymers.<sup>6-9</sup> To this end, high-molecular-weight polymers are able to degrade into small fragments that can be cleared from the body by renal filtration after use. One example is methoxy-poly(ethyleneglycol)-*b*-poly( $\epsilon$ -caprolactone)-*b*-poly[2-(dimethylamino) ethyl methacrylate] (MPEG-PCL-PDMAEMA) triblock copolymer. It was reported as an

efficient transgene carrier and the incorporation of MPEG and biodegradable PCL imparted low cytotoxicity and high gene expression level to the polymer.<sup>6,7</sup> Recently, we investigated the MPEG-PCL-PDMAEMA copolymers anchored cyclodextrins supramolecular hydrogels as an effectively sustained gene delivery carrier.<sup>10</sup> In addition, PDMAEMA-PCL-PDMAEMA triblock copolymer was also demonstrated as a biodegradable gene delivery vector with high transfection efficiency.<sup>8</sup> However, lack of affinity could make these carriers unable to differentiate receptor-mediated endocytosis of human cancer cell lines from the non-specific uptake of normal tissues when applied them as gene vectors. Folate has been previously exploited to enhance the specific targeting of non-viral gene delivery since its target, folate receptor (FR), is frequently amplified in many cancer cells but generally absent in normal cell surface.<sup>2</sup> Copolymerizing of DMAEMA monomer with other vinyl derivatives has been utilized to provide the frames for further modification with folate as targeting reagent. Results show an enhanced endocytosis by the targeted cells.<sup>11,12</sup> Nevertheless, this type of study is very limited and, as mentioned earlier, the vinyl-based polymers are non-degradable and may have a safety concern after repeated administration.<sup>5</sup>

Cyclodextrins (CDs) are a series of cyclic oligosaccharides composed of 6, 7, or 8 glucose units linked by  $\alpha$ -1,4-linkages and named  $\alpha$ -,  $\beta$ -, and  $\gamma$ -CD, respectively. The hydroxyl groups on CDs surface make them possible for various functionalization procedures, and the inner hydrophobic cavity has the ability to form inclusion complexes with different guest molecules.<sup>13-16</sup> With these advantages, CDs are adopted with significant precedence in designing gene delivery carriers to meet various objectives. Recently, we have reported a group of novel CD-containing polymers as gene delivery vectors by functionalizing CDs exterior with cationic polymers, or utilizing its polyrotaxane formation with specific polymer chains.<sup>17-21</sup> Low cytotoxicity and high gene transfection efficiency were achieved on those newly developed polymers. In the present study, we designed a site-specific cell targeting gene delivery carrier based on a biodegradable polyrotaxane (PR) comprising of PCL and  $\alpha$ -CD. For this strategy, bromoisobutyryl-terminated PCL (PCL-diBr) was used for PR preparation via its inclusion complexation with  $\alpha$ -CD for the first time, and the obtained PR was further used as an atom transfer radical polymerization (ATRP) macroinitiator to polymerize DMAEMA into the polymer backbone subsequently. As such, triblock copolymers containing a biodegradable PR flanked by various PDMAEMA segments (D-PR-D) were obtained. Folate, as an active targeting ligand, was covalently attached to the hydroxyl groups in  $\alpha$ -CD exterior by using PEG as a spacer. Physicochemical and biological properties of the desired polymers (FA-PEG-(D-PR-D)) were evaluated in this study. To study the cell specificity of the system,

two cell lines with FR positive (KB) and negative control (A549), were investigated using a plasmid containing a luciferase reporter gene. More importantly, this study provides a new approach for designing receptor-mediated gene delivery system based on CDs and its inclusion complexes.

## 5.2 Experimental Section

### 5.2.1 Materials

Hydroxyl terminated poly( $\epsilon$ -caprolactone) (PCL-diol,  $M_n = 1250$ ) and  $\alpha$ -CD ( $\geq 98\%$ ) were purchased from Aldrich and they were vacuum-dried overnight at  $75^\circ\text{C}$  and  $100^\circ\text{C}$ , respectively, before use. Diamine terminated poly(ethylene glycol) (PEG-*bis*-amine,  $M_n = 3400$ ) was purchased from CreativePEGWorks and used as received. Folic acid ( $\geq 97\%$ ), N-Hydroxysuccinimide (98%), N,N'-Dicyclohexylcarbodiimide (99%), 1,1'-Carbonyldiimidazole (CDI,  $\geq 97\%$ ), 2-bromoisobutyryl bromide (98%), 1,1,4,7,10,10-hexamethyltriethylenetetramine (HMTETA, 99%), copper(I) bromide (CuBr, 99%), triethylamine ( $>99\%$ ), 1,6-diphenyl-1,3,5-hexatriene (DPH), anhydrous dimethyl sulfoxide (DMSO,  $\geq 99.9\%$ ), tetrahydrofuran (THF, 99.9%) and N,N-dimethylformamide (DMF, 99.8%) were purchased from Sigma-Aldrich. 2-(dimethylamino)ethyl methacrylate (DMAEMA) stabilized with hydroquinone monomethyl ether was obtained from Merck and used as received.

### 5.2.2 Synthesis of Polyrotaxane-Based Triblock Copolymers and FA-PEG-(D-PR-D) Conjugates

Folate-PEG-NH<sub>2</sub> was prepared according to the following protocol. N-Hydroxysuccinimide ester of folic acid (NHS-FA ( $\gamma$ )) was prepared in accordance to a reported procedure as shown in Scheme 5.1A.<sup>22</sup> Vacuum dried NHS-FA (23.4 mg, 0.043 mmol) was then dissolved in 5.0 mL dry DMF and the obtained solution was added dropwise into 5.0 mL DMF contained an equal molar amount of PEG-*bis*-amine (147.8 mg, 0.043 mmol) under continuous stirring over a 1 h period. The reaction was carried out in the dark overnight. Based on the molecular weight of PEG-*bis*-amine given by the supplier, we estimate from <sup>1</sup>H-NMR spectra that  $\sim 49.1\%$  of the total amino groups were conjugated to FA. The resulting

FA-PEG-NH<sub>2</sub> containing a free amino group at the distal end of the PEG was for subsequent use in the preparation of D-PR-D triblock copolymer based conjugation (Scheme 5.1B).

PCL-diol was modified into ATRP macroinitiator by esterification of its hydroxyl end groups with 2-bromoisobutyryl bromide (Scheme 1B).<sup>23, 24</sup> Typically, 10.0 g PCL-diol ( $M_n = 1250$ , -OH end groups = 16.0 mmol) was dissolved in 50 mL of anhydrous tetrahydrofuran (THF) containing 1.6 g (16.0 mmol) of triethylamine. The reaction was cooled to 4 °C and then 3.8 g (16.5 mmol) of 2-bromoisobutyryl bromide dissolved in 15 mL dry THF was added dropwise under continuous stirring over a 1 h period in nitrogen atmosphere. After addition, the reaction was sealed and kept at room temperature for another 48 h. The resultant solution was centrifuged to remove triethylamine·HCl salt before it was precipitated in excess hexane/methanol (95/5, v/v) for precipitation. After another cycle of THF dissolution, hexane/methanol (95/5, v/v) re-precipitation, PCL-diBr was filtered and dried under vacuum to give the purified product, yield 82%.

PDMAEMA-Polyrotaxane-PDMAEMA (D-PR-D) triblock copolymers were prepared according to the following two steps (Scheme 5.1B, **3** → **5**). First, a typical polypseudorotaxane (PPR) of PCL-diBr threaded with  $\alpha$ -CD were prepared as follows.  $\alpha$ -CD (3.0 g, 3.0 mmol) and PCL-diBr (1.5 g, 0.97 mmol) were dissolved in a 30 mL dry DMF and heated to 70 °C with vigorous stirring. After being stirred at 70 °C for 6 h, the mixture was cooled to room temperature and stirred vigorously for another 24 h. The precipitated product was collected by centrifugation and three times washed with fresh DMF (15.0 mL) to remove free polymer and unthreaded  $\alpha$ -CD. After washing, the PPR slurry was used as macroinitiator by suspending it in dry DMF containing ATRP reactants. To study the average number of  $\alpha$ -CDs threaded and the crystallinity behavior of PPR prepared in this step, the PPR slurry was then dried overnight in high vacuum to give a white powder before characterization. Molecular characteristic of PPRs obtained under different feed ratios were tabulated in Table 5.1. Second, D-PR-D triblock copolymers were prepared by controlled ATRP. Molar feed ratio of [PPR2] : [DMAEMA] : [HMTETA] : [CuBr] = 1 : 1000 : 2 : 1 was applied for all polymer syntheses. In a typical experiment, 2.5 mL dry DMF and 4.8 g (31.3 mmol) of DMAEMA were first introduced into a nitrogen filled round bottom flask (RBF) followed by successive addition of CuBr (4.5 mg, 0.031 mmol) and HMTETA (14.4 mg, 0.062 mmol) under nitrogen atmosphere. Then, the RBF was purged and refilled with nitrogen using *vacuum-nitrogen-cycling* system three times. After 30 min equilibration, the mixture was transferred into a PPR2 slurry (0.2 g, 0.031 mmol) contained RBF through syringe injection. The RBF was again purged and refilled with nitrogen using *vacuum-nitrogen-cycling* system three times. Polymerization was allowed to proceed

under continuous stirring at room temperature for 24 h and then heated to 40 °C for another 24 - 72 h to give various lengths of PDMAEMA segments. D-PR-D triblock copolymers are depicted as D-PR-D-1 and D-PR-D-2, which represents different PDMAEMA segment lengths in the polymer composition (Table 5.2). The reaction was stopped by precipitating the mixture in excess ether. For a further purification, the product was again dissolved in 5mL DMF at 60 °C, followed by dialysis for 24 h with frequent water change (MWCO 3500 Da, Spectrum Laboratories, USA) to remove the catalyst complex. The resulting solution was freeze dried before further analysis.

In a typical synthesis of D-PR-D copolymer derived conjugates, the polyrotaxane-based triblock copolymer 5 (D-PR-D-1, 58.5 mg, 0.0043 mmol) was dried in a flask at 40 °C under vacuum overnight. After the flask had cooled, 5 mL of anhydrous DMF was injected under nitrogen to dissolve D-PR-D-1 polymer. Then, the polymer solution of 5 was added dropwise over a period of 1 h under nitrogen to another 5 mL of anhydrous DMF solution in which CDI (5.3 mg, 0.032 mmol) was dissolved. The mixture was stirred overnight under nitrogen at room temperature and this solution was slowly added dropwise during a period of 2 h into 10 mL dry DMF dissolved with 0.043 mmol of FA-PEG-NH<sub>2</sub>. The reaction was kept in the dark at room temperature, followed by stirring the mixture for 48 h. The synthesized product was dialyzed against PBS buffer (10 mM, pH 7.4, 24 h) and DI water (12 h) consecutively in dialysis tube (MWCO 8000 Da). The final products were collected by freeze drying. PEG-(D-PR-D) was prepared by using PEG-*bis*-amine instead of FA-PEG-NH<sub>2</sub> in a similar protocol for comparison study in the biological characterization.

### 5.2.3 Methods and Characterization

**Molecular Characterization.** <sup>1</sup>H and <sup>13</sup>C NMR spectra were recorded on a Bruker AV-400 NMR spectrometer at room temperature. The chemical peaks are reported in ppm with reference to solvent peaks (DMF: δ 8.03, 2.92 and 2.75 ppm for <sup>1</sup>H NMR and δ163.15, 34.89 and 29.76 ppm for <sup>13</sup>C NMR; DMSO: δ 2.50 ppm for <sup>1</sup>H NMR).

**Molecular Weight Determination.** The weight-averaged molecular weight ( $M_w$ ) of the as-synthesized polymers was determined by Gel Permeation Chromatography/Light Scattering (GPC/LS) analysis. GPC was performed on two 10-μm PLgel MIXED-B columns (size: 300 × 7.5 mm) in series with a DMF (0.1M LiBr) flow rate of 1 mLmin<sup>-1</sup>. Light scattering and refractive index measurements were acquired using an Alliance Waters 2690 separation module equipped with a Waters 410 differential refractometer and a Wyatt MiniDAWN light scattering



detector. The LS detection measures the light-scattering intensity at 90° and the RI detection measures the concentration of the copolymers. The data were processed using Astra 4.50 software.

**Nitrogen Content Characterization.** Nitrogen content was determined on an EA1112 Automatic Elemental Analyzer. Samples of about 1.80 - 2.00 mg were loaded into aluminium sample cups for analyses. The analyses were performed at 950 °C with a constant carrier gas flow of 140 mL/min. Sulfanilamide was used as a standard and was analyzed before use.

**Folic Acid Content of FA-PEG-(D-PR-D).** Folic acid content conjugated in FA-PEG-(D-PR-D) was obtained on the basis of the standard curve by using the UV-Vis spectrophotometer (Shimadzu UV 2501, Japan) in the wavelength range of 200 - 400 nm. FA-PEG-(D-PR-D) and folic acid were dissolved in PBS buffer solution. FA-PEG-(D-PR-D) solution of 200 mg/L, and folic acid solution of 2.9 - 50 mg/L were prepared. The absorbance values of the peak intensities at 280 nm of the absorbance spectra were analyzed as a function of folic acid concentration.<sup>25</sup> The concentration of the folic acid in FA-PEG-(D-PR-D) solution was calculated according to the calibration curve made from free folic acid, while the content of folic acid was calculated by the concentration ratio of the folic acid and FA-PEG-(D-PR-D).<sup>26</sup>

**Critical Micellization Concentration Determination.** Critical micellization concentration (CMC) values were determined using dye solubilization method.<sup>27</sup> Hydrophobic dye 1,6-diphenyl-1,3,5-hexatriene (DPH) was dissolved in methanol to give a concentration of 0.6 mM. Ten microliters of this solution was mixed with 1.0 mL of copolymer aqueous solution with concentrations ranging from  $1 \times 10^{-4}$  to 5 mg/mL and equilibrated overnight at 4 °C. A Shimadzu UV-2501PC UV-Vis spectrophotometer was used to obtain the UV-Vis spectra in the range of 330 - 430 nm at 25 °C. CMC values were determined from the plot of the difference in absorbance at 378 nm and at 400 nm ( $A_{378}-A_{400}$ ) versus the logarithmic of the copolymer concentrations.

**Crystallinity Behavior.** Wide angle X-ray scattering (WAXS) was carried out on Bruker GADDS X-ray diffractometer with an area detector, operating under Cu-K $\alpha$  (1.5418 Å) radiation (40kV, 40mA) at room temperature. The samples were scanned from 5 to 40° (2 $\theta$ ).

### 5.2.4 Plasmid Amplification, Cell Lines and Gene Transfection Evaluation

**Plasmid Amplification and Cell Line.** Plasmid pRL-CMV (Promega, USA) was used as reporter gene in this study, which encodes *Renilla* luciferase originally cloned from the

marine organism *Renilla reniformis*. The pDNA was amplified using reported protocol.<sup>3</sup> Human nasopharyngeal cells (KB) and FR negative human lung epithelial carcinoma cells (A549) were purchased from ATCC (Rockville, MD) and maintained respectively in MEM and DMEM/F12 supplemented with 10% fetal bovine serum, 100 units/mg penicillin, 100 mg/mL streptomycin at 37 °C and 5% CO<sub>2</sub>. RPMI 1640 medium (FA free) supplemented with 10% FBS, 100 units/mg of penicillin, and 100 µg/mL of streptomycin was used during cell viability and gene transfection test. MEM, DMEM/F-12, and RPMI-1640 medium (FA free) was purchased from Invitrogen (Carlsbad, CA).

**Formation and Characterization of Polymer/pDNA Polyplexes.** The mean particle size and surface charge of the polymer/pDNA polyplexes were measured on a Zetasizer Nano ZS (Malvern Instruments Ltd., MA, USA), with a laser light wavelength of 633 nm at 173°. 100 µL polyplex solution containing 3 µg of DNA was prepared at various N/P ratios from 2 to 15. The mixture was vortexed for 10 s, incubated for 30 min at room temperature and diluted to 1 mL with filtered distilled water at the time of measurements. Zeta potential measurements were performed using a capillary zeta potential cell in automatic mode. The morphologies of the polyplexes were observed on a high-resolution transmission electron microscope (Philips CM300 FEGTEM) (TEM) operated at an accelerating voltage of 300 kV.

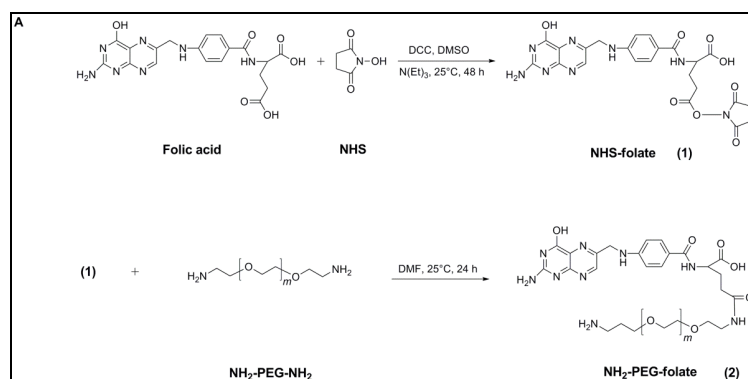
**Gel Retardation Assay.** The polymer/pDNA polyplexes at various N/P ratios were prepared to examine the binding ability of the as-synthesized polymers to pDNA by gel electrophoresis. After adding 10 × loading buffer with polyplex solutions, samples were loaded on a 0.8% agarose gel stained with 1 × SYBR® Safe DNA Gel Stain. The gels were run in 1 × TAE buffer (40 mM Tris-acetate, 1 mM EDTA) at 100 V for 40 min in a Sub-Cell system (Bio-Rad Laboratories, CA). DNA bands were visualized with a UV lamp on GelDoc system (Synoptics Ltd., UK).

**Cell Viability Assay.** Two cell lines (A549 and KB) were cultured in DMEM/F12 and MEM medium supplemented with 10% FBS at 37 °C with 5% CO<sub>2</sub> in a humidified incubator. 100 µL of cell suspension in serum-supplemented RPMI 1640 medium (FA free) were seeded into 96-well plates (NUNC, Wiesbaden, Germany) at a density of  $1.5 \times 10^5$  cells/mL. After 24 h, culture medium were replaced with serum-supplemented RPMI 1640 medium (FA free) containing serial dilutions of polymer, in which the cells were cultured for another 24 h. Then, 20 µL MTS/PMS solution was added into each well and the absorbance of soluble formazan produced by cellular reduction of the MTS was recorded on a microplate reader (Spectra Plus, TECAN) at a wavelength of 490 nm.

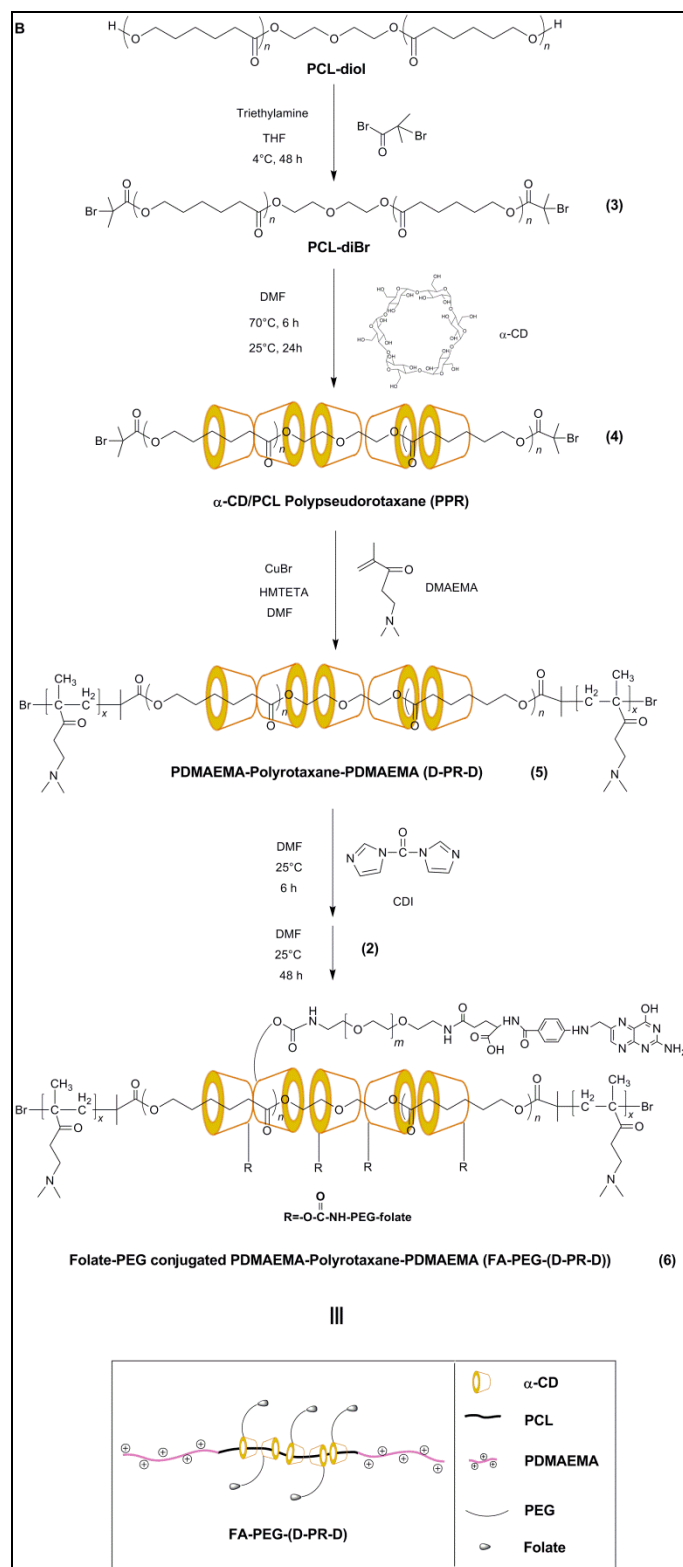
**Transfection Efficiency Study.** KB and A549 cells were grown in folic acid-free RPMI-1640 medium in 24-well plates to 70 - 80% confluence one day prior to the transfection study. The cells were then transfected with freshly prepared gene delivery polyplexes containing 1  $\mu$ g of pDNA at 37 °C for 4 h. After that, the polyplexes solution was replaced with serum supplemented folic acid-free RPMI-1640 medium and the cells were further incubated for 20 h under standard culture conditions. At the end of transfection, the cells were washed with preheated PBS twice, lysed with 100  $\mu$ l of cell lysis buffer (Promega, USA) for 30 min. The luciferase activity in cell extracts was measured using a luciferase assay kit (Promega, USA) on a Berthold Centro LB960 microplate luminometer and monitored with MikroWin 2000 software. The relative light units (RLU) were normalized against protein concentration in the cell extracts, which was measured using Coomassie Plus Protein Assay Reagent (Pierce, Rpckford, IL, USA). Absorption was measured on a microplate reader (Spectra Plus, TECAN) at 595 nm and compared to a standard curve calibrated with BSA samples of known concentrations. Results are expressed as relative light units per milligram of cell protein lysate (RLU/mg protein).<sup>28</sup> For the folic acid competition study, KB and A549 cells were cultured in the same conditions as that for the transfection tests while polyplex solutions at the same N/P ratios were added in the presence of 10  $\mu$ g/mL free folic acid. The transfection efficiency was then assessed using the same way described in this section.

### 5.3 Results and Discussion

#### 5.3.1 Synthesis and Characterization of Polyrotaxane-Based Triblock Copolymers (D-PR-D)



Synthesis route to be continued in the next page.



**Scheme 5.1. Synthetic procedure of Folate-PEG-NH<sub>2</sub> (A) and the final product FA-PEG-(D-PR-D) (B) with D-PR-D triblock copolymer as intermediate.**

To prepare the FA-PEG-(D-PR-D) conjugates, self-assembling PCL/ $\alpha$ -CD PPR, D-PR-D triblock copolymer and folate-PEG-NH<sub>2</sub> were designed and synthesized to develop a new synthetic protocol of using  $\alpha$ -CD to introduce functional groups for conjugation (Scheme 5.1) As a macroinitiator, PCL-diBr was prepared from the reaction of PCL-diol with 2-bromoisobutyryl bromide according to our previous report.<sup>23,24</sup> As shown in Scheme 5.1B, the self-assembly of this macroinitiator with  $\alpha$ -CD gave a PPR suspension after simultaneously stirring with  $\alpha$ -CD in DMF at 70 °C. After cooling to room temperature and washing with fresh DMF, pure PPR slurry was harvested.

Table 5.1 shows the composition and yields of the purified PPRs after drying. As we can see, the yields and coverage ratios of  $\alpha$ -CD change with the feeding ratios and these two values are lower than the PPRs prepared from ultrasonic technique.<sup>29</sup> At optimized condition of PPR2, there are *ca.* 5.3  $\alpha$ -CD molecules trapped in the backbone of PCL-diBr with the yield of 28.9%, as estimated from <sup>1</sup>H NMR in DMSO-d<sub>6</sub> (Figure 5.1B). This clearly indicates that the number of threaded  $\alpha$ -CDs is tunable by altering the feed ratios. More importantly, the purified PPR slurry was stable when dispersed as a suspension in ATRP reactants dissolved DMF solution at room temperature.

The effect of ATRP reaction system on the average-in-chain number of  $\alpha$ -CD in the PPR was monitored by NMR. The  $\alpha$ -CD/PCL molar ratio was found to be *ca.* 4.9 when DMAEMA signals was observed in the NMR spectra monitoring during the reaction, indicating an intact PPR structure for DMAEMA polymerization. The PPR slurry would thus be able to serve as an ATRP macroinitiator to yield the mechanically locked PR-based triblock copolymers (D-PR-D).

**Table 5.1. Compositions and yields of PCL-diBr /  $\alpha$ -CD based polypseudorotaxanes.<sup>a</sup>**

Sample	Molar composition (PCL1250-diBr : $\alpha$ -CD)		Coverage ratio of CDs (%) <sup>c</sup>	Yield (%) <sup>d</sup>
	Feed ratio	Found ratio <sup>b</sup>		
PPR1	1.0 : 2.0	1.0 : 3.1	18.2	17.5
PPR2	1.0 : 3.1	1.0 : 5.3	45.6	28.9
PPR3	1.0 : 11.0	1.0 : 2.7	24.9	23.6

<sup>a)</sup> Polypseudorotaxane, denoted as PPR, was prepared by directly mixing of PCL1250-diBr and  $\alpha$ -CD in DMF.

<sup>b)</sup> Determined by <sup>1</sup>H NMR analysis in DMSO-d<sub>6</sub>.

<sup>c)</sup> Coverage ratio is defined as the ratio of the CL units covered by CDs to the whole CL units based on the fact that one CL unit is covered by one CD molecule.

<sup>d)</sup> Yield is calculated based on the weight of the product divided by that of all raw materials.

On the basis of these trials, the ATRP reaction was firstly controlled to proceed at room temperature for 24 h to sufficiently depress the dethreading of  $\alpha$ -CDs.<sup>30</sup> Then, PR flanked by PDMAEMA with different chain lengths was synthesized by carefully controlling the polymerization time and temperature during the end-capping reaction. The polymer compositions and the molecular characteristics are listed in Table 5.2. During the synthesis of D-PR-D copolymers, the length of PDMAEMA on either side PPR was deliberately restricted to a molecular weight of < 20 000 g/mol so as to allow the final degraded fragment to be easily excreted from the body via renal filtration (Table 5.2).<sup>31</sup>

**Table 5.2. Molecular characteristics of PR-based triblock copolymers and conjugates**

Sample	M <sub>w</sub> <sup>a</sup> (×10 <sup>4</sup> )	PDI <sup>a</sup>	DMAEMA Unit NO. <sup>b</sup>	Conjugated Chain No. <sup>c</sup>	N % <sup>d</sup>	CMC <sup>e</sup> (mg/mL)
D-PR-D-1	1.39 ± 0.12	1.51 ± 0.27	53	- (-) <sup>f</sup>	5.1	0.28
D-PR-D-2	3.49 ± 0.23	1.32 ± 0.28	183	- (-) <sup>f</sup>	7.9	0.35
PEG-(D-PR-D-1)	3.03 ± 0.61	1.63 ± 0.13	46	4.8 (-) <sup>f</sup>	3.2	- <sup>f</sup>
PEG-(D-PR-D-2)	5.01 ± 0.54	1.50 ± 0.16	179	4.5 (-) <sup>f</sup>	6.8	- <sup>f</sup>
FA-PEG-(D-PR-D-1)	2.98 ± 0.32	1.56 ± 0.21	49	4.2 (4.0)	3.7	- <sup>f</sup>
FA-PEG-(D-PR-D-2)	4.98 ± 1.25	1.42 ± 0.25	174	3.9 (3.5)	6.3	- <sup>f</sup>

<sup>a)</sup> The weight-averaged molecular weight ( $M_w$ ) and polydispersity index (PDI) were determined by GPC with light scattering and differential refractometer as detectors. DMF containing 0.1 M LiBr was used as eluent.

<sup>b)</sup> Determined by <sup>1</sup>H NMR.

<sup>c)</sup> Conjugated chain number was determined by GPC. The value in the parentheses was determined by the standard curve based calculation of UV-Vis absorption at 280 nm of FA-PEG-(D-PR-D) solution.

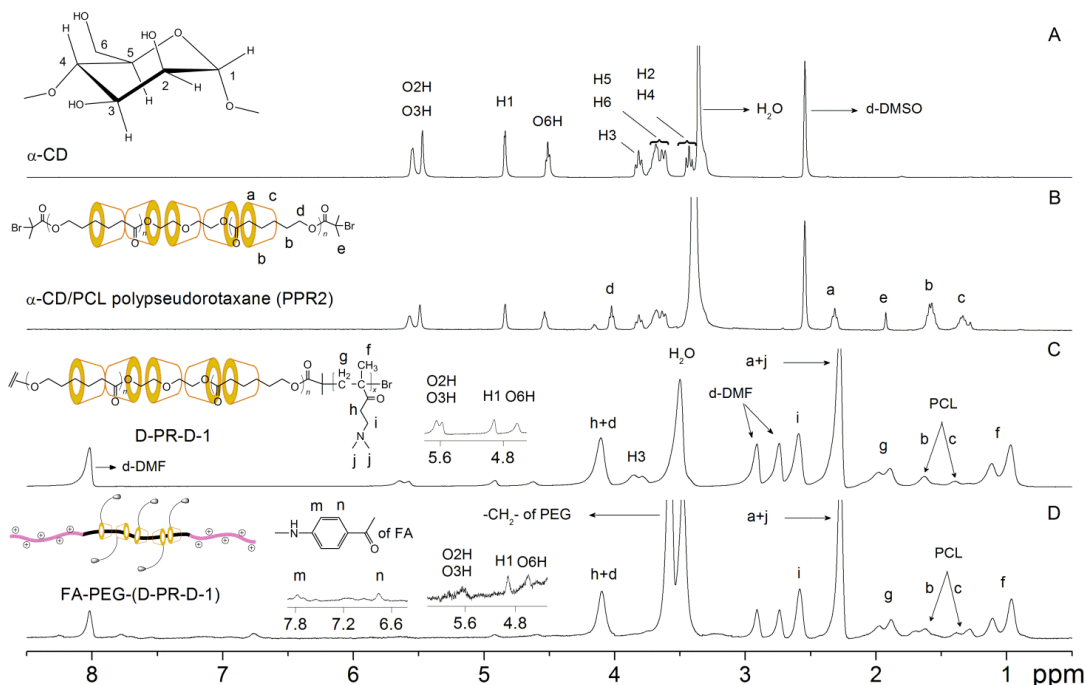
<sup>d)</sup> Nitrogen weight content was evaluated from elemental analyses.

<sup>e)</sup> Critical micellization concentration (CMC) was determined using dye solubilization method.

<sup>f)</sup> Not determined.

The D-PR-D triblock copolymers structure was characterized by NMR analysis. As shown in Figure 5.1C, all resonance peaks of PDMAEMA protons were discernable in D-PR-D-1, indicating that the DMAEMA monomers were successfully polymerized by PCL-diBr with threaded  $\alpha$ -CDs. Evidence can be seen from the new peaks at  $\delta$  2.6 ppm and  $\delta$  0.85 - 1.15 ppm, which are corresponding to the protons of -CH<sub>2</sub>N= and -CH<sub>3</sub> groups in PDMAEMA segments. O2H and O3H of  $\alpha$ -CD appear at  $\delta$  5.52 - 5.73 ppm, and O6H at  $\delta$  4.56 - 4.70 ppm, respectively. The broadening resonance of  $\alpha$ -CDs peaks are observed in D-PR-D-1 spectrum because of the chemical environment change after the channeled structure

was formed between  $\alpha$ -CDs and polymer chains.<sup>14, 30</sup> All resonance peaks of  $\alpha$ -CDs in D-PR-D-1 are obviously broadened and the corresponding hydroxyl groups of O2H, O3H and O6H are in different shapes with those signals observed on pure  $\alpha$ -CD (Figure 5.1 A and C). However, the methylene protons signals of PCL at  $\delta$  4.1 and 2.3 ppm are superposed with protons signals of  $-\text{COCH}_2-$  and  $-\text{N}(\text{CH}_3)_2$  groups of PDMAEMA. The unit number of DMAEMA was hence estimated by integrating the proton chemical shifts of  $-\text{CH}_2-$  in PCL unit at  $\delta$  1.4 ppm and the area of  $-\text{CH}_2\text{N}=\text{}$  at  $\delta$  2.6 ppm in PDMAEMA (Figure 5.1C).

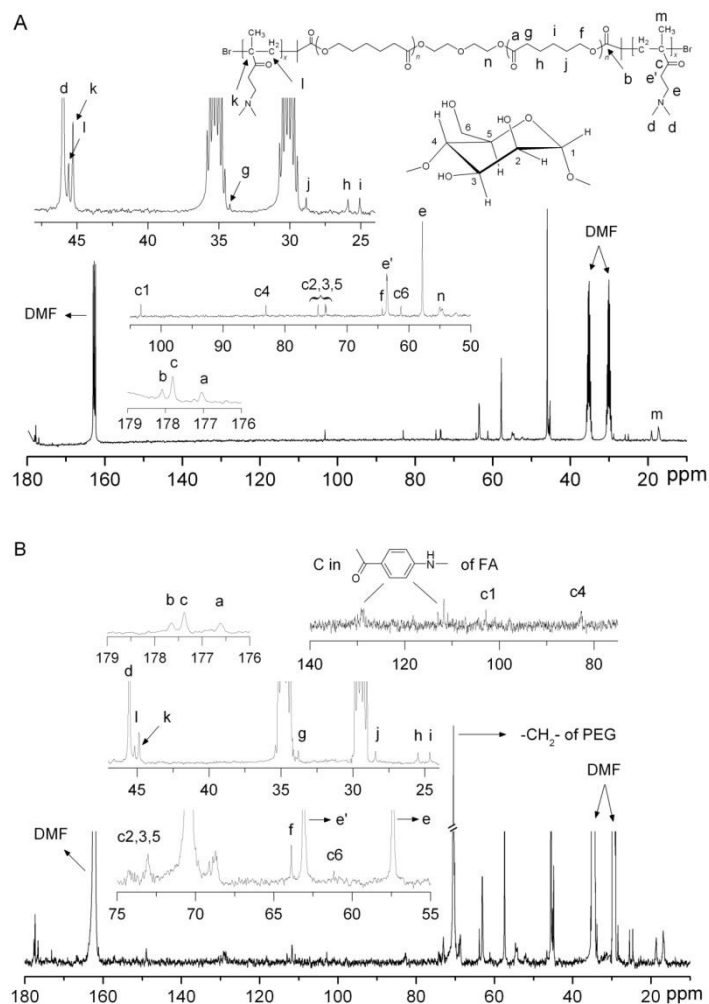


**Figure 5.1.**  $^1\text{H}$  NMR spectra of pure  $\alpha$ -CD (A), PPR2 (B) in  $\text{DMSO-d}_6$ , and D-PR-D-1 (C), FA-PEG-(D-PR-D-1) (D) in  $\text{DMF-d}_7$ .

All these observations indicate that  $\alpha$ -CDs are threaded along the middle PCL block and end stopped by the PDMAEMA blocks as well.  $^{13}\text{C}$  NMR was further applied to investigate the D-PR-D triblock copolymer architecture. As shown in Figure 5.2A, all the signals that belong to the three components are split. The signals corresponding to the methylene carbon alpha to the ester group of PCL segment are observed at  $\delta$  64.5 ppm, while the signals at  $\delta$  46.2 ppm are associated with the methyl carbon adjacent to the tertiary amino moiety in PDMAEMA segments. More importantly, the resonance peaks of the carbons associated with  $\alpha$ -CD from  $\delta$  61.3 to 103.3 ppm are well resolved and can be clearly identified, providing additional evidence on the successful synthesis of D-PR-D triblock copolymer. Nitrogen contents of the D-PR-D

copolymer were obtained from elemental analysis. These data were applied for the stoichiometry of pDNA binding, as reflected by specific N/P ratios.

### 5.3.2 Synthesis and Characterization of D-PR-D Triblock Copolymer Based Conjugates

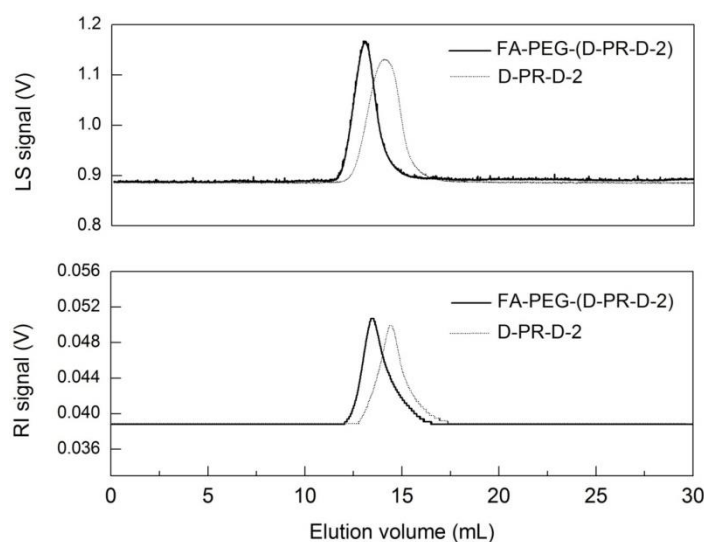


**Figure 5.2.**  $^{13}\text{C}$  NMR spectra of D-PR-D-1 (A) and FA-PEG-(D-PR-D-1) (B) in  $\text{DMF-d}_7$ .

As shown in Scheme 5.1B, the hydroxyl groups of  $\alpha$ -CD rings placed in the central segment of D-PR-D triblock copolymer can be activated with CDI. As such, the activated hydroxyl groups enable the easy coupling reaction with the primary amino group at the distal end of the  $\text{NH}_2$ -PEG-folate as prepared in Scheme 1A. The conjugation procedure was similar to that of our previously reported  $\alpha$ -CD-oligoethylenimine star polymer and PEG/poly(propylene glycol) (PPG) block copolymer based cationic polyrotaxanes.<sup>17, 18, 21, 32</sup> Through this



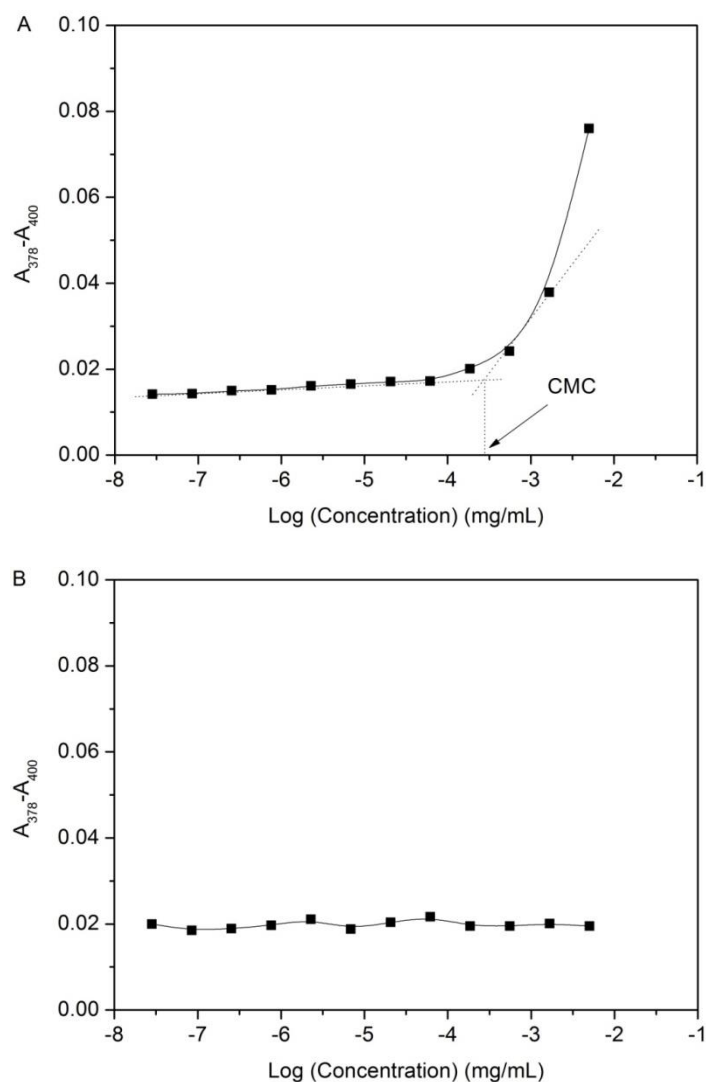
coupling reaction, the targeting molecules were conjugated to D-PR-D polymer backbone via PEG as a spacer to give the final product of FA-PEG-(D-PR-D). Moreover, the desired content of the folic acid in the product was carefully controlled by reactant feed ratios. PEG at molecular weight of 3400 was applied in the designed reaction. This is because long PEG chain can extend the distance between folic acid and the cationic groups of the polymer, which provides more accessibility to the FR positive cells in gene delivery.<sup>33, 34</sup>



**Figure 5.3.** GPC traces of D-PR-D-2 triblock copolymer and the conjugated FA-PEG-(D-PR-D-2) polymer measured with light scattering and differential refractometer as detectors. DMF containing 0.1 M LiBr was used as eluent at 40 °C.

The polymer architecture of FA-PEG-(D-PR-D) was also investigated by NMR measurement. In the spectra of Figure 5.1D, the signals for  $\alpha$ -CD, end-capping PDMAEMA chains and the threading PCL are observed. Also, the  $\alpha$ -CD resonance peaks are much broadened due to the restriction of the molecular motion by molecular interlocking.<sup>14, 30</sup> More importantly, new born peaks corresponding to the methylene protons of PEG segments are observed at  $\delta$  3.6 ppm in comparison with the spectra recorded on D-PR-D before conjugation reaction. The signals appeared at  $\delta$  6.8 and 7.6 ppm are ascribed to the *p*-aminobenzoic acid in folic acid molecules, which gives another evidence for the success of the conjugation reaction.<sup>35</sup> Further structure determination was performed by  $^{13}\text{C}$  NMR. In the spectra of Figure 5.2B, the peaks belong to all components in FA-PEG-(D-PR-D) polymer are observed clearly, and the peak intensity of C6 in  $\alpha$ -CD is reduced at  $\delta$  61.3 ppm and shifts as superposition at  $\delta$  64.0 ppm as compared to Figure 5.2A. This is evidence that the conjugation of  $\text{NH}_2$ -PEG-FA mainly happened at the 6 position hydroxyl group of  $\alpha$ -CD as previously accounted.<sup>17, 18, 36</sup> The relevant signals of folic acid are much weaker than the broad and strong proton signals of PEG

and PDMAEMA. Therefore, for more accurate evaluation, the conjugated folate content was assessed from UV spectroscopy, as discussed later. All these findings show the successful synthesis of the desired FA-PEG-(D-PR-D) supramolecular system through a biodegradable PCL/ $\alpha$ -CD polyrotaxane derived conjugation reaction.



**Figure 5.4. CMC determination of D-PR-D-1 (A) by extrapolation of the difference in absorbance at 378 and 400 nm by using DPH as probe. CMC of FA-PEG-(D-PR-D-1) (B) is not determined in the measured concentration range.**

GPC was performed to determine the molecular weights and molecular weight distribution of the as-synthesized polymers. DMF containing 0.1 M LiBr was used as eluent, given that  $\text{Li}^+$  ion can effectively depress the hydrogen bonding strength between polyrotaxane blocks. Typical GPC signals of D-PR-D-2 triblock copolymer and its derived

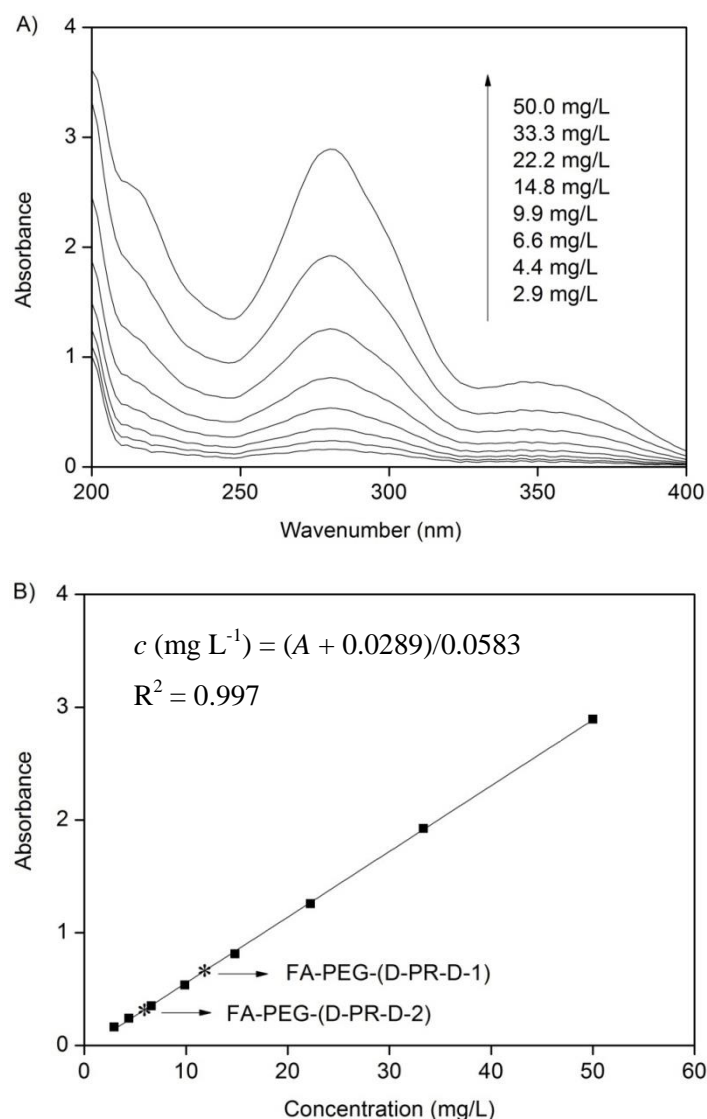
FA-PEG-(D-PR-D-2) conjugate measured by light scattering and differential refractometer detectors is displayed in Figure 5.3. All the traces show a nearly symmetrical and unimodal peak of the molecular weight distributions reveals the high purity of tested samples. In addition, the molecular weight of the FA-PEG-(D-PR-D-2) increases and experiences a shorter elution time as comparison to D-PR-D trace. This clearly illustrates the success of the conjugation reaction between activated hydroxyl groups in  $\alpha$ -CD rings and the amino groups of PEG. The molecular weight difference between D-PR-D triblock copolymers and their conjugates can be used to approximately evaluate the arms attached to the polyrotaxane blocks. The results are presented in Table 5.2.

The number of chain conjugated to one polyrotaxanes is about 4.2 for D-PR-D-1; nearly every  $\alpha$ -CD molecules was conjugated with one FA-PEG arm. In the meantime, about 3.9 molecules FA-PEG were reacted onto D-PR-D-2. It is likely that the longer PDMAEMA chains resulted in more difficult conjugation, properly because of the spatial hindrance. However, the conjugated chain number increases slightly when PEG-*bis*-amine was used instead of FA-PEG. PEG-(D-PR-D) samples will be used as controls in the biological characterization. GPC results confirm the successful synthesis of the target and the conjugated chain number in FA-PEG-(D-PR-D) is tunable by changing the polymer compositions and feed ratios.

CMC values were determined using dye solubilization method at 25 °C.<sup>27</sup> All of the studied polymers are soluble in water. This experiment was carried out by varying the aqueous polymer concentration in the range of  $1 \times 10^{-4}$  to 5 mg/mL, while keeping the concentration of DPH constant. The CMC was determined by plotting the difference in the absorbance at 378 nm and 400 nm ( $A_{378}-A_{400}$ ) versus the logarithmic of the polymer concentrations (Figure 5.4). As shown in Table 5.2, the CMC values of the D-PR-D triblock copolymers increase from 0.28 to 0.35 mg/mL with increasing PDMAEMA block length. This is due to the increased hydrophilicity in D-PR-D-2 copolymers as a result of longer PDMAEMA chains.<sup>37</sup>

Polyrotaxanes comprising  $\alpha$ -CDs and PCL in the central block lead to a high crystalline capability and hydrophobicity, which may provide the main driving force for the self-assembly of micelle formation.<sup>38</sup> This observation is also confirmed by the results measured on FA-PEG-(D-PR-D) sample. In Figure 5.4B, the CMC of FA-PEG-(D-PR-D-1) is not determined in the measured concentration range due to the significant reduction of the non-covalent hydrogen bonding interactions between polyrotaxanes after the consumption of the hydroxyl groups in  $\alpha$ -CD rings. Similar phenomenon was also observed on PEG-(D-PR-D) specimens. The CMC results reveal the conjugation of PEG contained arms onto D-PR-D

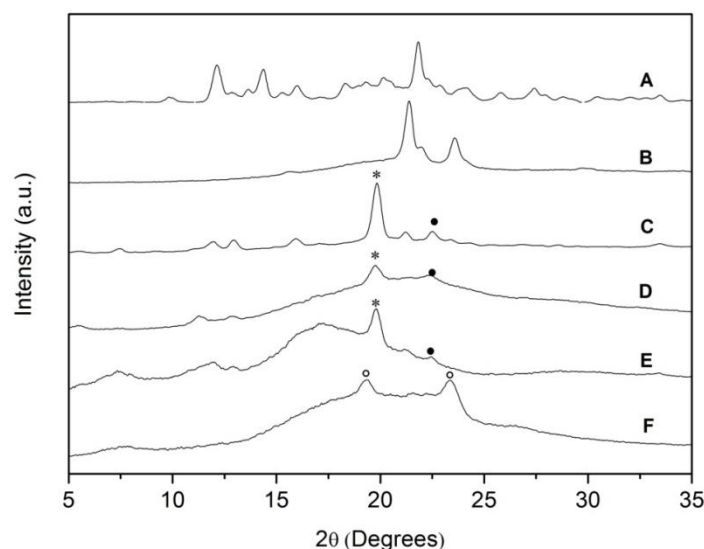
copolymers improves the water solubility of the product and may make it as a PEGylated gene vector.<sup>39</sup>



**Figure 5.5.** UV absorbance of folic acid PBS solutions (A) and the standard curve based folic acid content determination of FA-PEG-(D-PR-D) supramolecules (B). Light absorption of FA-PEG-(D-PR-D) solution was measured from 200 to 400 nm by UV-Vis spectrometer.

The folic acid amount in the final product FA-PEG-(D-PR-D) was measured using UV absorbance at 280 nm.<sup>25, 26</sup> The concentration of the folic acid in FA-PEG-(D-PR-D) PBS solution ( $c$ ) was obtained based on the standard curve of free folic acid (Figure 5.5A):  $c \text{ (mg L}^{-1}\text{)} = (A + 0.0289)/0.0583$ , where  $A$  is the UV absorbance at 280 nm. As shown in Figure 5.5B, the content of folic acid conjugated in FA-PEG-(D-PR-D-1) and FA-PEG-(D-PR-D-2) polymer is

11.7 and 6.2 mg/L, corresponding to the molar ratio of folic acid/polymer at around 4.0 and 3.5, respectively. Basing on the assumption of one  $\gamma$ -carboxyl group in the folic acid molecule was reacted with PEG-*bis*-amine, these numbers are in good agreement with the conjugated arms determined by GPC (Table 5.2).



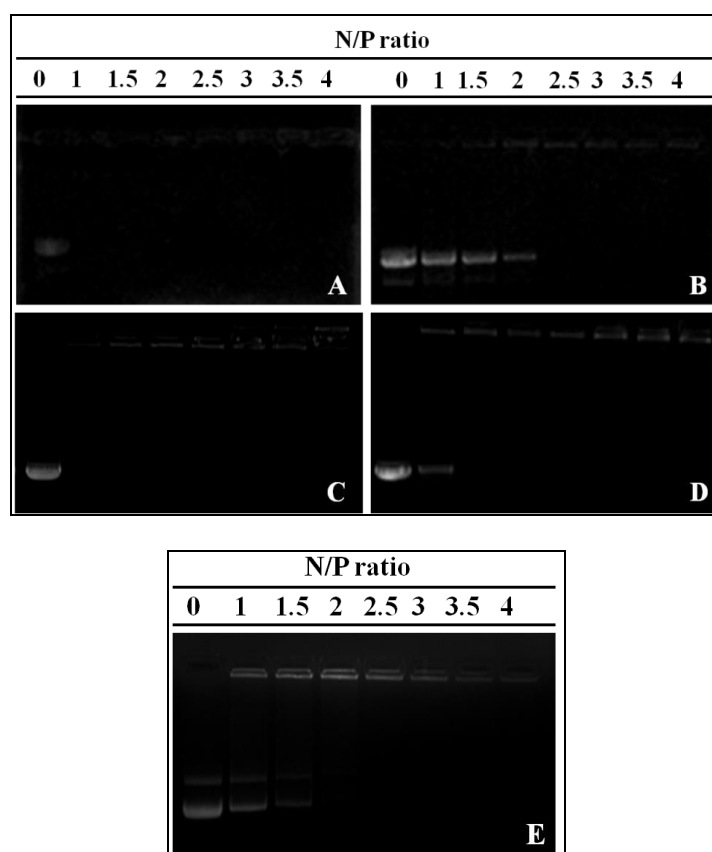
**Figure 5.6.** Wide-angle X-ray diffraction patterns of  $\alpha$ -CD (A), PCL-diBr (B), dried PCL/ $\alpha$ -CD PPR2 (C), PCL/ $\alpha$ -CD PPR2 slurry in DMF (D), D-PR-D-1 (E) and FA-PEG-(D-PR-D-1) (F). The characteristic X-ray diffraction peaks of crystalline columnar  $\alpha$ -CD at  $2\theta = 19.8^\circ$  and  $22.6^\circ$  are labelled with \* and •, respectively. PEG peaks at around  $2\theta = 19.3^\circ$  and  $23.5^\circ$  are labelled with ○.

Figure 5.6 demonstrates the crystalline structure of FA-PEG-(D-PR-D) and its precursors investigated by wide-angle X-ray diffraction (WAXD). As shown, the main reflection of pure  $\alpha$ -CD are observed at  $12.1^\circ$ ,  $14.4^\circ$ ,  $18.3^\circ$  and  $21.8^\circ$  and the characteristic peaks of PCL crystal are formed at about  $21.4^\circ$  and  $23.6^\circ$ , respectively (Figure 5.6 A and B). However, the diffractogram PPR shows quite a different diffraction pattern from those of PCL and  $\alpha$ -CD (Figure 5.6C). The strong peaks at approximately  $19.8^\circ$  and  $22.6^\circ$  indicate that the  $\alpha$ -CD rings are stacked along the PCL chain axis to form the channel-type crystalline structure.<sup>29</sup> The presence of this crystalline columnar  $\alpha$ -CD structure can also be detected in PPR slurry in XRD at  $2\theta = 19.8^\circ$ , albeit with some peak attenuated (Figure 5.6D), which is not unexpected due to a lower crystallinity in the presence of DMF. More importantly, the characteristic peaks of polyrotaxane structure are clearly evidenced in D-PR-D triblock copolymer (Figure 5.6E), giving another evidence for the successful preparation of the polyrotaxane flanked by PDMAEMA copolymer architecture. However, the crystalline capability between polyrotaxanes is eliminated after the consumption of the hydroxyl groups in

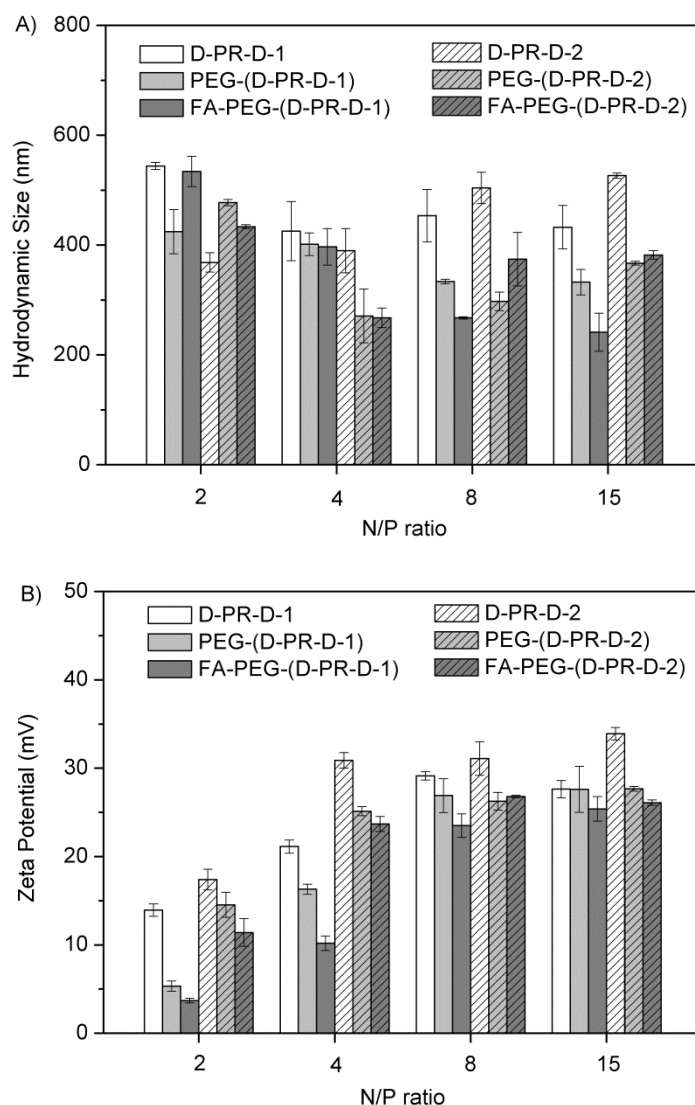
$\alpha$ -CDs. Compared with the reflection of D-PR-D, only the major crystal peaks of PEG at 19.3° and 23.5° are observed on conjugated FA-PEG-(D-PR-D) supramolecules, confirming the success for the conjugation reaction.

### 5.3.3 pDNA Condensation and Particle Size Characterization

To function as polymeric gene vectors, a particular polymer must be able to condense DNA into polyplexes suitable for cellular uptake. The condensed form of the polymer/pDNA polyplex protects the pDNA from cell barriers during gene delivery.<sup>26</sup> In this study, the complexation and condensation capability of D-PR-D triblock copolymers and their conjugated FA-PEG-(D-PR-D) supramolecules to pDNA were examined using gel electrophoresis, with golden standard PEI ( $M_n = 25$  kDa) as control. Electrophoresis results are shown in Figure 5.7.



**Figure 5.7.** Agarose gel electrophoresis retardation assays for D-PR-D-1/pDNA (A), FA-PEG-(D-PR-D-1)/pDNA (B), D-PR-D-2/pDNA (C), FA-PEG-(D-PR-D-2)/pDNA (D) and PEI/pDNA (E). Lane 1 (most left) is the pDNA control and Lanes 2 → 8 correspond to the polymer/pDNA polyplexes in different N/P ratios.



**Figure 5.8. Particle size (A) and zeta potential (B) of polyplexes formed by D-PR-D triblock copolymers and their conjugated supramolecules at different transfection N/P ratios.**

As can be seen, both D-PR-D-1 and D-PR-D-2 are found to condense pDNA efficiently at N/P ratio of 1.0, in comparison to N/P ratio of 2.0 for PEI. This illustrates that D-PR-D triblock copolymers have strong pDNA binding ability (Figure 5.7 A and C). For the conjugated FA-PEG-(D-PR-D) supramolecules, free DNA band could be seen in the image at low N/P ratios (Figure 5.7 B and D). As the N/P ratio increased, DNA bands gradually became fainter. At N/P ratio of 2.5 for FA-PEG-(D-PR-D-1) and 1.5 for FA-PEG-(D-PR-D-2), no DNA bands could be observed but the fluorescence could still be detected in the loading well, suggesting a complete binding of pDNA. At this level, the binding efficiencies of the two conjugates are comparable to PEI. However, the conjugated FA-PEG-(D-PR-D)

supramolecules show a lower pDNA binding efficiency when compared with the N/P ratios of the corresponding D-PR-D triblock copolymers. This may be caused by the reduced charge density of PDMAEMA within the polymer, as imparted from the PEGylation effect of the conjugated PEG chains.<sup>12, 40, 41</sup> Moreover, this effect is highly dependent on the PEG chain number as well as the D-PR-D triblock copolymer compositions.

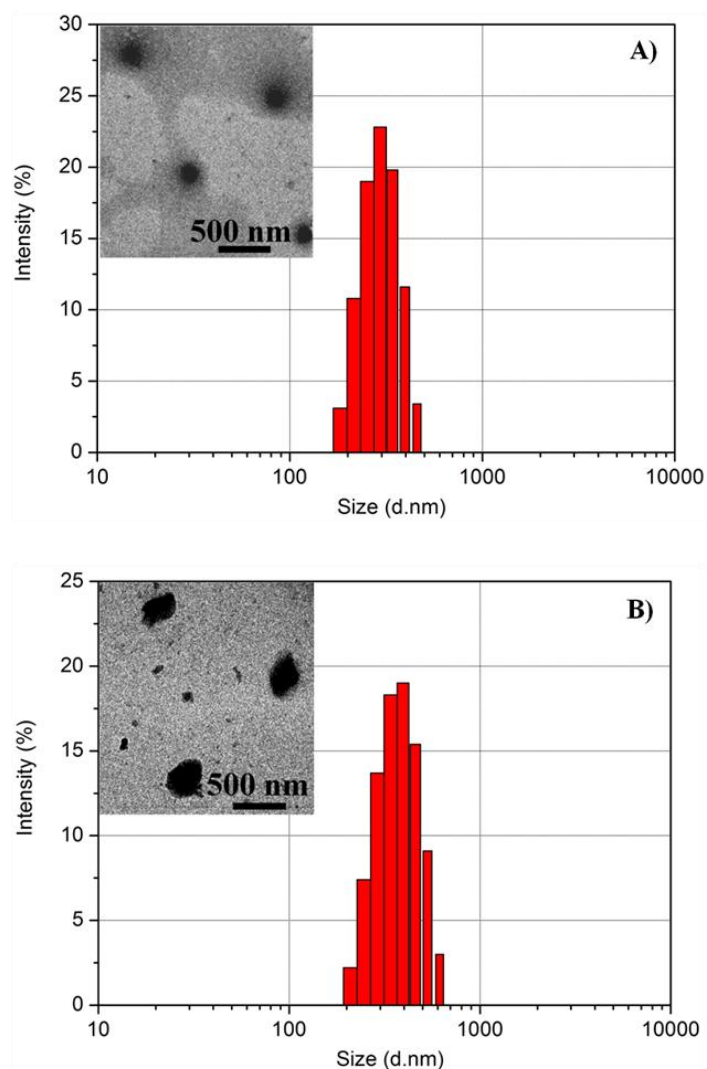
The particle size of the as-synthesized polymer/pDNA polyplexes at different N/P ratios are shown in Figure 5.8A. At the lowest N/P ratio, the average particle size measured on D-PR-D-1/pDNA polyplexes is 544 nm in comparison with 368 nm of its counterpart D-PR-D-2/pDNA polyplexes. This observation may be due to the stronger condensation ability of the longer PDMAEMA chains in D-PR-D-2 triblock copolymer which leads to the polyplexes more compact in a smaller size.<sup>6, 20</sup> Due to the difference in DMAEMA unit number in the two D-PR-D triblock copolymers, the polyplexes showed an inverted trend as the N/P ratio increases, in which the D-PR-D-1 copolymer formed more condensed particles while a bigger complex size of D-PR-D-2/pDNA polyplexes was observed at high N/P ratio. Obviously, the particle size of the D-PR-D copolymer/pDNA polyplexes depends on the N/P ratios as well as the copolymer compositions. For D-PR-D triblock copolymers conjugated polymers, the particle sizes at high N/P ratios are generally smaller than those measured at the lowest N/P ratio of 2. In addition, the two conjugated supramolecules/pDNA polyplexes, *i.e.*, PEG-(D-PR-D)/pDNA and FA-PEG-(D-PR-D)/pDNA have similar particle size at the same N/P ratio.

As presented in Figure 5.8A, a gradual decreasing trend from 534 to 241 nm for D-PE-D-1 conjugated polymers is observed as the ratios increase from 2 to 15. This may be caused by the shielding effect of conjugated PEG chains on the charge density that the formation of loose and unstable complex structures were formed at low N/P ratios. The reduced surface charge distribution resulted from PEGylation effect would need more polymers for effective condensation of pDNA as stable and compact polyplexes.<sup>12, 40, 41</sup> On the other hand, the particle size for D-PR-D-2 conjugates/pDNA polyplexes decreased from 477 to 271 nm but increased slightly when N/P ratios were further increased from 8 to 15. This is probably due to the long PDMAEMA segment together with the low number of the conjugated PEG chains make the charge shielding effect not prominent. This finding is consistent with previously reported data of FA-PEI-PEG system with strong pDNA condensation capability, in which the so formed polyplex size increased as increasing the polymer /pDNA ratio.<sup>26</sup>

Figure 5.8B shows the zeta potentials of the polyplexes. As can be seen, the zeta potentials of D-PR-D-1 copolymer/pDNA polyplexes increase from 13.9 to 29.1 mV with



increasing N/P ratio while those for the D-PR-D-2 copolymer/pDNA polyplexes increase from 17.4 to 33.9 mV correspondingly. At higher N/P ratio, the copolymer/pDNA polyplexes possess a higher zeta potential due to the increasing amount of cationic moiety. The effect of PEGylation (with or without FA) on the surface charge of polyplexes is also shown in Figure 5.8B.



**Figure 5.9. Particle size distribution and transmission electron micrographs of FA-PEG-(D-PR-D-2)/pDNA polyplexes at N/P of 4 (A) and 15 (B), respectively.**

As illustrated, the conjugation of PEG to D-PR-D copolymers led to a drastic drop in zeta potential, demonstrating that the PEG chains effectively shielded the surface charge. With FA-PEG, the decrease of zeta potential is even more pronounced, dropping to the range of 3.7 ~ 25.4 mV and 11.4 ~ 26.8 mV for FA-PEG-(D-PR-D-1) and FA-PEG-(D-PR-D-2) polymers prepared polyplexes, respectively. This is probably caused by the negatively charged carboxylic

acid group of the folic acid ligand.<sup>12</sup> It should be noted that the zeta potentials of all the investigated polymer/pDNA polyplexes are positive, which is necessary to ensure the uptake of polyplexes by cells due to electrostatic interaction between negatively charged cellular membranes and positively charged polyplexes.<sup>42</sup>

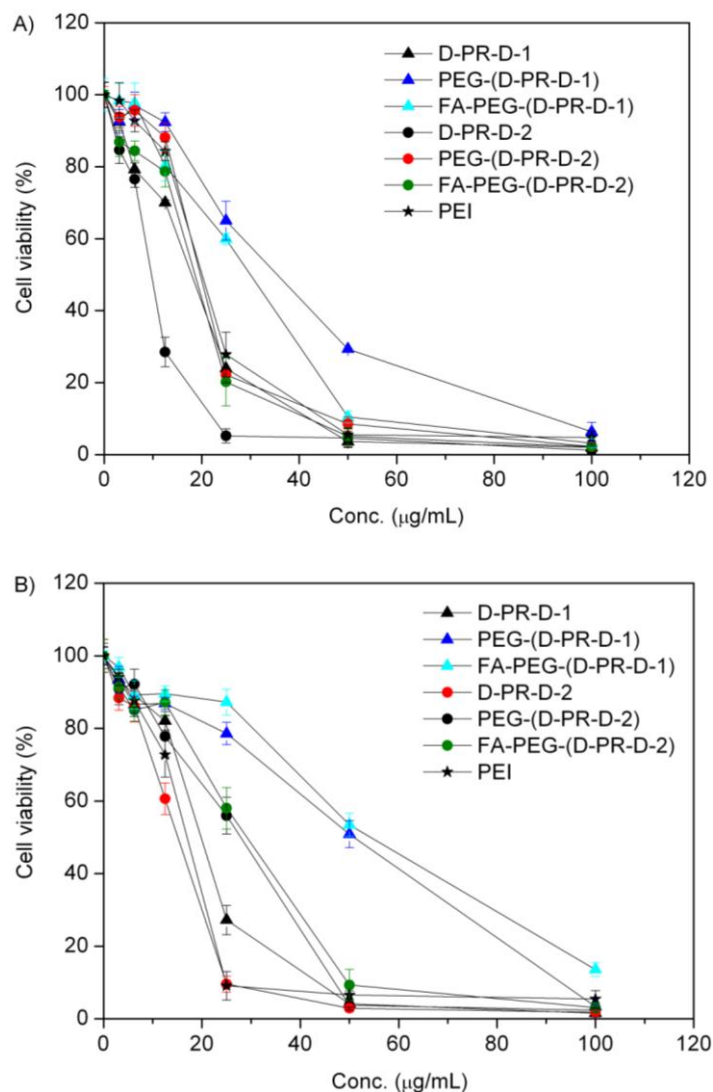
The polyplexes were further characterized by TEM visualization. Representative images of FA-PEG-(D-PR-D-2)/pDNA complexes at the N/P ratios of 4 and 15 are shown in Figure 5.9. After complexation, the morphologies of both polyplexes are spherical, and there is no obvious agglomeration of polyplexes in the field of vision. The sizes viewed by TEM are in good agreement with the results measured on DLS (Figure 5.8). These results indicate that the complexation of pDNA by the polymers could lead to the formation of compact nanoparticles which can be endocytosed by cells at certain N/P ratios.

### 5.3.4 Cytotoxicity and *In Vitro* Transfection Efficiency Studies

**Cytotoxicity:** Cytotoxicity is one of the most important factors to be considered in developing polymeric gene carriers. In order to evaluate the potential toxicity of the resulting polymers, the viability of two different cell lines was investigated in the presence of the as-synthesized polymers at various concentrations. PEI (25 kDa, branched) was used as control. As shown in Figure 5.10, all the studied polymers exhibit dose-dependent cytotoxicity effect. Notably, the conjugation of PEG with or without FA exhibits significantly lower cytotoxicity compared with that of unconjugated D-PR-D triblock copolymers regardless of cell lines, and the difference of cytotoxicity between PEG-(D-PR-D) and FA-PEG-(D-PR-D) is not significant for both series.

In general, cytotoxicity of these cationic polymers is related to their high amino group concentration.<sup>6, 19</sup> In this work, toxicity of the unmodified D-PR-D triblock copolymers increases with increasing PDMAEMA chain length, in the order of D-PR-D-1 < D-PR-D-2, following the trend of increasing amino group density (Table 5.2). At this stage, the unmodified D-PR-D copolymers are either comparable or more toxic than PEI in the tested cells lines (Figure 5.10 A & B). However, after conjugation, the reduced amino density as imparted from the PEGylation effect, leads to a remarkable increase in the relative viability. In addition, the results also show a cell type-dependent cytotoxicity effect, in which the cytotoxicity of the as-synthesized polymers are much lower in A549 cells than that in KB cells. Taking PEI and FA-PEG-(D-PR-D-1) for example, the calculated median inhibitory concentration (IC<sub>50</sub>) value in A549 cells is 16.9 µg/mL and 53.8 µg/mL while the corresponding value determined in KB

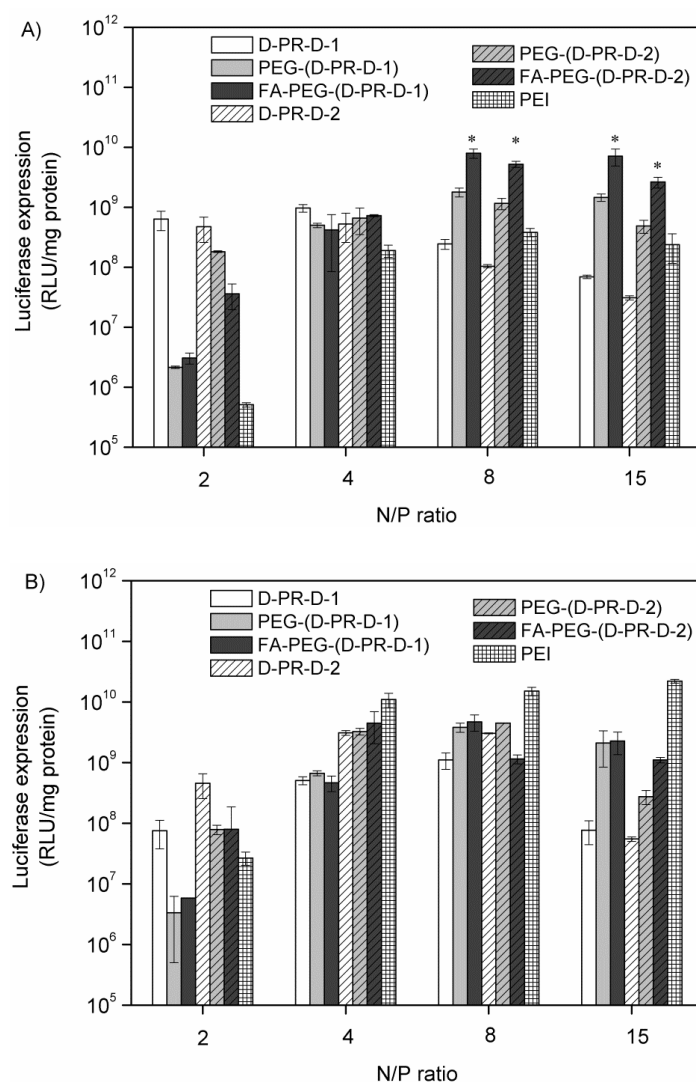
cells for each polymer is 19.7  $\mu\text{g/mL}$  and 29.6  $\mu\text{g/mL}$ , respectively. These results indicate FA-PEG-(D-PR-D-1) exhibits much lower toxicity in the both cell lines than that of PEI.



**Figure 5.10.** Cytotoxicity of D-PR-D triblock copolymers and their conjugated supramolecules in comparison with PEI (25 kDa, branched) in KB cells (A) and A549 cells (B).

*In Vitro* Transfection Study: As FR expression is frequently elevated in a variety of human cancers and in tumor cell lines, the folic acid molecule was conjugated to D-PR-D triblock copolymer using PEG as a spacer to obtain the desired FA-PEG-(D-PR-D) supramolecules. The conjugation design aimed to introduce the tumor-target effect as well as PEGylation of the gene delivery carrier. For comparison, PEG-(D-PR-D) without FA at the PEG distal end was prepared for control. To quantify the transfection efficiency mediated by D-PR-D triblock copolymers and their conjugated supramolecules, we performed *in vitro*

transfection activity assays using luciferase as marker gene in both FR-positive (KB) and FR-negative (A549) cells. Transfection experiments were carried out in folate-depleted medium.



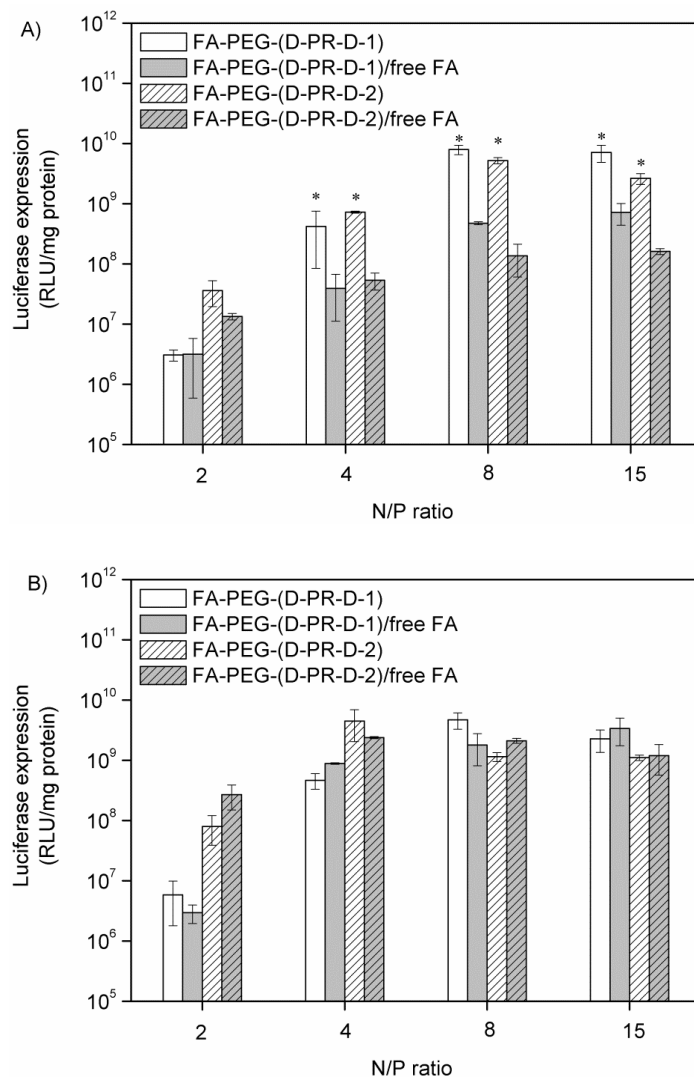
**Figure 5.11.** *In vitro* gene transfection efficiency of D-PR-D/pDNA, PEG-(D-PR-D)/pDNA and FA-PEG-(D-PR-D)/pDNA polyplexes at various N/P ratios in serum supplemented folic acid-free RPMI-1640 medium at KB (A) and A549 (B) cell lines, in comparison with PEI (25 kDa, branched). Data represent mean  $\pm$  SD ( $n = 3$ , Student's *t*-test, \* $P < 0.05$  as compared with the data of PEG-(D-PR-D)).

Figure 5.11A shows the results for KB cells, the unconjugated D-PR-D triblock copolymers exhibit much higher transgene expression level than PEI at low N/P ratios of 2 and 4, while the transfection efficiency decreases with an increasing N/P ratio of copolymer/pDNA up to 15. This can be explained by the strong pDNA condensation capability of D-PR-D

copolymers, giving positive surface charge and leading to an enhanced non-specific cellular association and internalization at this N/P ratio range. The decreasing efficiency at  $N/P > 4$  was attributed to the toxicity of the free polymer present in the transfection medium at these high ratios.<sup>43</sup> Considering the transfection efficiencies of the conjugated supramolecular systems at N/P ratio of 2, these are significantly decreased as compared to D-PR-D/pDNA polyplexes, probably due to the charge shielding effect by PEGylation that reduced the non-specific adhesion to the cell surface, as was shown previously.<sup>40</sup> Nevertheless, the transfection efficiencies on both conjugated systems increase readily at N/P ratios above 4 and show higher luciferase activities at certain N/P ratios when compared with that of PEI and the unconjugated D-PR-D copolymers as carriers, respectively (Figure 5.11A). This observation indicates that the PEGylation effect could reduce cytotoxicity of the copolymers and increase the gene expression to some extent. In addition, it is interesting to note that there is statistically significant difference ( $p < 0.05$ ) in the level of transfection between FA-PEG-(D-PR-D) and PEG-(D-PR-D) at certain N/P ratios of 8 and 15. This illustrates the incorporation of FA increases transfection efficiency of the system in FR-positive KB cells, relative to the unmodified D-PR-D triblock copolymers, PEI and PEG-(D-PR-D) conjugates. The increase in gene expression is not observed at N/P ratios of 2 and 4 for both conjugated FA-PEG-(D-PR-D) supramolecules. One of the reasons could be that the polyplexes formed by FA-PEG-(D-PR-D) system at low N/P ratios would be expected to have fewer ligands per particle compared to that at high N/P ratios, thereby potentially reducing occurrence of the polyplexes to interact with the receptors on the cell surface.<sup>11</sup> It has been previously reported that specific surface binding is initially proportional to the density of targeting ligands on particle surface.<sup>44, 45</sup> In the present study, the gene transfection efficiency could be adjusted by controlling the polymer/pDNA ratios in the polyplexes.

In A549 cells, the results became different from those described above. As shown in Figure 5.11B, the optimal transfection capabilities of the unmodified D-PR-D triblock copolymers are observed at N/P ratio of 8 and the efficiency further decreases till N/P ratio 15 because of the toxicity of the polymer at high concentrations. At N/P ratios over 4, PEI possessed the highest transfection efficiency in A549 cells among all the investigated polymers. More importantly, the transfection efficiency mediated by FA-PEG-(D-PR-D)/pDNA and PEG-(D-PR-D)/pDNA polyplexes does not show significant difference and the improved luciferase expression of both polyplexes is only observed at the highest N/P ratio of 15 as related to D-PR-D copolymers under the experimental conditions. These results indicate that the transfection efficiency depends on cell types. FA-PEG-(D-PR-D)/pDNA polyplexes

exhibited higher transfection efficiency than that of PEG-(D-PR-D)/pDNA polyplexes in FR-positive KB cells, whereas no obvious difference in FR-negative A549 cells was found.



**Figure 5.12. Transfection efficiency of FA-PEG-(D-PR-D)/pDNA polyplexes in KB (A) and A549 (B) cell lines in the presence or absence of free folic acid at various N/P ratios. Data represent mean  $\pm$  SD ( $n = 3$ , Student's  $t$ -test,  $*P < 0.05$  as compared with the data of FA-PEG-(D-PR-D)/free FA).**

In order to further assess the targeting effect of FA-PEG-(D-PR-D) system, transgene expression level was evaluated with the presence of free folic acid in FR-positive KB cells with FR-negative A549 cells transfection process as control. Free folic acid at concentration of 10  $\mu\text{g}/\text{mL}$  was added to saturate the FRs. As seen in Figure 5.12A, the luciferase expression in KB cells is significantly decreased at certain effectively transfected N/P ratios when pDNA was condensed with FA-PEG-(D-PR-D)/free FA transfection than when the polyplexes were

prepared with FA-PEG-(D-PR-D). Due to the existence of free folic acid added in the culture medium, the binding competition of free folic acid to the FRs on the cell surface would reduce receptor-specific cellular association with the polyplexes.<sup>11, 26, 46, 47</sup> Hence, the transfection efficiency decreased greatly. By contrast, there is no significant difference was found when A549 cells were transfected in the presence of free folic acid in the medium (Figure 5.12B). These findings illustrate that the incorporation of folic acid molecules improves the transfection efficiency of FA-PEG-(D-PR-D) supramolecules for FR-positive cells, implying the potential of such system for specific targeting gene delivery.

### 5.4 Conclusion

In this study, cationic D-PR-D triblock copolymers with biodegradable PCL/ $\alpha$ -CD self-assembled PR as the central block flanked by various PDMAEMA segments were prepared; thereafter, FA was conjugated to  $\alpha$ -CD exterior by using PEG as a spacer to prepare the FA-PEG-(D-PR-D) as a targeting gene vector. Their molecular and structural properties were characterized by EA, GPC, NMR and XRD. The conjugated arm numbers were evaluated by the molecular weight difference before and after the conjugation reaction and these numbers were in good agreement with the results determined by UV spectroscopy. All the studied polymers showed good pDNA complexation capability to form nano-sized polyplexes. In addition, the conjugated PEG and FA-PEG could reduce the cytotoxicity of D-PR-D copolymers by shielding the amino group density and increase the gene expression to some extent. More importantly, FA-PEG-(D-PR-D)/pDNA complexes exhibited higher transfection efficiency than that of PEG-(D-PR-D) in FR-positive KB cells, whereas no significant difference in FR-negative A549 cells was found. Competitive assay in the presence of free folic acid demonstrated that there was a reduced gene expression as compared with FA-PEG-(D-PR-D) polyplexes, clearly indicating the targeting effect. On the basis of the obtained results, FA-PEG-(D-PR-D) might be a potential safe and efficient system for specific targeting to cells that exhibit the overexpression of FRs.

### 5.5 References

1. W. Walther and U. Stein, *Drugs*, 2000, **60**, 249-271.

2. C. Shih-Jiuan and L. Robert, in *Polymeric Gene Delivery*, CRC Press, 2004.
3. A. Agarwal, R. Unfer and S. K. Mallapragada, *J. Controlled Release*, 2005, **103**, 245-258.
4. P. Van de Wetering, J. Y. Cherng, H. Talsma and W. E. Hennink, *J. Controlled Release*, 1997, **49**, 59-69.
5. P. Dubruel and E. Schacht, *Macromol. Biosci.*, 2006, **6**, 789-810.
6. W. Zhang, J. He, Z. Liu, P. Ni and X. Zhu, *J. Polym. Sci., Part A: Polym. Chem.*, 2010, **48**, 1079-1091.
7. X. Yue, Y. Qiao, N. Qiao, S. Guo, J. Xing, L. Deng, J. Xu and A. Dong, *Biomacromolecules*, 2010, **11**, 2306-2312.
8. C. Zhu, S. Jung, S. Luo, F. Meng, X. Zhu, T. G. Park and Z. Zhong, *Biomaterials*, 2010, **31**, 2408-2416.
9. S. Motala-Timol and D. Jhurry, *Eur. Polym. J.*, 2007, **43**, 3042-3049.
10. Z. Li, H. Yin, Z. Zhang, K. L. Liu and J. Li, *Biomacromolecules*, 2012, **13**, 3162-3172.
11. J. K. W. Lam, S. P. Armes, A. L. Lewis and S. Stolnik, *J. Drug Targeting*, 2009, **17**, 512-523.
12. J. H. van Steenis, E. M. van Maarseveen, F. J. Verbaan, R. Verrijck, D. J. A. Crommelin, G. Storm and W. E. Hennink, *J. Controlled Release*, 2003, **87**, 167-176.
13. Y. L. Wu and J. Li, *Angew. Chem. Int. Ed.*, 2009, **48**, 3842-3845.
14. A. Harada, J. Li and M. Kamachi, *Nature*, 1992, **356**, 325-327.
15. Z. X. Zhang, X. Liu, F. J. Xu, X. J. Loh, E. T. Kang, K. G. Neoh and J. Li, *Macromolecules*, 2008, **41**, 5967-5970.
16. C. Yang, J. Yang, X. Ni and J. Li, *Macromolecules*, 2009, **42**, 3856-3859.
17. C. Yang, X. Wang, H. Li, S. H. Goh and J. Li, *Biomacromolecules*, 2007, **8**, 3365-3374.
18. J. Li, C. Yang, H. Z. Li, X. Wang, S. H. Goh, J. L. Ding, D. Y. Wang and K. W. Leong, *Adv. Mater.*, 2006, **18**, 2969-2974.
19. F. J. Xu, H. Li, J. Li, Z. Zhang, E. T. Kang and K. G. Neoh, *Biomaterials*, 2008, **29**, 3023-3033.
20. F. J. Xu, Z. X. Zhang, Y. Ping, J. Li, E. T. Kang and K. G. Neoh, *Biomacromolecules*, 2009, **10**, 285-293.
21. C. Yang, H. Li, S. H. Goh and J. Li, *Biomaterials*, 2007, **28**, 3245-3254.



22. R. J. Lee and P. S. Low, *J. Biol. Chem.*, 1994, **269**, 3198-3204.
23. X. J. Loh, Y. L. Wu, W. T. J. Seow, M. N. I. Norimzan, Z. X. Zhang, F. Xu, E. T. Kang, K. G. Neoh and J. Li, *Polymer*, 2008, **49**, 5084-5094.
24. F. J. Xu, J. Li, S. J. Yuan, Z. X. Zhang, E. T. Kang and K. G. Neoh, *Biomacromolecules*, 2008, **9**, 331-339.
25. H. K. Mitchell, *J. Am. Chem. Soc.*, 1944, **66**, 274-278.
26. H. Cheng, J. L. Zhu, X. Zeng, Y. Jing, X. Z. Zhang and R. X. Zhuo, *Bioconjugate Chem.*, 2009, **20**, 481-487.
27. X. J. Loh, S. H. Goh and J. Li, *Biomacromolecules*, 2007, **8**, 585-593.
28. Y. Ping, C. Liu, Z. Zhang, K. L. Liu, J. Chen and J. Li, *Biomaterials*, 2011, **32**, 8328-8341.
29. L. Huang, E. Allen and A. E. Tonelli, *Polymer*, 1998, **39**, 4857-4865.
30. X. Tong, X. Zhang, L. Ye, A.-y. Zhang and Z.-g. Feng, *Soft Matter*, 2009, **5**, 1848-1855.
31. R. Nakaoka, Y. Tabata, T. Yamaoka and Y. Ikada, *J. Controlled Release*, 1997, **46**, 253-261.
32. C. A. Yang, H. Z. Li, X. Wang and J. Li, *J. Biomed. Mater. Res., Part A*, 2009, **89A**, 13-23.
33. C. P. Leamon, D. Weigl and R. W. Hendren, *Bioconjugate Chem.*, 1999, **10**, 947-957.
34. P. Chan, M. Kurisawa, J. E. Chung and Y.-Y. Yang, *Biomaterials*, 2007, **28**, 540-549.
35. Y. Bae, W.-D. Jang, N. Nishiyama, S. Fukushima and K. Kataoka, *Molecular BioSystems*, 2005, **1**, 242-250.
36. A. R. Khan, P. Forgo, K. J. Stine and V. T. D'Souza, *Chem. Rev.*, 1998, **98**, 1977-1996.
37. V. San Miguel, A. J. Limer, D. M. Haddleton, F. Catalina and C. Peinado, *Eur. Polym. J.*, 2008, **44**, 3853-3863.
38. J. Li, X. Li, X. P. Ni, X. Wang, H. Z. Li and K. W. Leong, *Biomaterials*, 2006, **27**, 4132-4140.
39. S. Üzgün, O. z. r. Akdemir, G. n. Hasenpusch, C. Maucksch, M. M. Golas, B. Sander, H. Stark, R. Imker, J.-F. o. Lutz and C. Rudolph, *Biomacromolecules*, 2009, **11**, 39-50.
40. N. J. Zuidam, G. Posthuma, E. T. J. de Vries, D. J. A. Crommelin, W. E. Hennink and G. Storm, *J. Drug Targeting*, 2000, **8**, 51-66.
41. P. Erbacher, T. Bettinger, P. Belguise-Valladier, S. M. Zou, J. L. Coll, J. P. Behr and J. S. Remy, *J. Gene Med.*, 1999, **1**, 210-222.

42. S. Mansouri, Y. Cuie, F. Winnik, Q. Shi, P. Lavigne, M. Benderdour, E. Beaumont and J. C. Fernandes, *Biomaterials*, 2006, **27**, 2060-2065.
43. F. Verbaan, D. Crommelin, W. Hennink and G. Storm, in *Polymeric Gene Delivery*, CRC Press, 2004.
44. K. B. Ghaghada, J. Saul, J. V. Natarajan, R. V. Bellamkonda and A. V. Annapragada, *J. Controlled Release*, 2005, **104**, 113-128.
45. D. W. Bartlett and M. E. Davis, *Bioconjugate Chem.*, 2007, **18**, 456-468.
46. W. Zhou, X. Yuan, A. Wilson, L. Yang, M. Mokotoff, B. Pitt and S. Li, *Bioconjugate Chem.*, 2002, **13**, 1220-1225.
47. J. M. Saul, A. Annapragada, J. V. Natarajan and R. V. Bellamkonda, *J. Controlled Release*, 2003, **92**, 49-67.

## CHAPTER 6 CONCLUSIONS AND FUTURE WORK

### 6.1 Conclusions

This thesis presented a study on the design of novel block copolymers containing biodegradable PCL and different functional components with well-defined macromolecular architectures to fulfill the specific requirements in tissue engineering field. The CD involved supramolecular self-assembly and biological activity modifications of the newly developed block copolymers were further explored as a site-specific delivery system.

Thermo-responsive P(PPOMA)-PCL-P(PPOMA) (PCP) hairy copolymers were carefully synthesized by ATRP and the molecular characterizations of the copolymers were performed by NMR, GPC, TGA and DSC. The well-defined macromolecular architecture favored reversible self-assembles of the PCP copolymer solutions as triggered by temperature. At low temperature, the micelles formation with a hydrophilic PPO corona and hydrophobic PCL core was formed whereas the PPO corona became hydrophobic and induced into larger hydrophobic nano-aggregates at elevated temperature. When applied the PCP block copolymers as surface coatings, they were examined to support good cells adhesion and spreading at 37 °C. The temperature-dependent dehydration to hydration transition of the P(PPOMA) segments was used as an approach to detach cells by cooling to 4 °C without trypsin digestion. The thermally detached cells showed good viability in cell sub-culture on normal culture dishes. The PCP hairy copolymer coated substrates allows for easy cell recovery under mild conditions and fast passage in good cell activity.

The research also explored the potential cell delivery application from a novel mechano-responsive hydrogel developed from hyperbranched EGC block copolymers containing biodegradable PCL, hydrophilic PEG and glycerol as branch units. EGC copolymers were characterized and their composition and branch length varied with the feeding ratio of PCL and PEG and the amount of glycerol used. Hydrogels were formed from these copolymers by swelling of water at low polymer concentrations. The porous morphology of the hydrogels provided good permeability for gas and nutrition. Together with the tunable rheological properties, the hydrogels were found to be suitable for 3D living cell encapsulation and delivery. The morphology of the solid copolymers was semi-crystalline, while the hydrogels were totally amorphous without crystallinity, providing a mild aqueous environment for living cells. When the encapsulated cells were recovered from the hydrogels followed by sub-culture, they showed good cell viability and proliferation ability. The results indicate that the hyperbranched EGC copolymers hydrogels system developed in this work may be promising candidates for potential injectable cell delivery application.

Besides the construction of biodegradable block copolymers for biomedical use in tissue engineering fields, this research also developed a novel targeting gene delivery carrier from polyrotaxane derived D-PR-D triblock copolymers composed of biodegradable PCL/ $\alpha$ -CD as chain-interlocked central block that were flanked by cationic PDMAEMA segments. FA was further conjugated to  $\alpha$ -CD exterior via PEG as spacer to obtain the FA-PEG-(D-PR-D) supramolecules for the specific affinity effect with FR overexpressed cells. To do so, the *in vitro* cellular toxicity was lowered considerably compared with the unconjugated D-PR-D copolymers. The gene transfection results of FA-PEG-(D-PR-D)/pDNA polyplexes exhibited higher transfection efficiency than that of PEG-(D-PR-D) in FR-positive KB cells but not FR-negative A549 cells. The transfection efficiency of FA-PEG-(D-PR-D) in the presence of free folic acid was much lower than that of the supramolecules without free folic acid on FR-positive KB cells, indicating the newly designed FA-PEG-(D-PR-D) system was a potential safe and efficient system for specific targeting to cells that exhibit the overexpression of FRs.

In short, the present studies have diversified a new group of PCL-based biodegradable block copolymers and the results obtained could be helpful in clarifying block copolymer design considerations for specific biomedical applications. The research carried out in this thesis has shown significant impact on the understanding of structure-property relations and applications of the newly developed block copolymers in various areas. Moreover, the

utilization of the inclusion complexes as building blocks opens new avenues for the design of site-specific delivery system.

### 6.2 Possible Future Research

From the scientific point of view, the strategies demonstrated in the block copolymers synthesis in this thesis can be expanded to the synthesis of other novel functional polymeric materials whereby the biodegradable components can be attached instead of PCL polyesters currently involved. The rearrangement of these segments into other polymer architectures by the versatile synthesis approaches as described previously could afford the as-prepared biodegradable block copolymers with very different and interesting properties.

Although PCP block copolymers coated substrates showed superiority over those surfaces modification through the commercialized F127 in thermo-responsive cell detachment application, in terms of fabrication process and cell recovery efficiency, the design could be extended to a 3D cell culture and recovery system by reformulating the block copolymers into a soft-tissue-like thermogel formation.<sup>1,2</sup> To this end, optimal hydrogel cell culture systems could be developed by fully understanding the relationship between polymer composition, hydrogel rheologies and cell migration behavior. The later recovery process by the easy temperature cooling and simple cell collection ( *e.g.* by centrifuge) could make the system as a promising cell storage container, which can encapsulate and transport cells, as well as study the cell specific functions.

Hyperbranched EGC block copolymers based hydrogels maintained good cell viability and allowed the spatial distribution of the seeded cells without aggregation. However, the cell morphology was circular with no discernible cell spreading and proliferation in the EGC hydrogel cultivation. Besides the hydrophilic/hydrophobic balance optimization of the EGC block copolymer, the next investigative step could be made in the hydrogel by presenting biological signals to the cells. For example, Arg-Gly-Asp-Ser (RGDS) or other peptide can be incorporated to stimulate cell adhesion and growth within the hydrogel. Further, it could be a potentially rich area to explore the control of hydrogel rheological properties in the direction of stem cell differentiation.<sup>3</sup>

In the area of gene delivery, sustained gene delivery systems is more effective than repetitive single dose administrations, and the extended release of genes could provide high transient expression for treatment of certain localized diseases.<sup>4</sup> It would be worthwhile to

develop sustained gene delivery carriers containing biodegradable block copolymer which can maintain the long term local availability of DNA vectors to surrounding tissues to achieve a sustained systemic protein production. The combination of supramolecular hydrogels as sustained gene delivery carriers and bioactive molecules as targeting groups can be designed to treat certain localized diseases effectively.<sup>5,6</sup> To this end, the desired system could be more effective than previously reported repetitive single dose administrations, and the biological affinity are able to make the system differentiate receptor-mediated endocytosis of targeted cell lines from the non-specific uptake of normal tissues.

### 6.3 References

1. A. Higuchi, N. Aoki, T. Yamamoto, T. Miyazaki, H. Fukushima, T. M. Tak, S. Jyujyoji, S. Egashira, Y. Matsuoka and S. H. Natori, *J. Biomed. Mater. Res., Part A*, 2006, **79A**, 380-392.
2. A. Higuchi, T. Yamamoto, K. Sugiyama, S. Hayashi, T. M. Tak and T. Nakagawa, *Biomacromolecules*, 2005, **6**, 691-696.
3. Y. S. Pek, A. C. A. Wan, A. Shekaran, L. Zhuo and J. Y. Ying, *Nat Nanotechnol*, 2008, **3**, 671-675.
4. A. Agarwal and S. K. Mallapragada, *Curr. Top. Med. Chem.*, 2008, **8**, 311-330.
5. Z. Li, H. Yin, Z. Zhang, K. L. Liu and J. Li, *Biomacromolecules*, 2012, **13**, 3162-3172.
6. H. Cheng, J. L. Zhu, X. Zeng, Y. Jing, X. Z. Zhang and R. X. Zhuo, *Bioconjugate Chem.*, 2009, **20**, 481-487.